

NASA Technical Memorandum 101641

**AERODYNAMIC CHARACTERISTICS OF A PROPOSED
PERSONNEL LAUNCH SYSTEM (PLS) LIFTING-BODY
CONFIGURATION AT MACH NUMBERS FROM 0.05 TO 20.3**

**Christopher I. Cruz, George M. Ware,
Sue B. Grafton, William C. Woods,
and James C. Young**

NOVEMBER 1989

NASA

National Aeronautics and
Space Administration

Langley Research Center
Hampton, Virginia 23665-5225

(NASA-TM-101641) AERODYNAMIC
CHARACTERISTICS OF A PROPOSED
PERSONNEL LAUNCH SYSTEM (PLS)
LIFTING-BODY CONFIGURATION AT MACH
NUMBERS FROM 0.05 TO 20.3 (Diskette
Supplement) (NASA) 161 p

N93-24522

Unclas

G3/16 0159782

AERODYNAMIC CHARACTERISTICS OF A PROPOSED PERSONNEL LAUNCH
SYSTEM (PLS) LIFTING-BODY CONFIGURATION AT MACH NUMBERS
FROM 0.05 TO 20.3

Christopher I. Cruz, George M. Ware, Sue B. Grafton,
William C. Woods and James C. Young

SUMMARY

A wind-tunnel investigation has been performed to determine the aerodynamic characteristics of a proposed lifting-body personnel launch system (PLS) configuration over a Mach range of 0.05 to 20.3. The test configuration had a low-aspect-ratio body with a flat undersurface and three fins on the upper aft body. Data are presented with a minimum of analysis.

INTRODUCTION

The purpose of this report is to present in one document the published results of two experimental investigations (refs. 1 and 2) and the previously unpublished results from two additional investigations of a lifting-body configuration which is being studied by the NASA Langley Research Center as a candidate for the NASA Assured Crew Return Capability (ACRC, ref. 3) vehicle. References 1 and 2 presented the transonic and supersonic wind-tunnel results. This report includes results of the low-speed and initial hypersonic (Mach 20.3 in helium) experimental investigations. References 1 and 2 discuss the lifting-body configuration as an ACRC candidate, whereas this report proposes the configuration for a larger role in the nation's space transportation system as a personnel launch system (PLS) configuration. The PLS has been proposed as a priority cargo vehicle to be used to supplement the Space Shuttle system. The PLS will be vertically launched on an expendable booster and will be used primarily to carry supplies or crew to and from the Space Station Freedom. The lifting body configuration for the ACRC study was sized to (1) carry an eight-man crew, (2) fit inside the Shuttle payload bay,

and (3) meet space station docking requirements. The same size vehicle is being retained as the initial lifting-body configuration considered for the PLS role. The design is 24.6 feet long and features a low-aspect-ratio body with a flat undersurface and three fins on the aft upper body. The outboard (tip) fins are rolled outboard 40° from the vertical. The concept has two sets of longitudinal control surfaces: (1) elevons on the aft portion of the outboard fins and (2) four body flaps on the aft fuselage. Lateral control can be maintained by deflection of the center fin or differential deflection of the elevons or body flaps.

A wind-tunnel investigation has been initiated at Langley to define the aerodynamic characteristics of the lifting body over a Mach number range from 0.05 to 20.3. The complete aerodynamic data base for the proposed lifting-body PLS configuration is still being defined. The study is now entering the "CFD code calibration" phase whereby high-fidelity models are being designed and fabricated to obtain highly accurate measurements of forces, moments, pressure distributions, and heat transfer distributions.

The use of high-fidelity models is necessary to determine the influence of Mach number, Reynolds number, ratio of specific heats, density ratio across the bow shock, and wall temperature on the lifting-body configuration throughout its flight regime. At hypersonic flight conditions, a blunt-nosed shape such as the proposed PLS will generally experience mostly supersonic flow over the windward surface at low angles of attack; thus, the configuration would exhibit "slender body" behavior (strong dependence on Mach number, Reynolds number, ratio of specific heats, and wall temperature). At high angles of attack (at hypersonic conditions), however, the configuration would experience mostly subsonic flow over the windward surface, thereby invoking the Mach number independence principle and lessening the effects of Reynolds number and wall temperature, but having a possibly strong dependence on shock density

ratio. At this time, three different scale models of moderate fidelity have been tested: (1) a 0.02-scale model in the Langley Hypersonic Helium Tunnel Facility, (2) a 0.07-scale model in the Unitary Plan Wind Tunnel and Calspan 8-Foot Transonic Tunnel, and (3) a 0.20-scale model in the Langley 30 x 60 Ft Tunnel. The tests encompassed a wide range of angles of attack and sideslip. Control effectiveness was studied for all Mach numbers except 20.3. The system of axes used for the determination of forces, moments, velocities, and angles is shown in figure 1. Data are presented in the form of plots and data files on an enclosed floppy disk. Instructions for reading the disk and accessing the data are given in the appendix.

SYMBOLS

b	body span, ft
C_D	drag coefficient, drag/ qS_{ref}
C_L	lift coefficient, lift/ qS_{ref}
C_l	rolling-moment coefficient, rolling moment/ $qS_{ref}b$
$C_{l\beta}$	$\Delta C_l / \Delta \beta$, per deg
$C_{l\delta_a}$	$\Delta C_l / \Delta \delta_a$, per deg
$C_{l\delta_r}$	$\Delta C_l / \Delta \delta_r$, per deg
C_m	pitching-moment coefficient, pitching moment/ $qS_{ref}l$
C_n	yawing-moment coefficient, yawing moment/ $qS_{ref}b$
$C_{n\beta}$	$\Delta C_n / \Delta \beta$, per deg
$C_{n\delta_a}$	$\Delta C_n / \Delta \delta_a$, per deg
$C_{n\delta_r}$	$\Delta C_n / \Delta \delta_r$, per deg
C_p	pressure coefficient, $(p_{local} - p_{free\ stream})/q$
C_y	side-force coefficient, side force/ qS_{ref}
$C_{y\beta}$	$\Delta C_y / \Delta \beta$, per deg
$C_{y\delta_a}$	$\Delta C_y / \Delta \delta_a$, per deg
$C_{y\delta_r}$	$\Delta C_y / \Delta \delta_r$, per deg

L/D	lift/drag ratio
ℓ	length of root chord (body length), ft
M	Mach number
p	pressure, lb/ft ²
q	free-stream dynamic pressure, lb/ft ²
S _{ref}	basic body planform area (excluding tip fins), ft ²
X	longitudinal model body axis
Y	lateral model body axis
Z	vertical model body axis
α	angle of attack, deg
β	angle of sideslip, deg
δ_a	differential control deflection angle $\frac{\delta_{e,L} - \delta_{e,R}}{2}$ or $\frac{\delta_{BF,L} - \delta_{BF,R}}{2}$, deg
δ_{BF}	body flap deflection angle (positive when deflected downward), deg
δ_e	elevon deflection angle (positive when deflected downward), deg
δ_r	rudder deflection angle (positive when deflected with the trailing edge to the left), deg

Subscripts

L	left
max	maximum value
R	right
trim	trimmed condition (zero moment)

DESCRIPTION OF MODELS

The three test models were scaled from the design flight-scale PLS vehicle shown in figure 2. The models were of moderate fidelity and were

constructed to obtain preliminary force and moment characteristics of the lifting-body configuration. A photograph of each of the models is shown in figure 3. The proposed PLS vehicle consists of a low-aspect-ratio body with a flat undersurface and a blunt base. Three fins are mounted on the upper aft portion of the model. The baseline center fin is relatively small, and the large outboard (tip) fins are rolled outward 40° from the vertical. A larger center fin was tested at low speeds on the 0.20-scale model. A comparison between the baseline center fin and the large center fin is shown in figure 2(c). All fins are characterized by a thick flat plate cross section with a cylindrical leading edge and a blunt trailing edge. The location of the control surfaces on the configuration is shown in figures 1-3, and the geometric characteristics of the baseline flight-scale PLS vehicle are shown in table 1. Additionally, a list of body coordinates is enclosed on a floppy disk, and information on accessing the coordinates is given in the appendix.

DESCRIPTION OF TESTS

The low-speed tests were conducted in the Langley 30 x 60-Foot Wind Tunnel (ref. 4) at a Mach number of approximately 0.05. The tunnel is a closed-circuit, double-return, continuous flow design with an open throat.

The transonic tests were conducted in the Calspan 8-Foot Transonic Wind Tunnel (ref. 4) at Mach numbers of 0.6, 0.8, 0.9, 0.95, 1.1, and 1.2. The tunnel is a closed-circuit, single-return, variable-density facility. The Reynolds number for the transonic tests was held constant at 3.5×10^6 per foot.

The supersonic tests were conducted in the Langley Unitary Plan Wind Tunnel (ref. 4) at Mach numbers of 1.6, 2.0, 2.5, 3.0, 3.5, 4.0, and 4.5. The tunnel is a supersonic, closed-circuit design with two test legs. The Reynolds number for the supersonic tests was held constant at 2×10^6 per foot.

The hypersonic tests were conducted in the Langley Hypersonic Helium Tunnel Facility (HHTF, ref. 4) at a Mach number of 20.3. The tunnel is an intermittent, blowdown design which utilizes purified helium. The Reynolds number for the hypersonic tests was held constant at 6.8×10^6 per foot.

Further details on all of the test facilities can be found in reference 4. All drag data presented are uncorrected for base pressure. Where applicable, customary corrections for sting deflection, balance deflection, and tunnel interference were applied to the data. A wind-tunnel test schedule detailing model configuration and test conditions is given in table 2.

RESULTS AND DISCUSSION

Low-Speed Aerodynamics - The low-speed aerodynamic characteristics of the proposed PLS vehicle are shown in figures 4-10. The basic configuration is longitudinally stable with nearly linear lift and pitching-moment coefficients up to an angle of attack of 23° (fig. 4(a)). The configuration is also seen to be directionally and laterally stable up to an angle of attack in excess of 25° (fig. 4(b)). As shown in figure 5, the body flaps provide trim for the vehicle over a wide angle-of-attack range. Effects of rudder, center fin size, and all-movable center fin are also presented.

Transonic Aerodynamics - The transonic aerodynamic characteristics of the proposed PLS vehicle are shown in figures 11-19. The complete model was found to be longitudinally and laterally stable throughout the transonic speed range. Elevon, body flap, and center fin effectiveness data are presented. The model trimmed near the maximum lift-to-drag value (3.1) at a Mach number of 0.6 and at low angles of attack (between 2° and 3°) through the transonic speed range.

Supersonic Aerodynamics - The supersonic aerodynamic characteristics of the proposed PLS vehicle are shown in figures 20-27. The PLS model was longitudinally stable about the design center-of-gravity location. With pitch controls undeflected, the model trimmed at negative angles of attack at Mach

numbers from 1.6 to 3.0. Above Mach 3.0, the basic longitudinal trim angle increased, and the configuration trimmed near maximum L/D. The directional stability level at longitudinal trim conditions decreased with increasing speed and became zero at Mach numbers from 2.5 to 3.0 before regaining stability at higher speeds.

Hypersonic Aerodynamics - The hypersonic aerodynamic characteristics of the proposed PLS vehicle are shown in figures 28 and 29. Experimental data at Mach 20.3 in helium are given along with estimates made using the Aerodynamic Preliminary Analysis System (APAS) (ref. 5). The calculations used Newtonian impact theory to approximate the pressures on the surface of the vehicle. The viscous shear stresses were calculated using the reference temperature and reference enthalpy methods. These techniques are discussed in detail in reference 5.

The maximum hypersonic L/D of the PLS model in helium was found to be 1.43. The vehicle was trimmed at an angle of attack of 26.5° , very near maximum L/D. Theoretical calculations predict a maximum L/D value of 1.41 and a trim angle of attack of 27.8° in helium at Mach 20.3. As another reference, APAS calculations are shown for the PLS vehicle at Mach 10 in air. The maximum predicted L/D in air was 1.36, and the trim angle of attack was identical to the APAS helium calculation. The experimental data showed the proposed PLS vehicle to be directionally stable in the angle-of-attack range for longitudinal trimmed conditions at hypersonic speeds. No control deflections were tested.

Experimental Data Base - All experimental data obtained on the proposed PLS vehicle have been placed on two floppy disks enclosed in the back of this report. The data base can be accessed using the R:BASE (ref. 6) system. Information on accessing the data using R:BASE can be found in the appendix.

CONCLUDING REMARKS

A wind-tunnel investigation has been made to determine the aerodynamics of a proposed PLS lifting-body vehicle throughout the speed range from Mach 0.05 to Mach 20.3. The configuration was found to be longitudinally and laterally stable about the design center-of-gravity of 54 percent of the body length. The configuration was controlled in the pitch plane with either elevons on the trailing edge of the rolled-out tip fins or body flaps mounted on the aft fuselage. A small all-movable center fin or rudder provided yaw control. A larger version of the center fin was tested at low subsonic speeds. No control deflection data were available at hypersonic speeds. The hypersonic helium data agreed well with theoretical calculations. Based on these calculations and past hypersonic tests for this class of vehicle, no major differences are expected between the hypersonic helium data and the hypersonic air data when they become available. All of the experimental data have been placed in a structured data base using the R:BASE system and are included on two floppy disks enclosed in the back of this report.

REFERENCES

1. Ware, G. M.: Transonic Aerodynamic Characteristics of a Proposed Assured Crew Return Capability (ACRC) Lifting-Body Configuration. NASA TM 4117, July 1989.
2. Ware, G. M.: Supersonic Aerodynamic Characteristics of a Proposed Assured Crew Return Capability (ACRC) Lifting-Body Configuration. NASA TM 4136, December 1989.
3. Ware, G. M.; Spencer, B.; and Micol, J.: Aerodynamic Characteristics of Proposed Assured Crew Return Capability (ACRC) Configurations. AIAA Paper No. 89-2172, July 1989.
4. Penaranda, Frank E. and Freda, M. Shannon, eds.: Aeronautical Facilities Catalogue. Volume 1 - Wind Tunnels. NASA RP-1132, 1985.

5. Cruz, C. I. and Wilhite, A. W.: Prediction of High-Speed Aerodynamic Characteristics Using the Aerodynamic Preliminary Analysis System (APAS). AIAA Paper No. 89-2173, July 1989.
6. R:BASE Series 4000 User's Manual Tutorial. MICRORIM. 1985.

APPENDIX

Aerodynamic Data. The data presented in plotted form within this report are available on the enclosed magnetic personal computer disk. The floppy disk will allow access to both body axis and stability axis data in ASCII test file format. Identification of the available data is presented in the Wind Tunnel Schedule (table 2).

To be able to use the disk, the following equipment is required:

- (1) An IBM Personal Computer (or equivalent) with a minimum of 640K or RAM.
- (2) A 5-1/4 inch 1.2M disk drive.
- (3) A hard disk drive.

The files included on the disk are:

- (1) READ_NOW.BAT - test file providing information not included herein.
- (2) LB0001F1.RBF - MICRORIM R:Base data base files. These binary
LB0001F2.RBF files require R:Base software to access. Data
LB0001F3.RBF base name is LB0001F.
- (3) LB0001.EXE - Compiled application files which will allow the
LB0001.OVL R:Base data base files to be manipulated as
LB0001.MSG outlined in the following paragraph.
- (4) INSTALLH.BAT - Installation program.

The LB0001 application program will allow:

- (1) Creating ASCII text files of the data in either stability or body axis system format for use in a variety of mainframe and PC software.
- (2) Printing the data in tabular form.
- (3) Printing a detailed run log for all the tests.

To access the data base, insert the disk in the 1.2M drive, enter <INSTALLH>, and follow the instructions displayed on the screen.

Test Facility Identification. The following identification codes will facilitate the retrieval of the data on the floppy disk.

	<u>Site</u>	<u>Facility</u>	<u>Test</u>
30 x 60 FST	1	C	9999
CALSPAN	3	D	100
UPWT TS #1	1	I	1636
UPWT TS #2	1	L	1497
HHTF	1	Q	497

Surface Geometry. A file containing the surface coordinates for the surface of the proposed lifting-body PLS vehicle is stored on the enclosed floppy disk. The geometry is based on a subset of the coordinates used by the numerical milling machine used to construct the 0.20-scale and 0.07-scale models. There are a total of 1429 surface grid points tabulated. The fuselage is defined at 21 stations and the number of points per station varies from 1 (at the nose) to 130 (at the base). The name of the geometry file on the disk is PLS.FUS.

Table 1. Geometric Characteristics of Flight-Scale PLS Vehicle

Body alone:	
Aspect ratio	0.6
Length (reference length), ft.	24.6
Span (reference span), ft.	11.6
Planform area (reference area), ft ²	216.8
Baseline area, ft ²	40.0
Height (maximum), ft	5.6
Body with fins:	
Aspect ratio	1.5
Length, ft	24.6
Span, ft	19.5
Planform area, ft ²	254.3
Base area, ft ²	40.0
Height (to tip of fin), ft	7.0
Elevons:	
Chord, ft.	1.3
Span, ft	4.9
Area (each), ft ²	5.0
Body flaps:	
Chord, ft.	1.8
Span, ft	3.3
Area (each), ft ²	6.0

Table 2. Run schedule for data on floppy disk.

TEST PARAMETERS					FST	CALSPAN						UPWT TS #1			UPWT TS #2				He
α , deg	β , deg	δ_e , deg L/R	CNTR FIN	δ_{BF} , deg L/R	MACH 0.05	MACH 0.6	MACH 0.8	MACH 0.9	MACH 0.95	MACH 1.1	MACH 1.2	MACH 1.6	MACH 2.0	MACH 2.5	MACH 3.0	MACH 3.5	MACH 4.0	MACH 4.5	MACH 20
A	0	0	0	0	5	54	40	39	20	64	166	48	41	28	1	9	17	25	4
A	-2	0	0	0	4	55	42	38	21	66	167	47	40	30	3	11	19	27	X
A	2	0	0	0	6	53	41	34	23	65	168	X	X	X	4	12	20	28	X
0	B	0	0	0	X	48	43	33	24	67	169	42	35	33	X	X	X	X	X
5	B	0	0	0	X	49	44	32	25	68	170	43	36	32	5	13	X	X	X
10	B	0	0	0	X	50	45	31	26	69	171	44	37	34	6	14	21	29	X
15	B	0	0	0	X	51	46	30	27	70	172	45	38	31	7	15	22	30	X
20	B	0	0	0	33	52	47	29	28	71	173	X	X	X	8	16	23	31	X
25	B	0	0	0	X	X	X	X	X	X	X	X	X	X	X	X	24	32	X
A	0	5	0	0	X	198	197	196	195	194	193	X	X	X	X	X	X	X	X
A	0	10	0	0	X	X	X	X	X	X	X	X	X	X	X	X	X	X	X
A	0	-5	0	0	X	210	209	208	207	206	205	49	50	51	X	X	X	X	X
A	0	-10	0	0	X	216	215	214	213	212	211	53	54	52	33	34	35	36	X
A	0	0	0	-10	13	180	179	178	177	176	175	58	59	60	41	43	44	45	X
A	0	0	0	10	15	192	191	190	189	188	187	X	X	X	X	X	X	X	X

NUMBERS UNDER MACH HEADING ARE RUNS IN DESIGNATED FACILITY

A = ANGLE-OF-ATTACK SWEEP

B = ANGLE-OF-SIDESLIP SWEEP

X = DATA NOT AVAILABLE

Table 2. Continued.

TEST PARAMETERS					FST	CALSPAN						UPWT TS #1			UPWT TS #2			
α , deg	β , deg	δ_e , deg L/R	CNTR FIN	δ_{BF} , deg L/R	MACH 0.05	MACH 0.6	MACH 0.8	MACH 0.9	MACH 0.95	MACH 1.1	MACH 1.2	MACH 1.6	MACH 2.0	MACH 2.5	MACH 3.0	MACH 3.5	MACH 4.0	MACH 4.5
A	0	0	OFF	0	43	101	97	83	75	132	111	70	74	67	83	86	89	92
A	-2	0	OFF	0	X	102	99	85	77	133	112	72	73	69	84	87	90	93
A	2	0	OFF	0	X	100	96	86	76	131	110	71	75	68	85	88	91	94
0	B	0	OFF	0	X	103	95	87	78	126	118	X	X	X	X	X	X	X
5	B	0	OFF	0	X	104	94	88	79	127	123	X	X	X	X	X	X	X
10	B	0	OFF	0	X	105	93	89	80	128	122	X	X	X	X	X	X	X
15	B	0	OFF	0	X	106	92	90	81	129	124	X	X	X	X	X	X	X
20	B	0	OFF	0	X	108	155	148	82	130	125	X	X	X	X	98	101	104
A	0	OFF	OFF	0	53	159	155	148	145	139	154	76	79	82	95	98	101	104
A	-2	OFF	OFF	0	X	158	157	149	146	140	152	78	81	84	96	99	102	105
A	0	5	OFF	0	X	160	156	147	144	138	153	77	80	83	97	100	103	106
A	0	0	5	0	X	223	222	220	219	218	217	64	65	66	X	X	X	X
A	0	0	0	-10/10	X	186	185	184	183	182	181	X	X	X	X	X	X	X
A	0	-5/5	0	0	X	204	203	202	201	200	199	X	X	X	X	X	X	X
A	0	-10/10	0	0	X	X	X	X	X	X	X	55	56	57	37	38	39	40
A	0	-10/10	5	0	X	X	X	X	X	X	X	X	X	X	50	51	52	53

NUMBERS UNDER MACH HEADING ARE RUNS IN DESIGNATED FACILITY

A = ANGLE-OF-ATTACK SWEEP

B = ANGLE-OF-SIDESLIP SWEEP

X = DATA NOT AVAILABLE

Table 2. Continued.

TEST PARAMETERS					FST	CALSPAN							UPWT TS #1			UPWT TS #2				He
α , deg	β , deg	δ_{θ} , deg L/R	CNTR FIN	δ_{BF} , deg L/R	MACH 0.05	MACH 0.6	MACH 0.8	MACH 0.9	MACH 0.95	MACH 1.1	MACH 1.2	MACH 1.6	MACH 2.0	MACH 2.5	MACH 3.0	MACH 3.5	MACH 4.0	MACH 4.5	MACH 20	
A	-3	0	0	0	X	X	X	X	X	X	X	X	X	X	X	X	X	X	12	
A	-10	0	0	0	2	X	X	X	X	X	X	X	X	X	X	X	X	X	X	
A	-5	0	0	0	3	X	X	X	X	X	X	X	X	X	X	X	X	X	X	
A	5	0	0	0	7	X	X	X	X	X	X	X	X	X	X	X	X	X	X	
A	10	0	0	0	8	X	X	X	X	X	X	X	X	X	X	X	X	X	X	
12	B	0	0	0	9	X	X	X	X	X	X	X	X	X	X	X	X	X	X	
14	B	0	0	0	10	X	X	X	X	X	X	X	X	X	X	X	X	X	X	
16	B	0	0	0	11	X	X	X	X	X	X	X	X	X	X	X	X	X	X	
A	0	0	0	-5	12	X	X	X	X	X	X	X	X	X	X	X	X	X	X	
A	0	0	0	5	14	X	X	X	X	X	X	X	X	X	X	X	X	X	X	
A	0	15/-15	0	0	16	X	X	X	X	X	X	X	X	X	X	X	X	X	X	
A	0	30/-30	0	0	17	X	X	X	X	X	X	X	X	X	X	X	X	X	X	
A	0	-15/15	0	0	18	X	X	X	X	X	X	X	X	X	X	X	X	X	X	
A	0	-30/30	0	0	19	X	X	X	X	X	X	X	X	X	X	X	X	X	X	
A	0	0	0	-30/30	21	X	X	X	X	X	X	X	X	X	X	X	X	X	X	

NUMBERS UNDER MACH HEADING ARE RUNS IN DESIGNATED FACILITY

A = ANGLE-OF-ATTACK SWEEP

B = ANGLE-OF-SIDESLIP SWEEP

X = DATA NOT AVAILABLE

Table 2. Continued.

TEST PARAMETERS					FST	CALSPAN						UPWT TS #1			UPWT TS #2				He
α , deg	β , deg	δ_{θ} , deg L/R	CNTR FIN	δ_{BF} , deg L/R	MACH 0.05	MACH 0.6	MACH 0.8	MACH 0.9	MACH 0.95	MACH 1.1	MACH 1.2	MACH 1.6	MACH 2.0	MACH 2.5	MACH 3.0	MACH 3.5	MACH 4.0	MACH 4.5	MACH 20
A	-10	0	0	-30/30	22	X	X	X	X	X	X	X	X	X	X	X	X	X	X
A	-5	0	0	-30/30	23	X	X	X	X	X	X	X	X	X	X	X	X	X	X
A	0	0	0	-30/30	24	X	X	X	X	X	X	X	X	X	X	X	X	X	X
A	5	0	0	-30/30	25	X	X	X	X	X	X	X	X	X	X	X	X	X	X
A	10	0	0	-30/30	26	X	X	X	X	X	X	X	X	X	X	X	X	X	X
A	0	0	0	0/30	27	X	X	X	X	X	X	X	X	X	X	X	X	X	X
A	0	0	15 ²	0	28	X	X	X	X	X	X	X	X	X	X	X	X	X	X
A	0	0	30 ²	0	29	X	X	X	X	X	X	X	X	X	X	X	X	X	X
A	0	0	30	0	30	X	X	X	X	X	X	X	X	X	X	X	X	X	X
A	0	0	15	0	31	X	X	X	X	X	X	X	X	X	X	X	X	X	X
18	B	0	0	0	32	X	X	X	X	X	X	X	X	X	X	X	X	X	X
A	0	0	0	30	34	X	X	X	X	X	X	X	X	X	X	X	X	X	X
A	0	0	OFF	-30	35	X	X	X	X	X	X	X	X	X	X	X	X	X	X
A	-5	0	OFF	0	42	X	X	X	X	X	X	X	X	X	X	X	X	X	X
A	5	0	0	0	44	X	X	X	X	X	X	X	X	X	X	X	X	X	X

NUMBERS UNDER MACH HEADING ARE RUNS IN DESIGNATED FACILITY

A = ANGLE-OF-ATTACK SWEEP

B = ANGLE-OF-SIDSLIP SWEEP

X = DATA NOT AVAILABLE

SUPERSCRIPTS

1 = LARGE CENTER FIN

2 = ALL-MOVABLE FIN

Table 2. Concluded.

TEST PARAMETERS					FST	CALSPAN							UPWT TS #1			UPWT TS #2				He
α , deg	β , deg	δ_e , deg L/R	CNTR FIN	δ_{BF} , deg L/R	MACH 0.05	MACH 0.6	MACH 0.8	MACH 0.9	MACH 0.95	MACH 1.1	MACH 1.2	MACH 1.6	MACH 2.0	MACH 2.5	MACH 3.0	MACH 3.5	MACH 4.0	MACH 4.5	MACH 20	
A	-5	0	0 ¹	0	45	X	X	X	X	X	X	X	X	X	X	X	X	X	X	
A	0	0	0 ¹	0	46	X	X	X	X	X	X	X	X	X	X	X	X	X	X	
A	5	0	0 ¹	0	47	X	X	X	X	X	X	X	X	X	X	X	X	X	X	
A	0	0	30 ¹	0	48	X	X	X	X	X	X	X	X	X	X	X	X	X	X	
A	0	0	15 ¹	0	49	X	X	X	X	X	X	X	X	X	X	X	X	X	X	
A	0	0	15 ^{1,2}	0	50	X	X	X	X	X	X	X	X	X	X	X	X	X	X	
A	0	0	30 ^{1,2}	0	51	X	X	X	X	X	X	X	X	X	X	X	X	X	X	
A	-5	OFF	OFF	0	52	X	X	X	X	X	X	X	X	X	X	X	X	X	X	
A	5	OFF	OFF	0	54	X	X	X	X	X	X	X	X	X	X	X	X	X	X	
A	-10	30/-30	0 ¹	0	58	X	X	X	X	X	X	X	X	X	X	X	X	X	X	
A	-5	30/-30	0 ¹	0	59	X	X	X	X	X	X	X	X	X	X	X	X	X	X	
A	5	30/-30	0 ¹	0	60	X	X	X	X	X	X	X	X	X	X	X	X	X	X	
A	10	30/-30	0 ¹	0	61	X	X	X	X	X	X	X	X	X	X	X	X	X	X	
A	-10	0	30	0	62	X	X	X	X	X	X	X	X	X	X	X	X	X	X	

NUMBERS UNDER MACH HEADING ARE RUNS IN DESIGNATED FACILITY

A = ANGLE-OF-ATTACK SWEEP

B = ANGLE-OF-SIDESLIP SWEEP

X = DATA NOT AVAILABLE

SUPERSCRIPITS

1 = LARGE CENTER FIN

2 = ALL-MOVABLE FIN

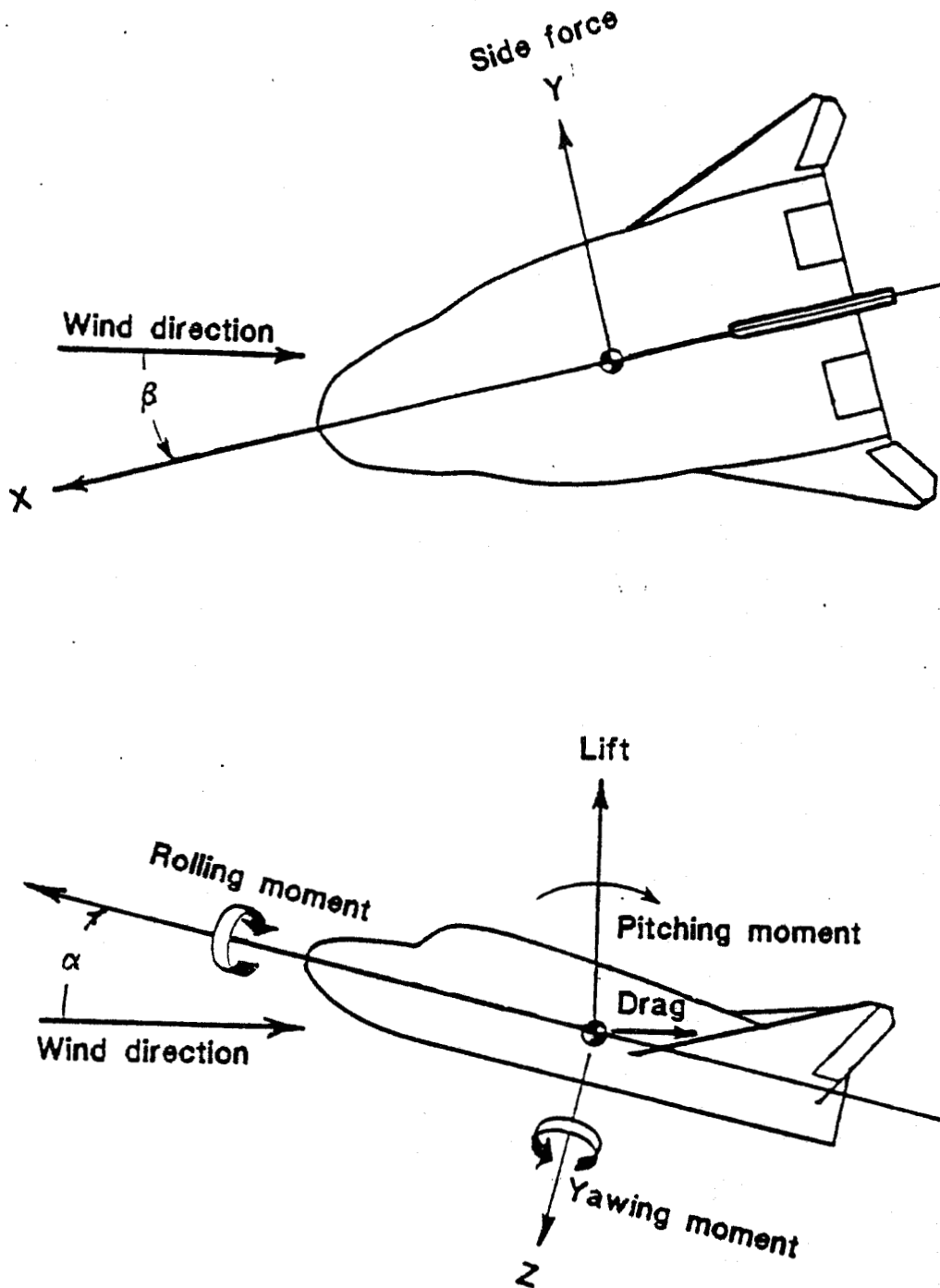
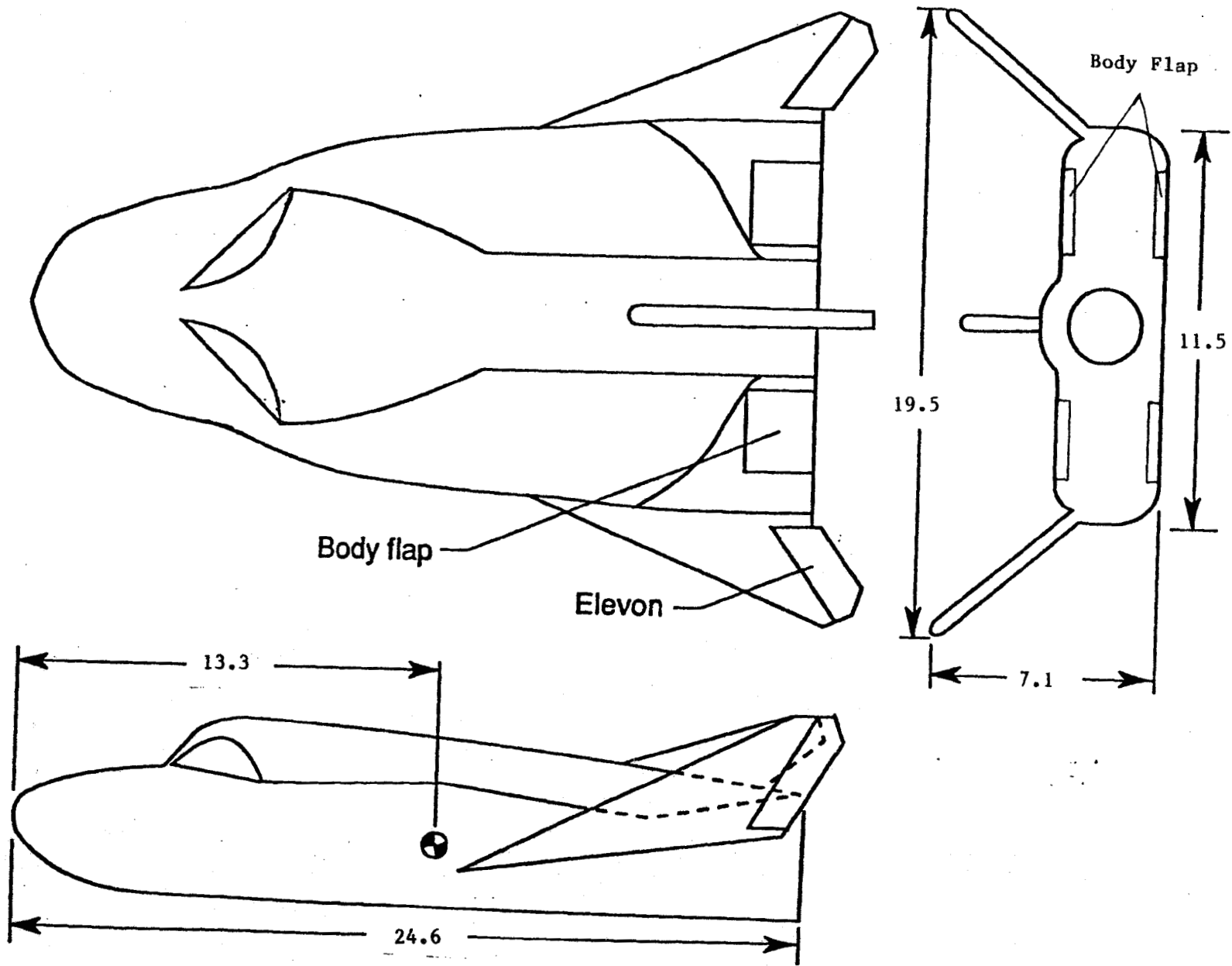
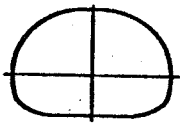


Figure 1. Sketch of system of axes used in the investigation, showing positive direction of forces, moments, velocities, and angles.

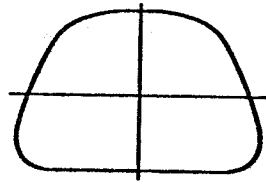


(a) Three-view

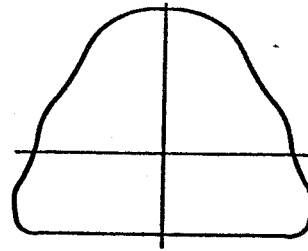
Figure 2. Sketch of flight-scale PLS vehicle. Dimensions are in feet.



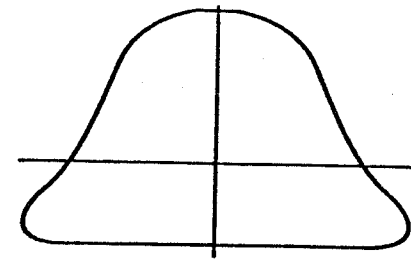
STA 1.19



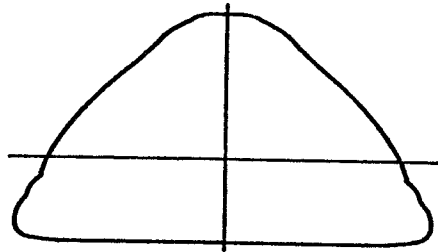
STA 3.57



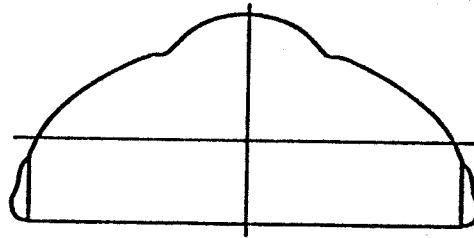
STA 6.07



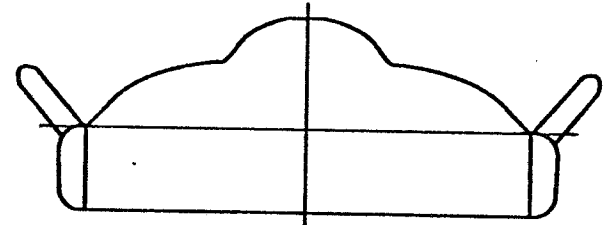
STA 8.45



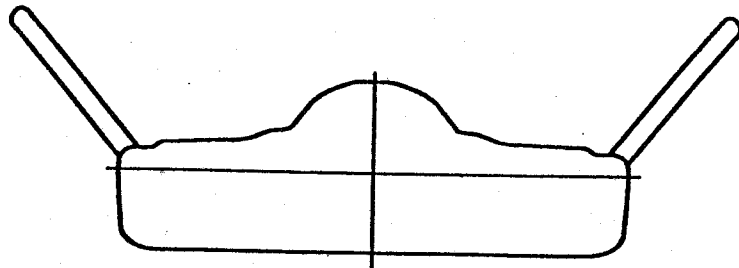
STA 10.95



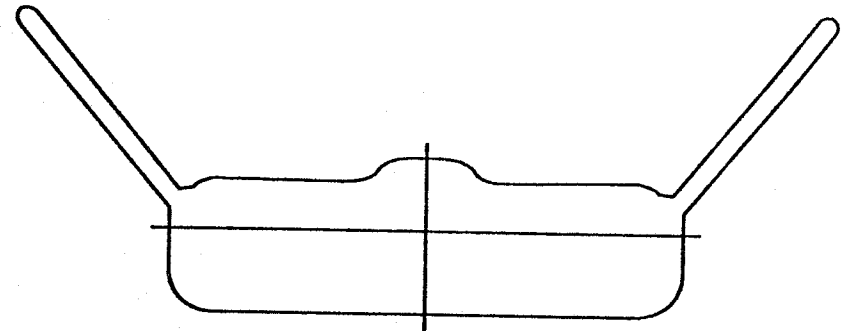
STA 14.76



STA 18.45



STA 22.14

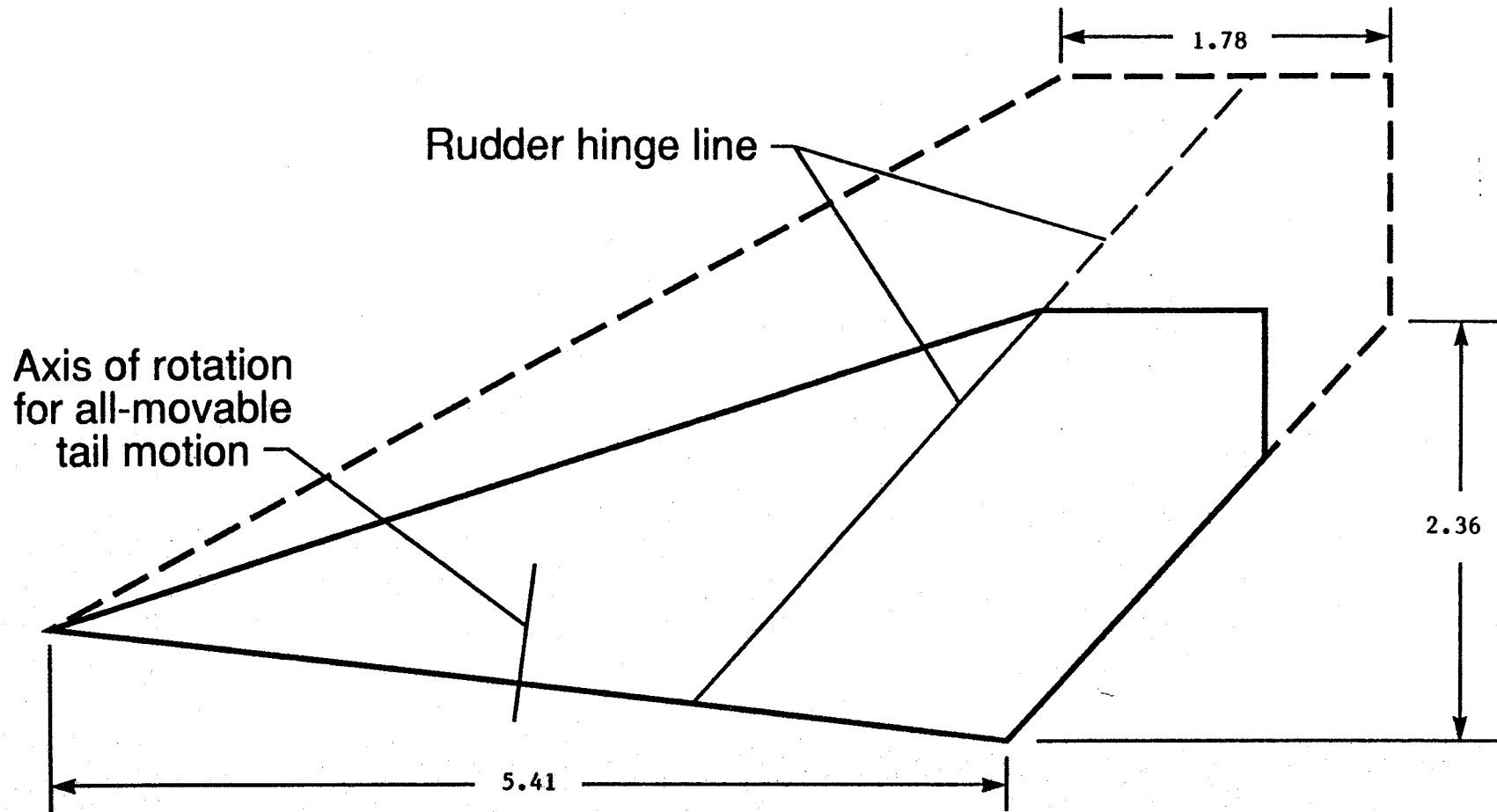


STA 24.56

(b) Vehicle section cuts

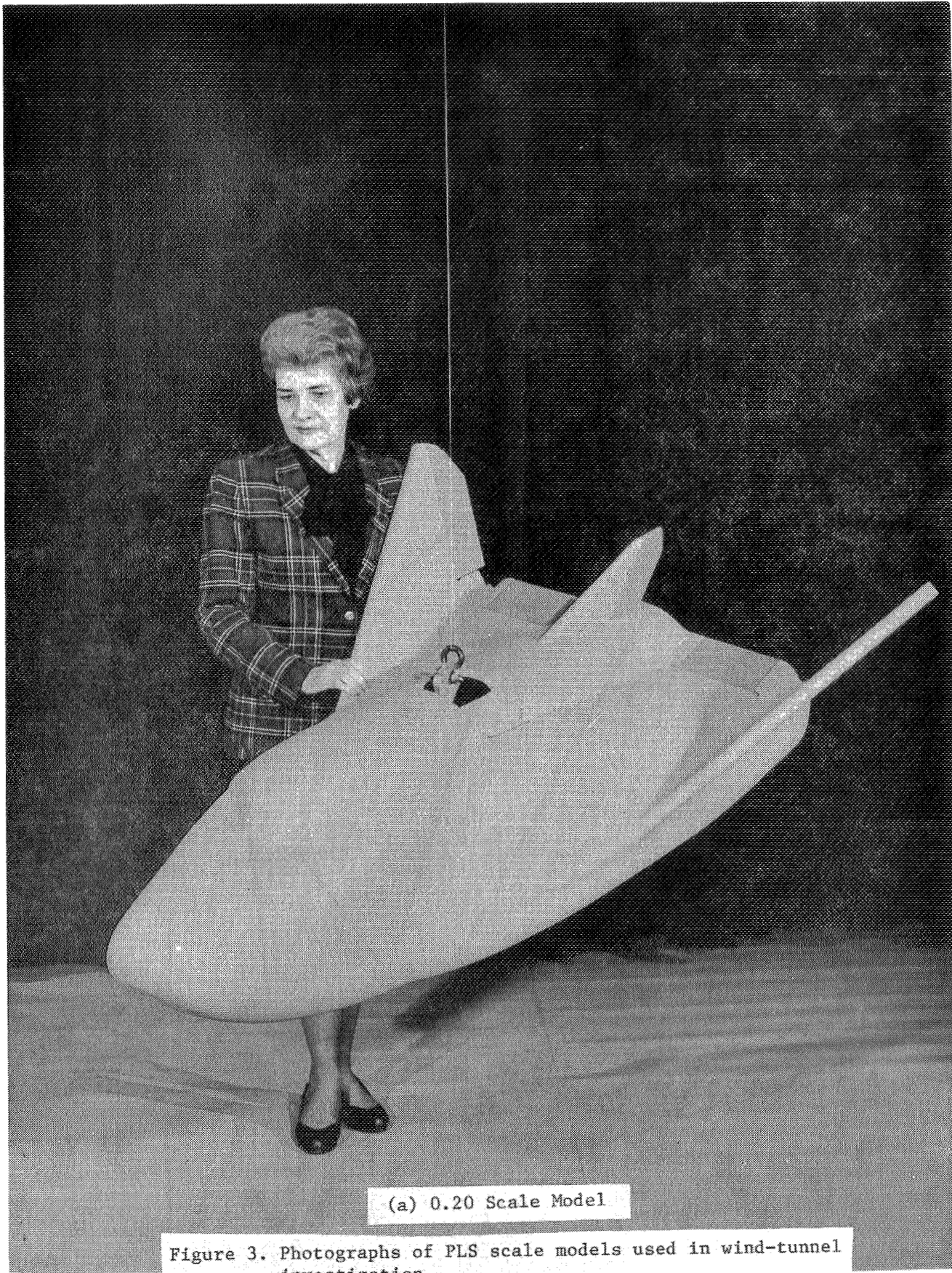
Figure 2. Continued.

- Baseline center fin (total area = 8.70 ft², rudder area = 4.29 ft²)
- - - - Large center fin (total area = 15.00 ft², rudder area = 6.33 ft²)



(c) Center fin geometry

Figure 2. Concluded.



NASA

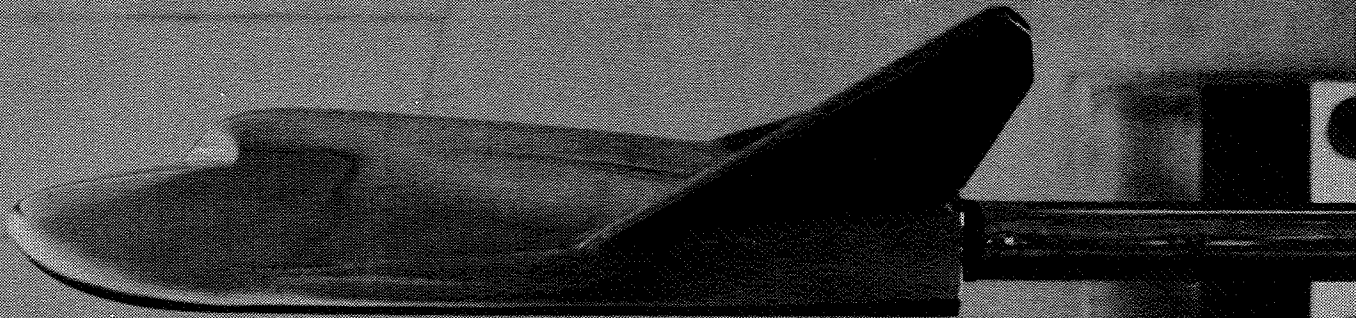
89-03306

Langer Research Center
Hampton, Virginia 22060-0223

(a) 0.20 Scale Model

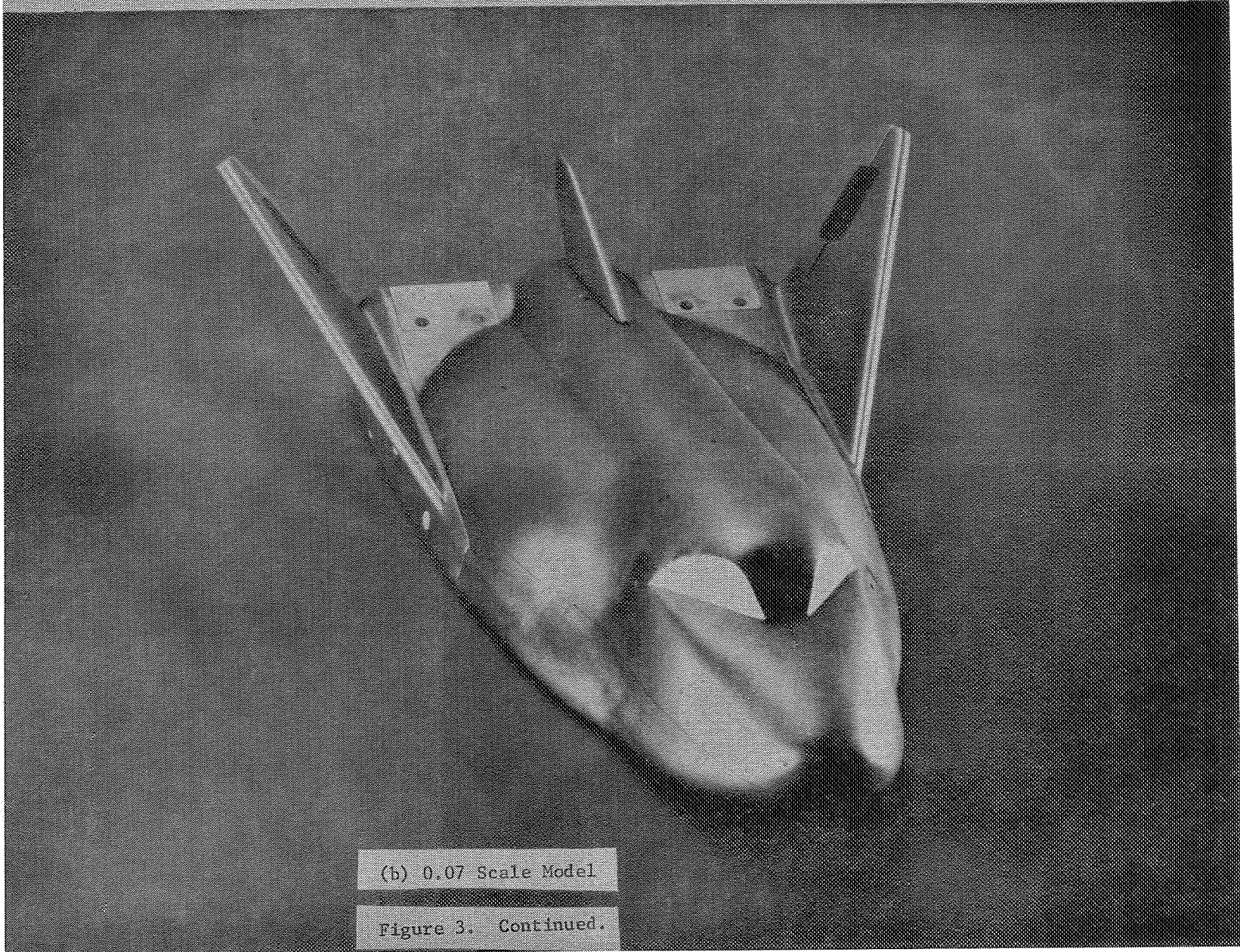
Figure 3. Photographs of PLS scale models used in wind-tunnel investigation.

31-INCH MACH 10 TUNNEL
EXPERIMENTAL AERODYNAMICS BRANCH
SPACE SYSTEMS DIVISION
NASA LANGLEY RESEARCH CENTER



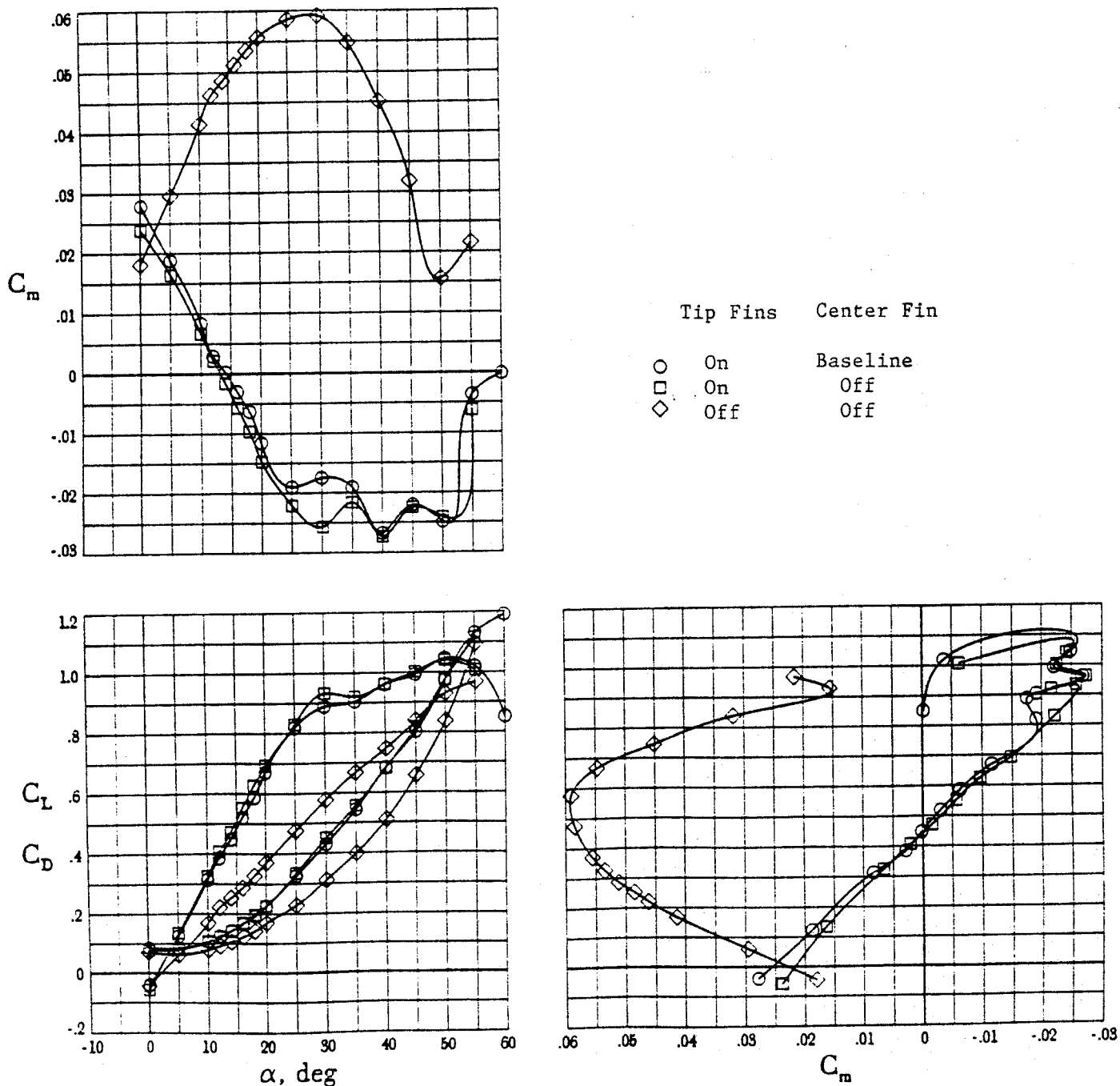
(c) 0.02 Scale Model

Figure 3. Concluded.



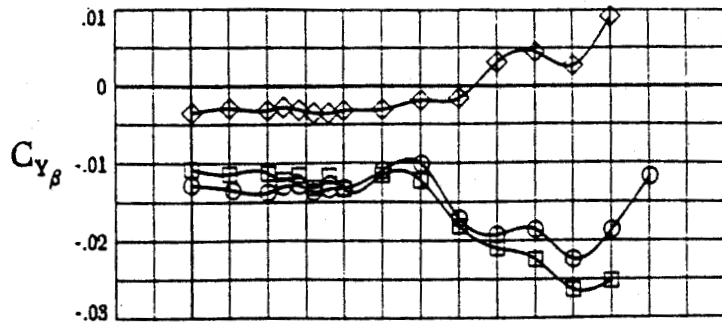
(b) 0.07 Scale Model

Figure 3. Continued.



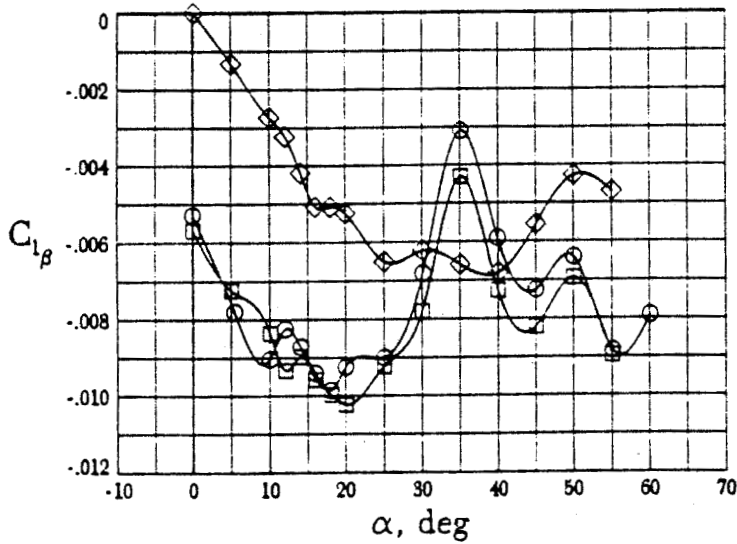
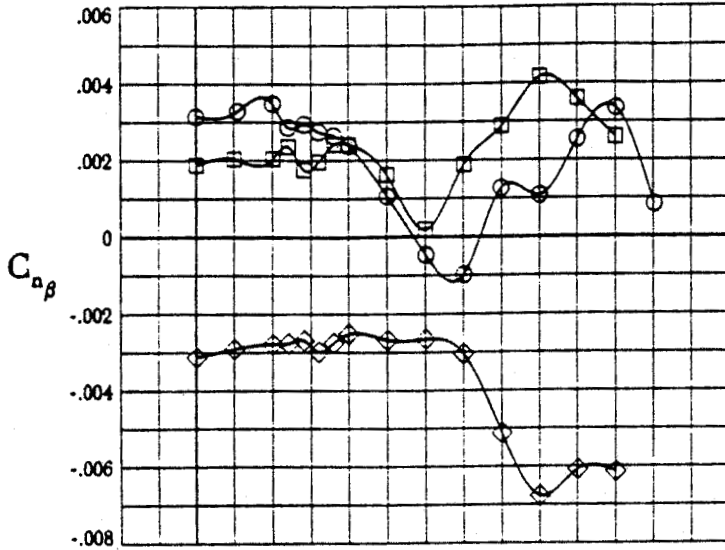
(a) Longitudinal characteristics.

Figure 4. Effect of center fin and tip fins on low-speed aerodynamics.



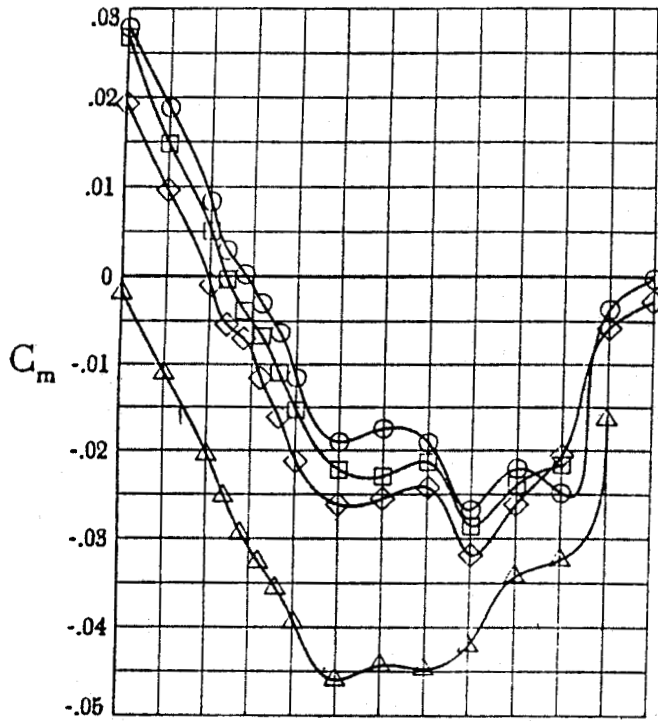
Tip Fins Center Fin

- On Baseline
- On Off
- ◇ Off Off

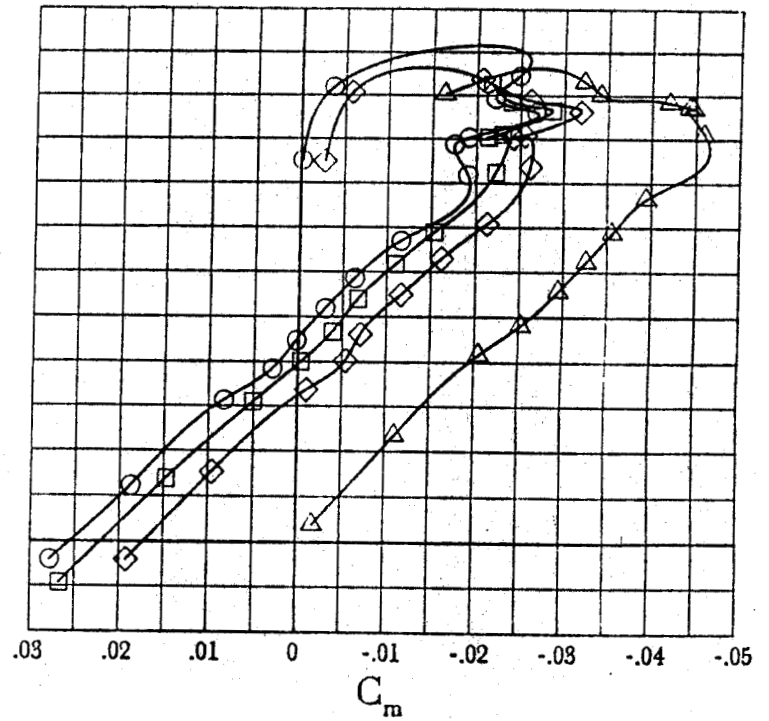
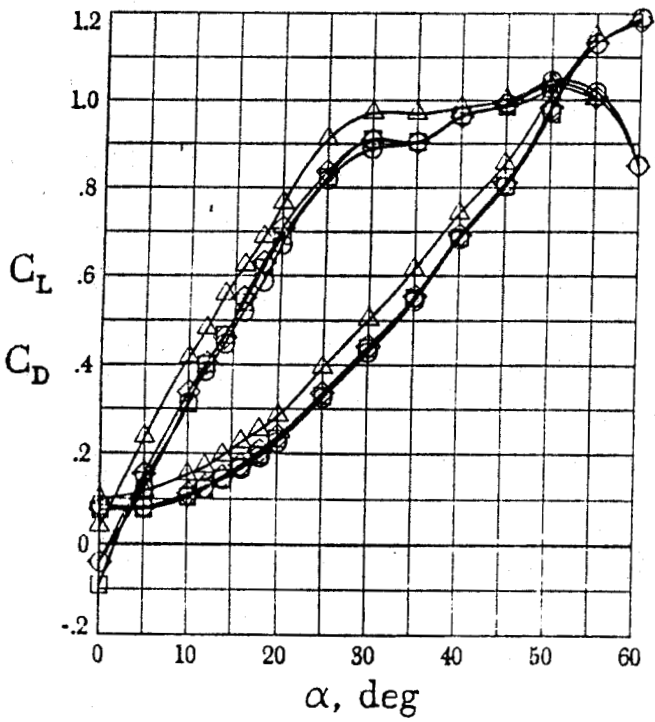


(b) Lateral-directional characteristics.

Figure 4. Concluded.

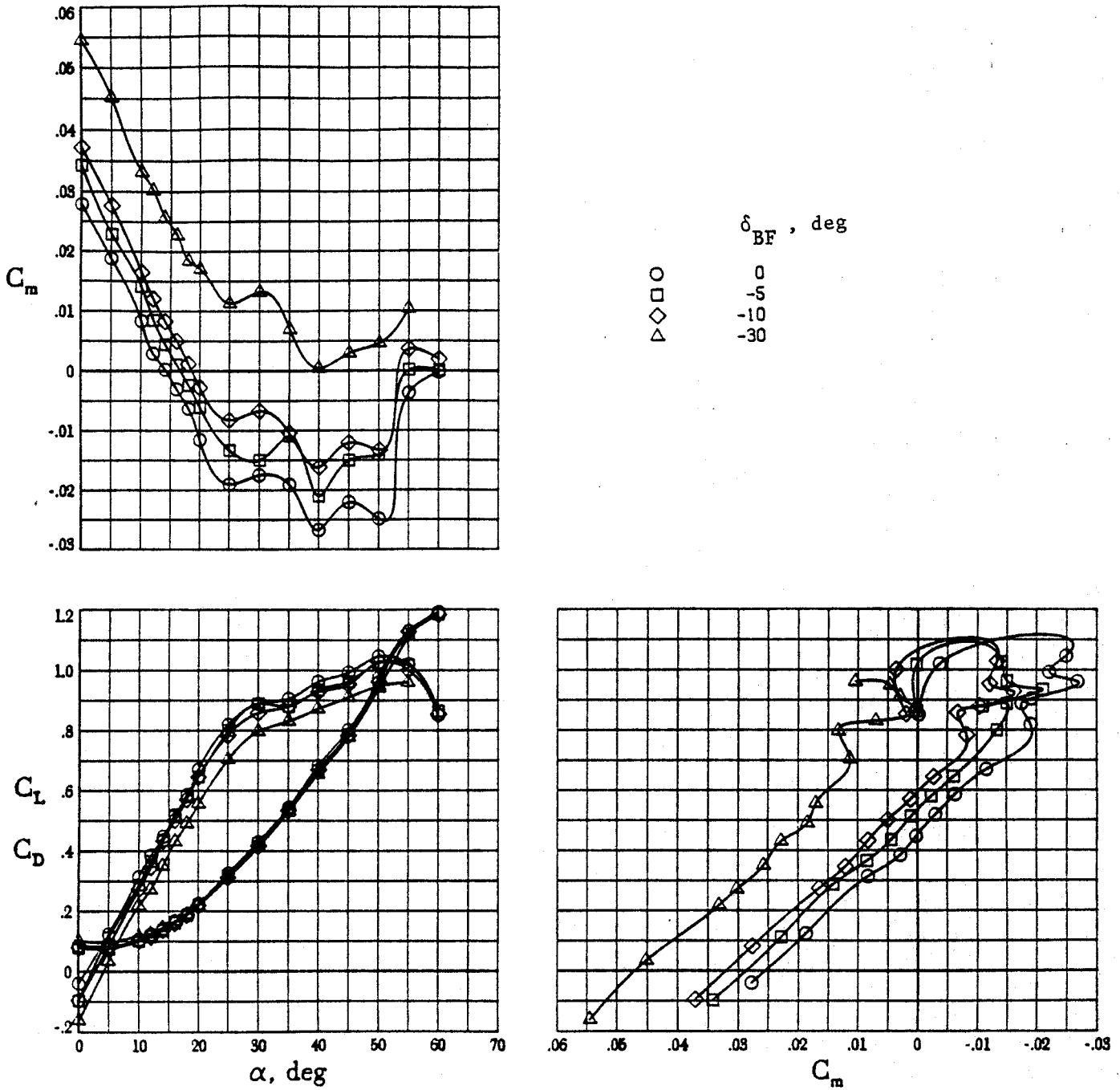


δ_{BF} , deg	Symbol
0	○
5	□
10	◇
30	△



(a) Positive body flap deflections.

Figure 5. Effect of body flaps on low-speed aerodynamics.
Baseline Configuration.



(b) Negative body flap deflections.

Figure 5. Concluded.

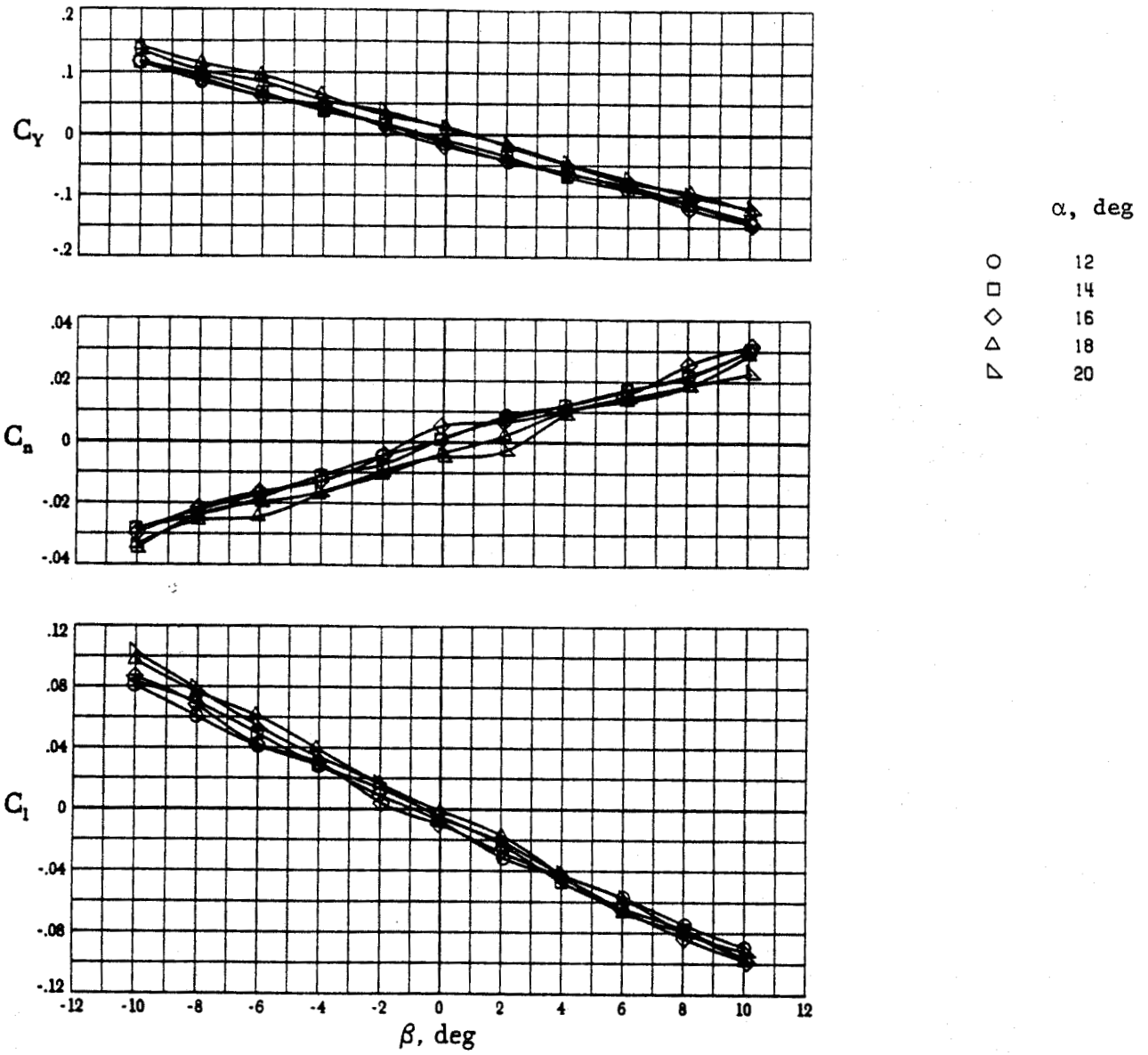


Figure 6. Effect of sideslip on low-speed lateral-directional aerodynamics. Baseline Configuration.

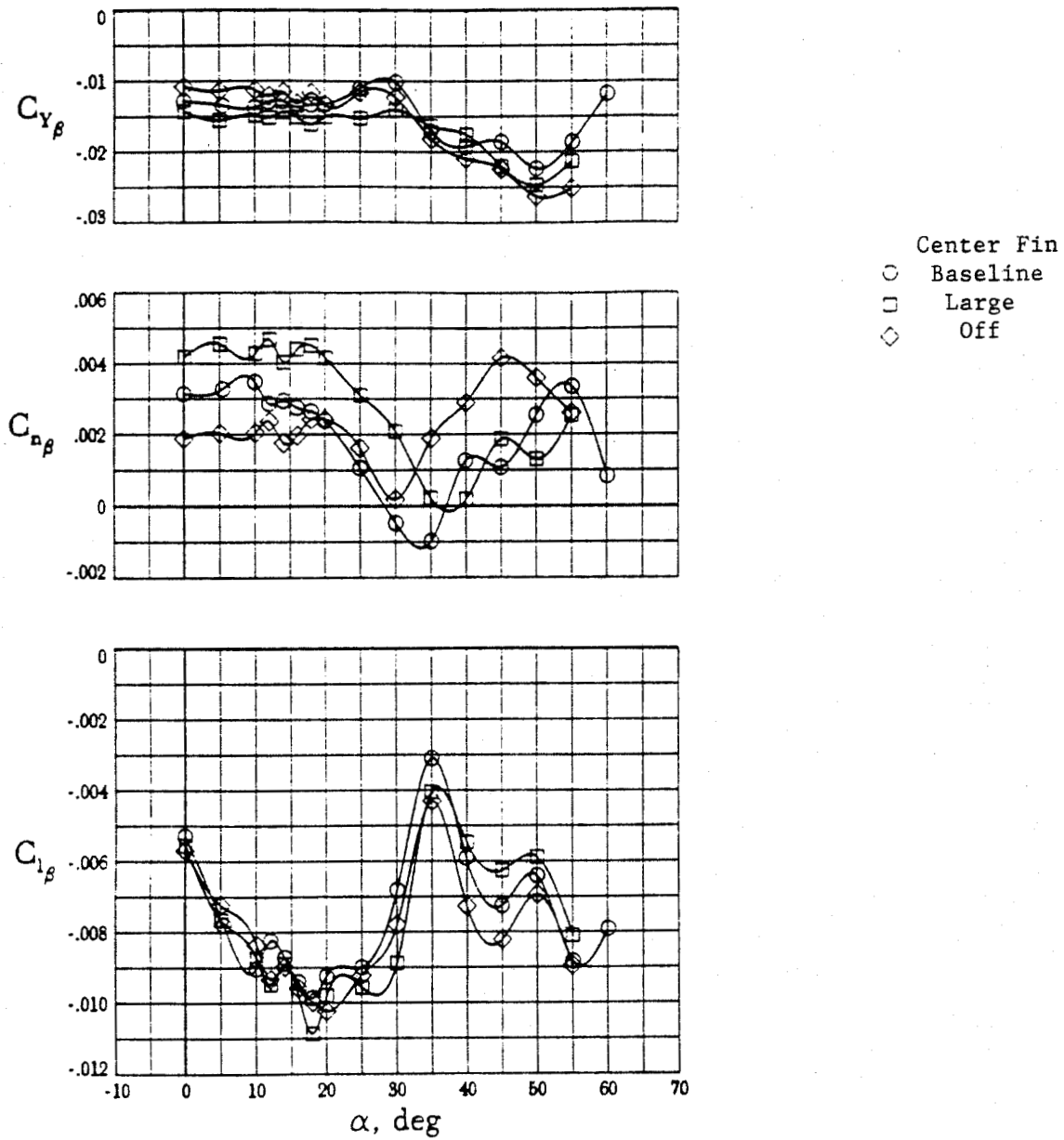


Figure 7. Effect of size of center fin on low-speed lateral-directional aerodynamics.

	$\delta_{BF,L}$	$\delta_{BF,R}$, deg
○	-30	0	
□	-30	30	
◇	0	30	

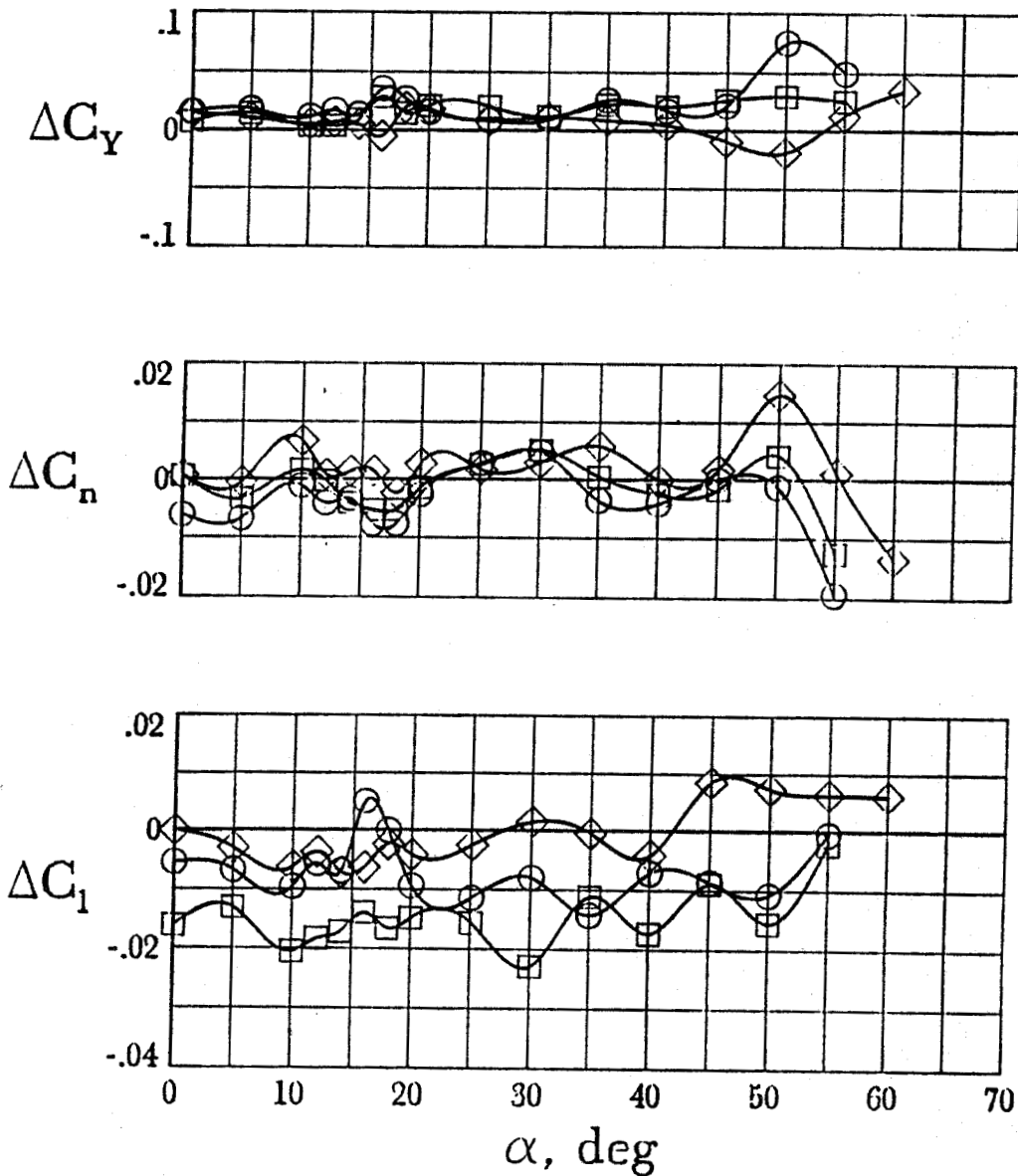


Figure 8. Effect of differentially deflected body flaps on low-speed lateral-directional aerodynamics. Baseline configuration.

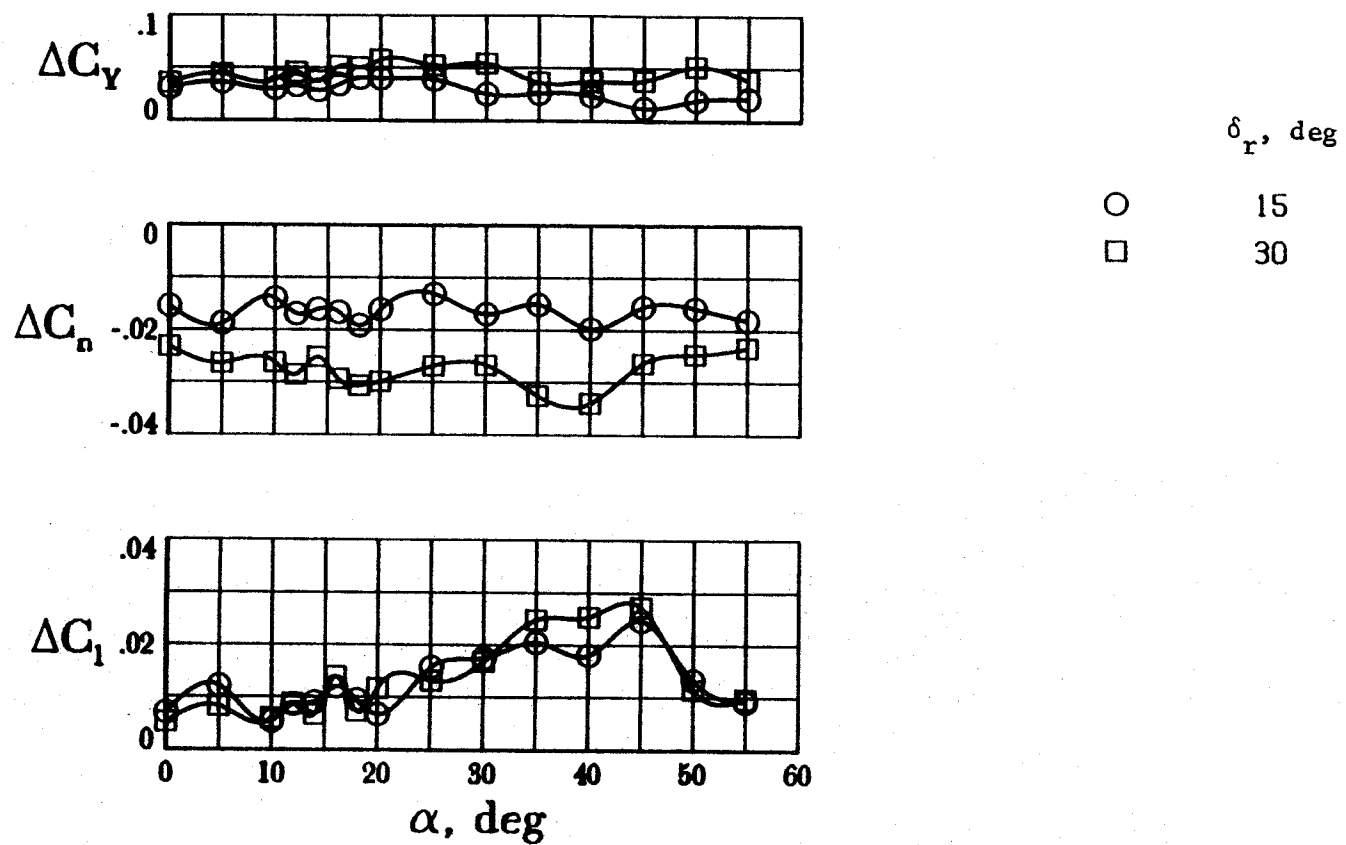


Figure 9. Low-speed baseline rudder control effectiveness.

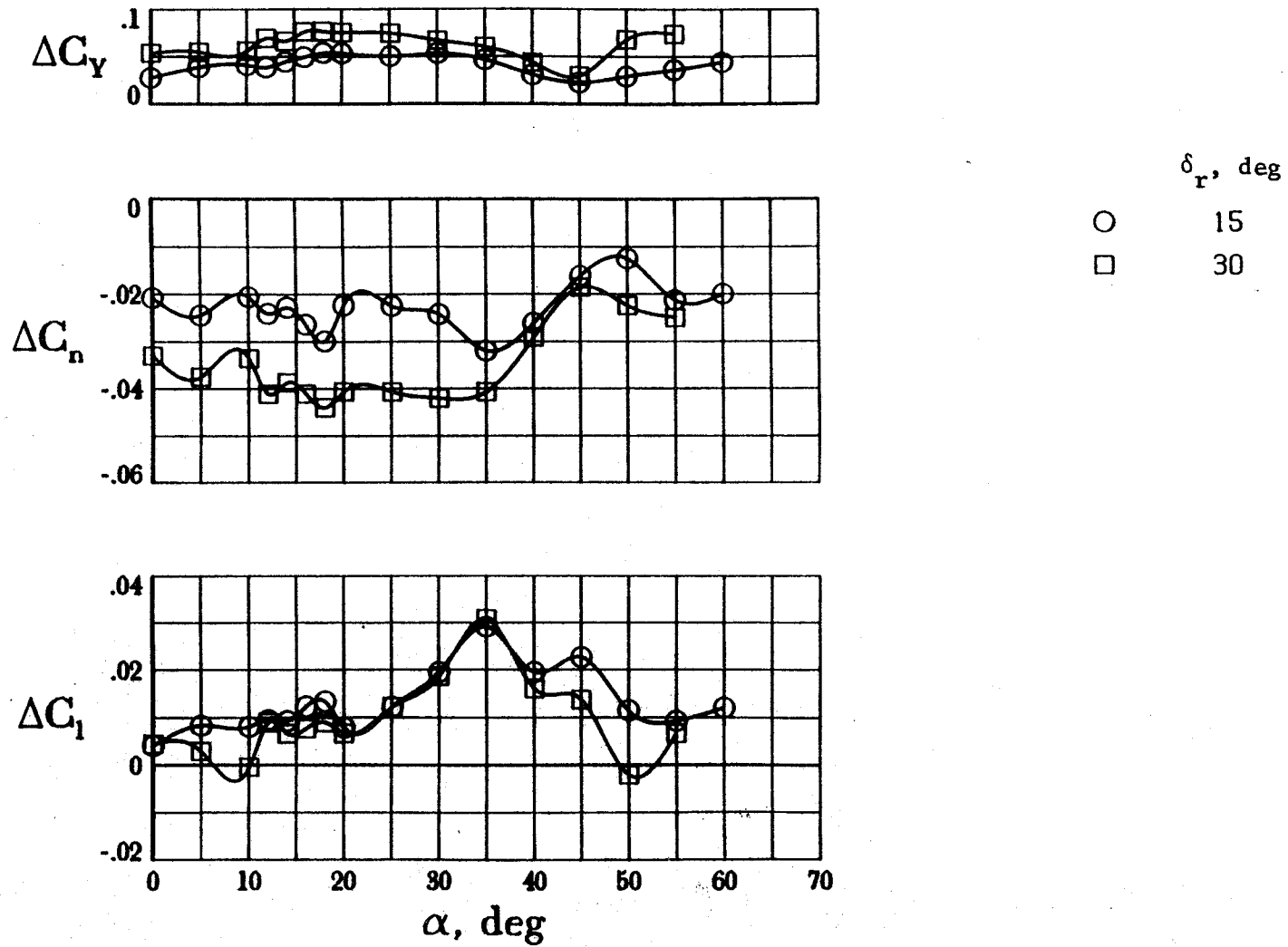


Figure 10. Low-speed control effectiveness with all-movable baseline center fin.

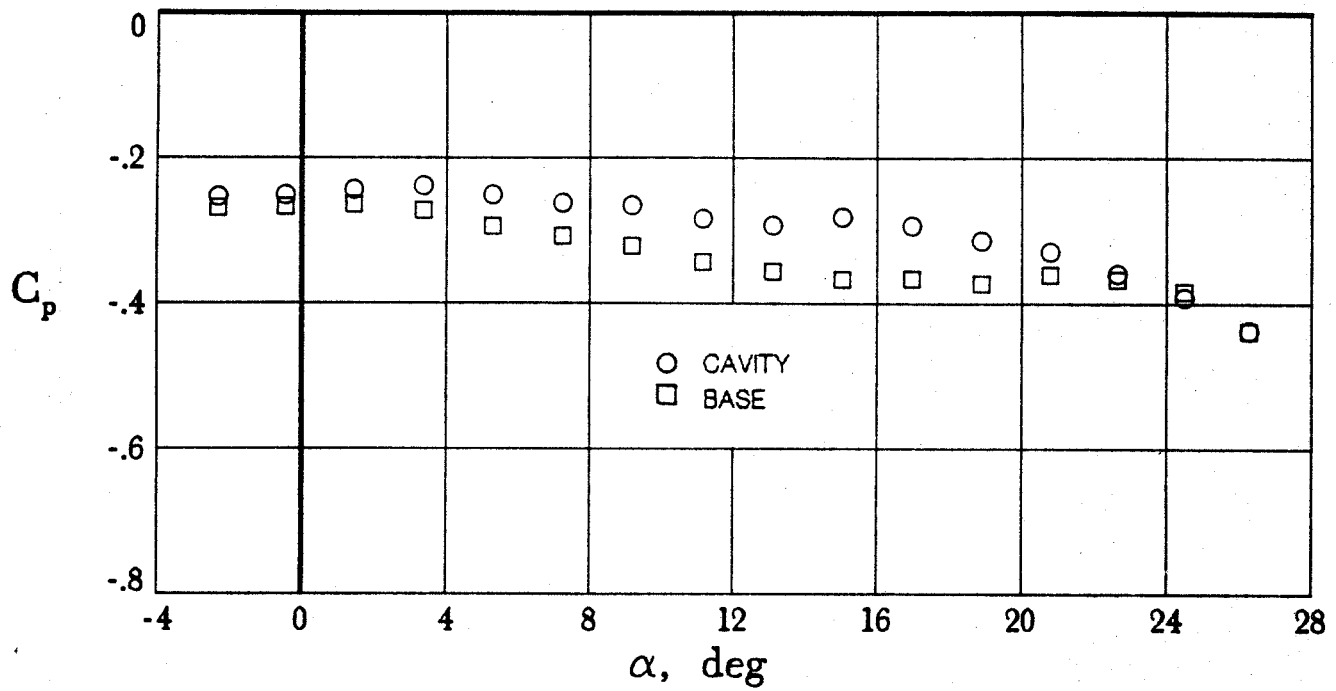
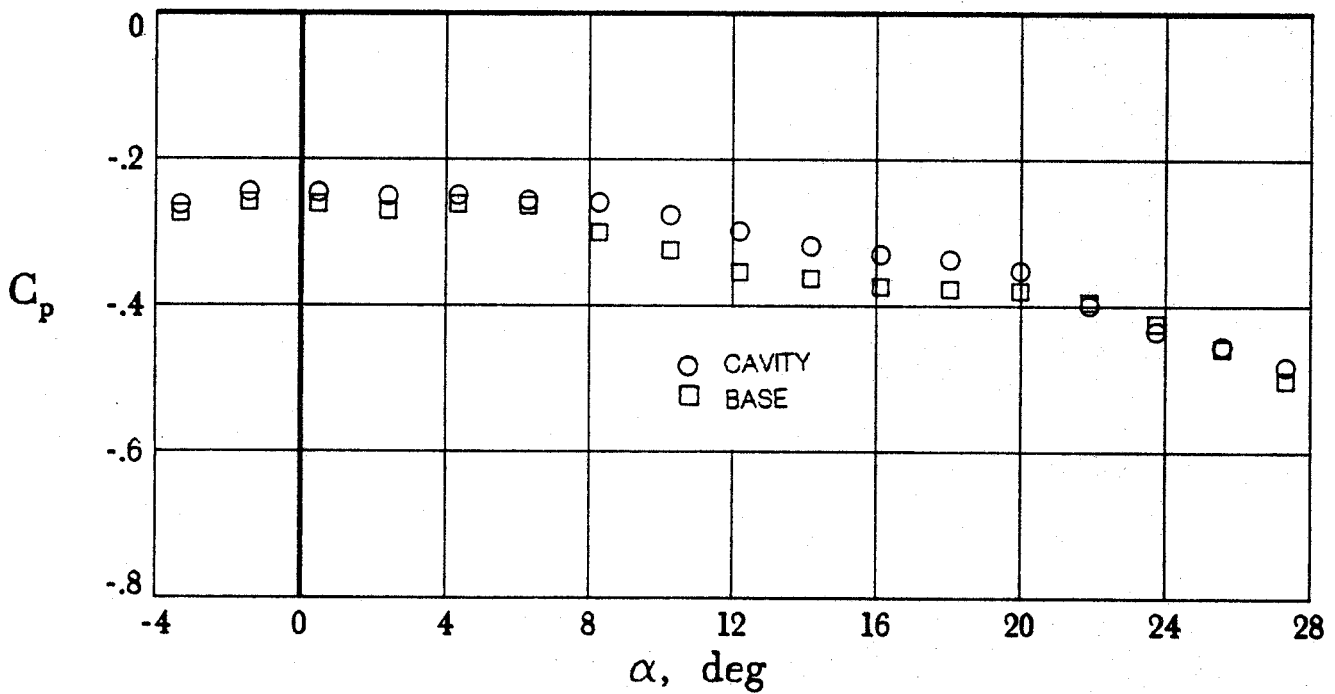
(a) $M = 0.6$.(b) $M = 0.8$.

Figure 11. Model base and sting-cavity pressures measured in transonic tests.

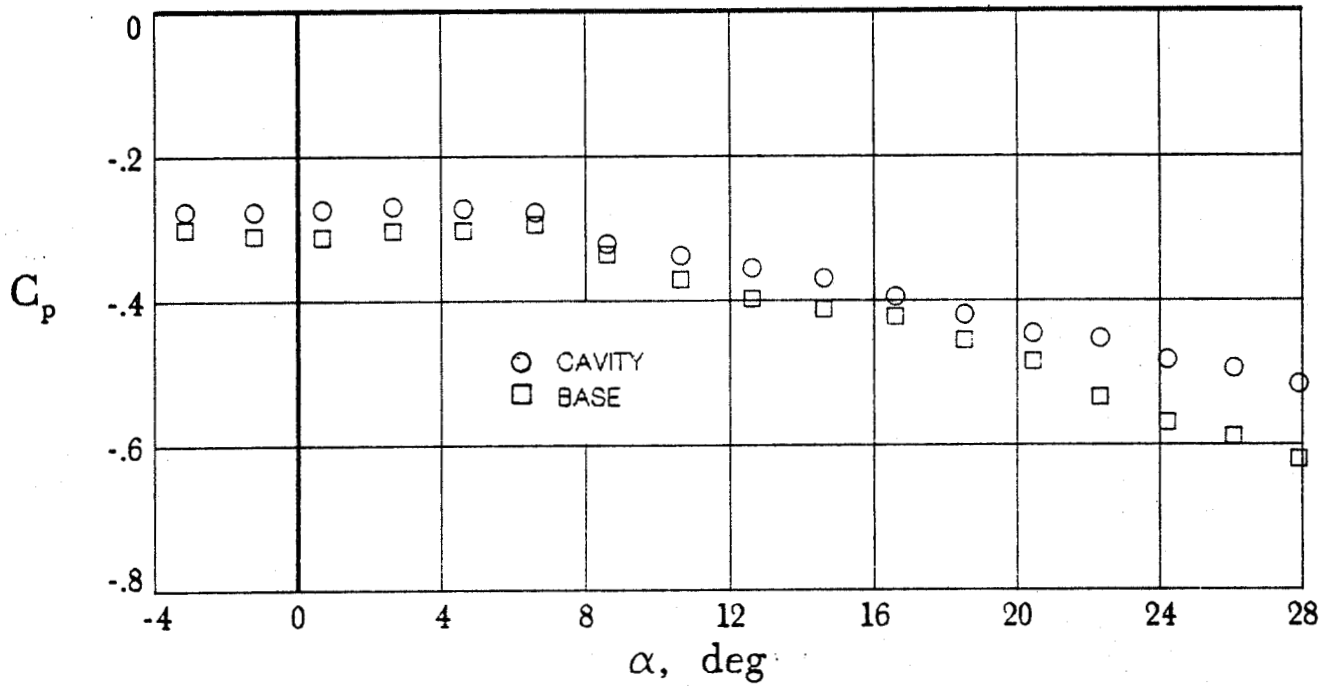
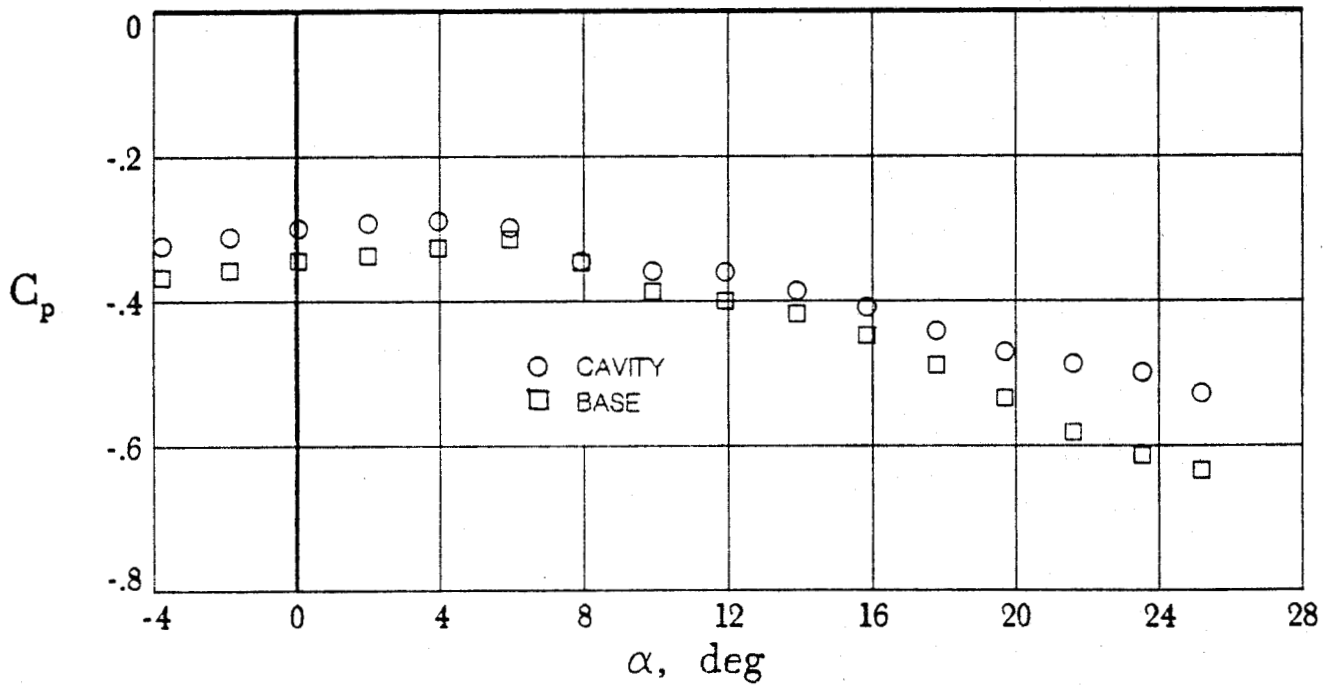
(c) $M = 0.9$.(d) $M = 0.95$.

Figure 11. Continued.

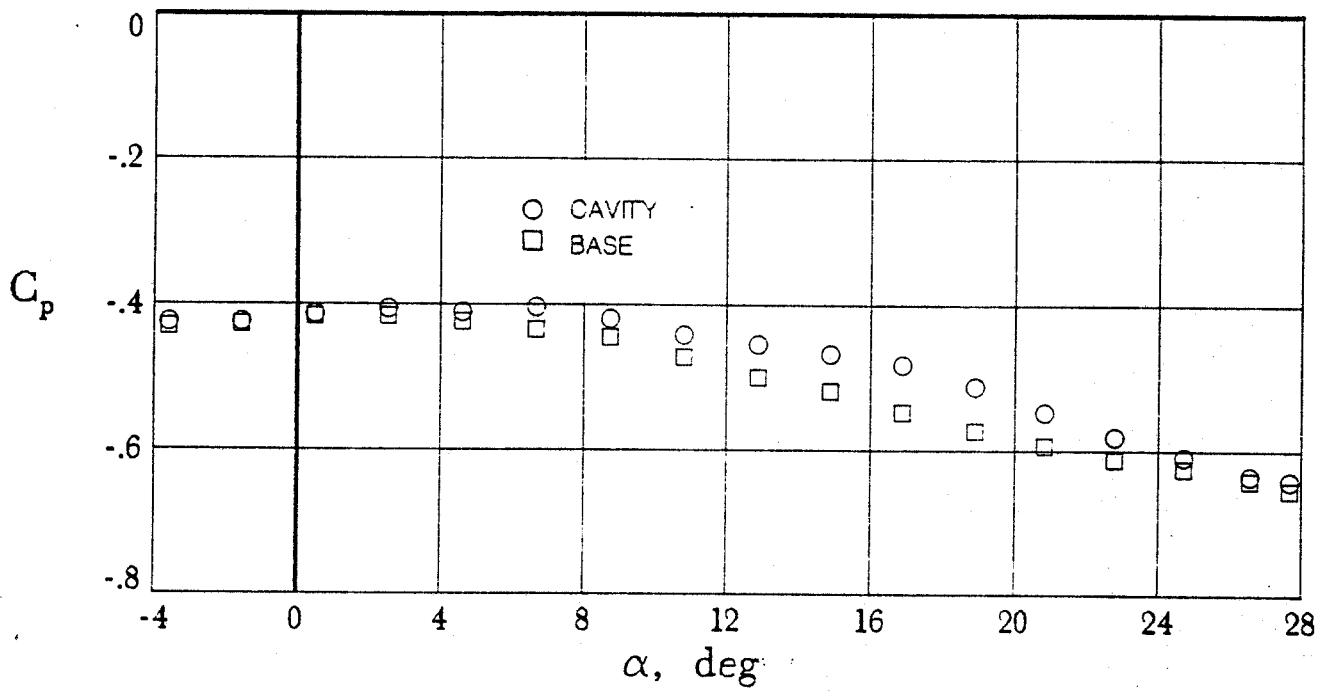
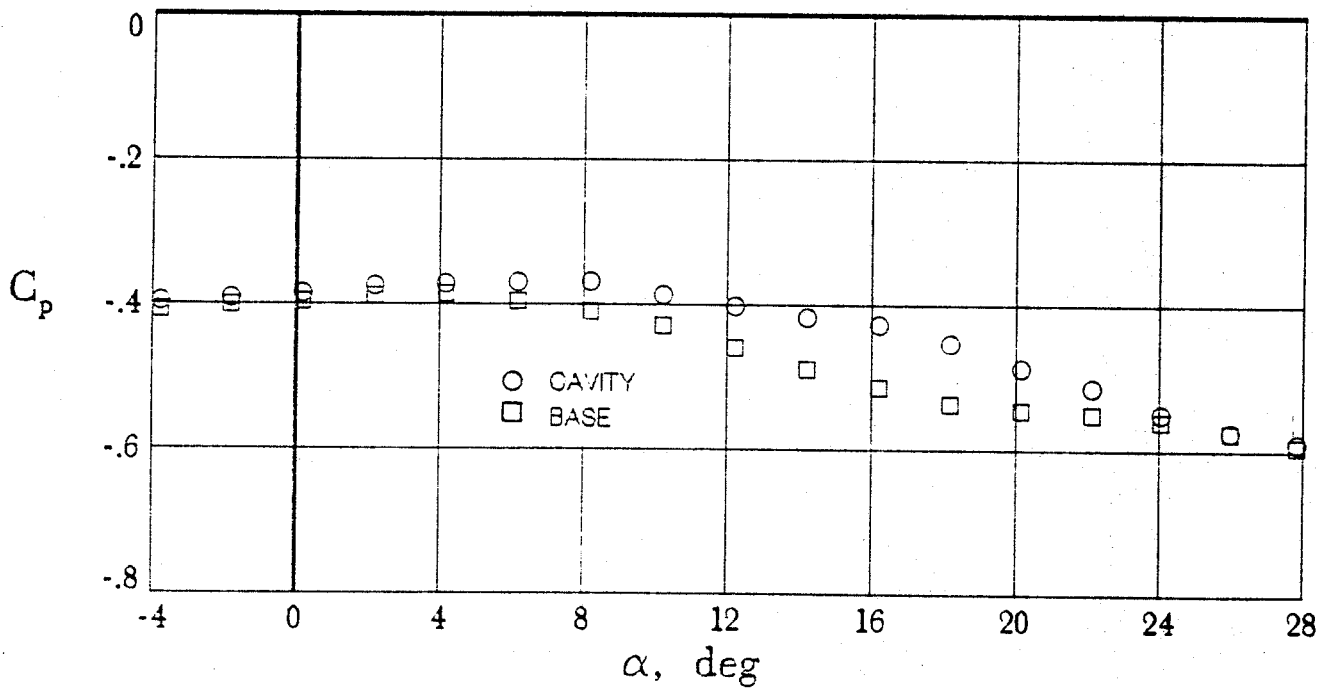
(e) $M = 1.1$.(f) $M = 1.2$.

Figure 11. Concluded.

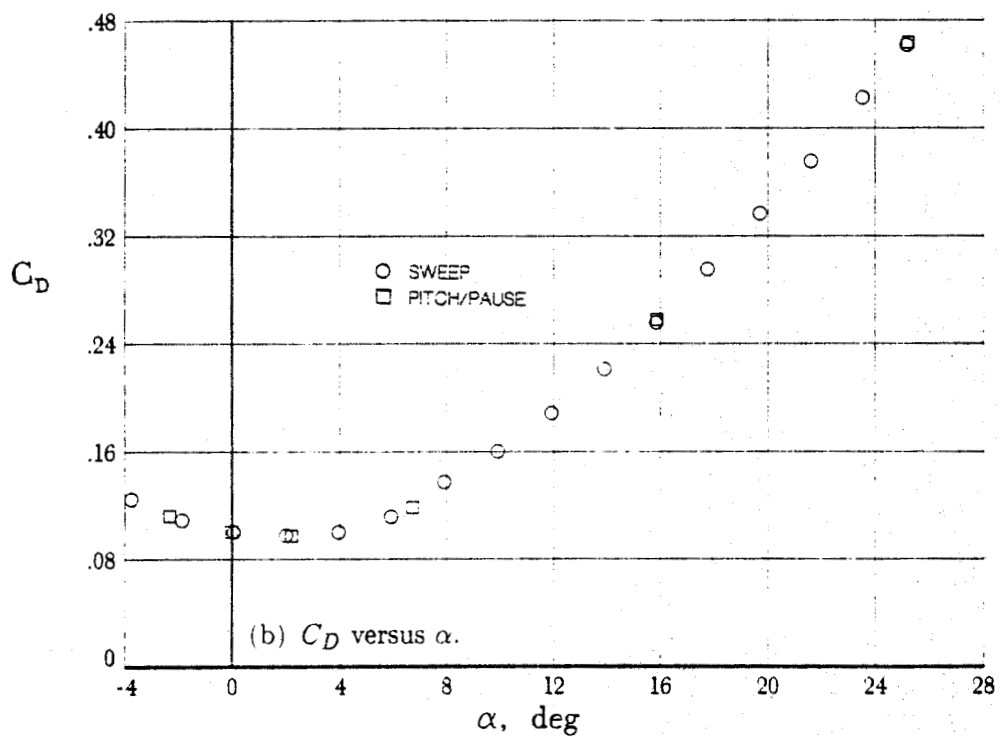
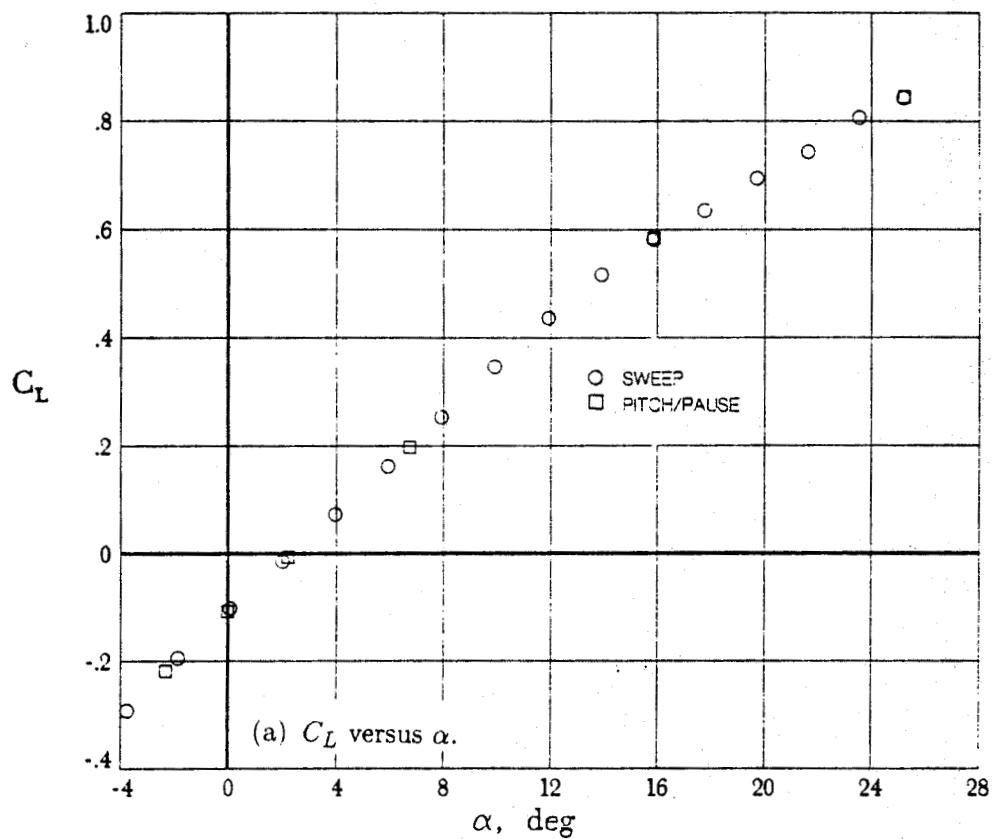


Figure 12. Comparison of data taken using sweep and pitch/pause methods. $M = 0.6$.

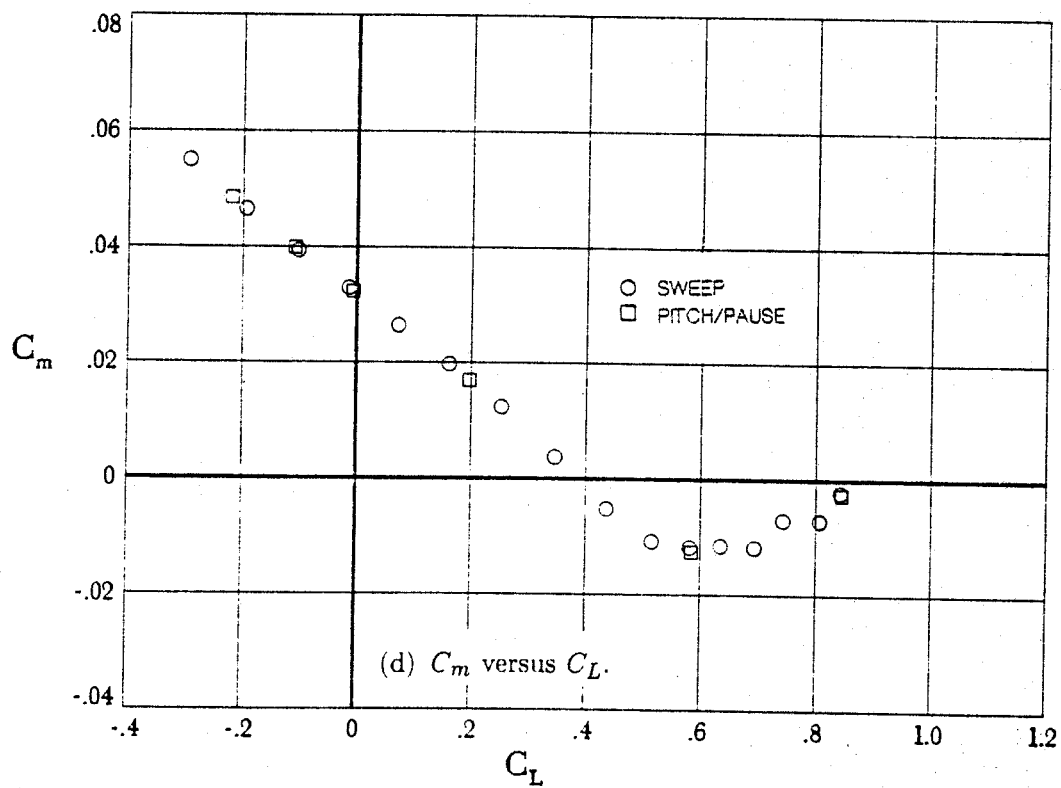
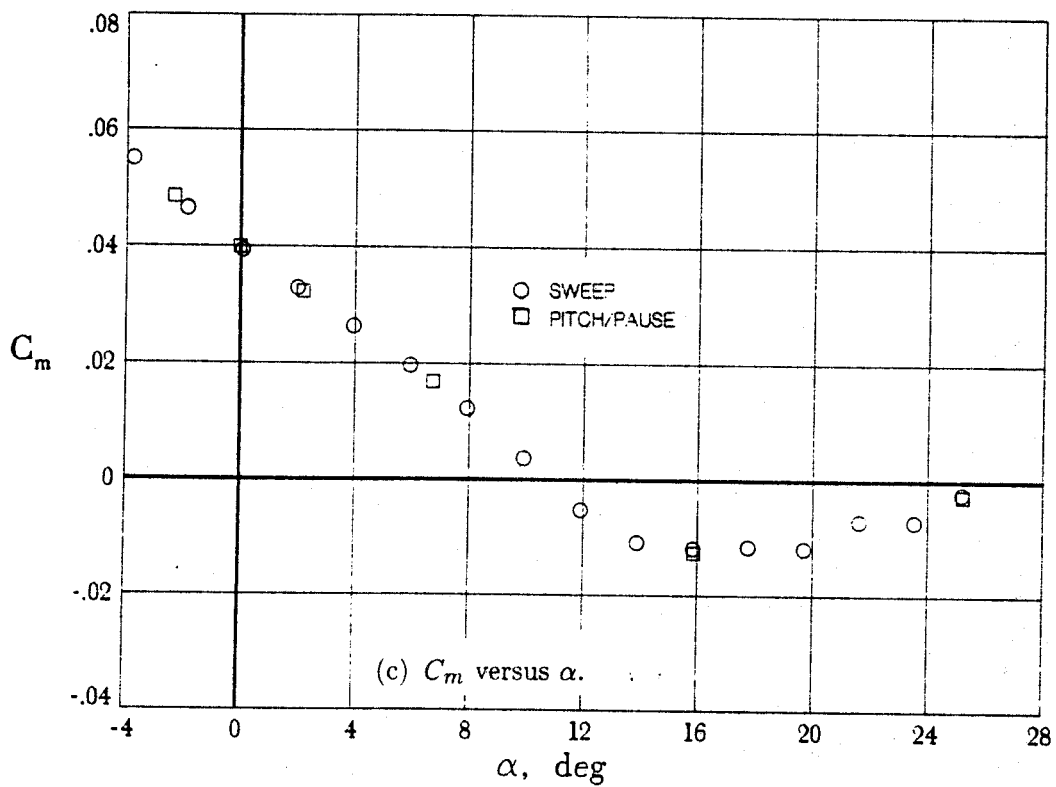


Figure 12. Continued.

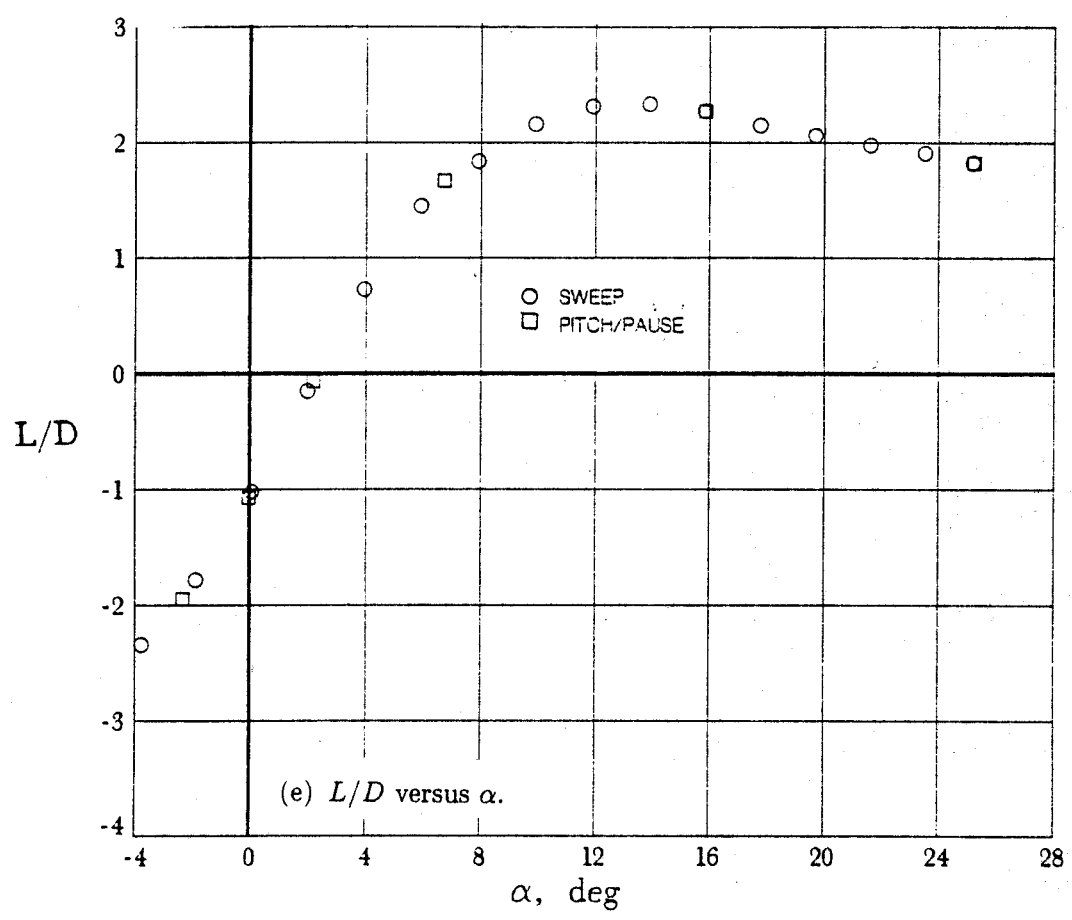


Figure 12. Concluded.

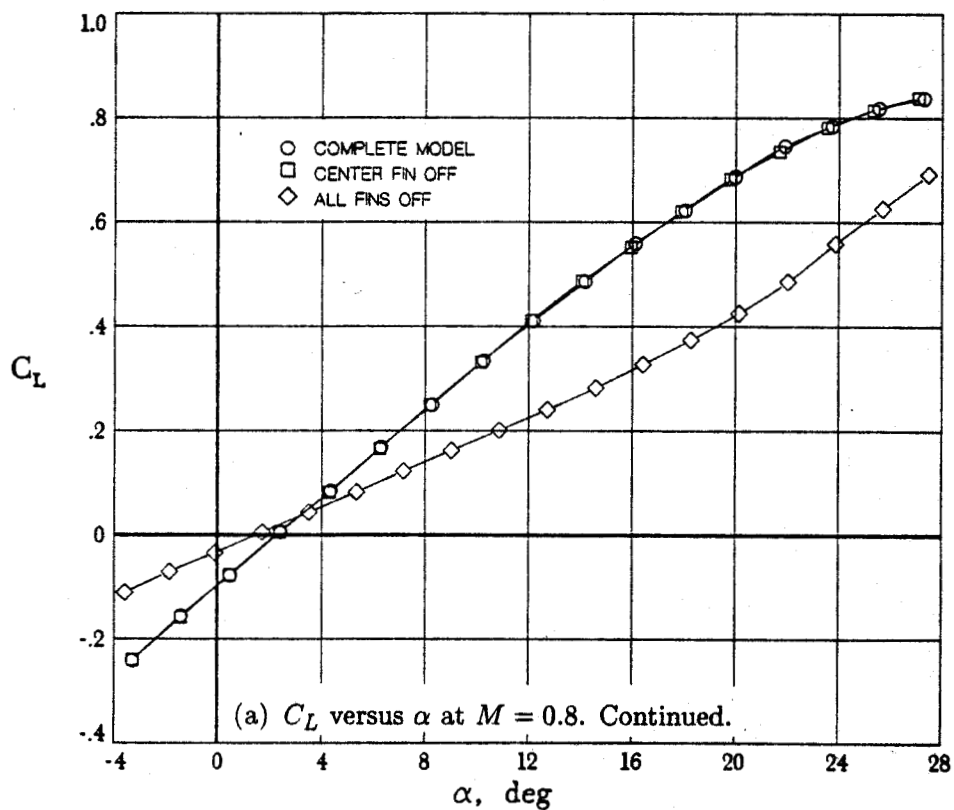
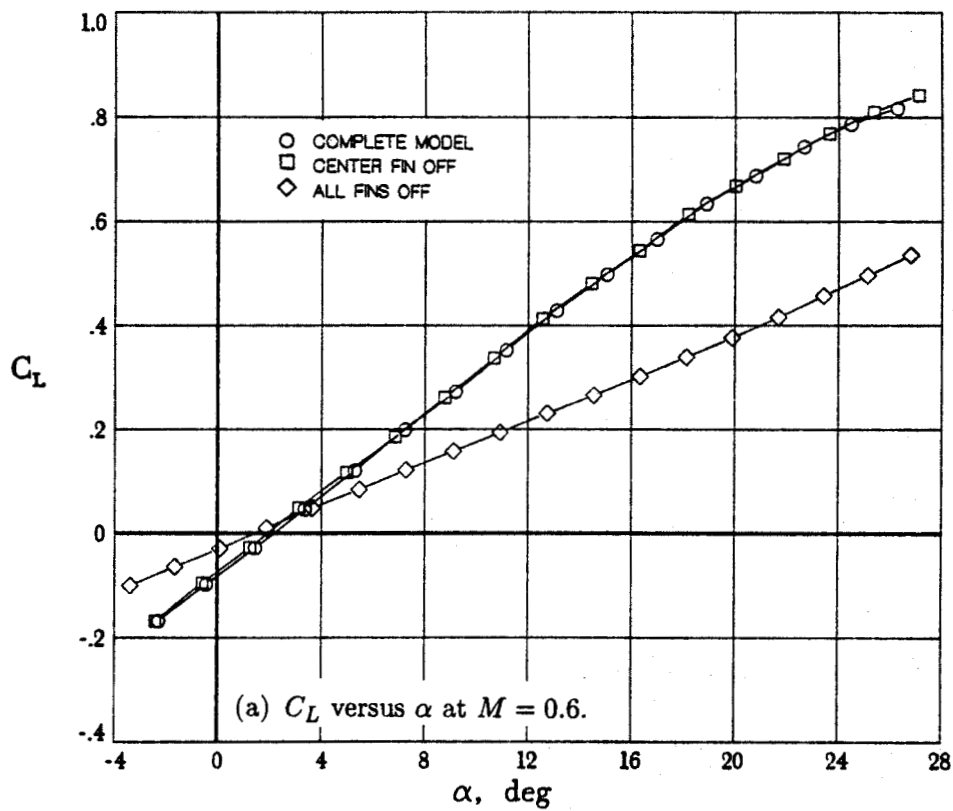


Figure 13. Effect of fins on longitudinal aerodynamic characteristics of model at transonic speeds.

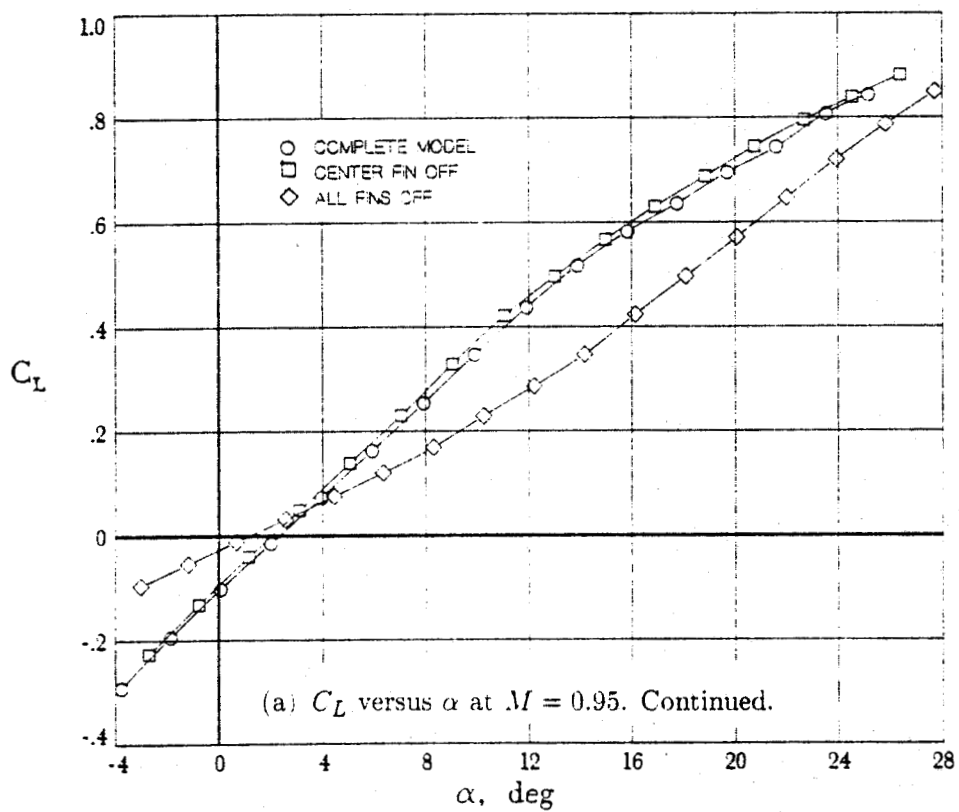
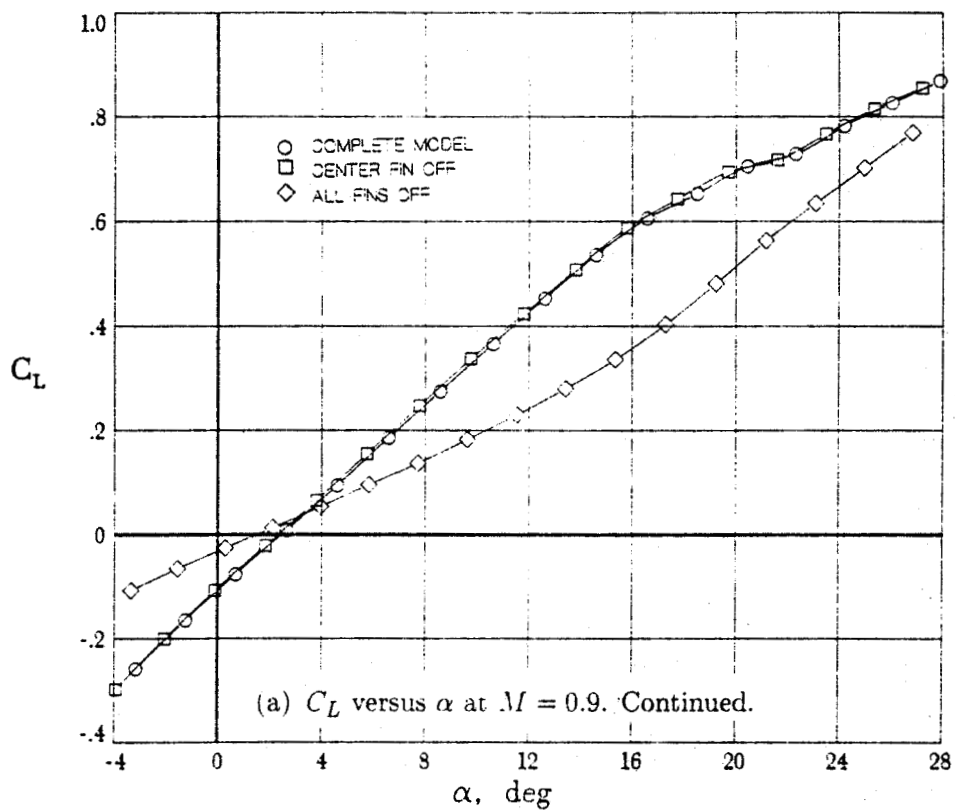


Figure 13. Continued.

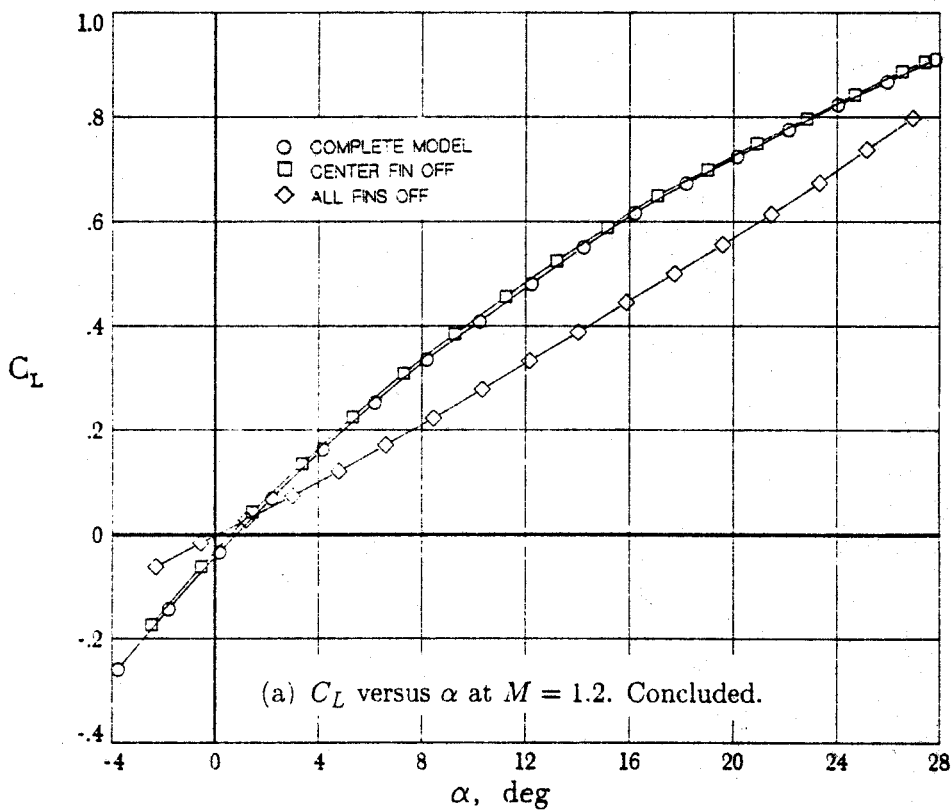
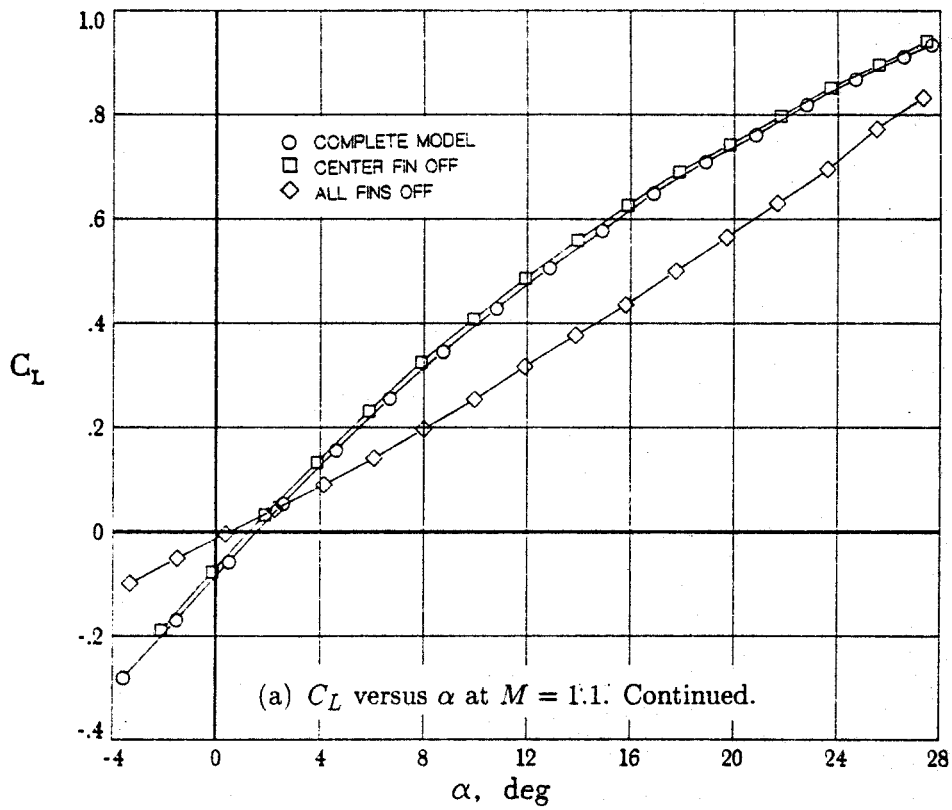


Figure 13. Continued.

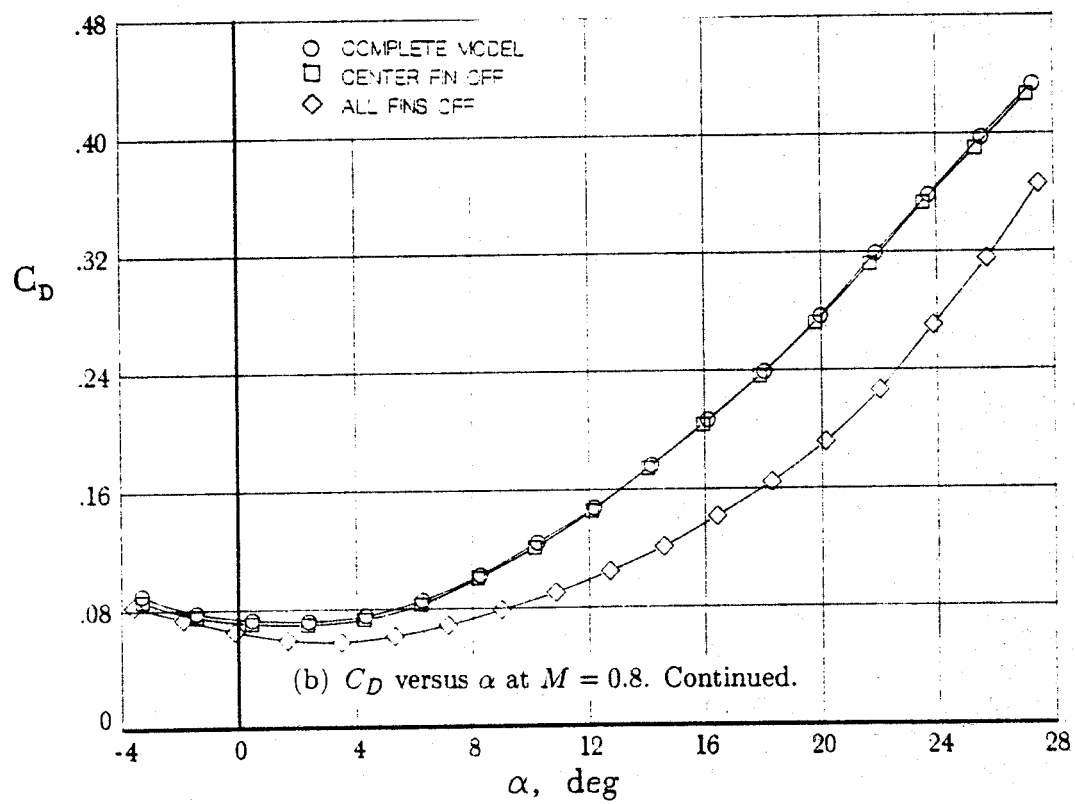
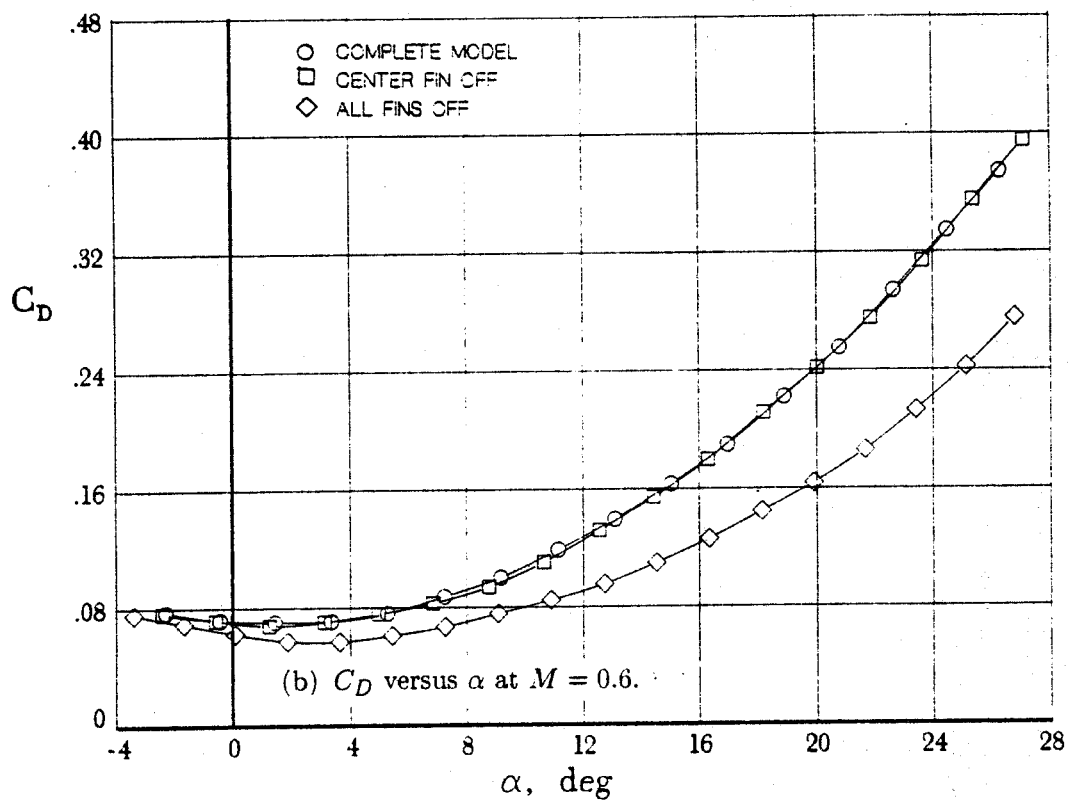


Figure 13. Continued.

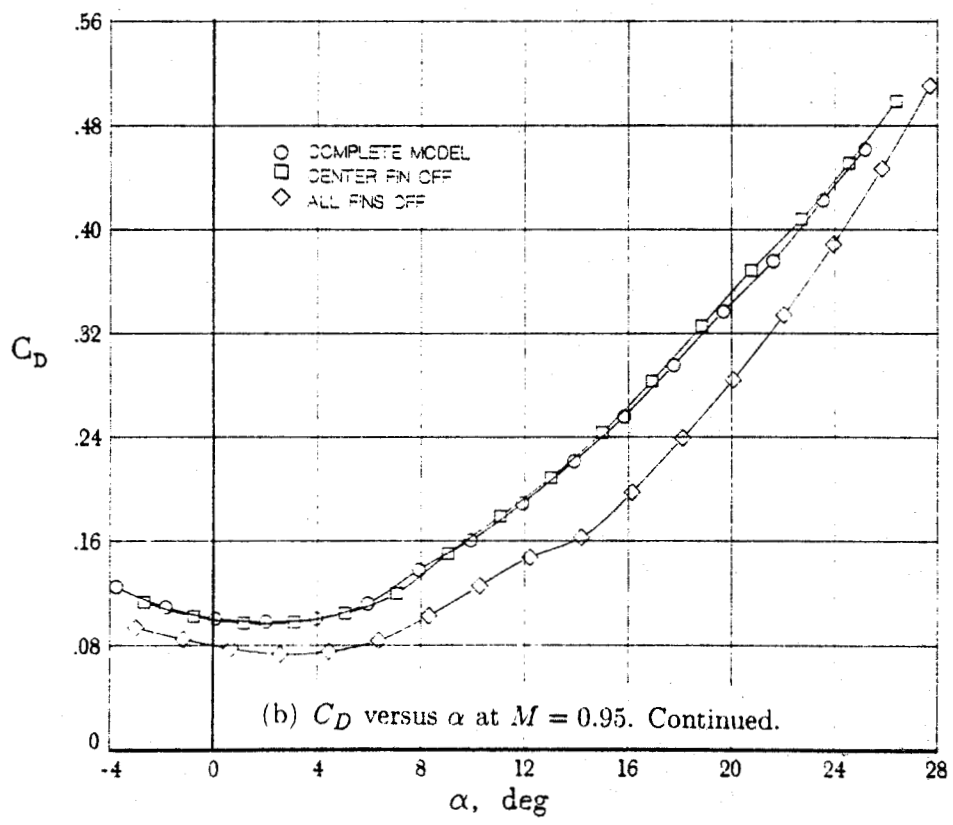
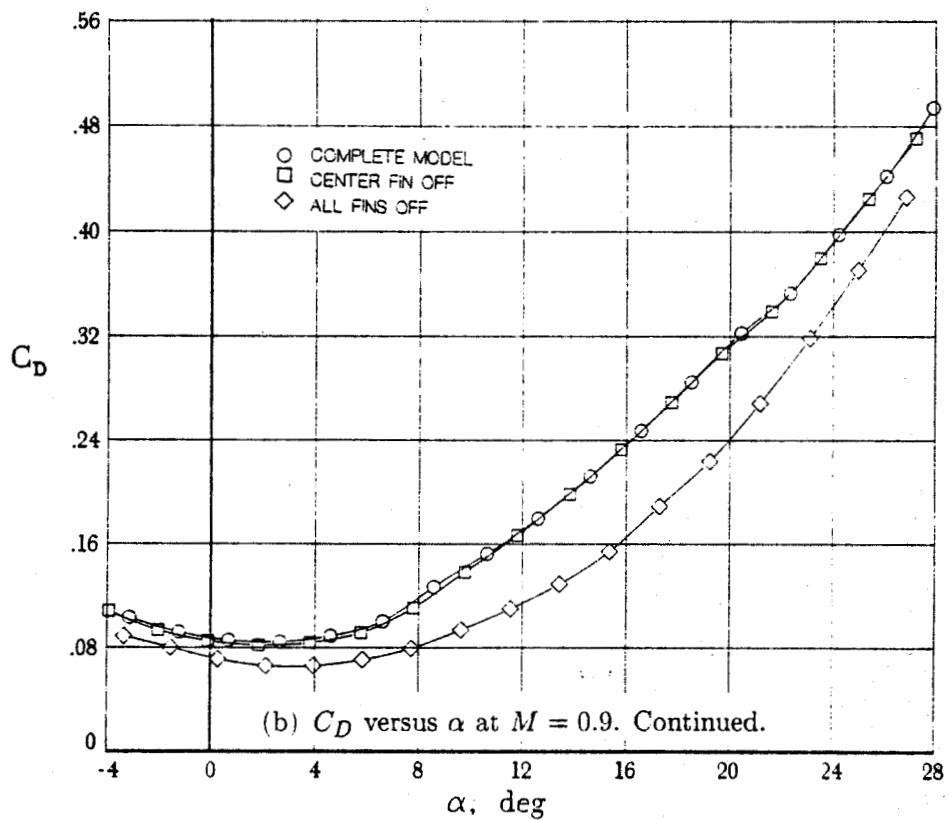


Figure 13. Continued.

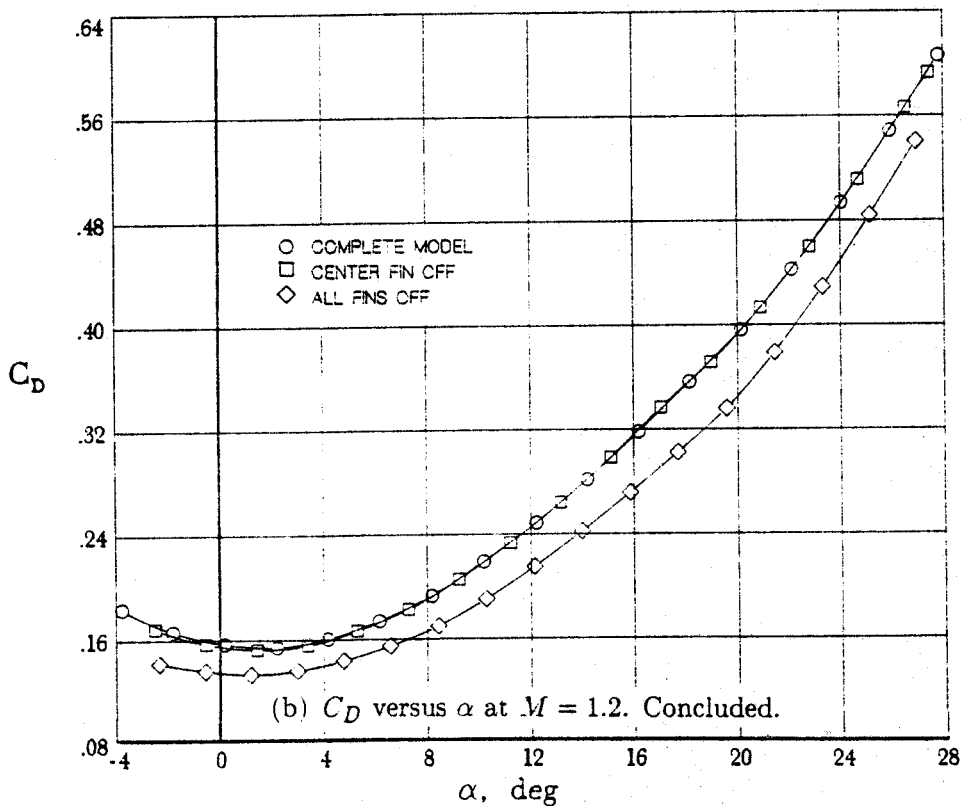
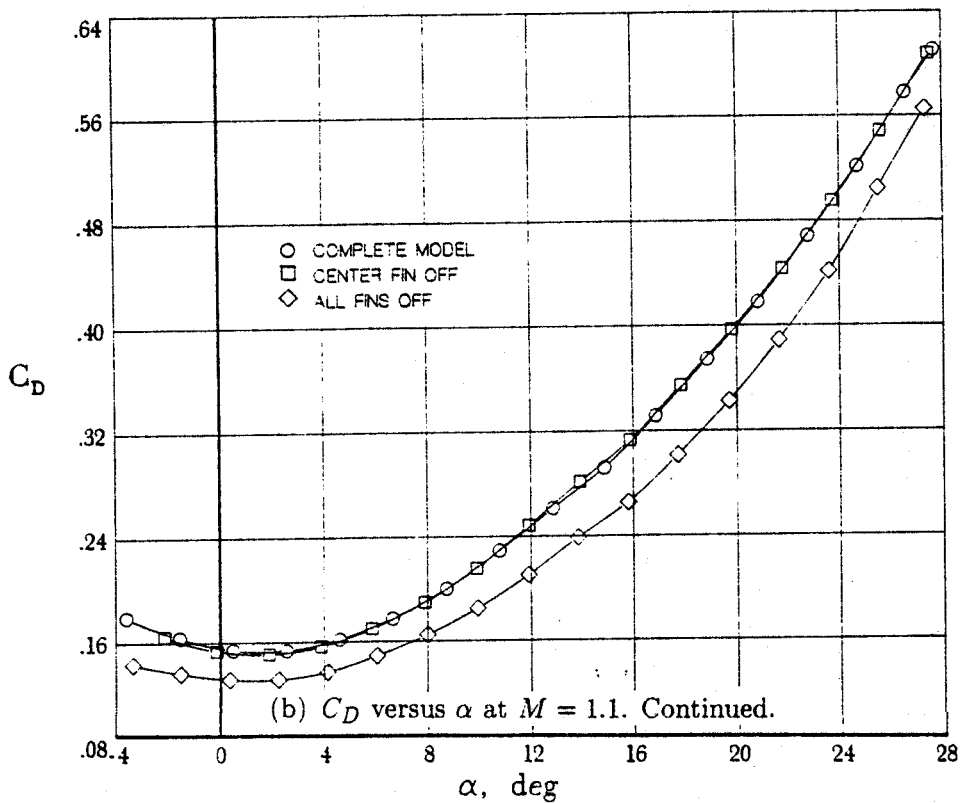


Figure 13. Continued.

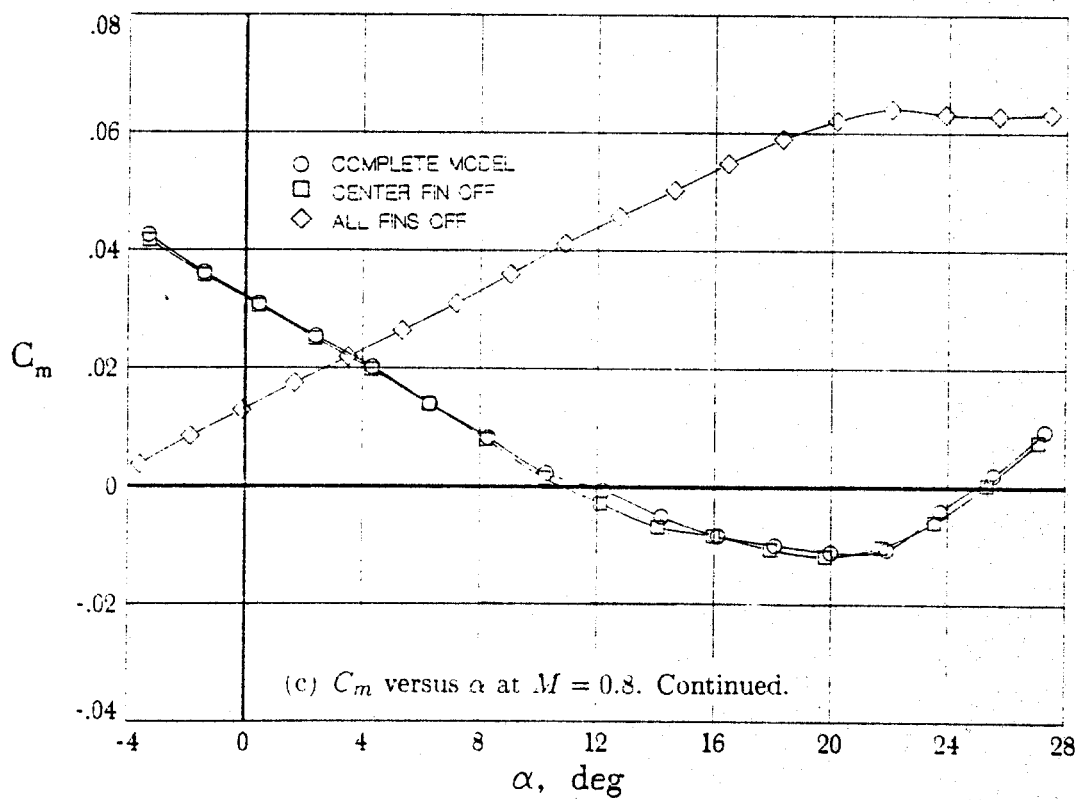
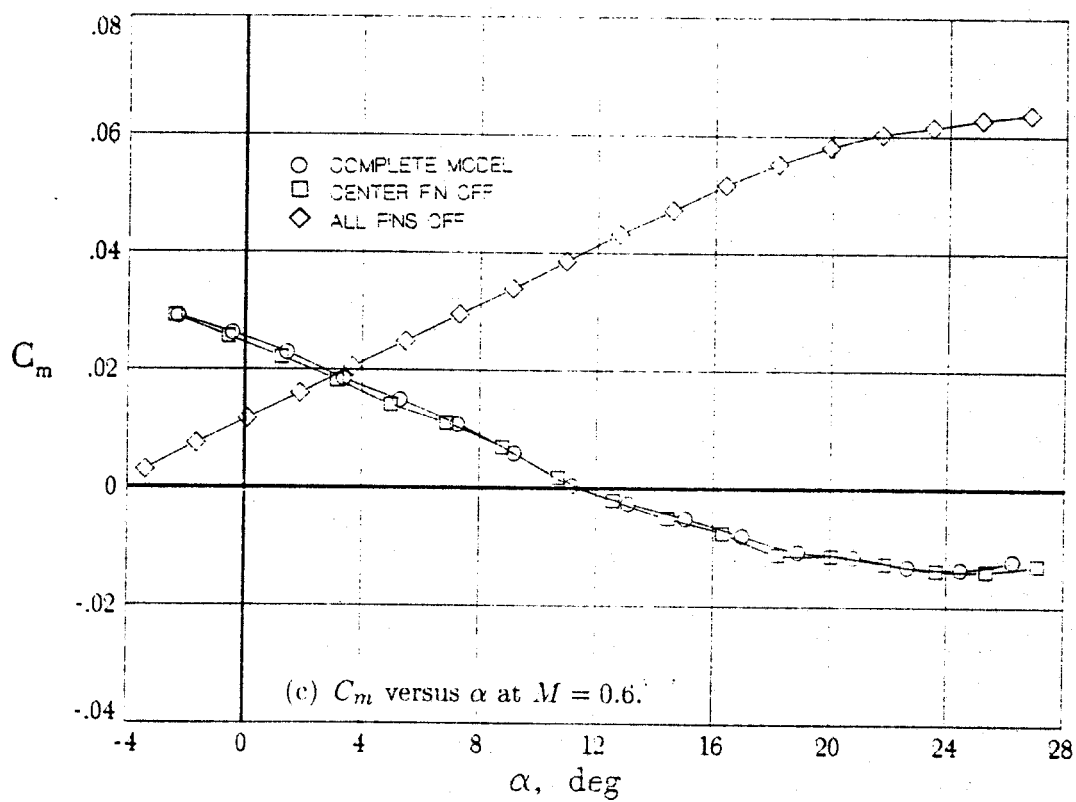


Figure 13. Continued.

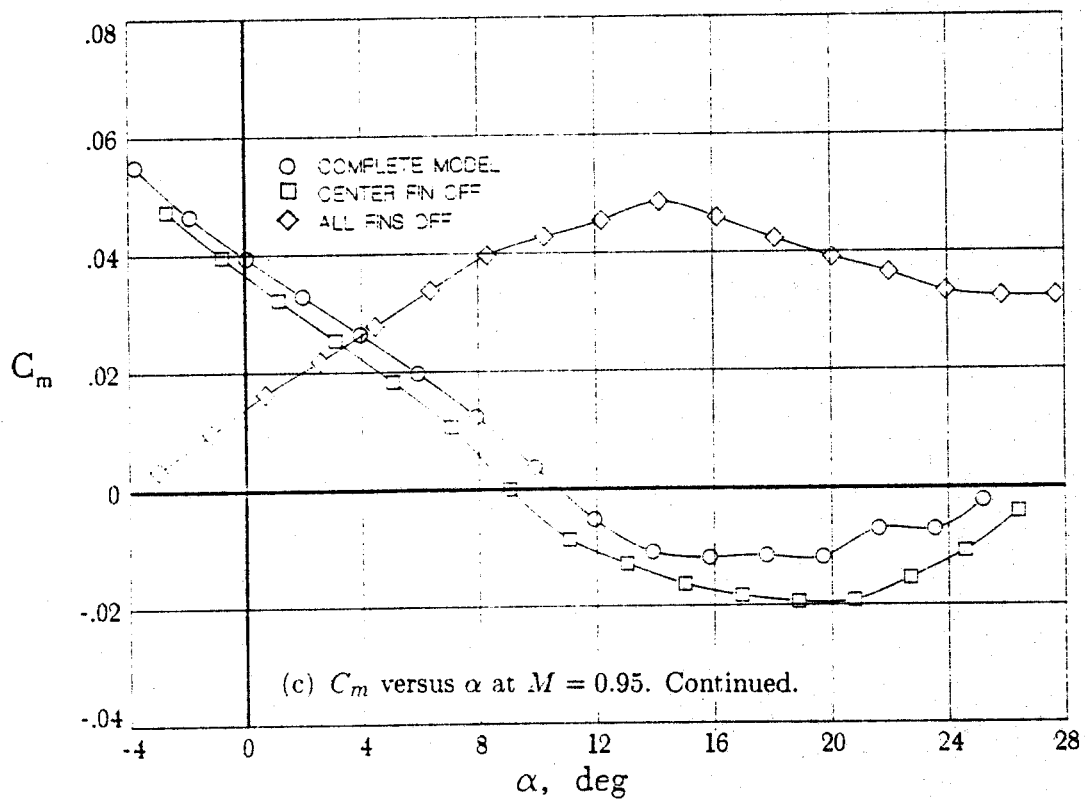
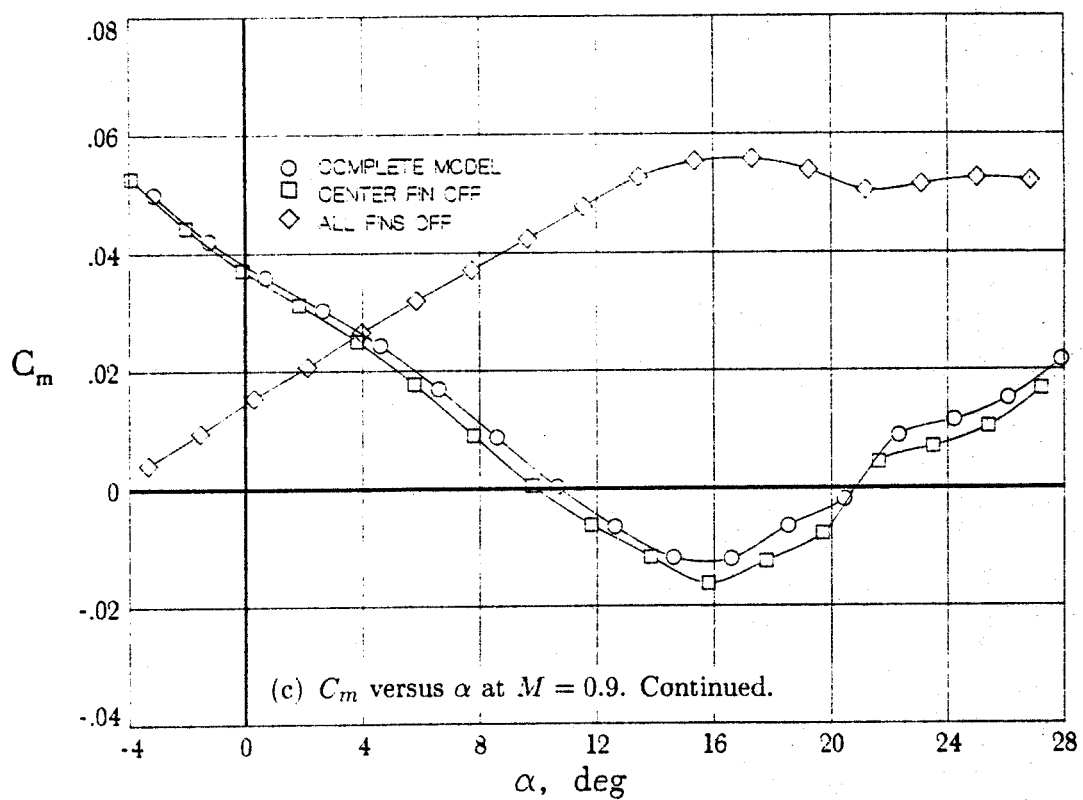


Figure 13. Continued.

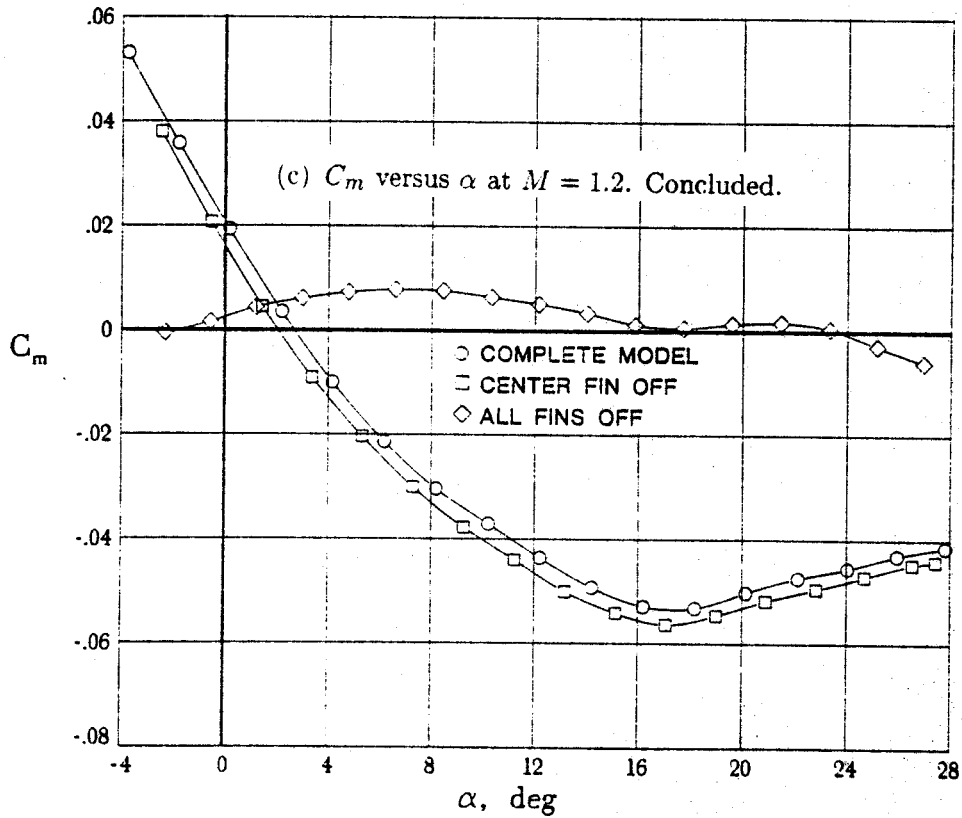
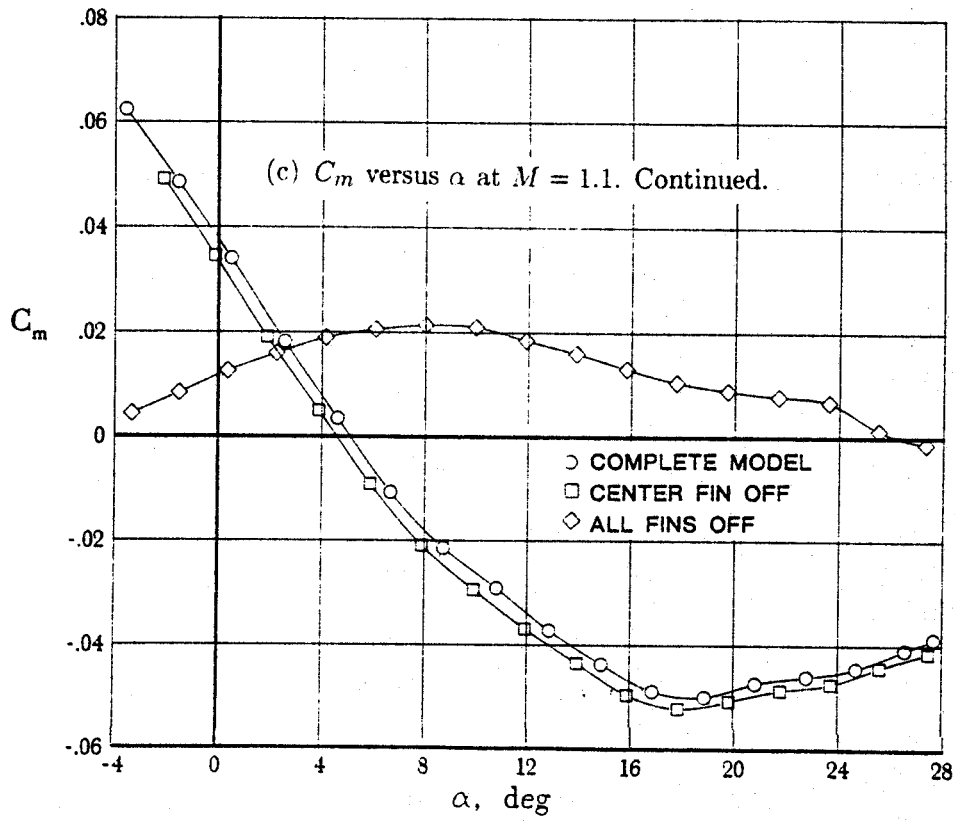


Figure 13. Continued.

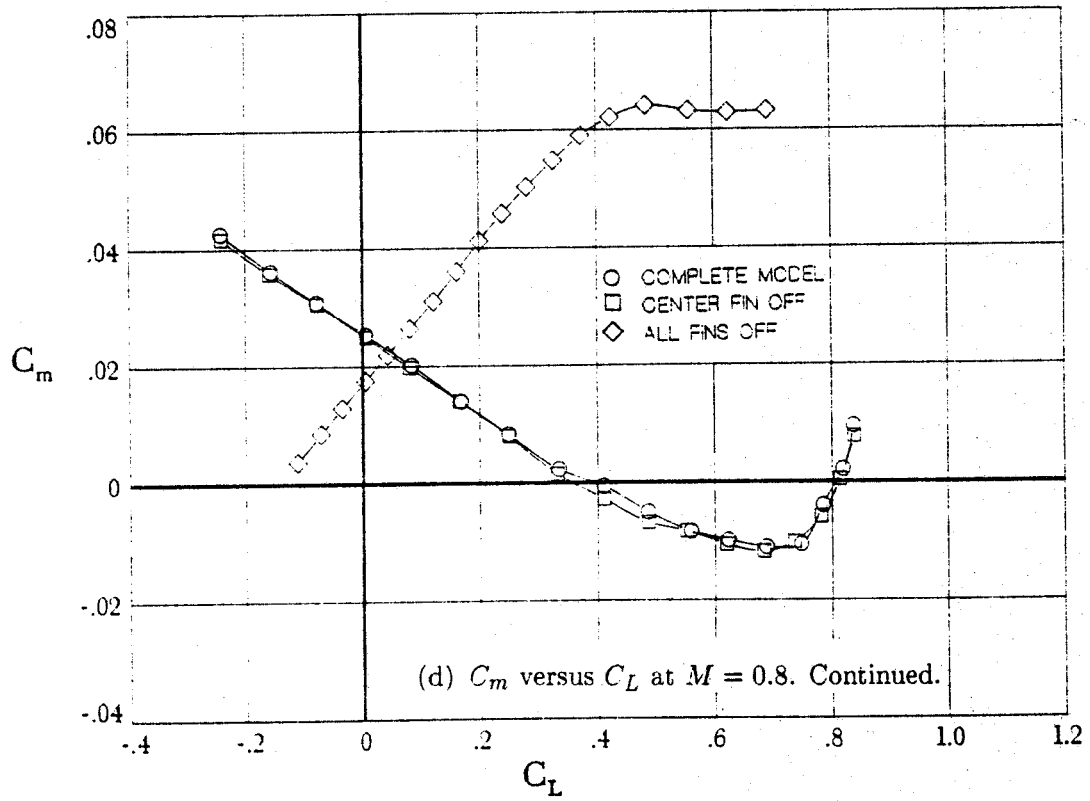
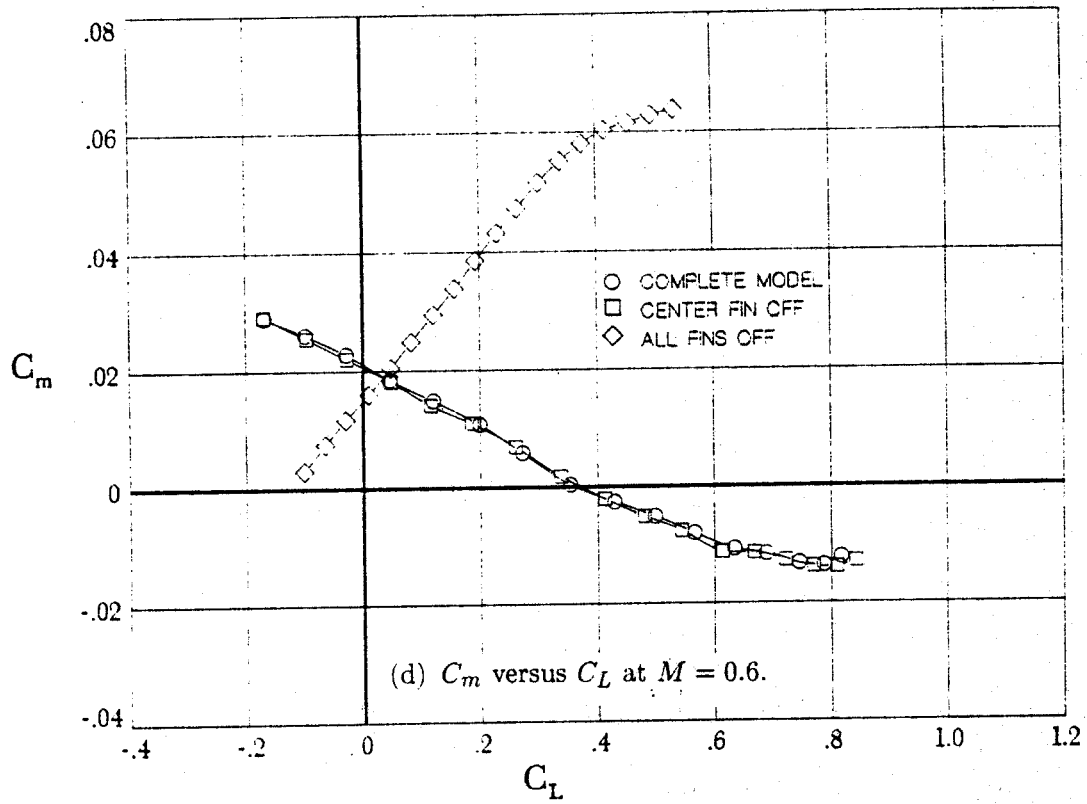


Figure 13. Continued.

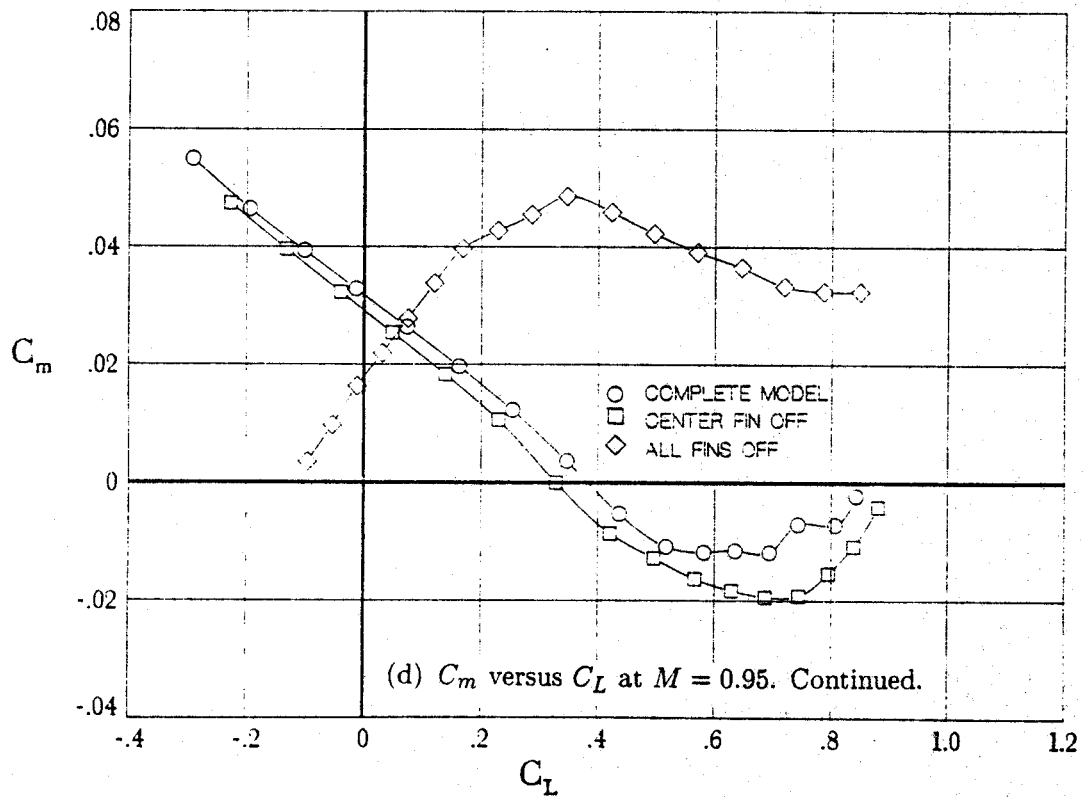
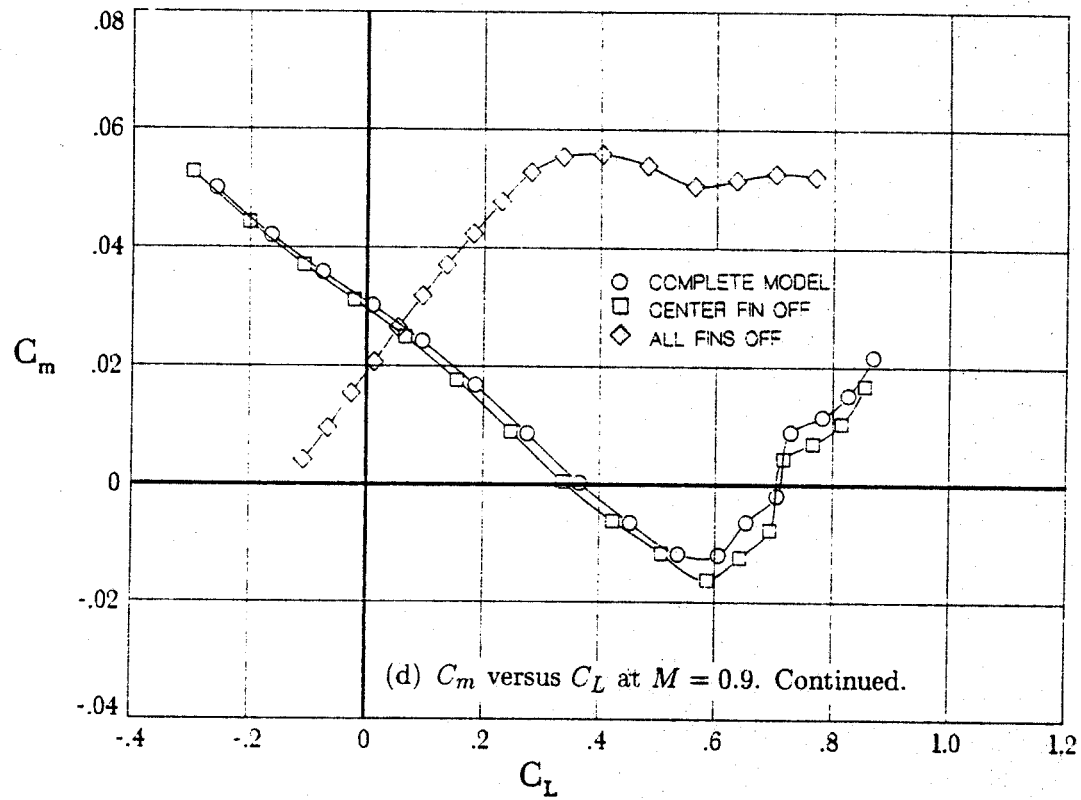


Figure 13. Continued.

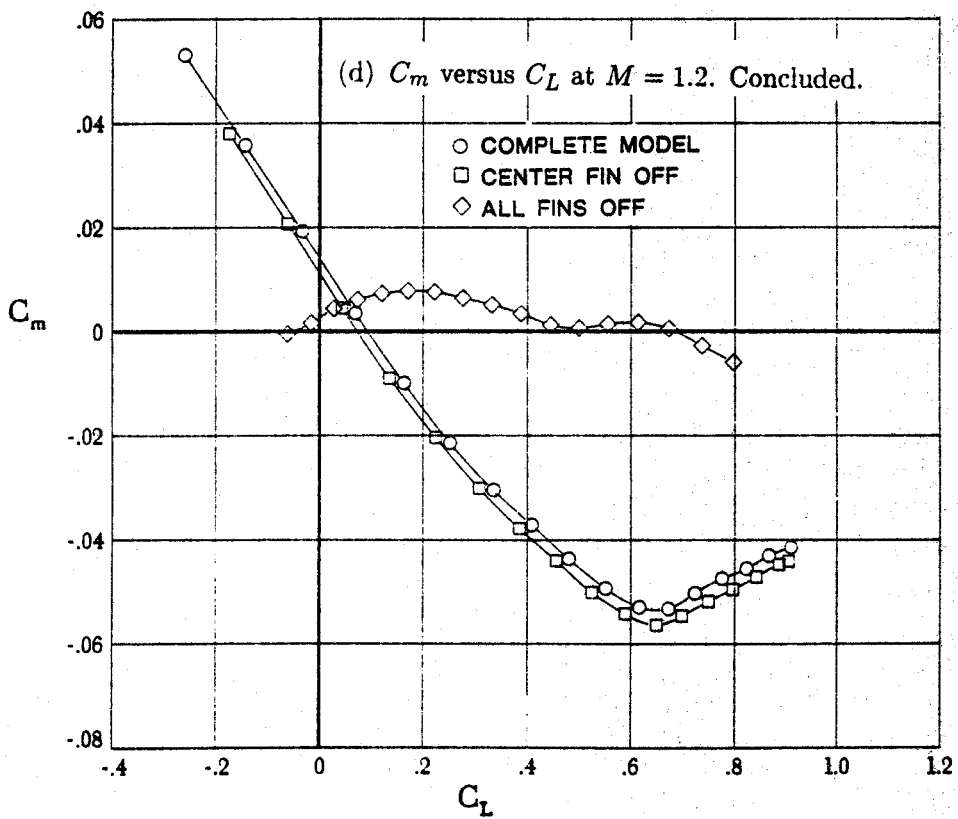
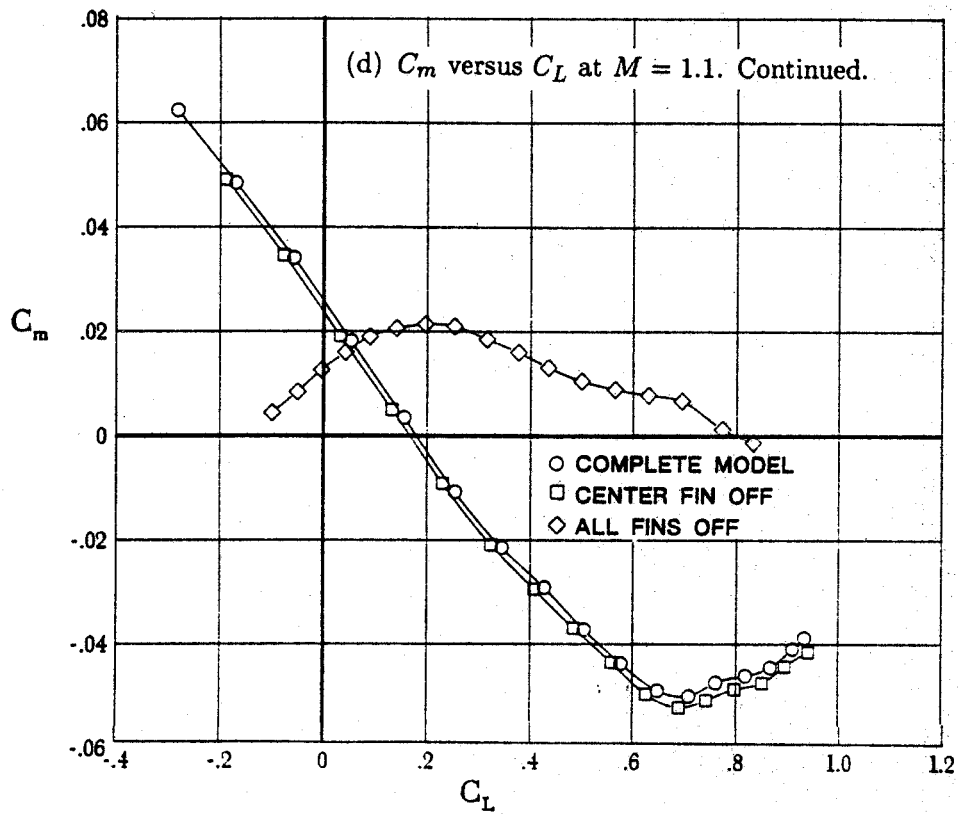


Figure 13. Continued.

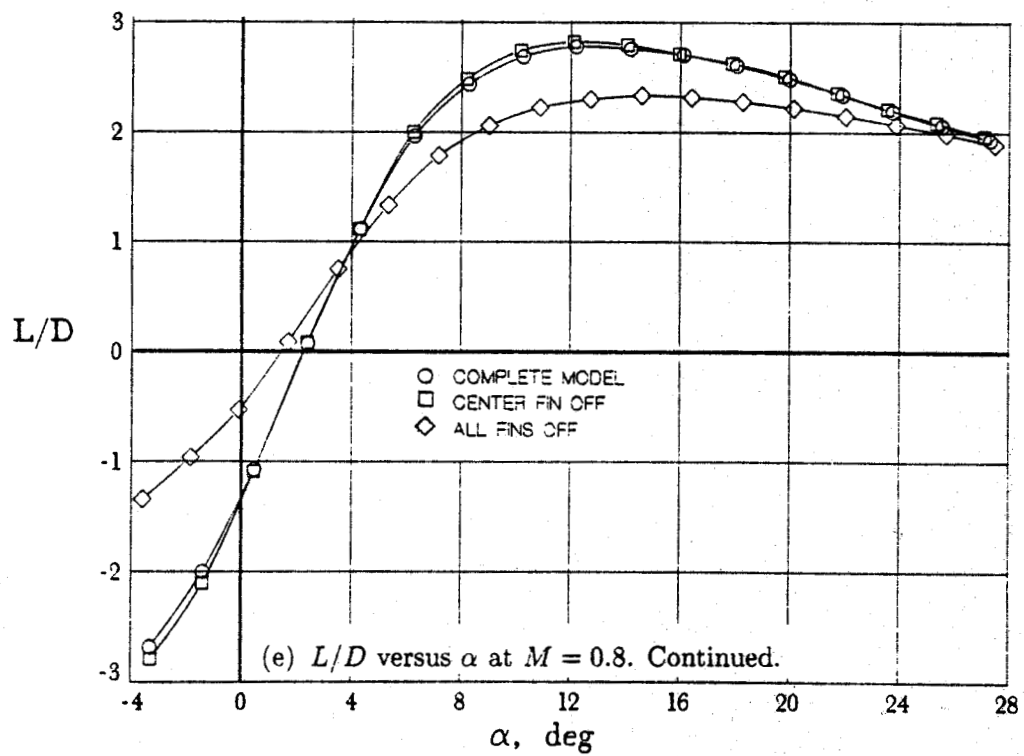
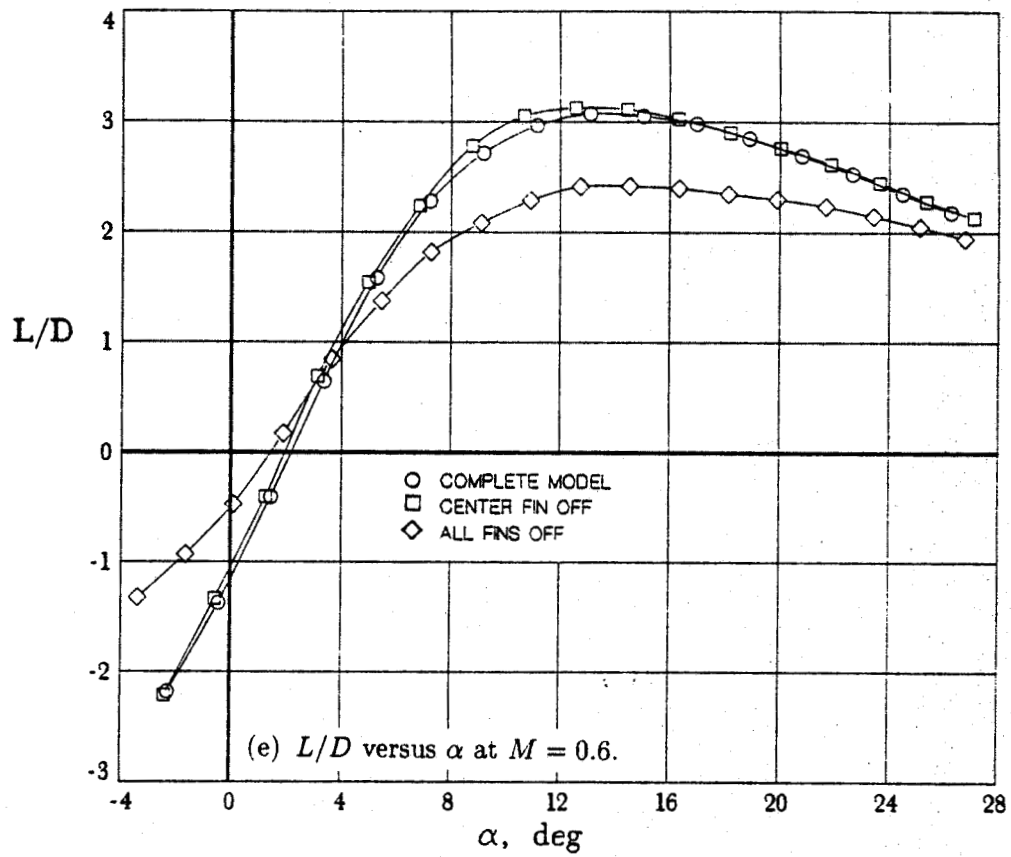


Figure 13. Continued.

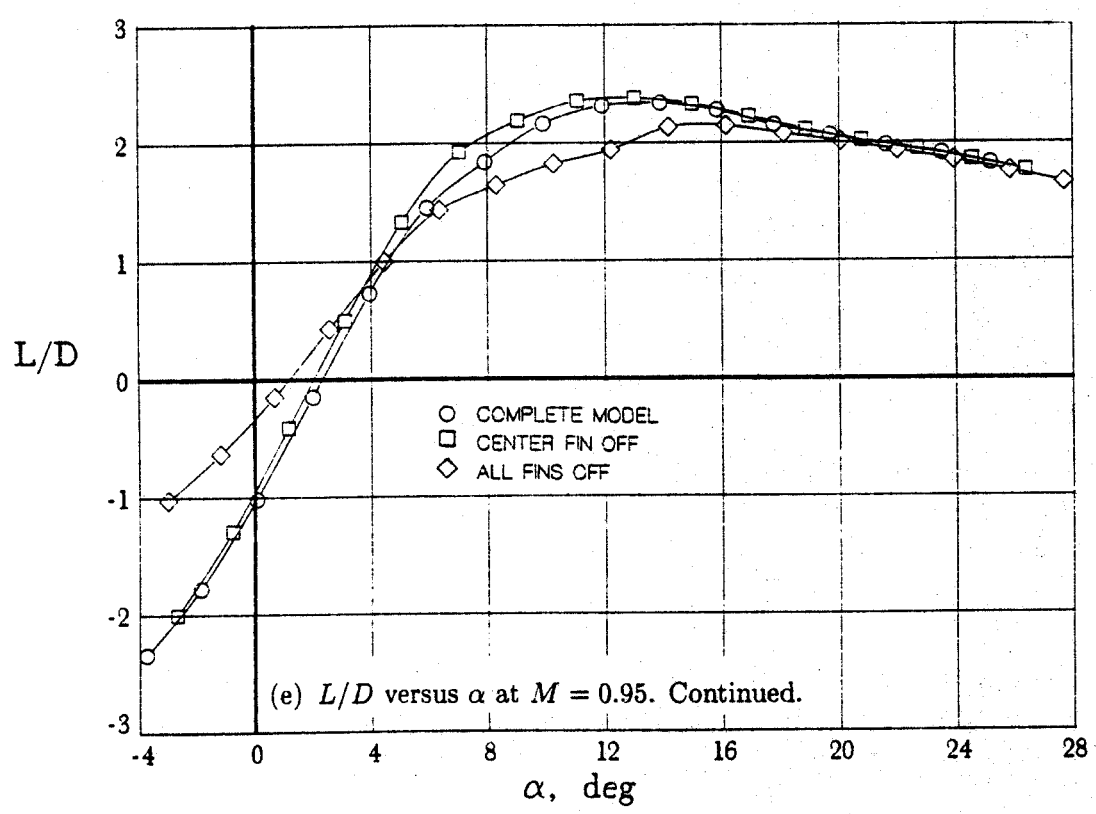
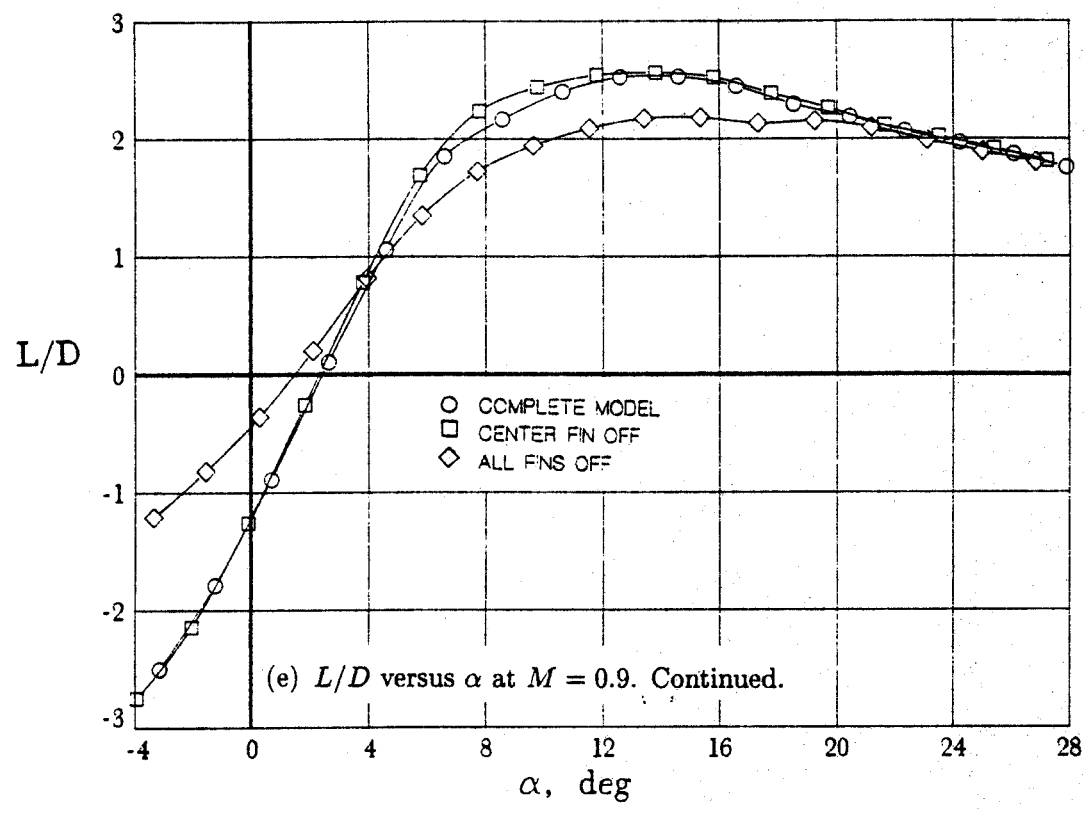


Figure 13. Continued.

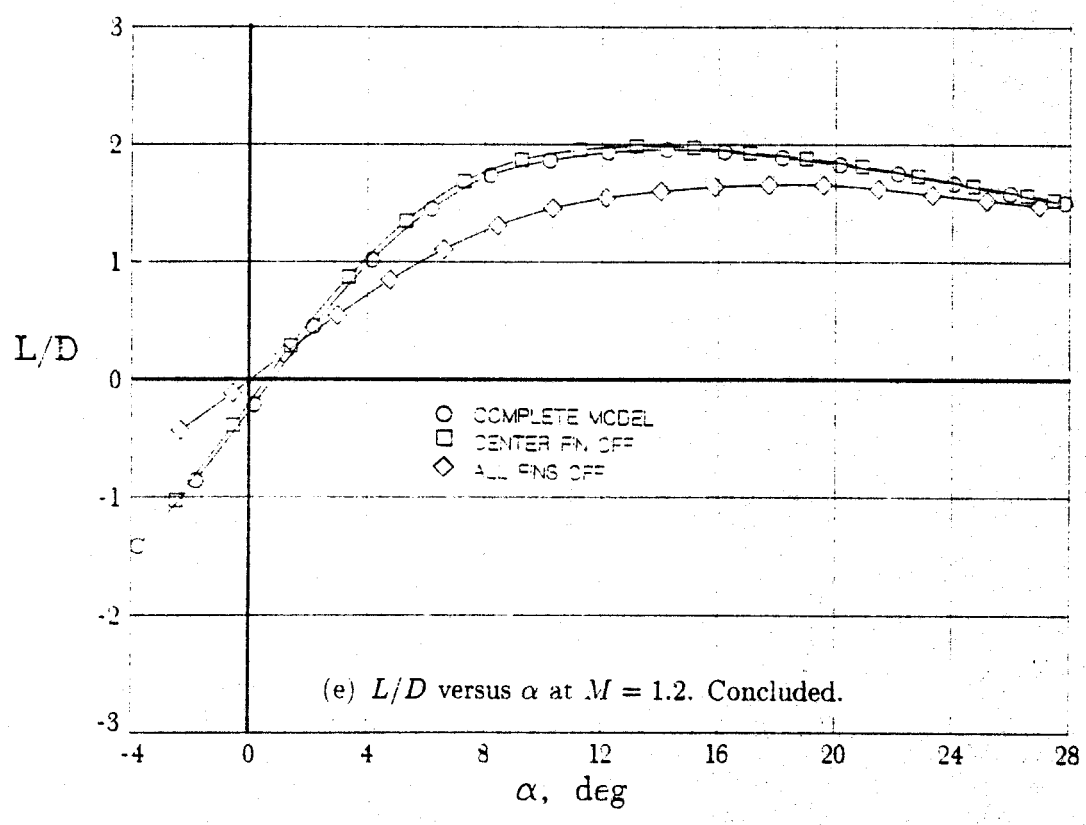
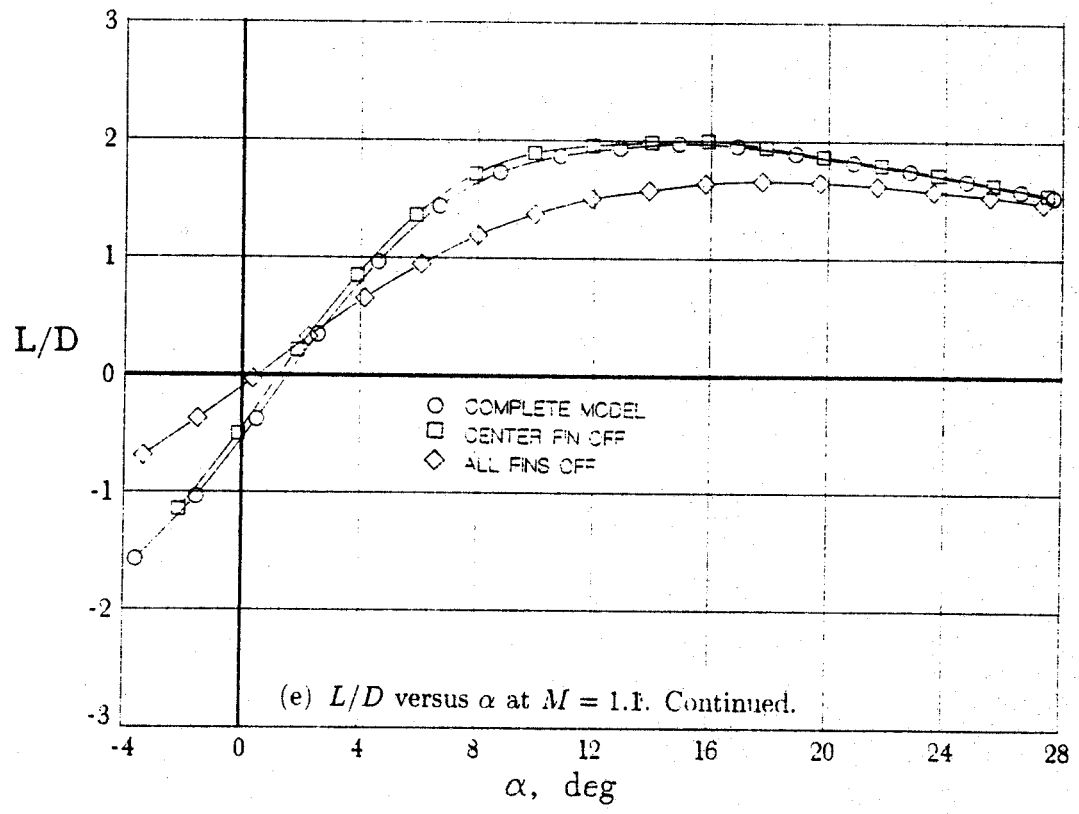


Figure 13. Concluded.

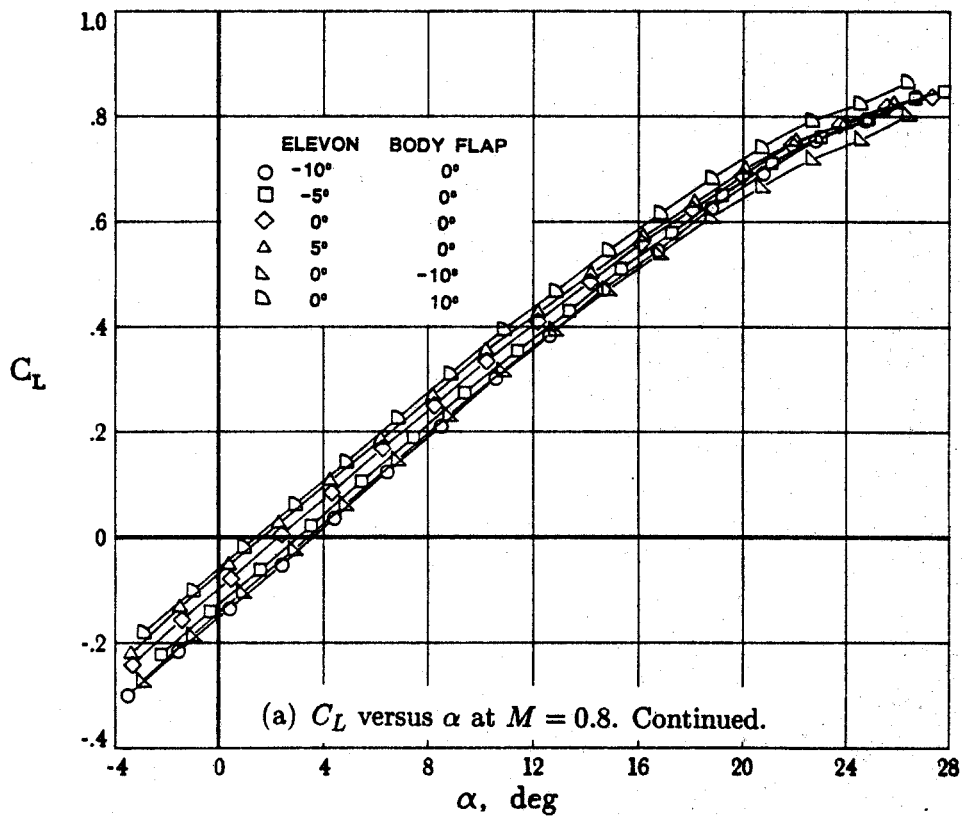
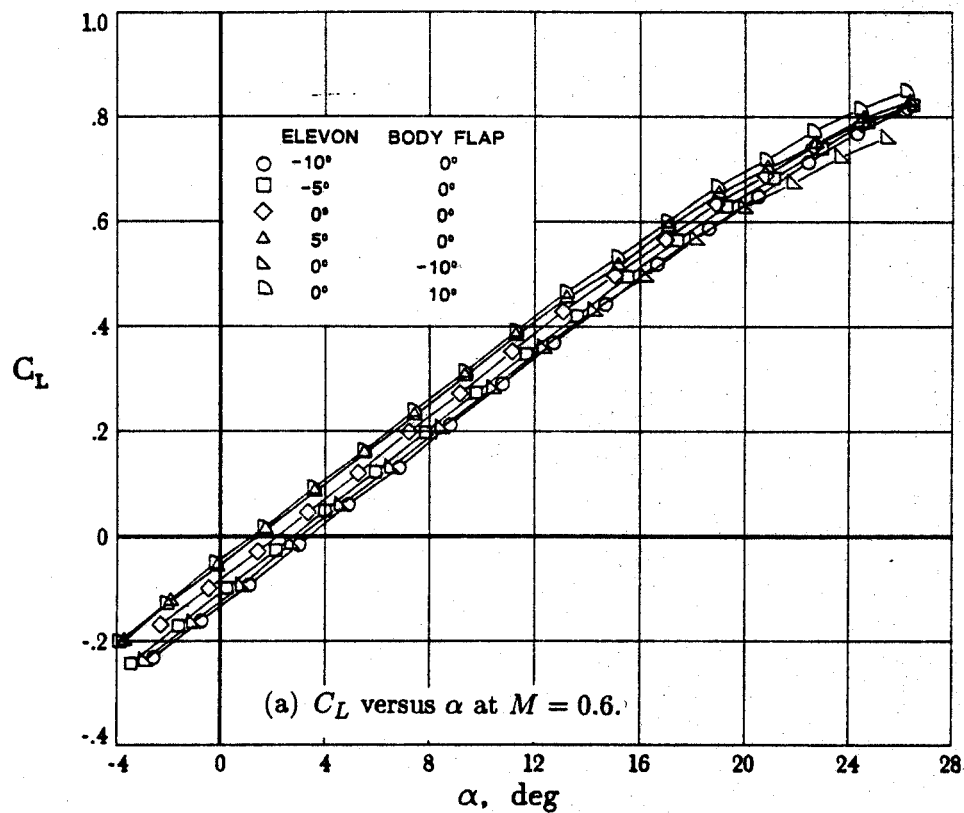


Figure 14. Effect of elevon and body flap on longitudinal aerodynamic characteristics of model at transonic speeds.

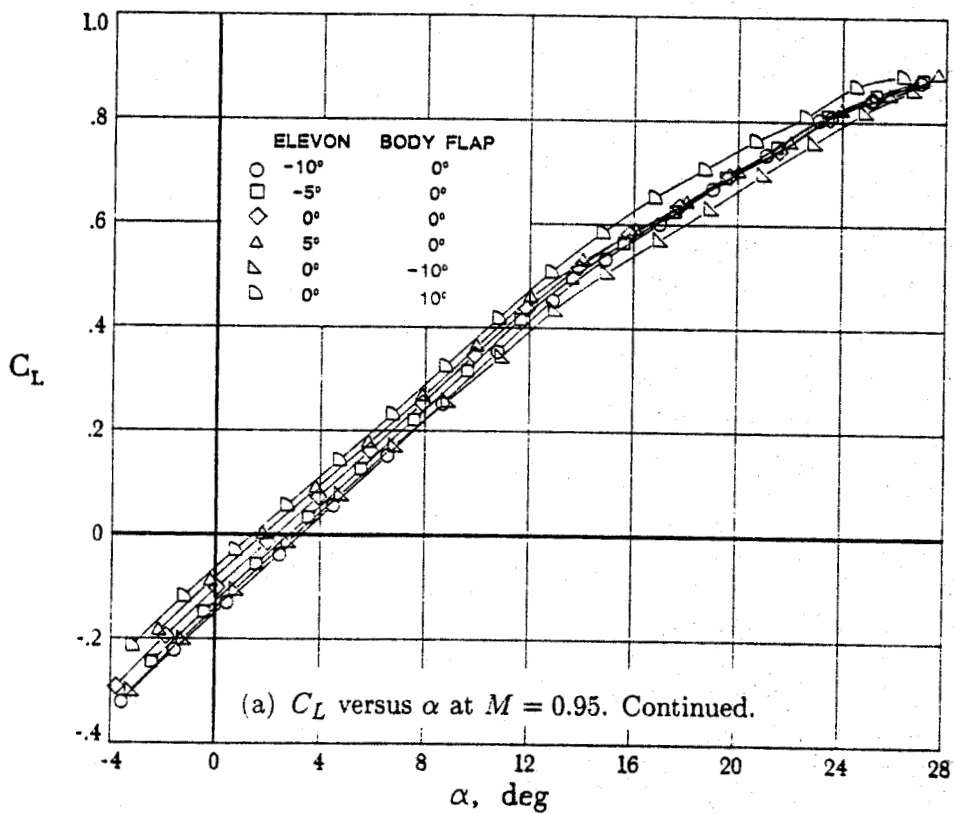
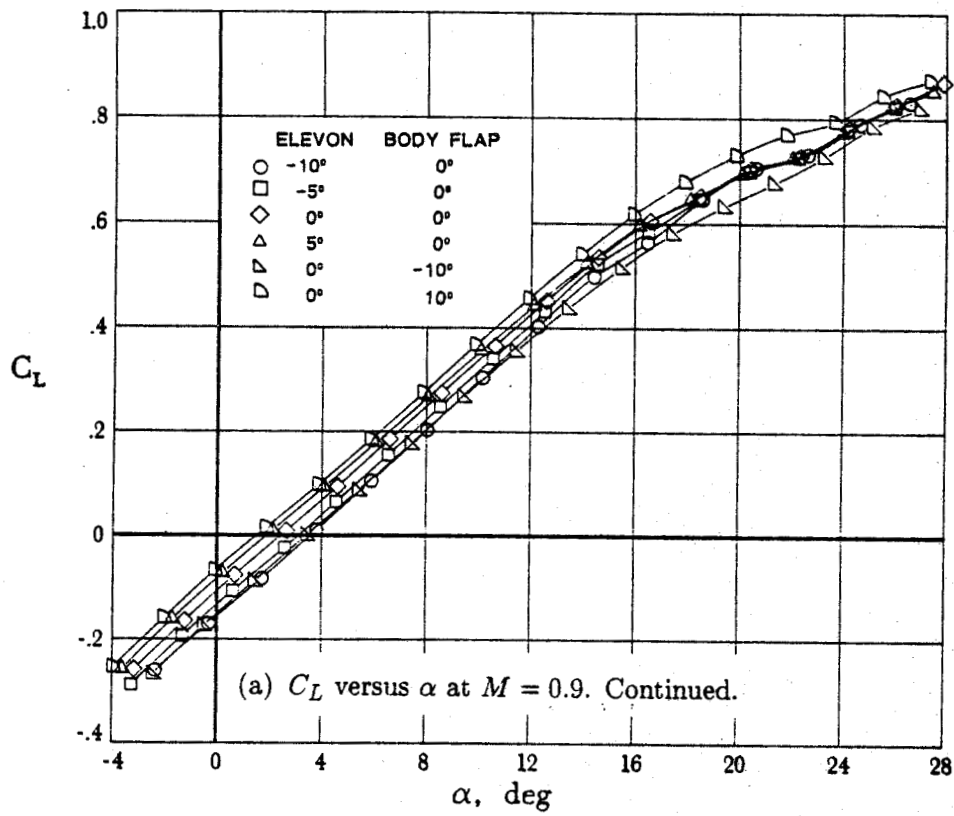


Figure 14. Continued.

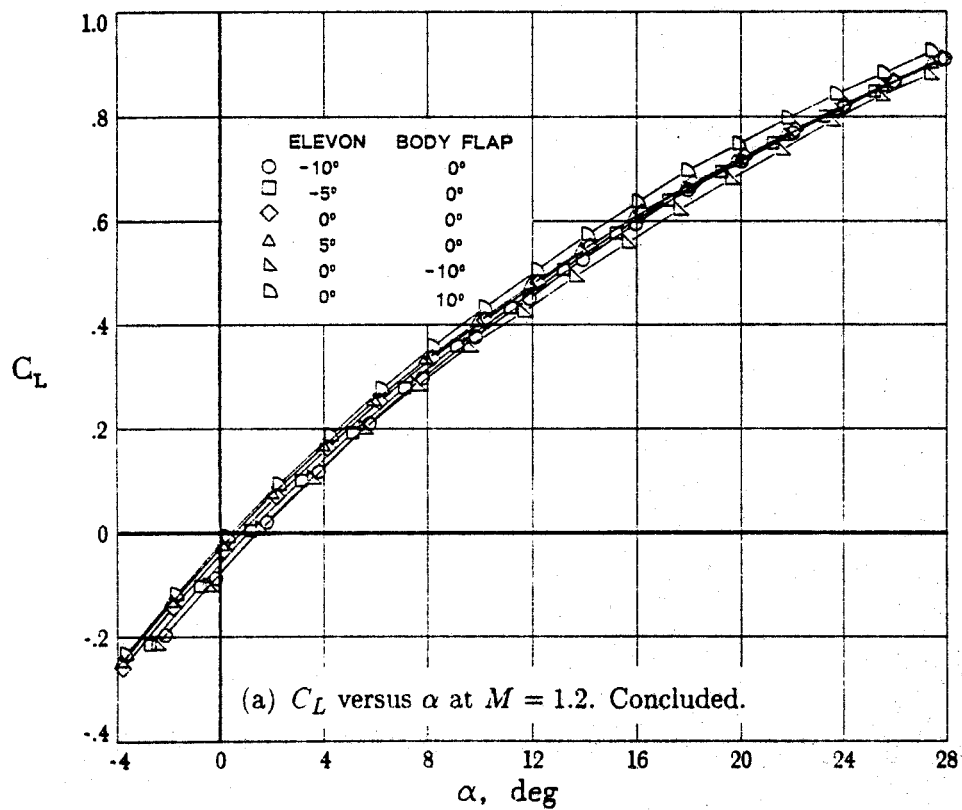
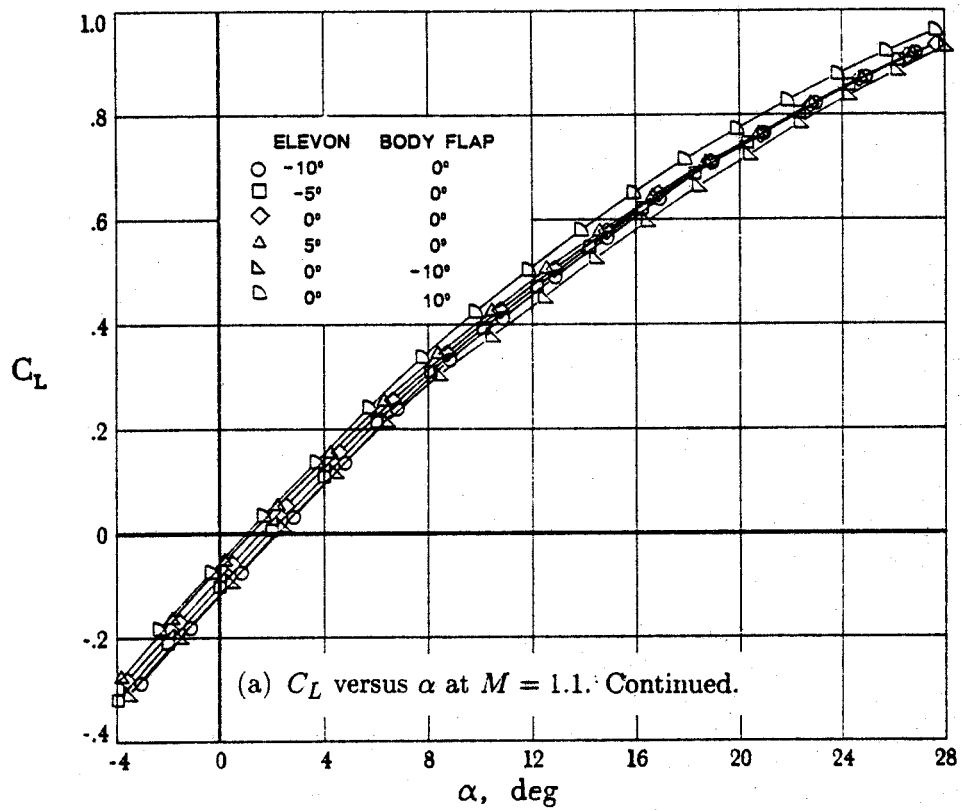


Figure 14. Continued.

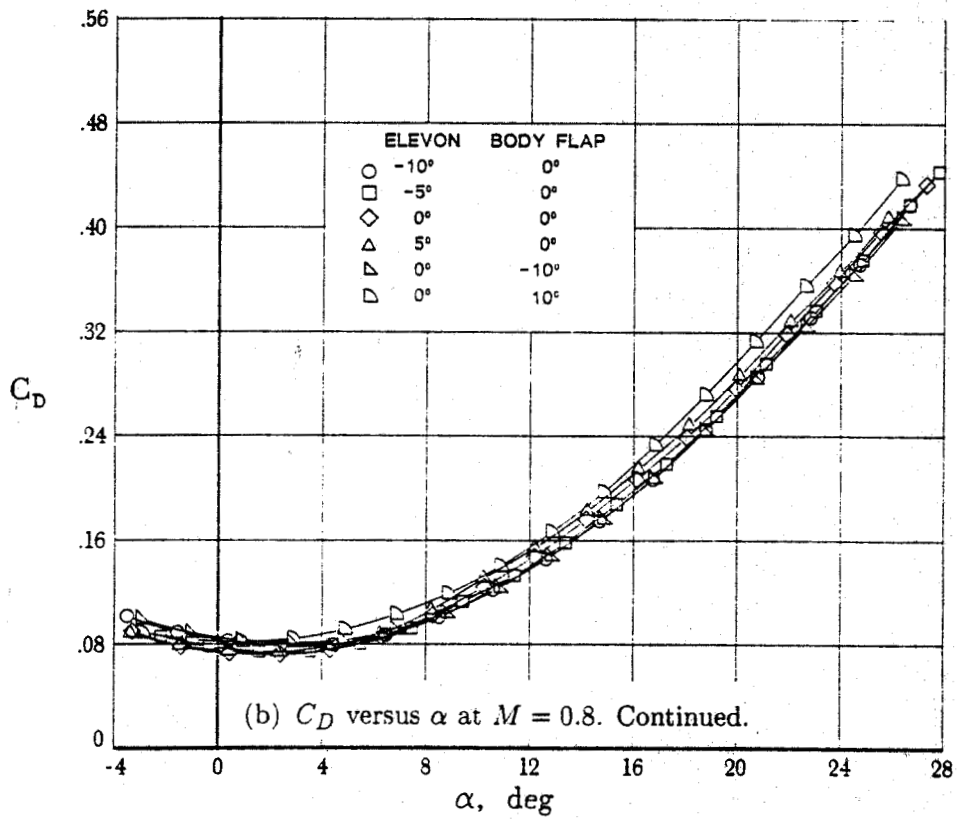
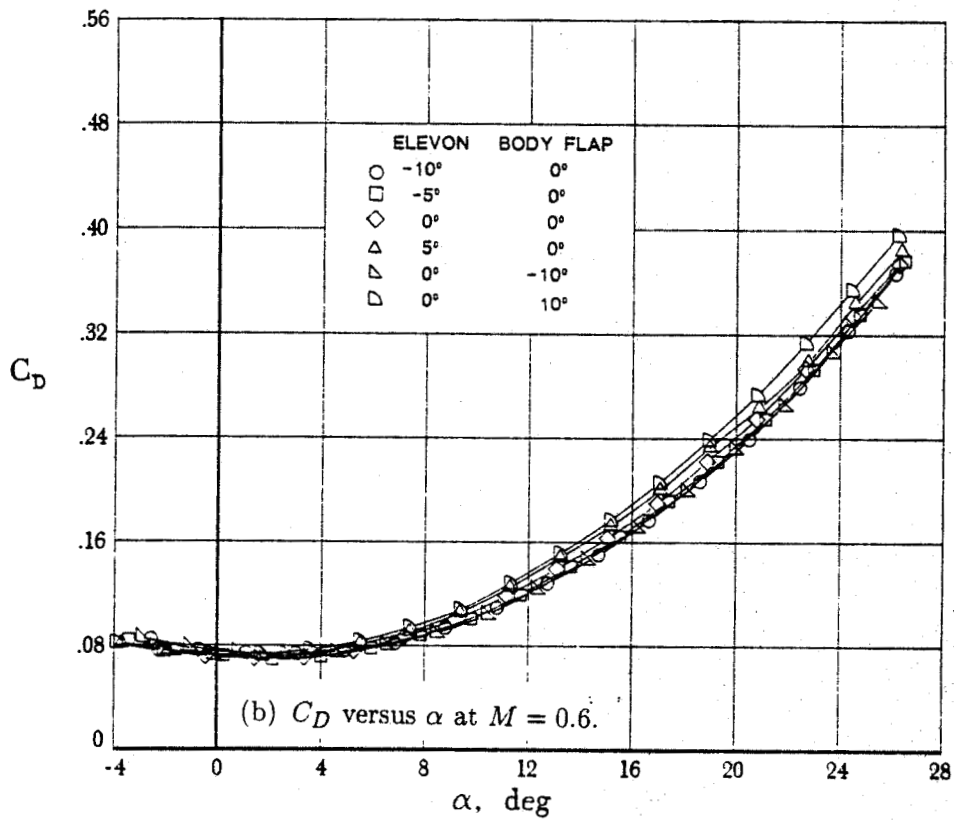


Figure 14. Continued.

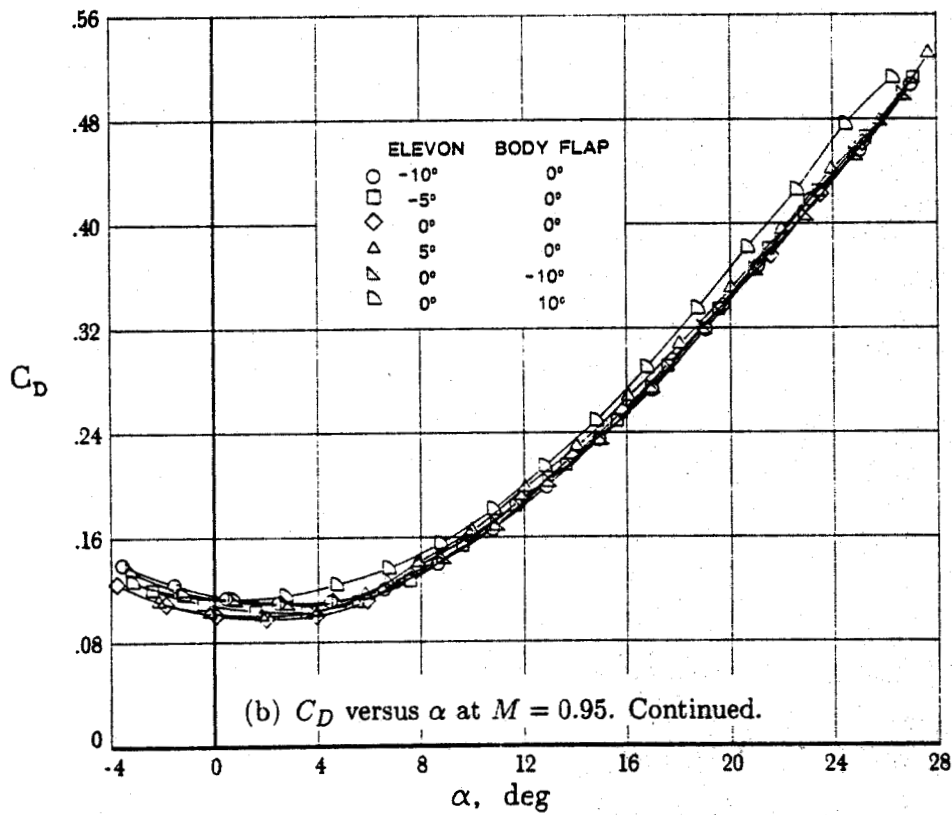
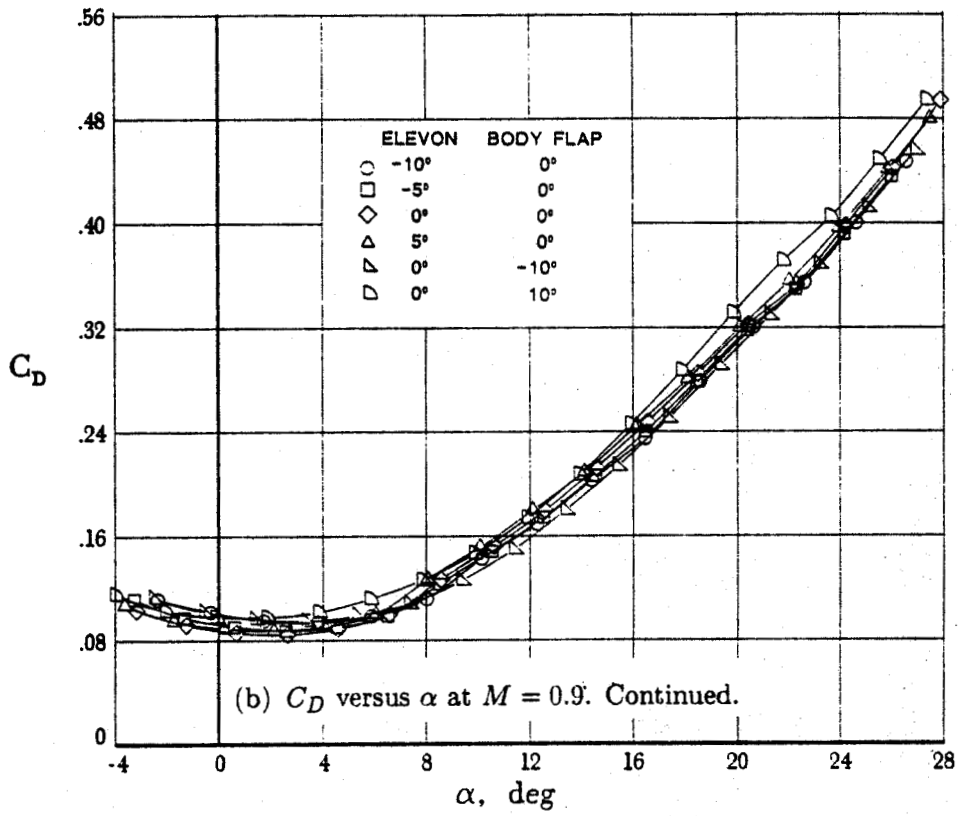


Figure 14. Continued.

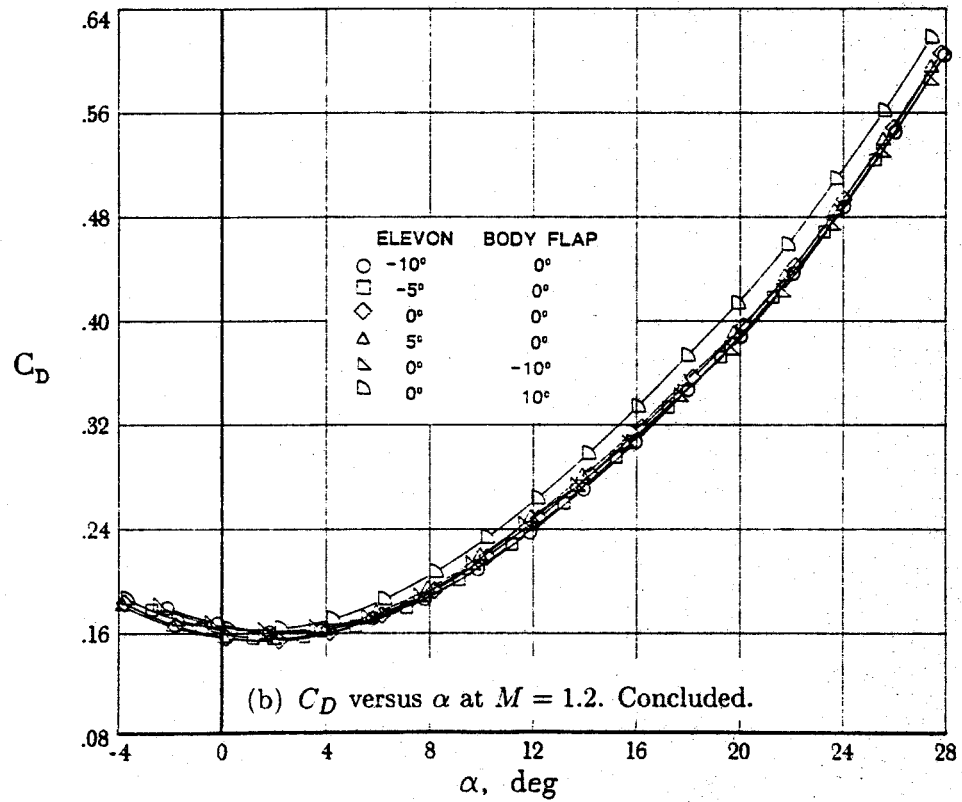
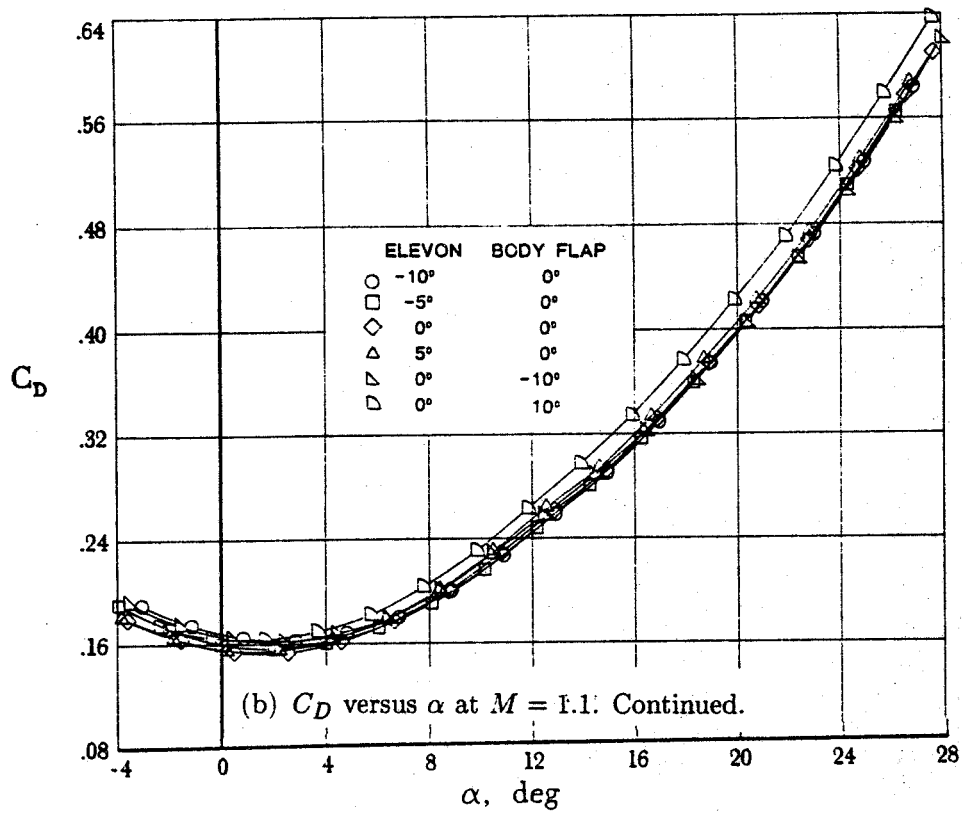


Figure 14. Continued.

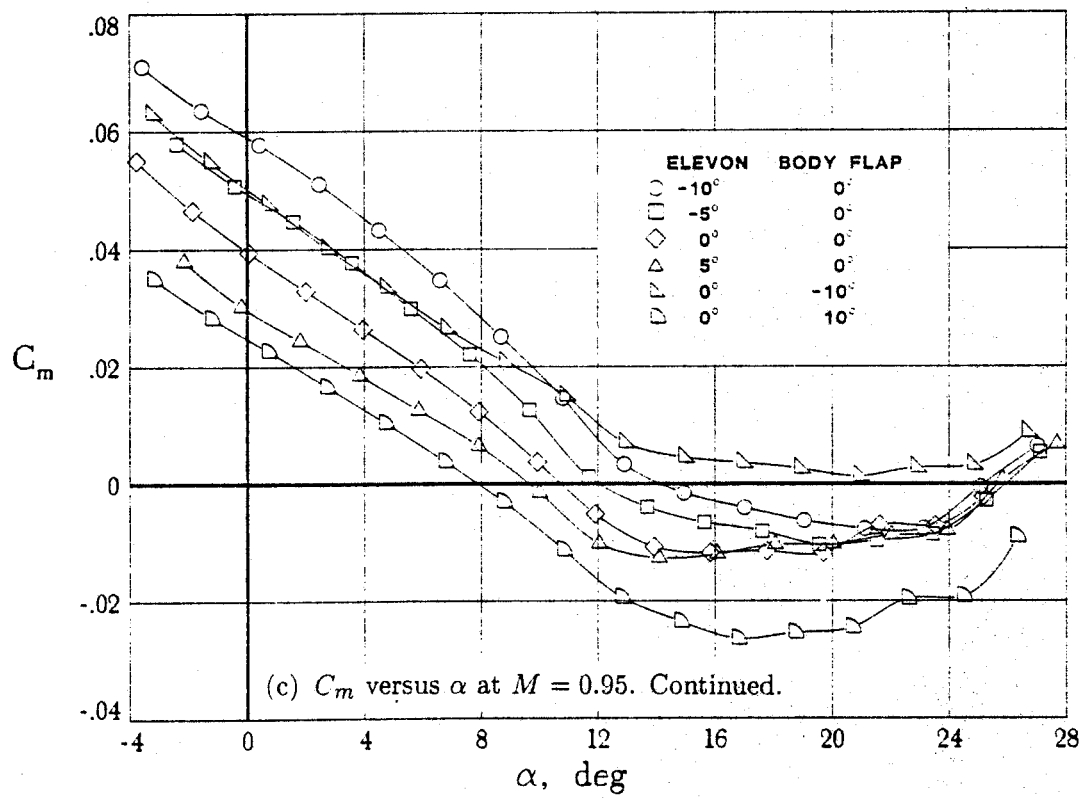
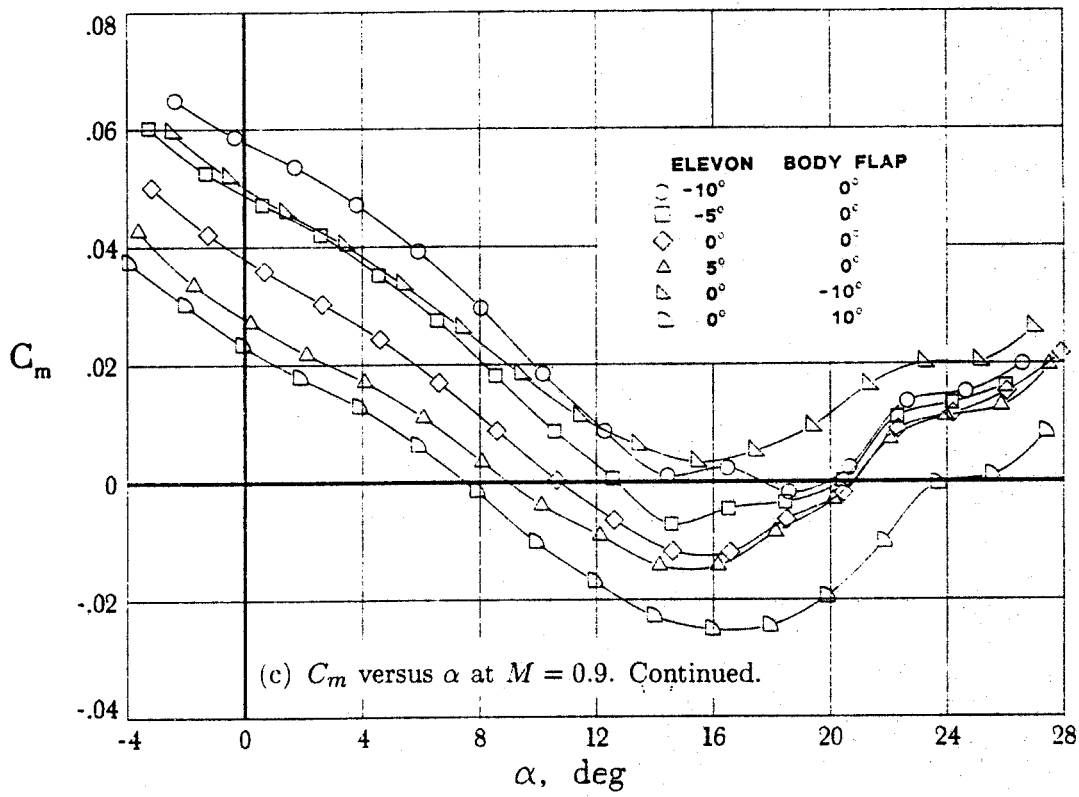


Figure 14. Continued.

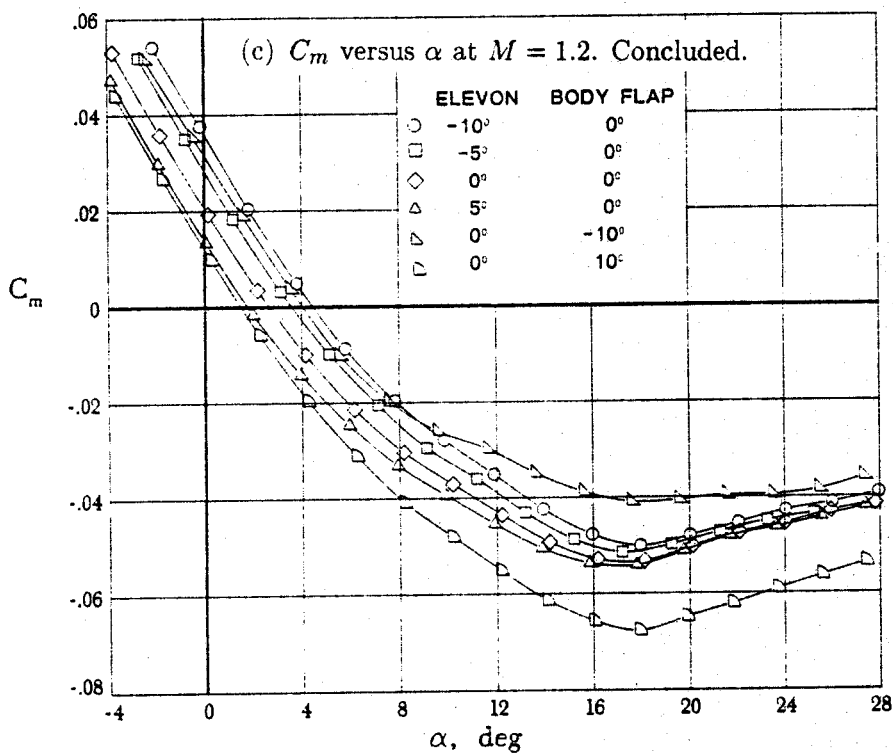
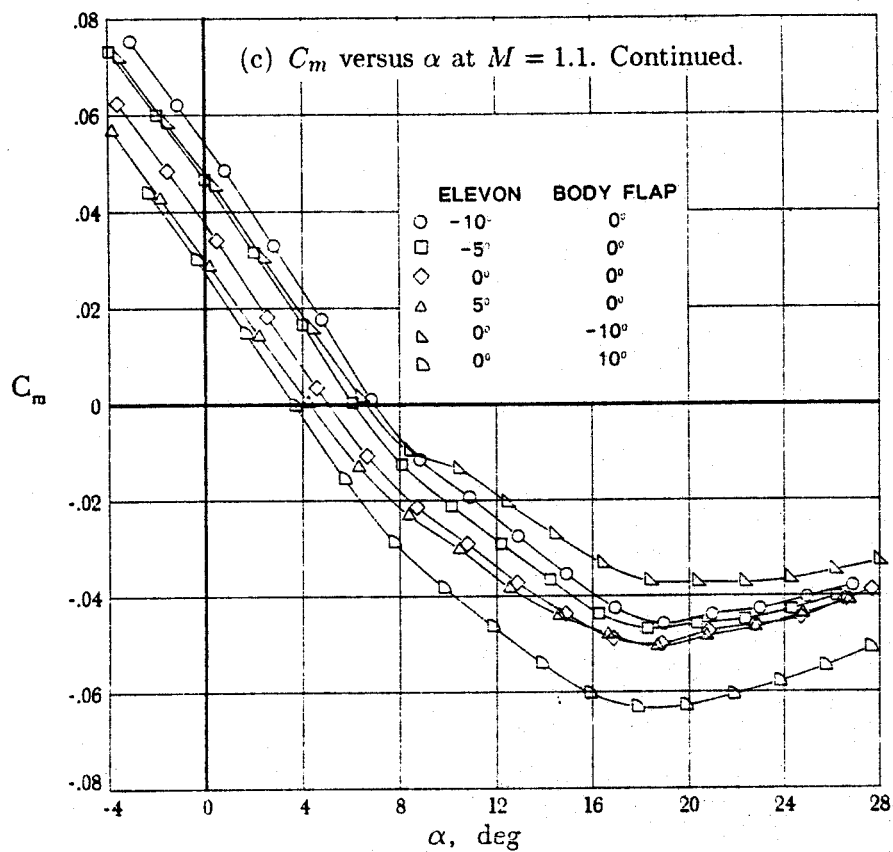


Figure 14. Continued.

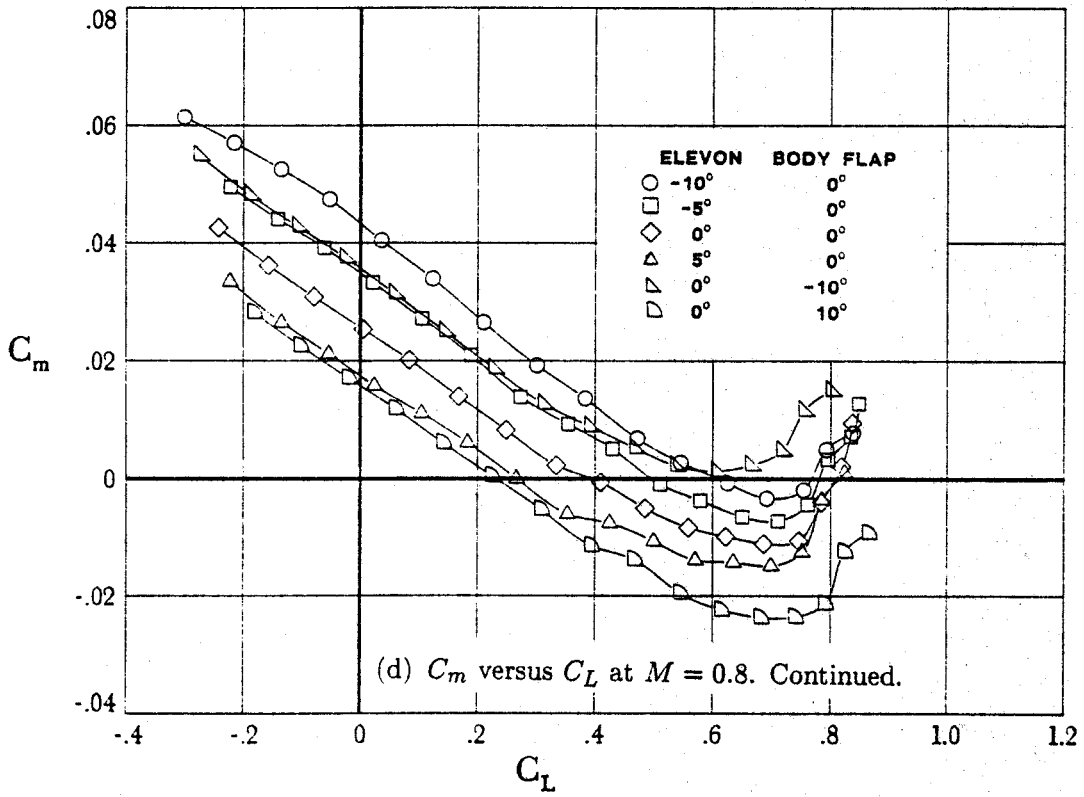
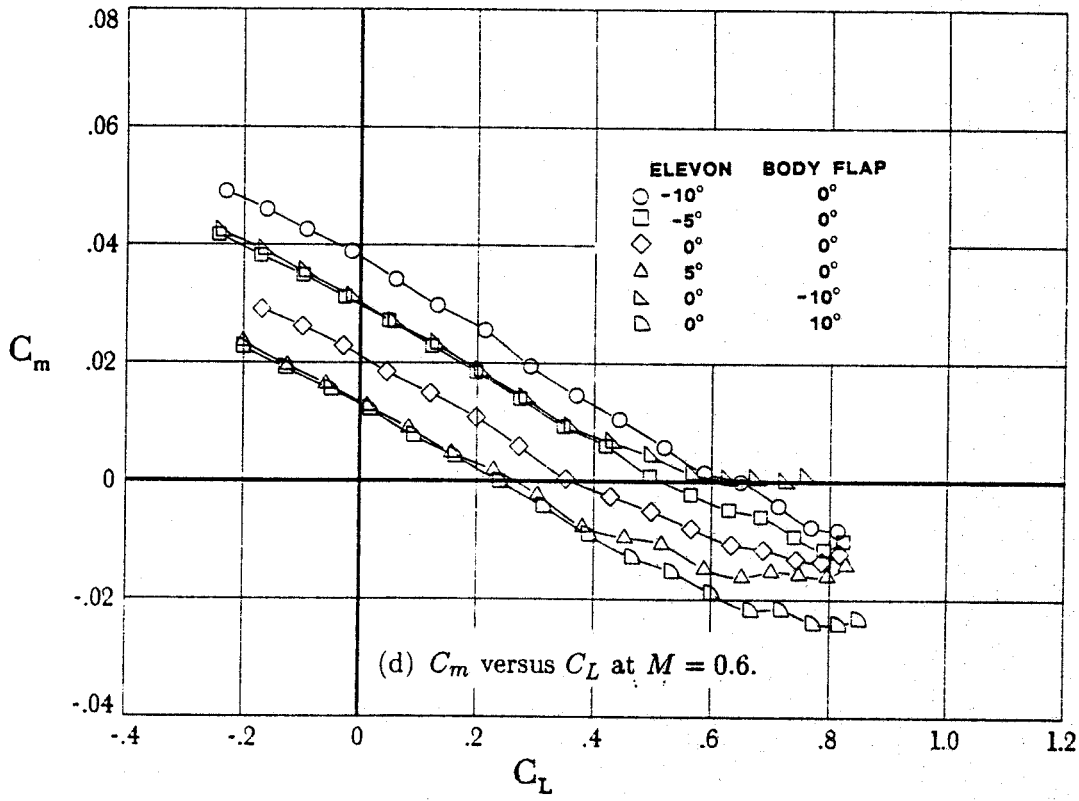


Figure 14. Continued.

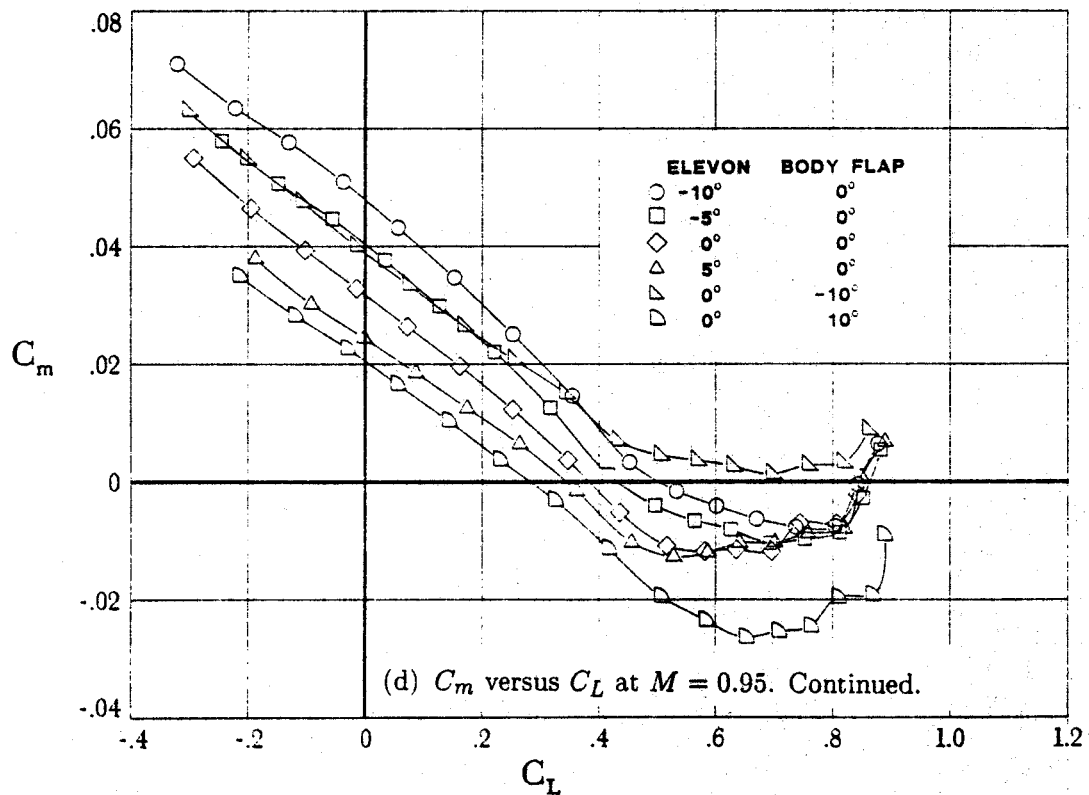
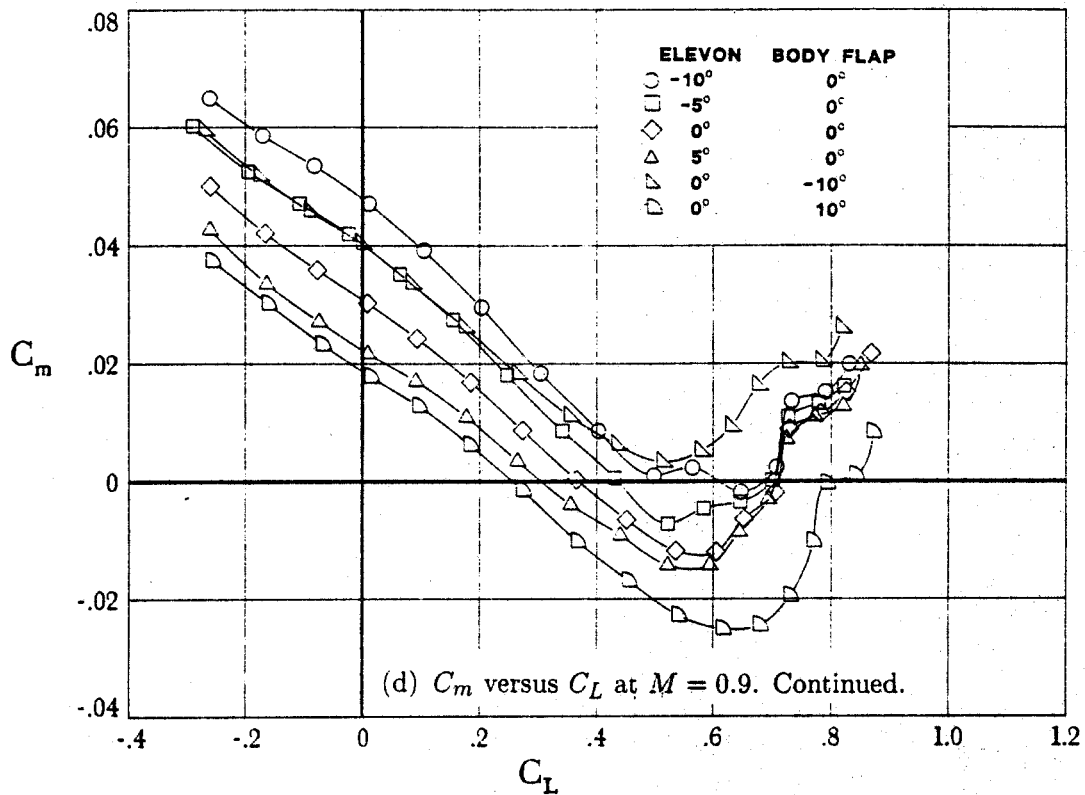


Figure 14. Continued.

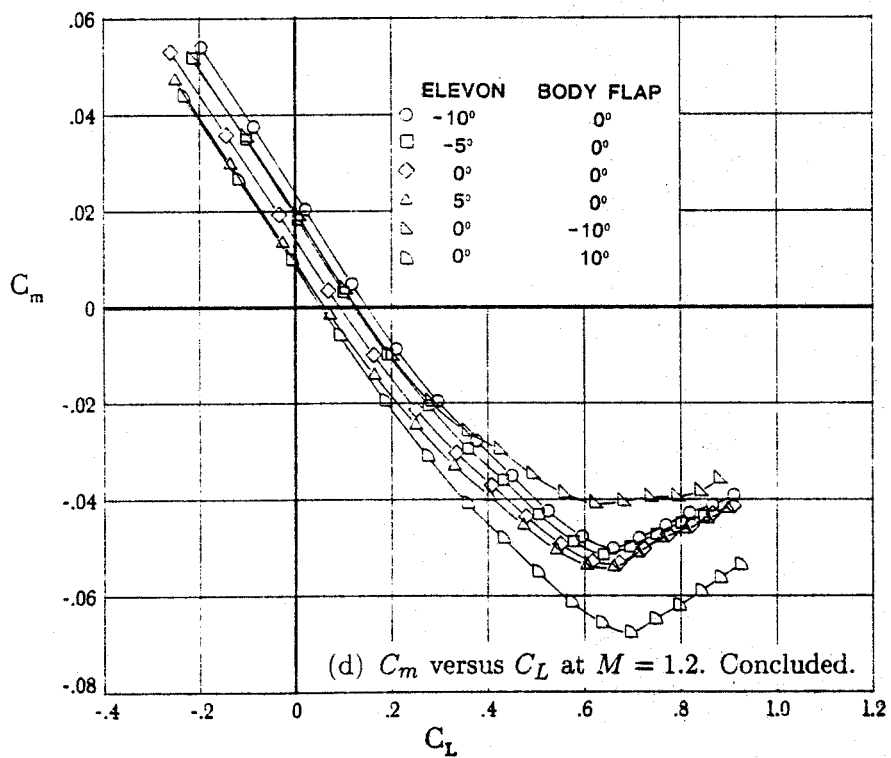
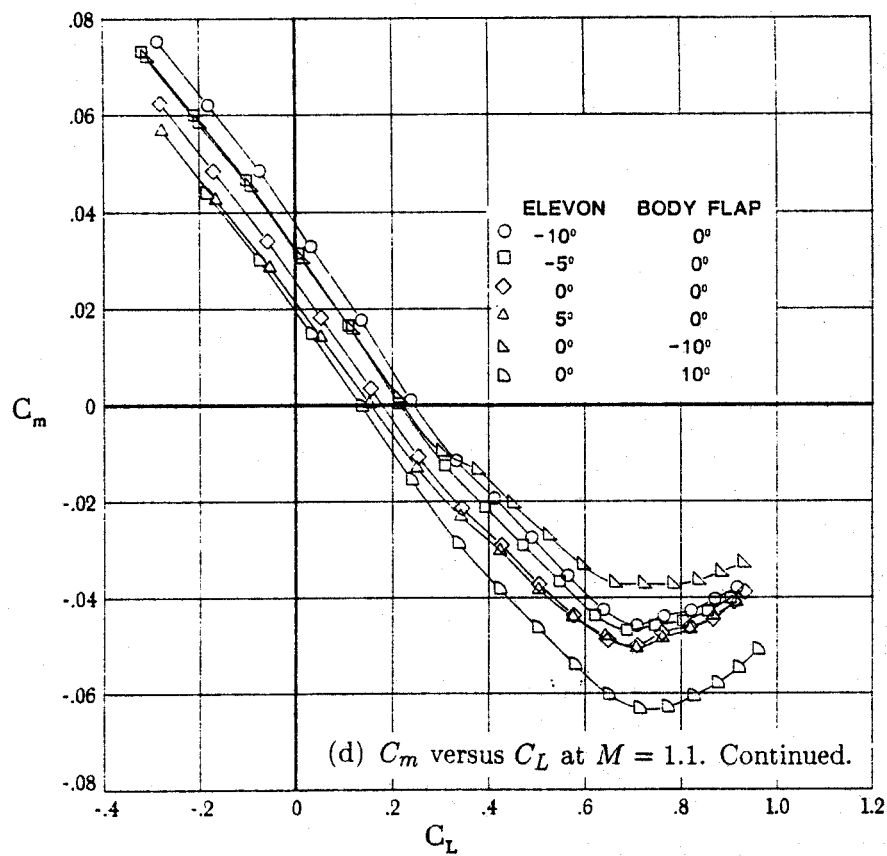


Figure 14. Continued.

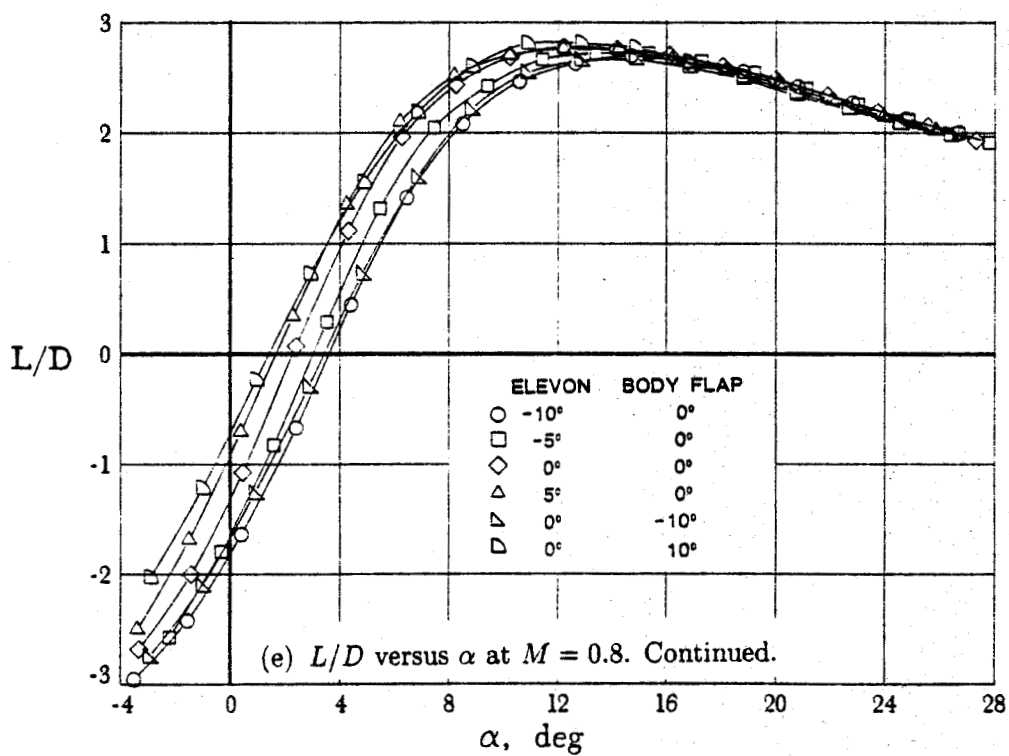
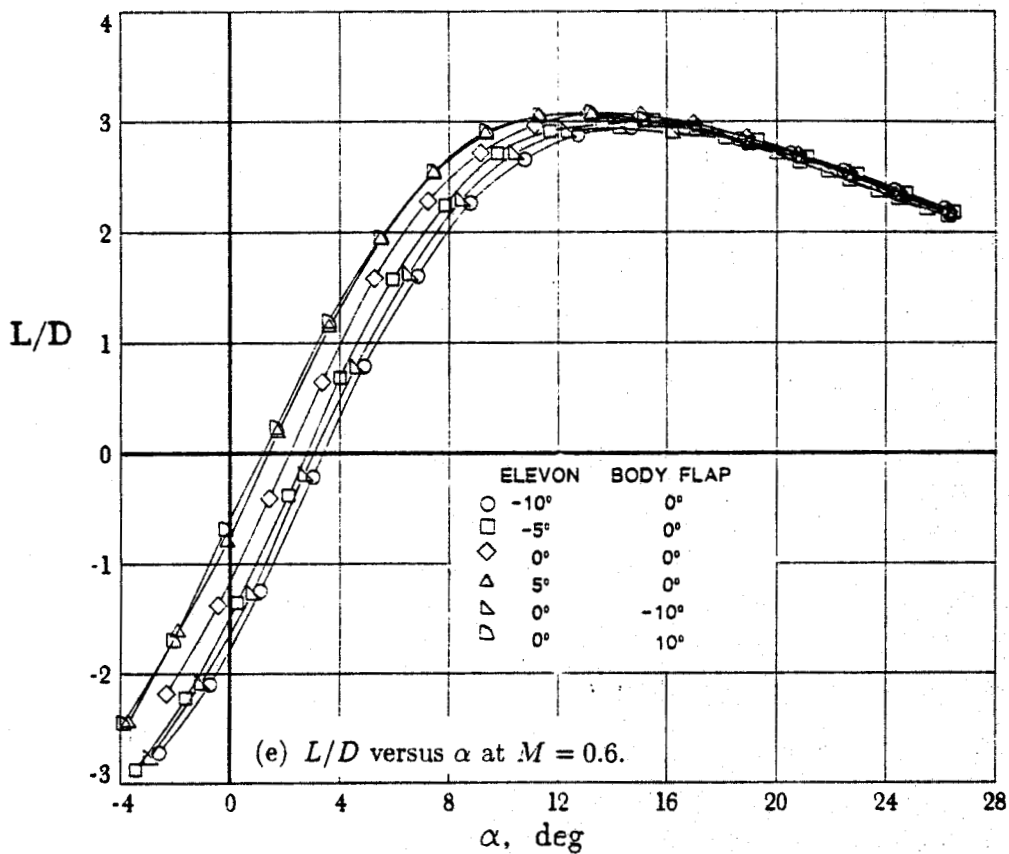


Figure 14. Continued.

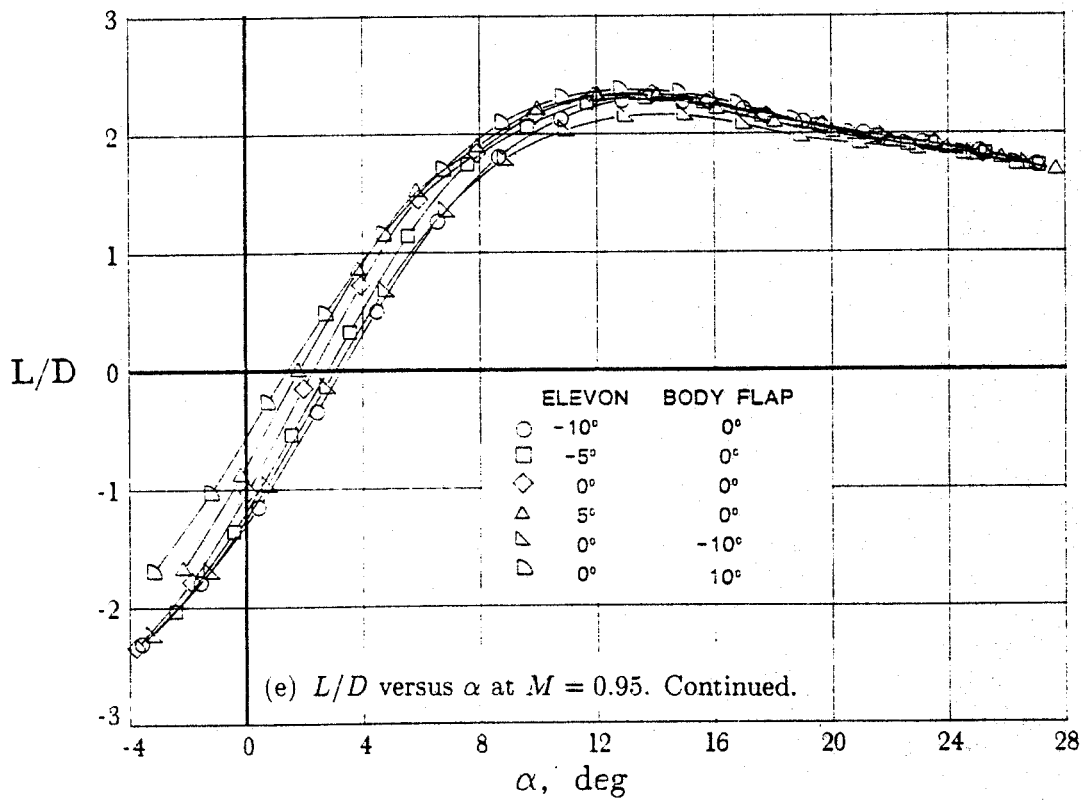
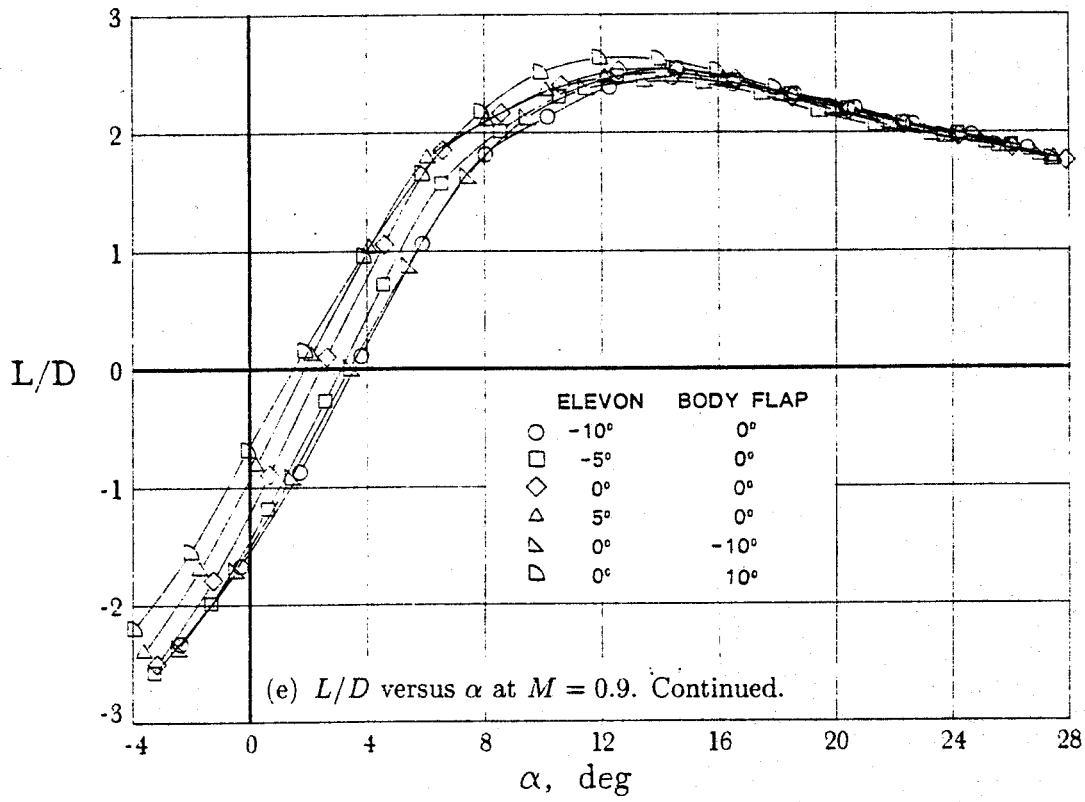


Figure 14. Continued.

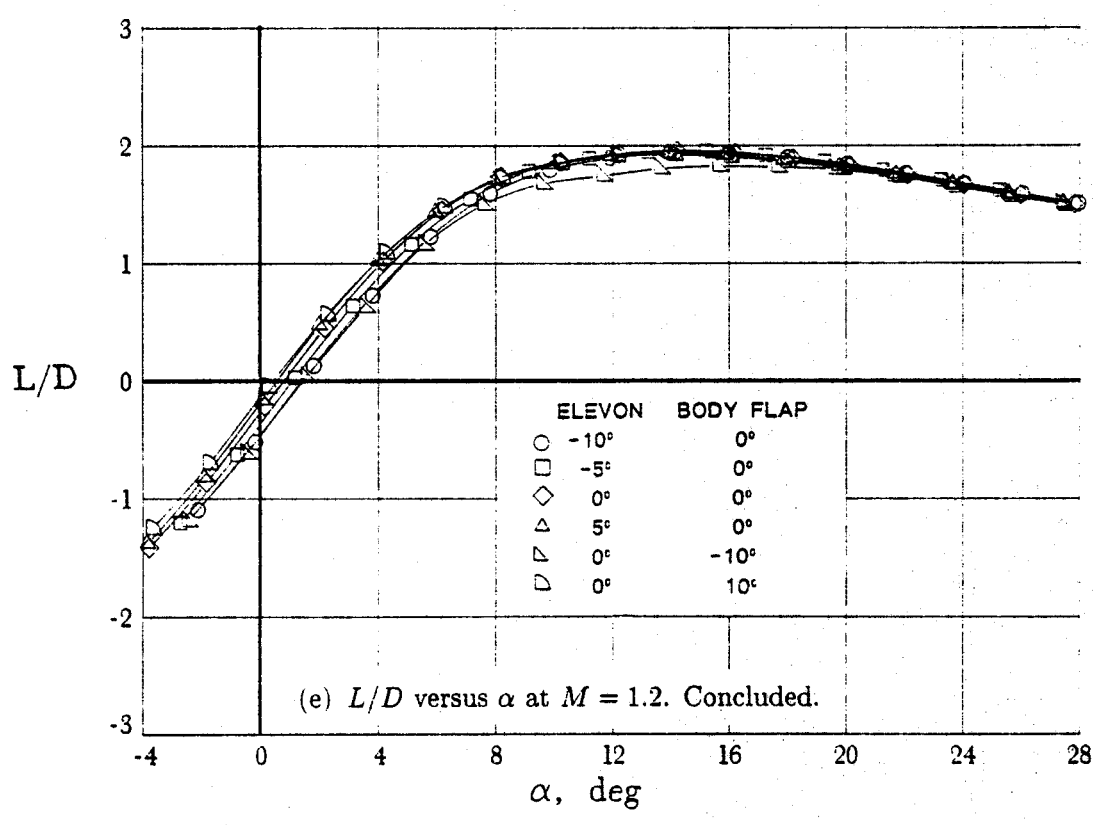
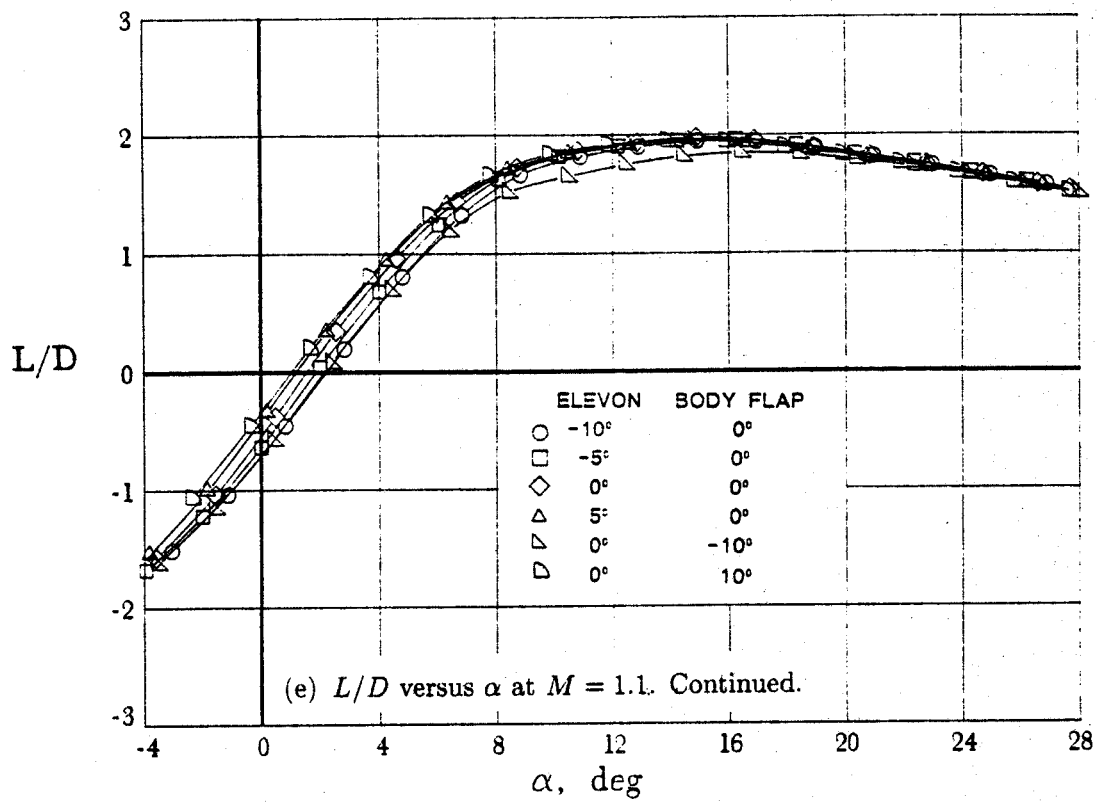


Figure 14. Concluded.

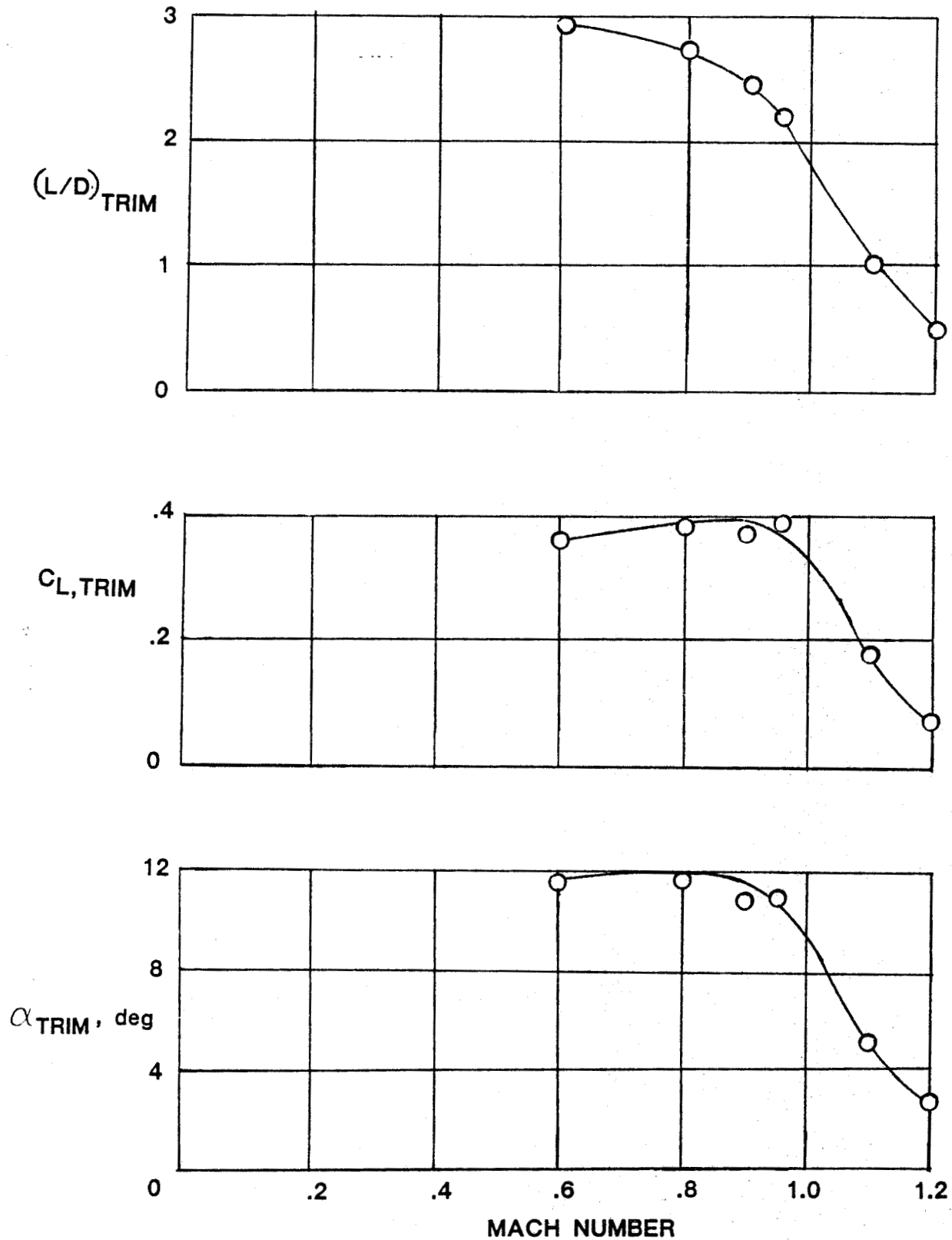


Figure 15. Variation of transonic longitudinal trim characteristics of baseline configuration with Mach number. No controls deflected.

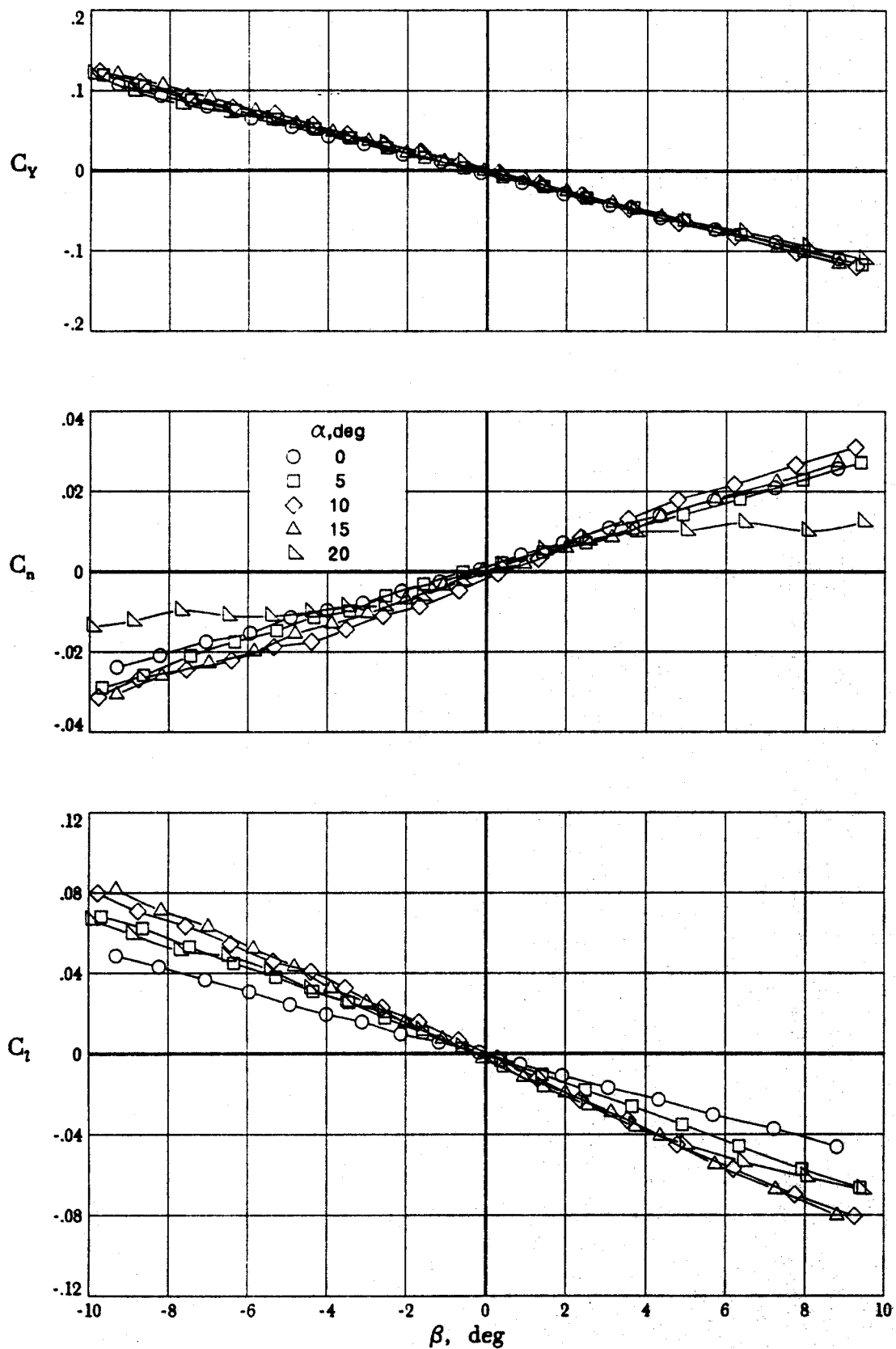
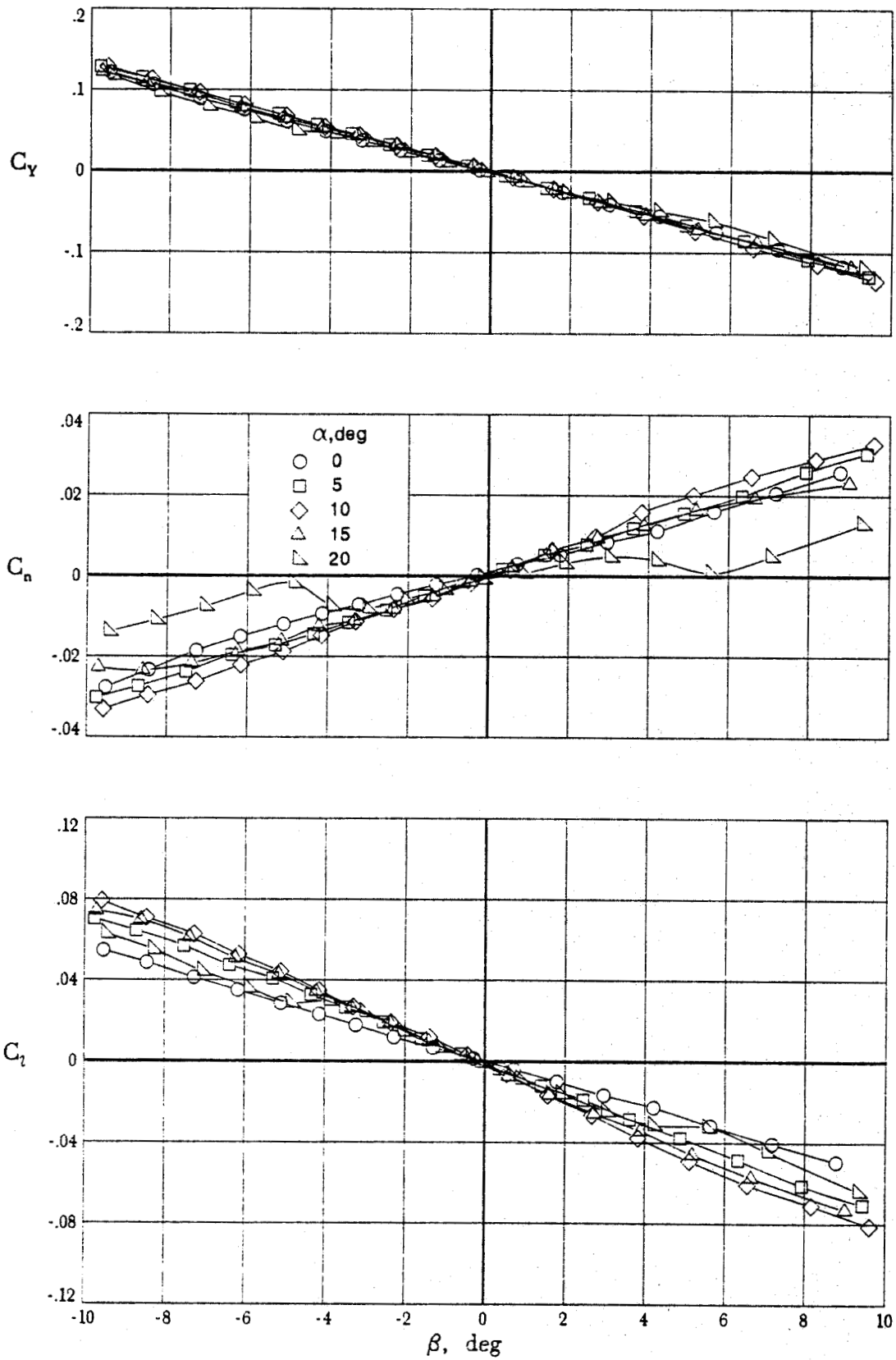
(a) $M = 0.6$.

Figure 16. Variation of transonic lateral aerodynamic characteristics with sideslip.



(b) $M = 0.8$.

Figure 16. Continued.

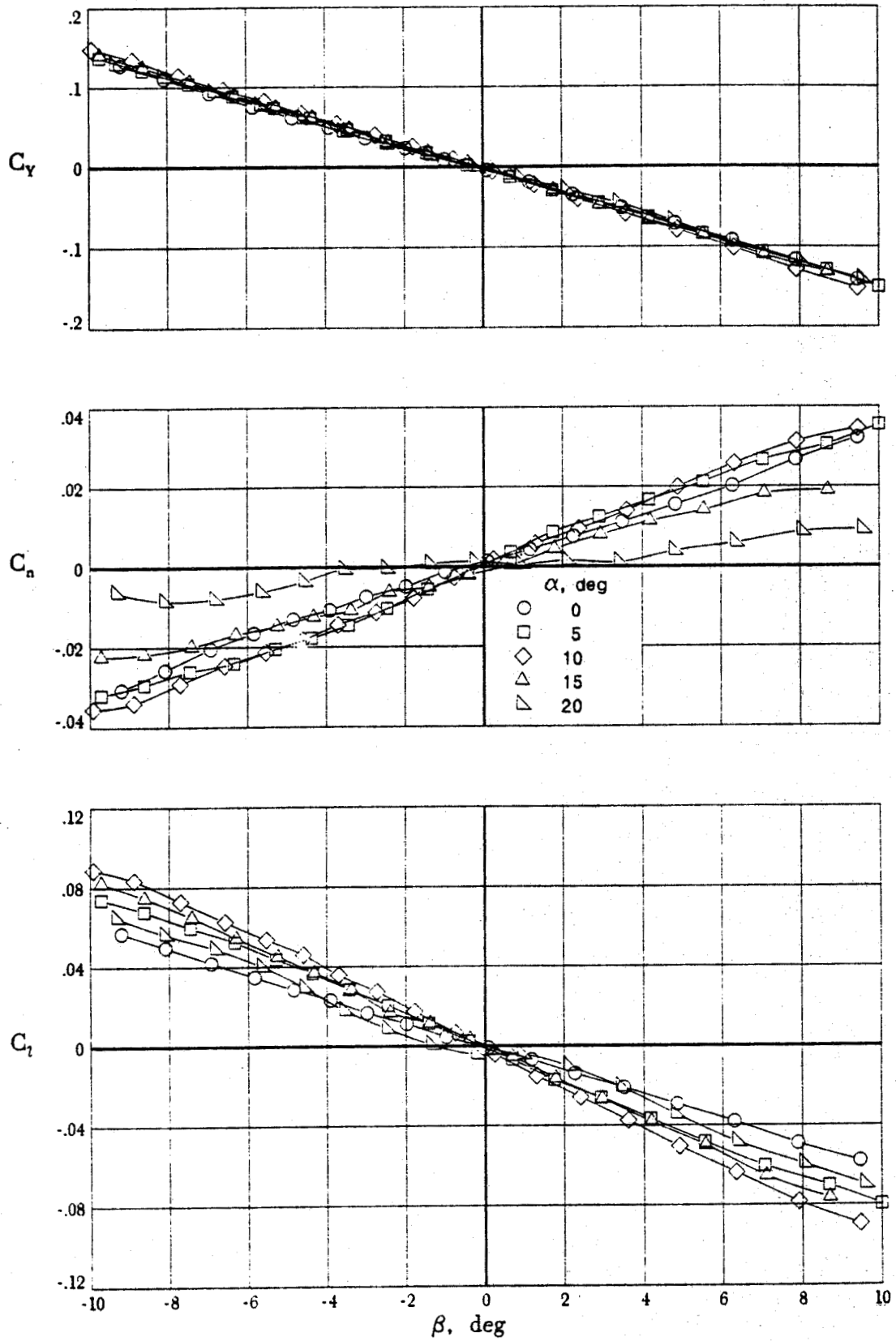
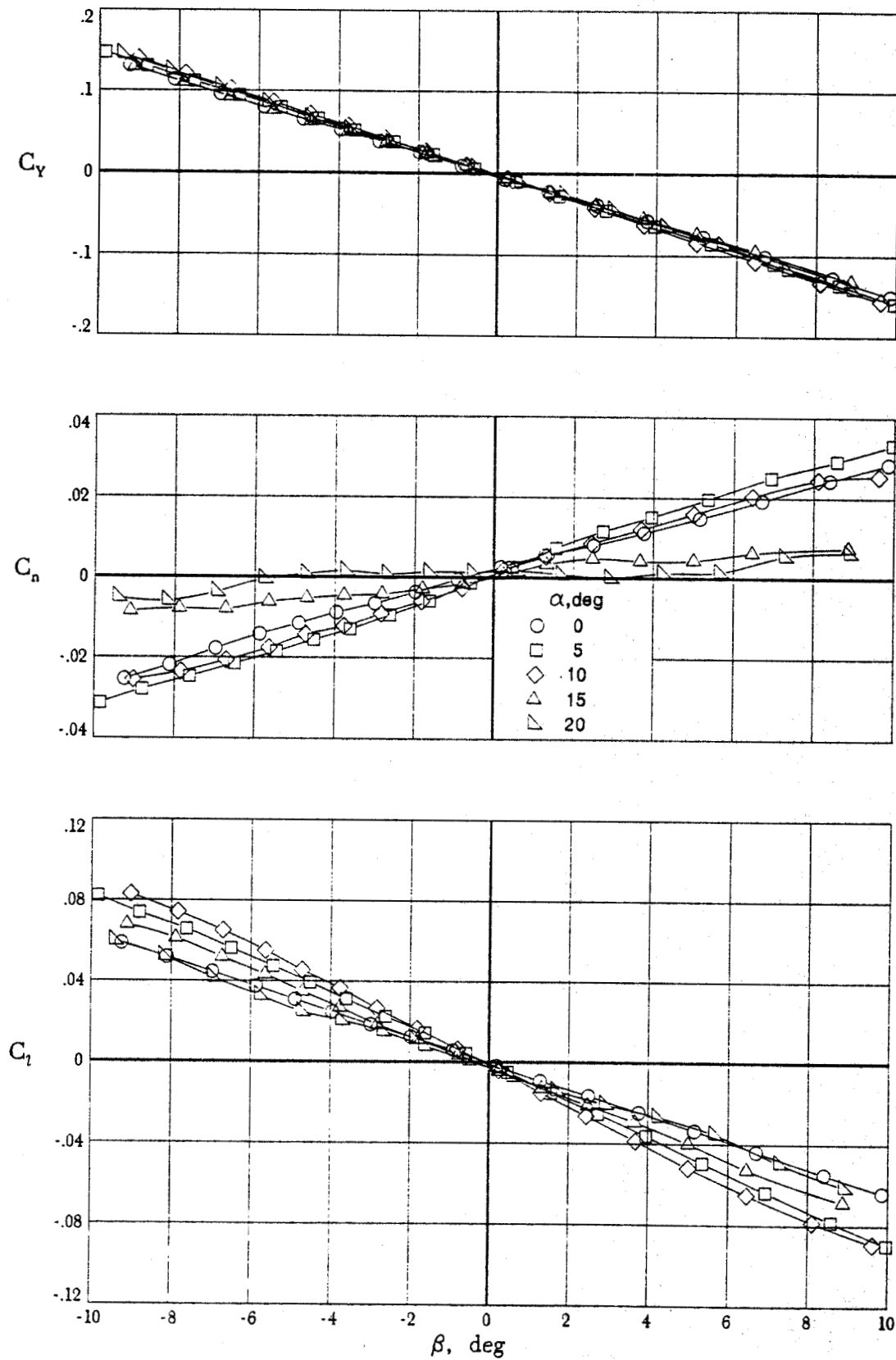
(c) $M = 0.9$.

Figure 16. Continued.



(d) $M = 0.95$.

Figure 16. Continued.

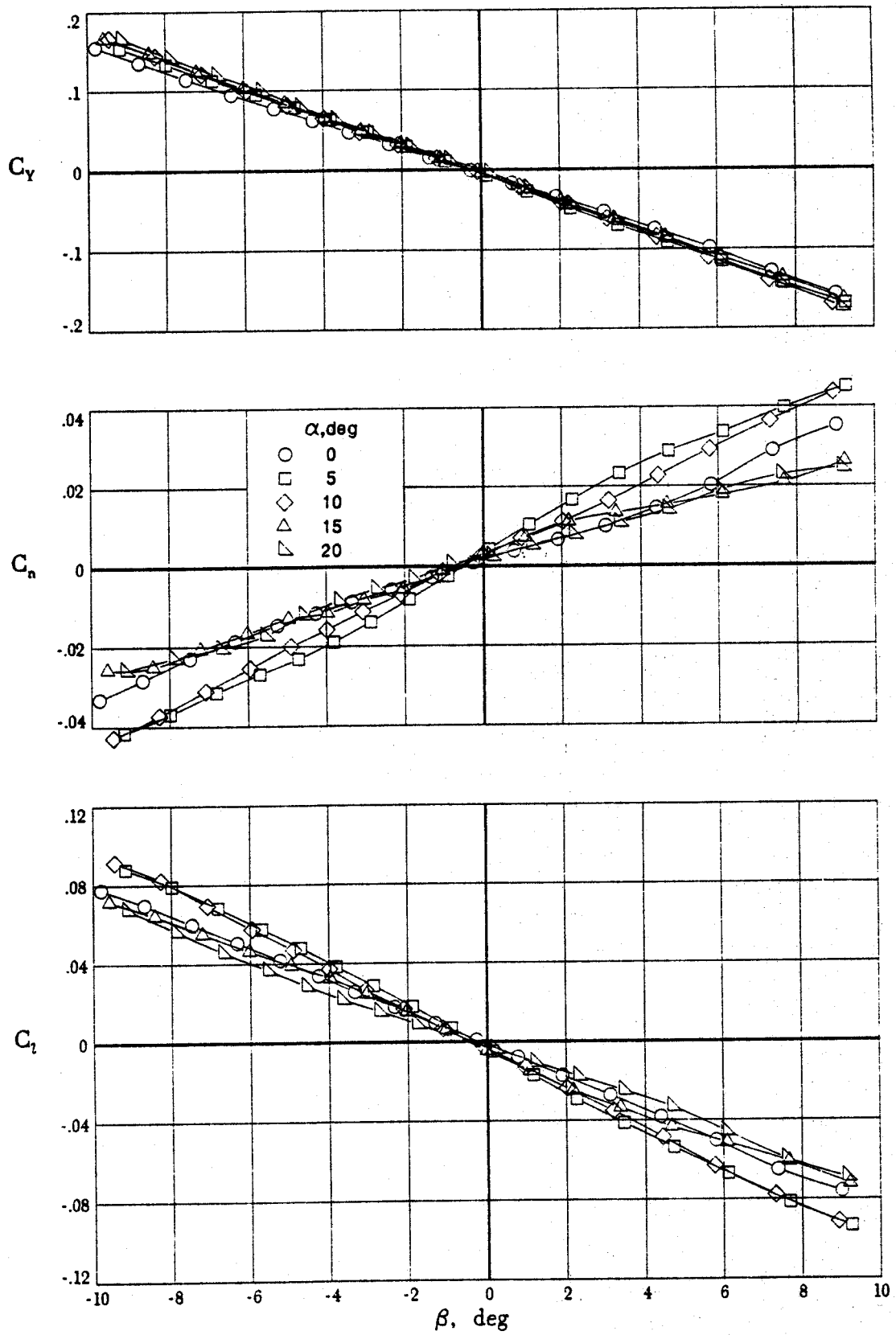
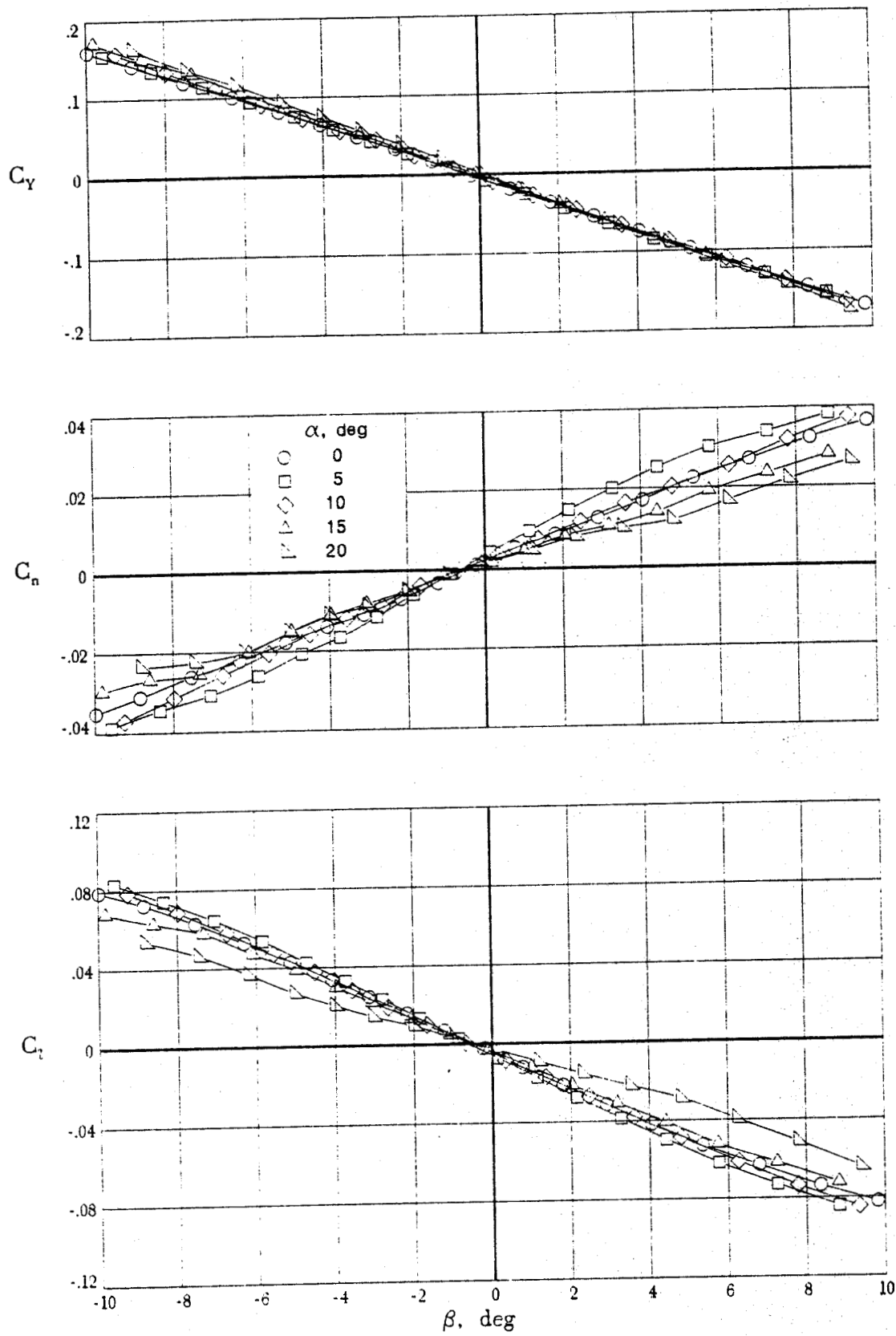
(e) $M = 1.1$.

Figure 16. Continued.



(f) $M = 1.2$.

Figure 16. Concluded.

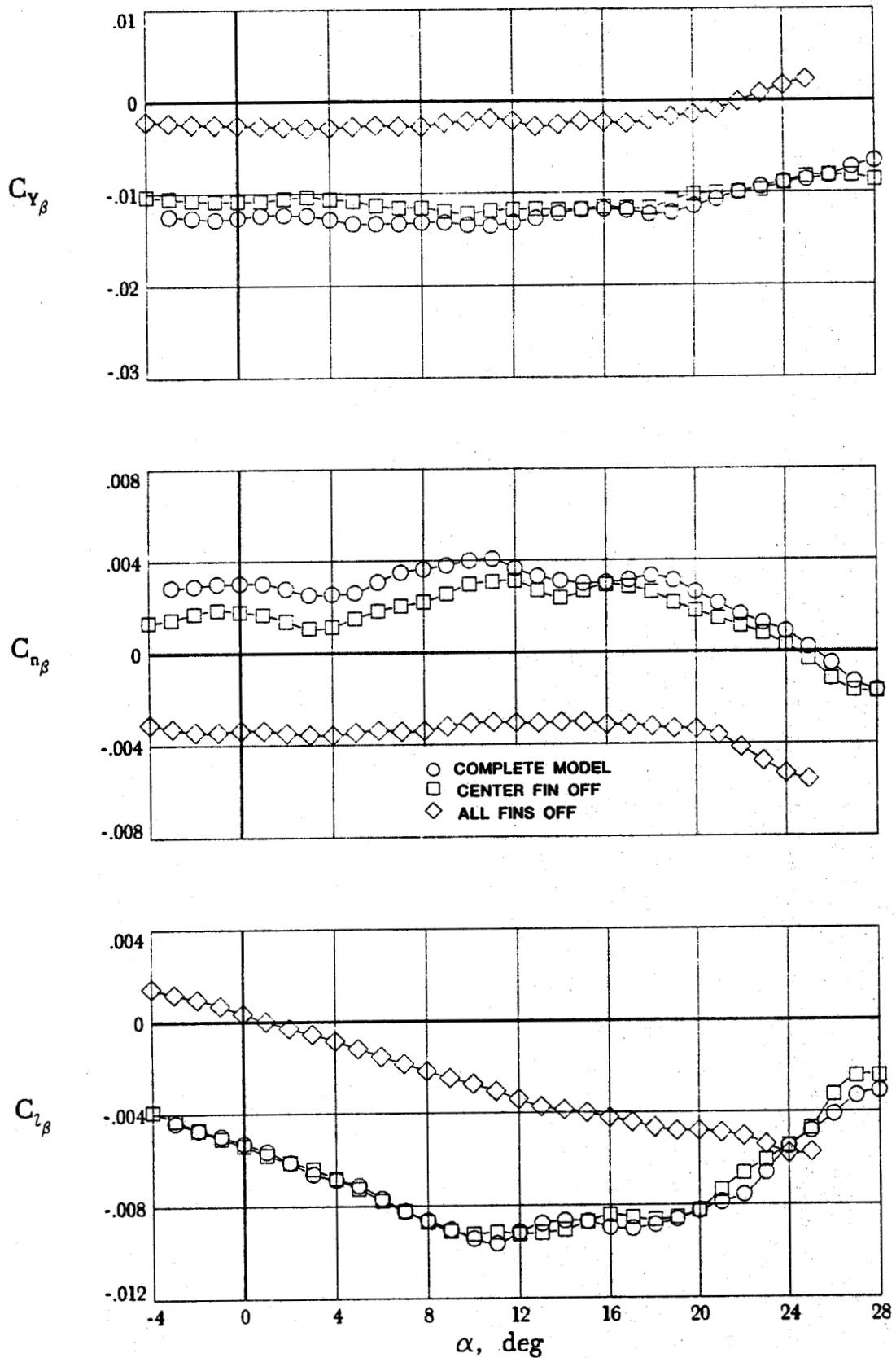
(a) $M = 0.6$.

Figure 17. Effect of fins on transonic lateral-directional stability characteristics.

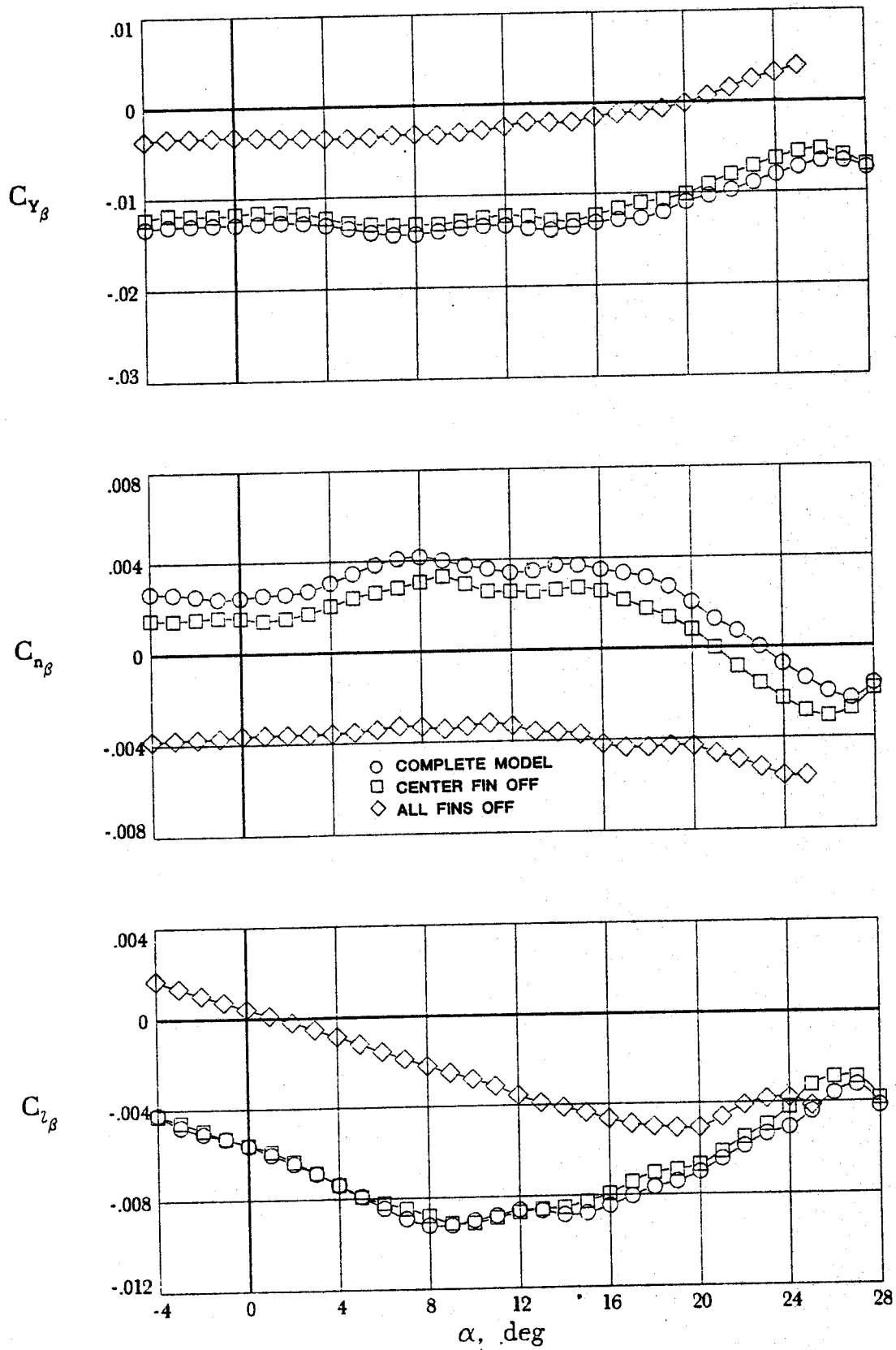
(b) $M = 0.8$.

Figure 17. Continued.

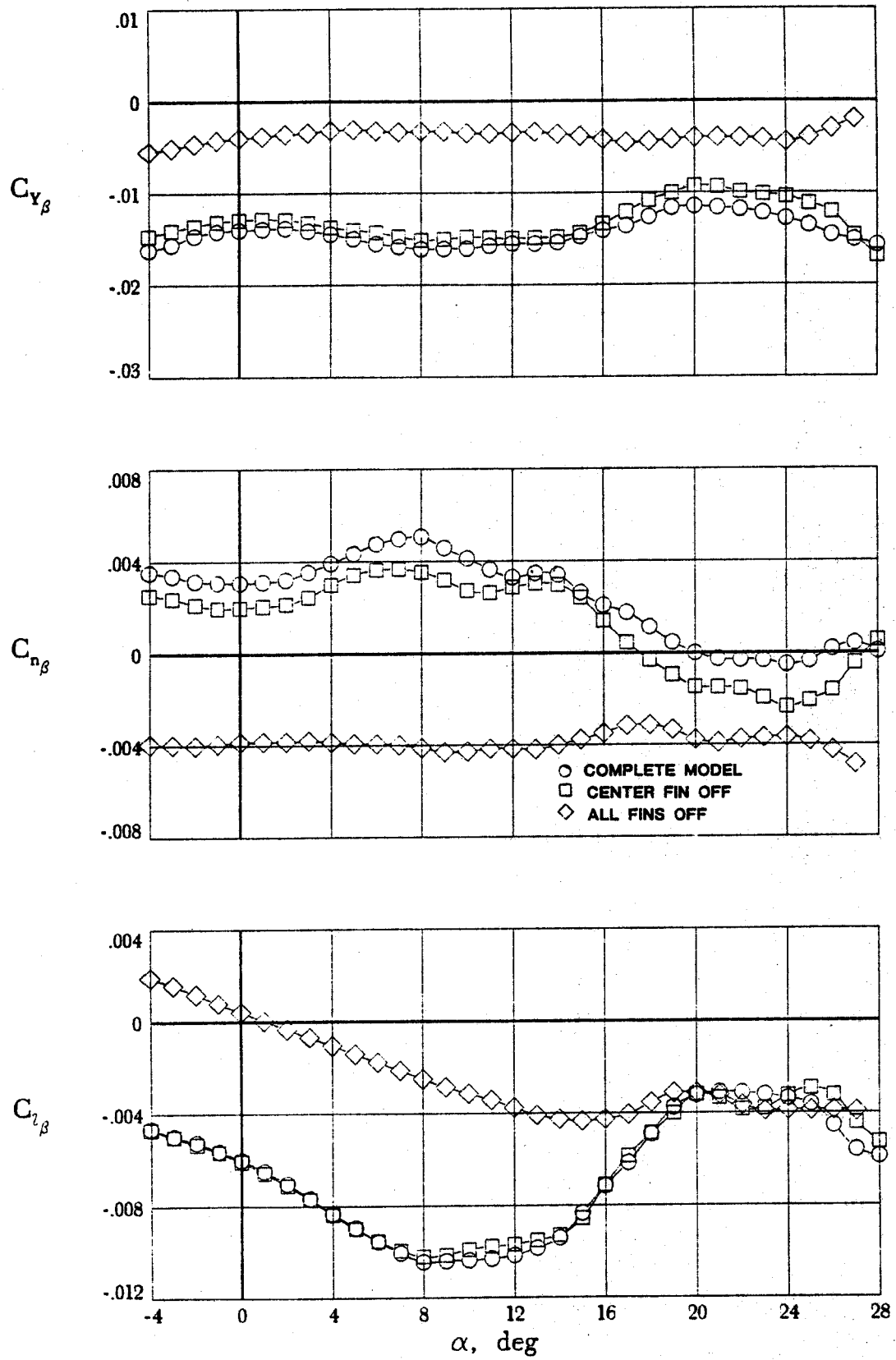
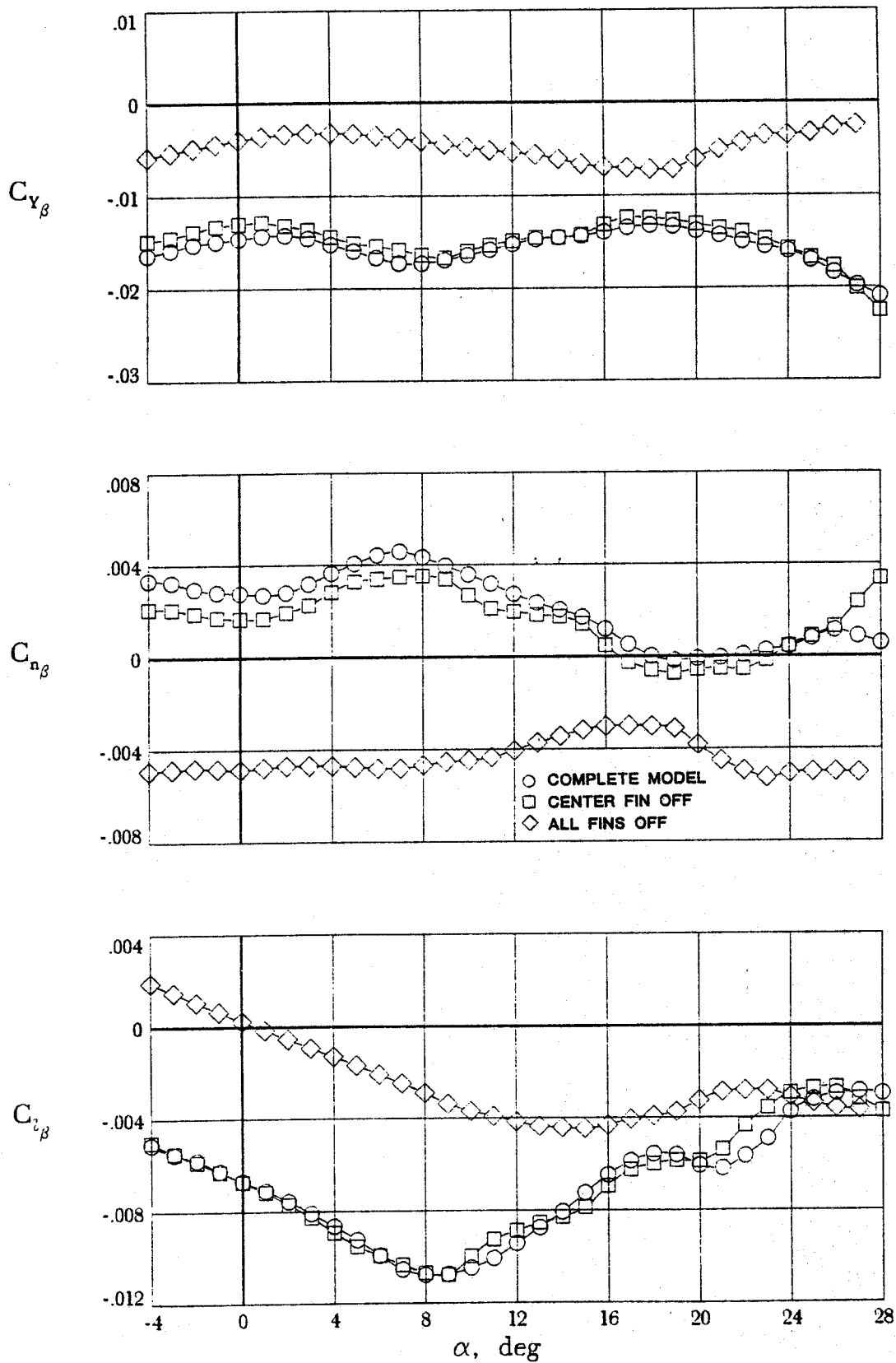
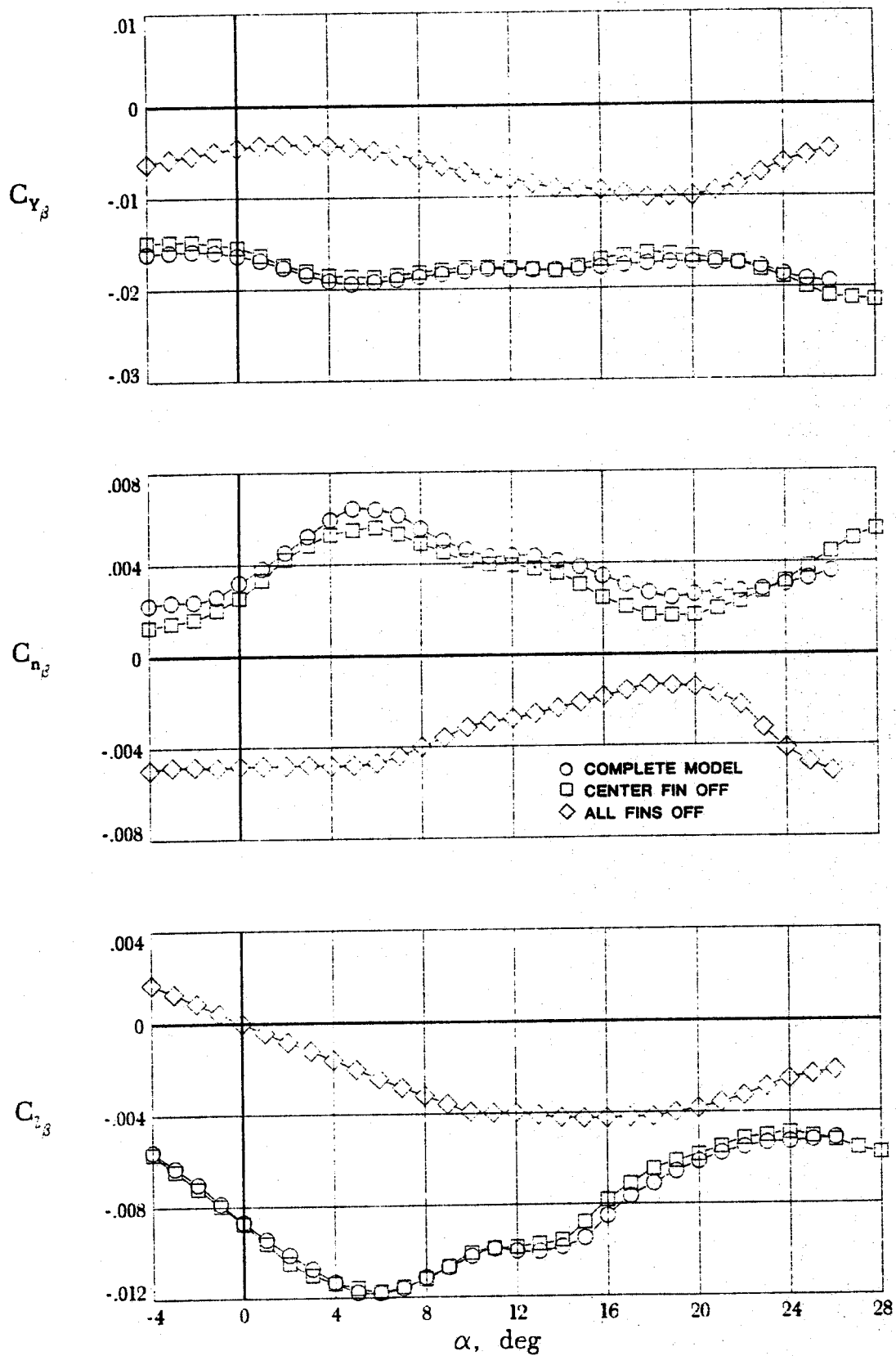
(c) $M = 0.9$.

Figure 17. Continued.



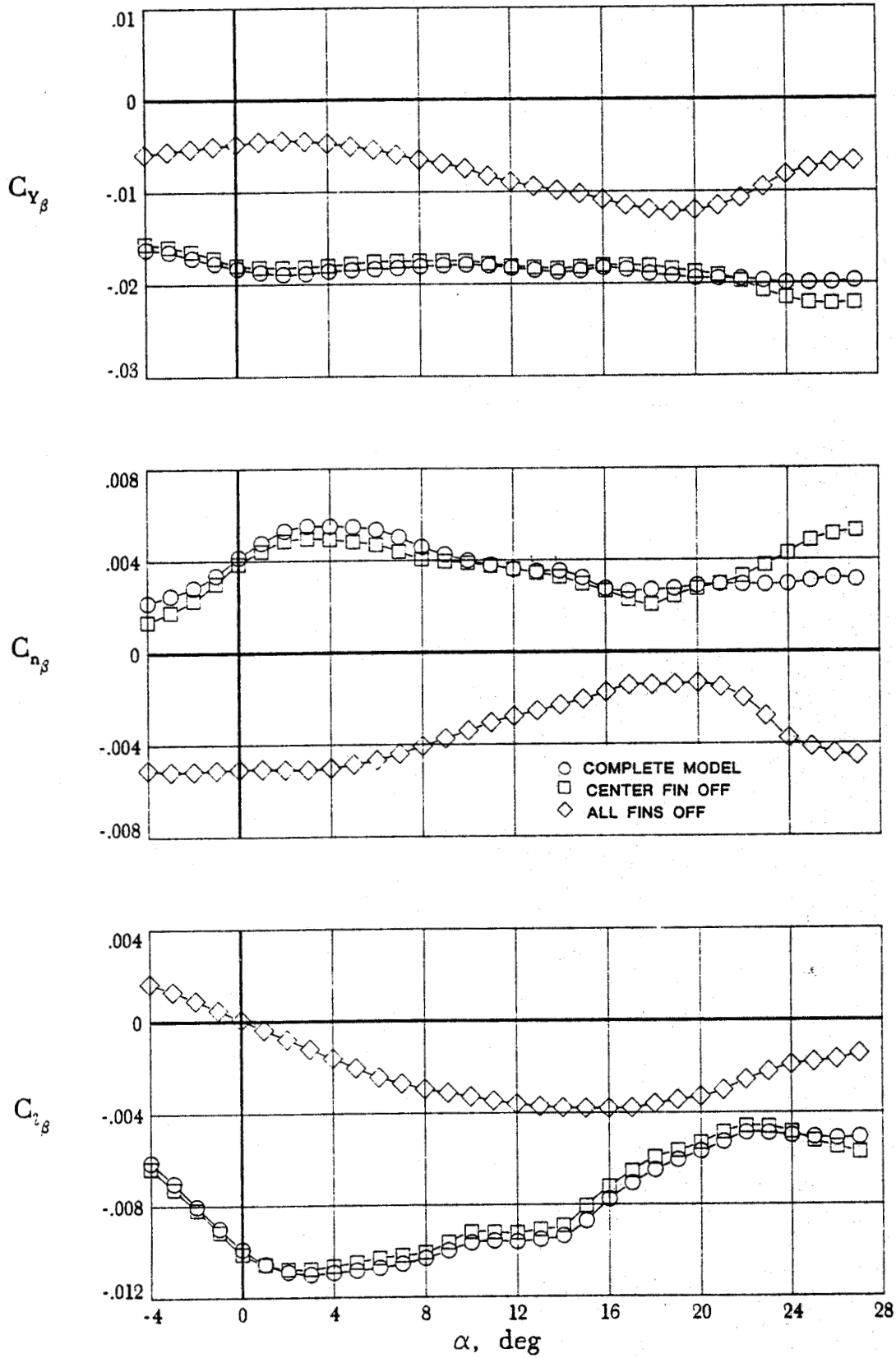
(d) $M = 0.95$.

Figure 17. Continued.



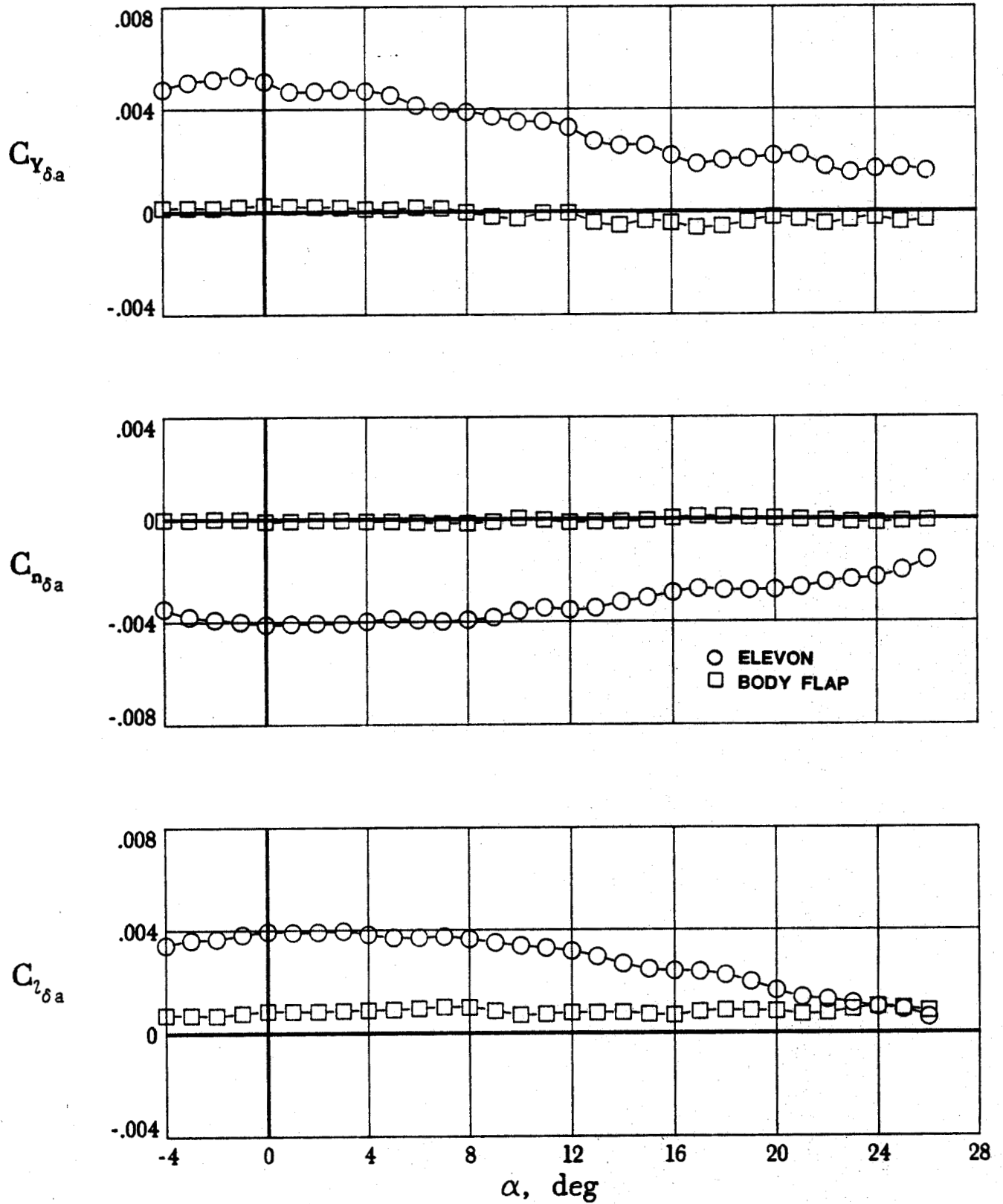
(e) $M = 1.1$.

Figure 17. Continued.



(f) $M = 1.2$.

Figure 17. Concluded.



(a) $M = 0.6$.

Figure 18. Transonic roll control effectiveness.

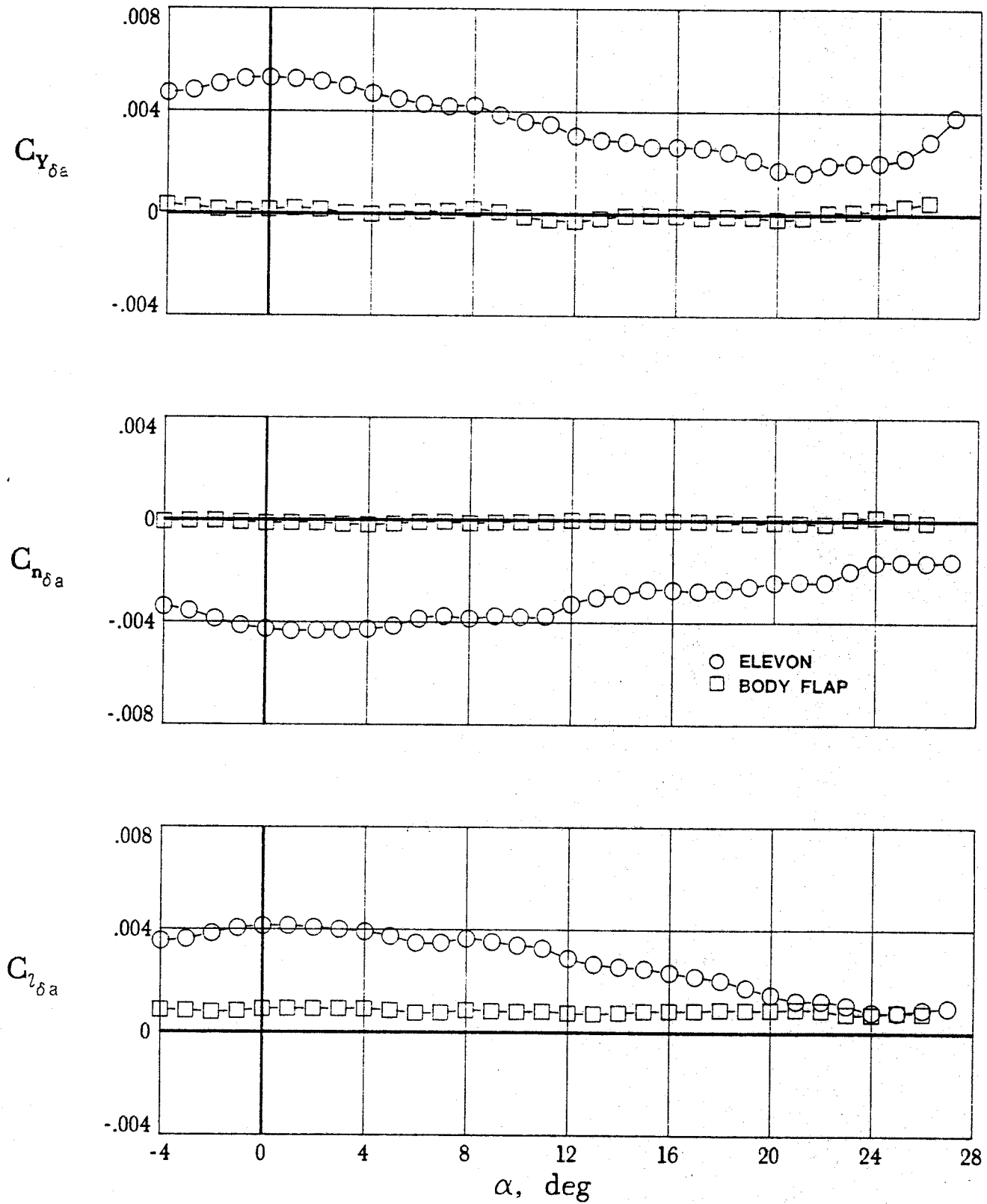
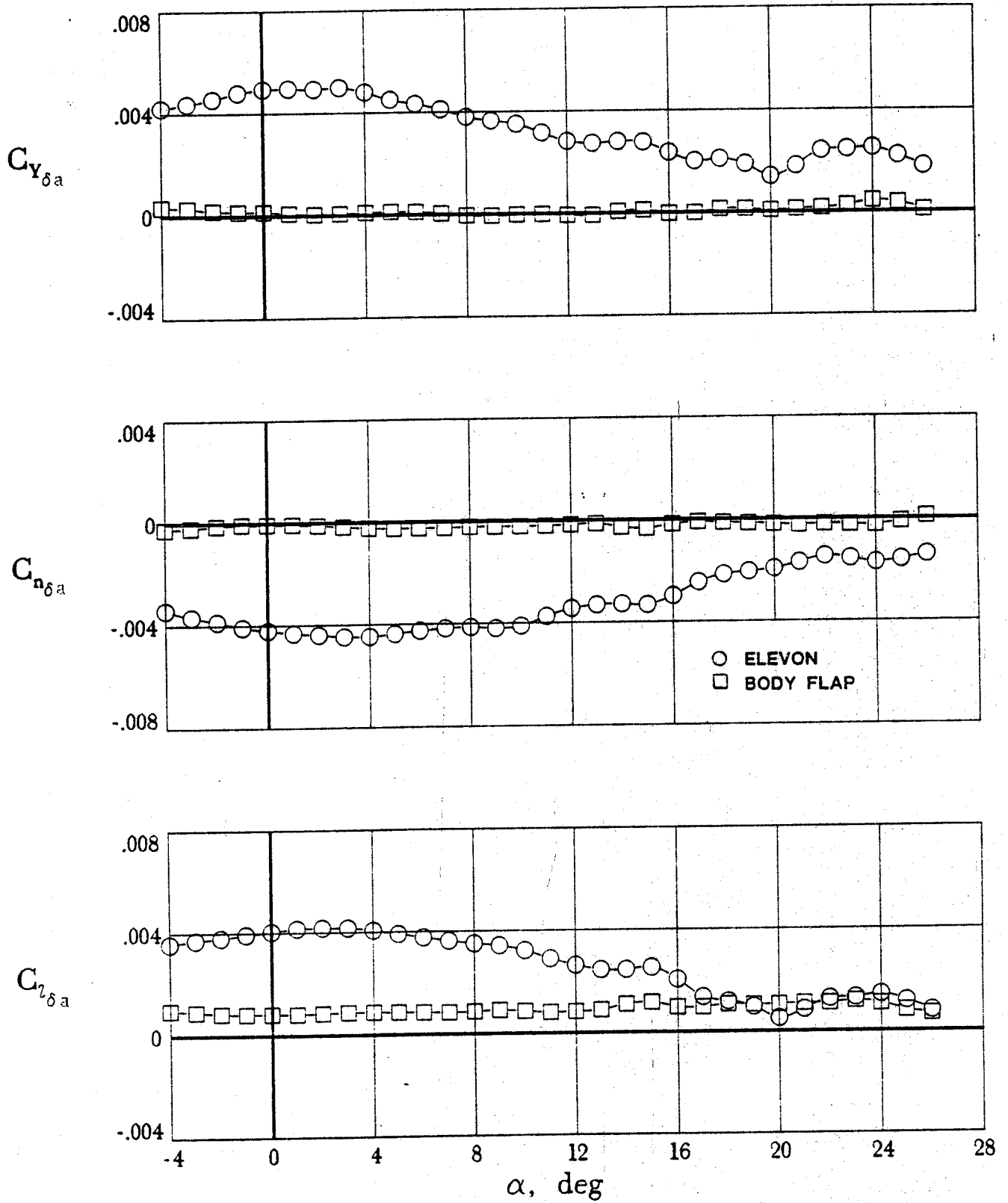
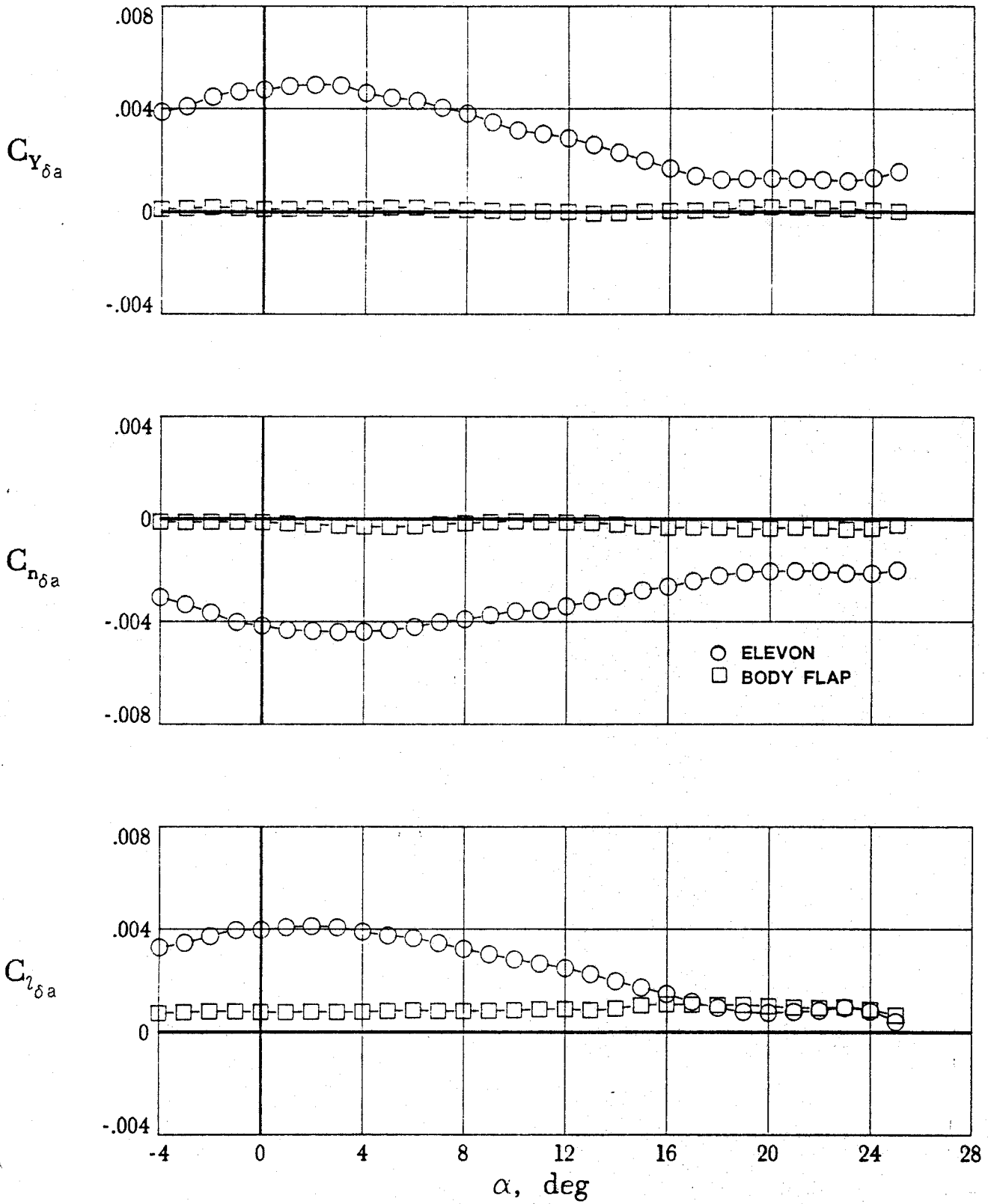
(b) $M = 0.8$.

Figure 18. Continued.



(c) $M = 0.9$.

Figure 18. Continued.



(d) $M = 0.95$.

Figure 18. Continued.

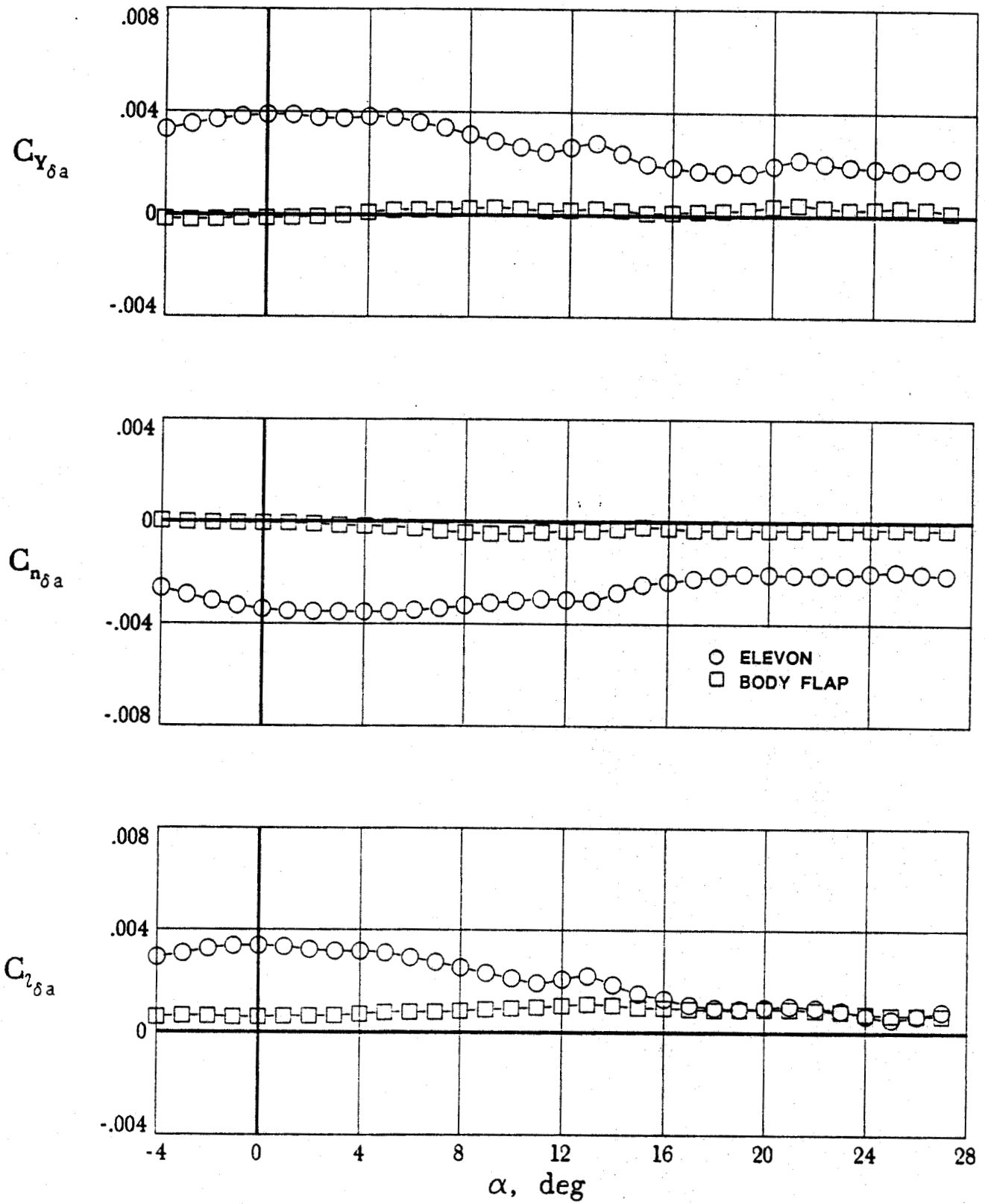
(e) $M = 1.1$.

Figure 18. Continued.

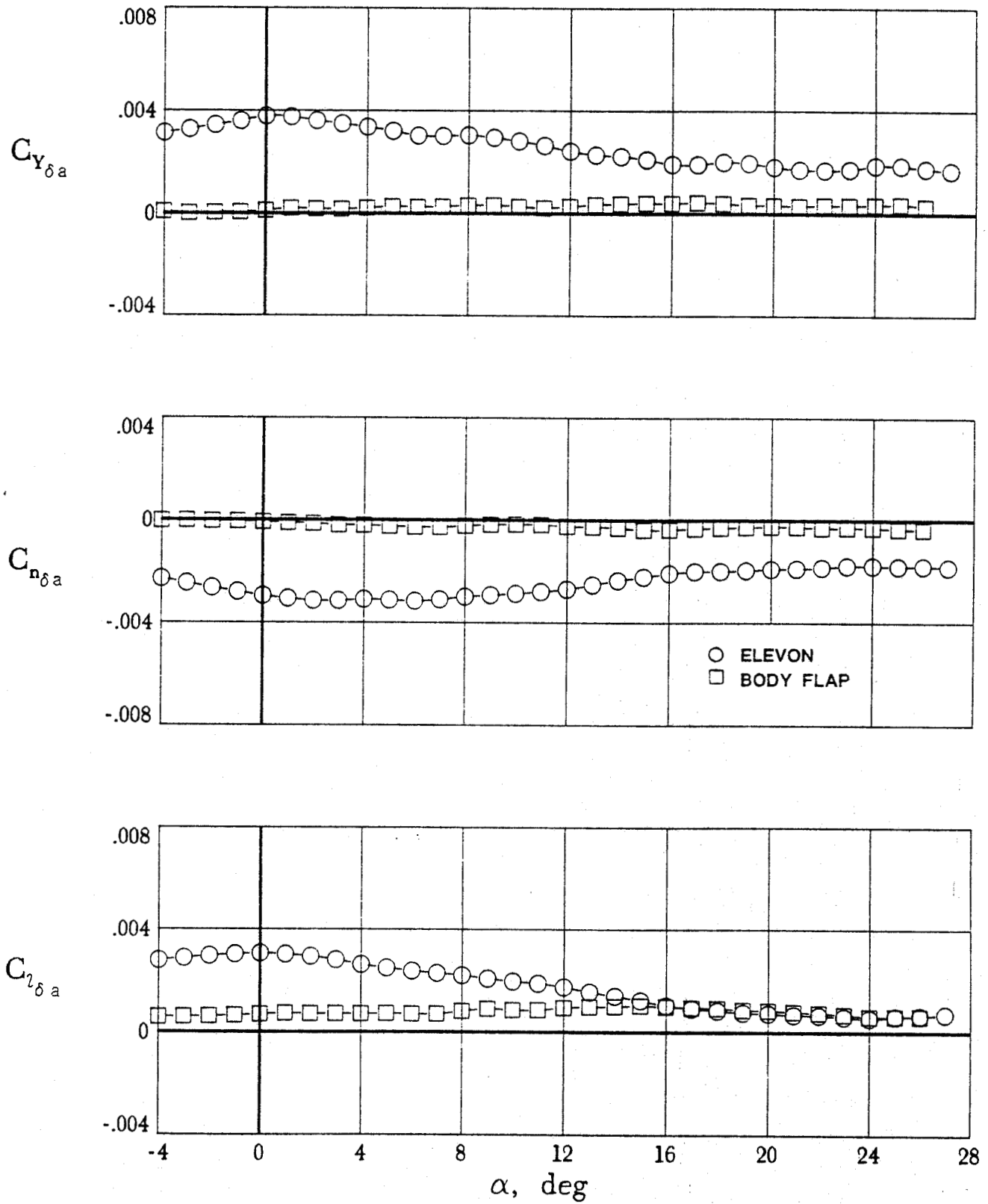
(f) $M = 1.2$.

Figure 18. Concluded.

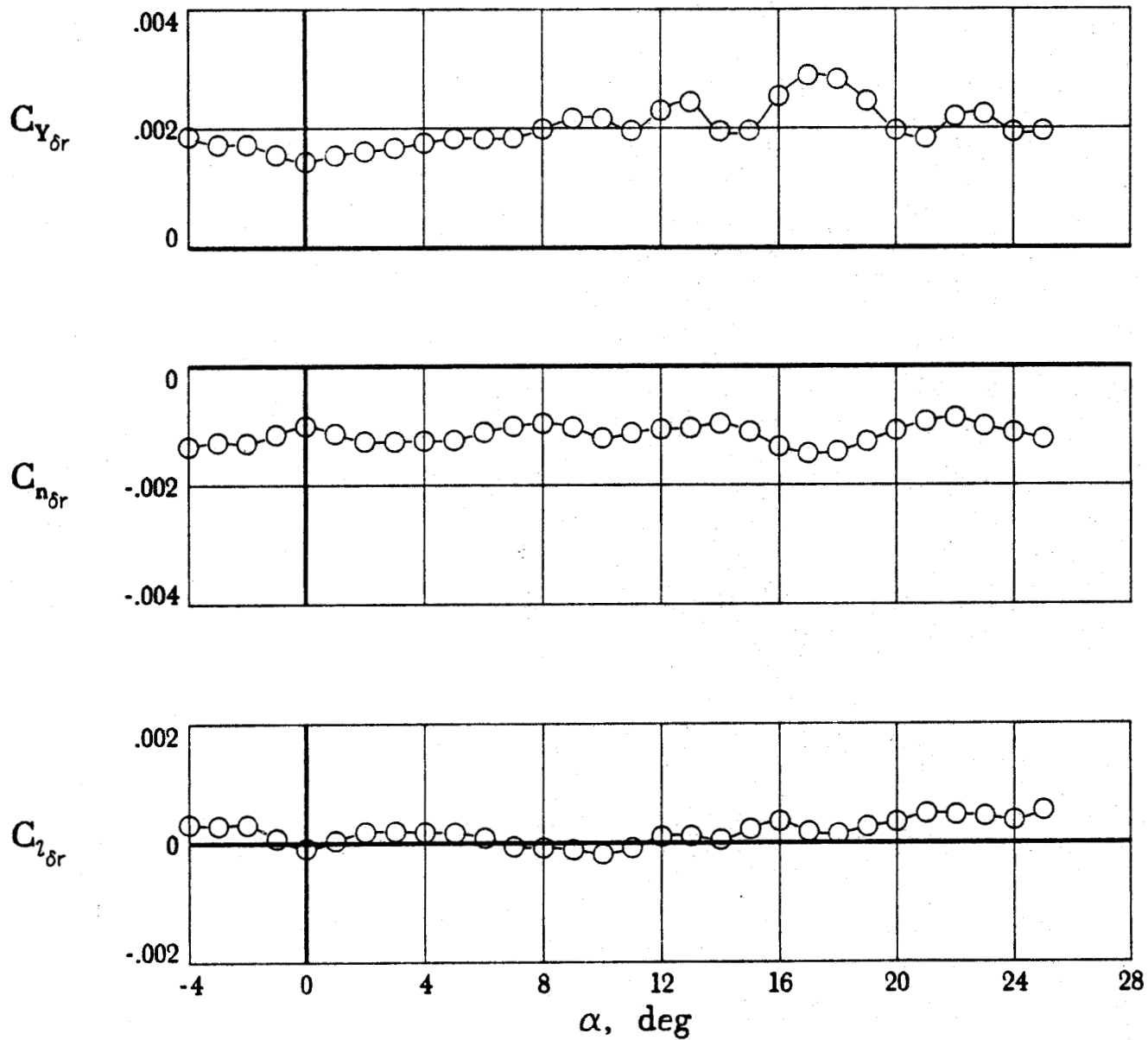
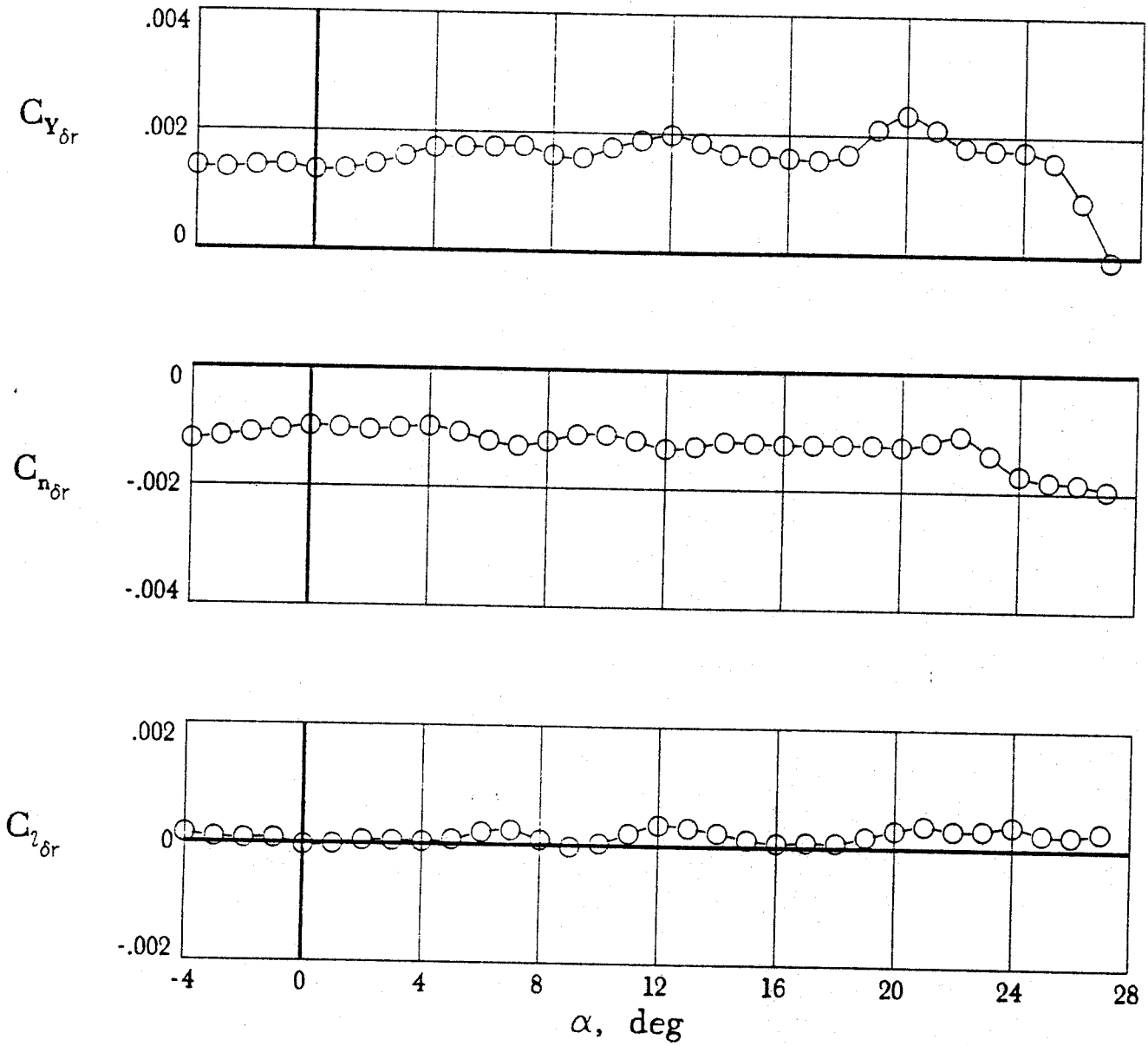
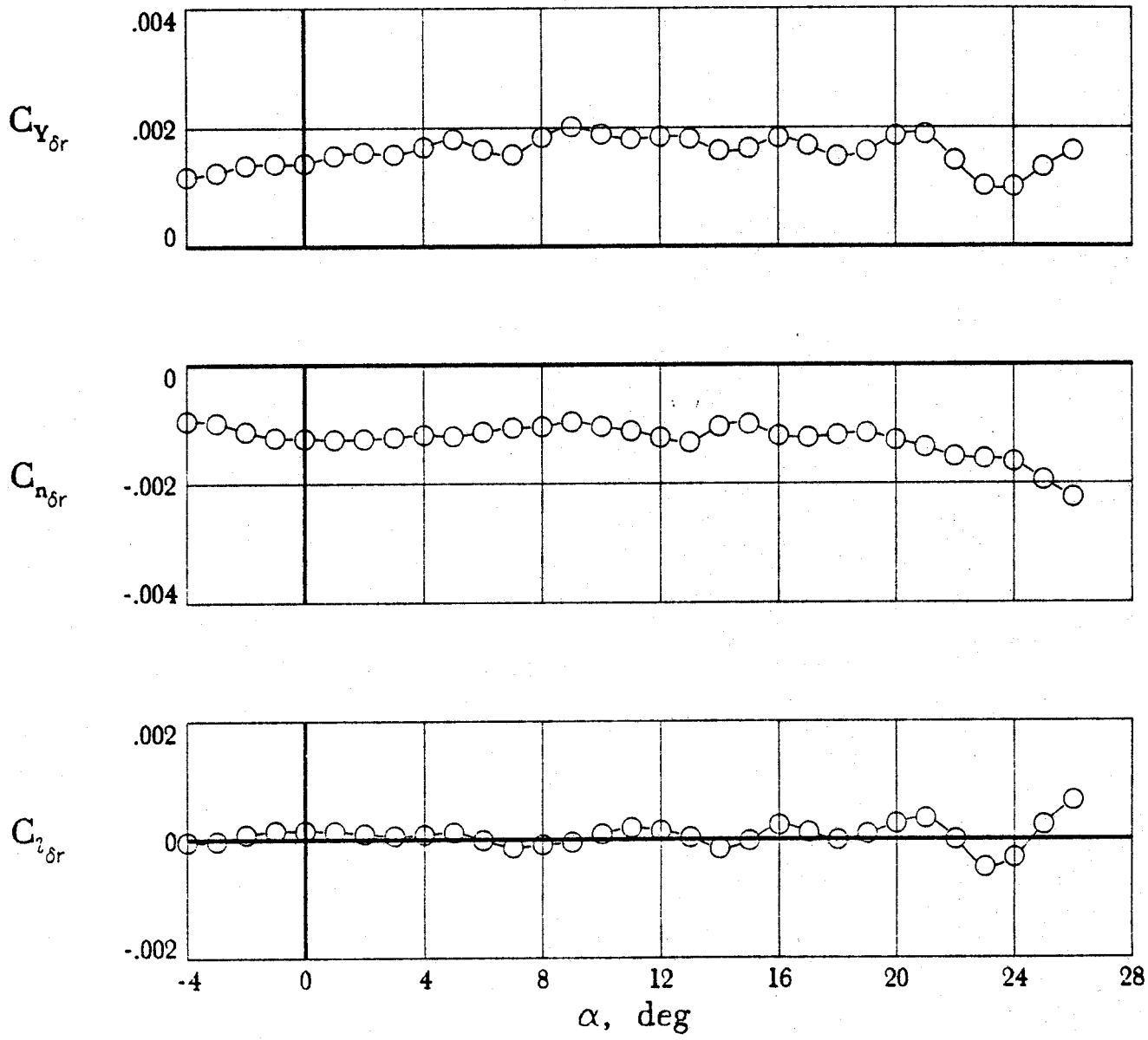
(a) $M = 0.6$.

Figure 19. Transonic yaw control effectiveness.



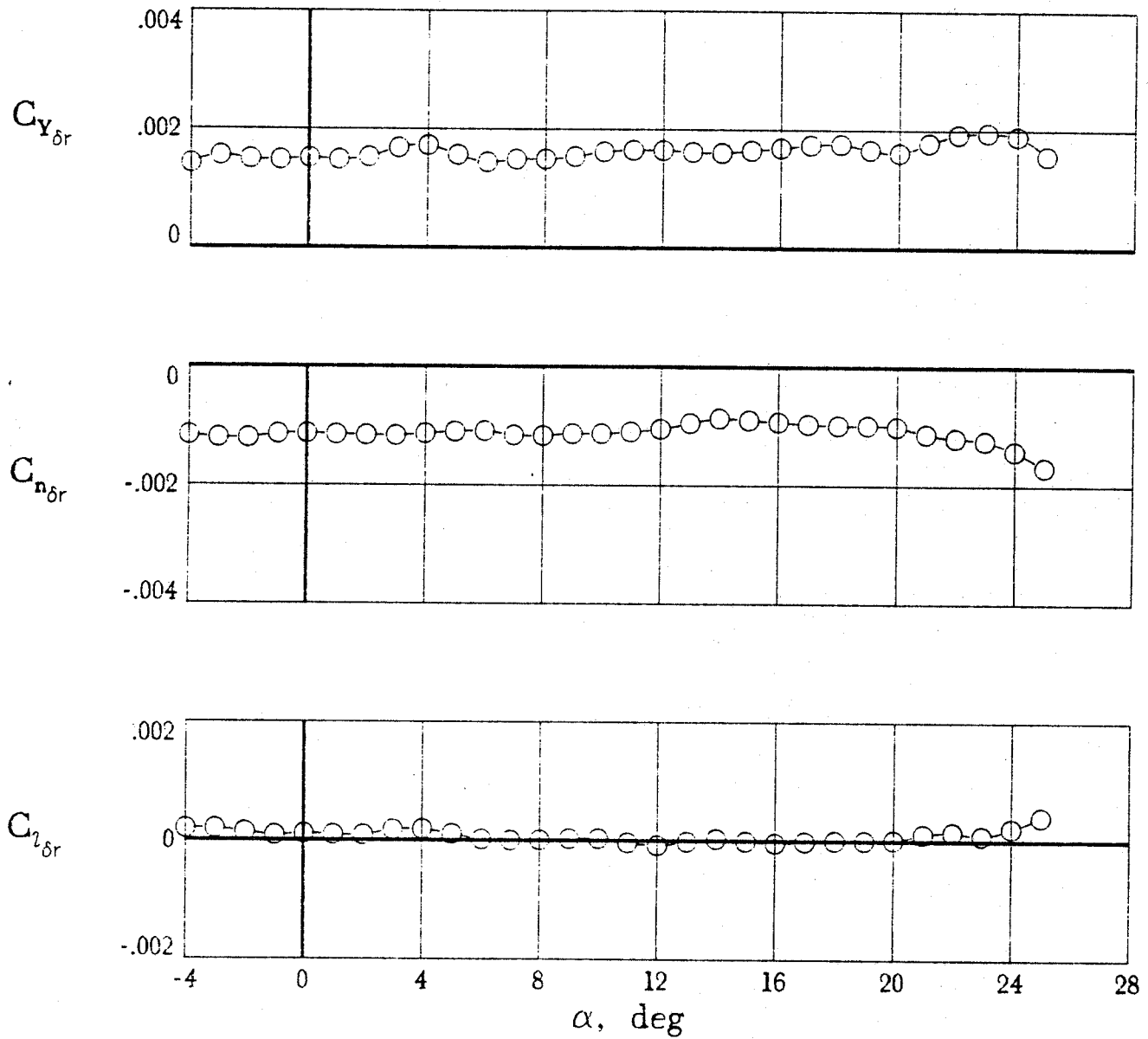
(b) $M = 0.8$.

Figure 19. Continued.



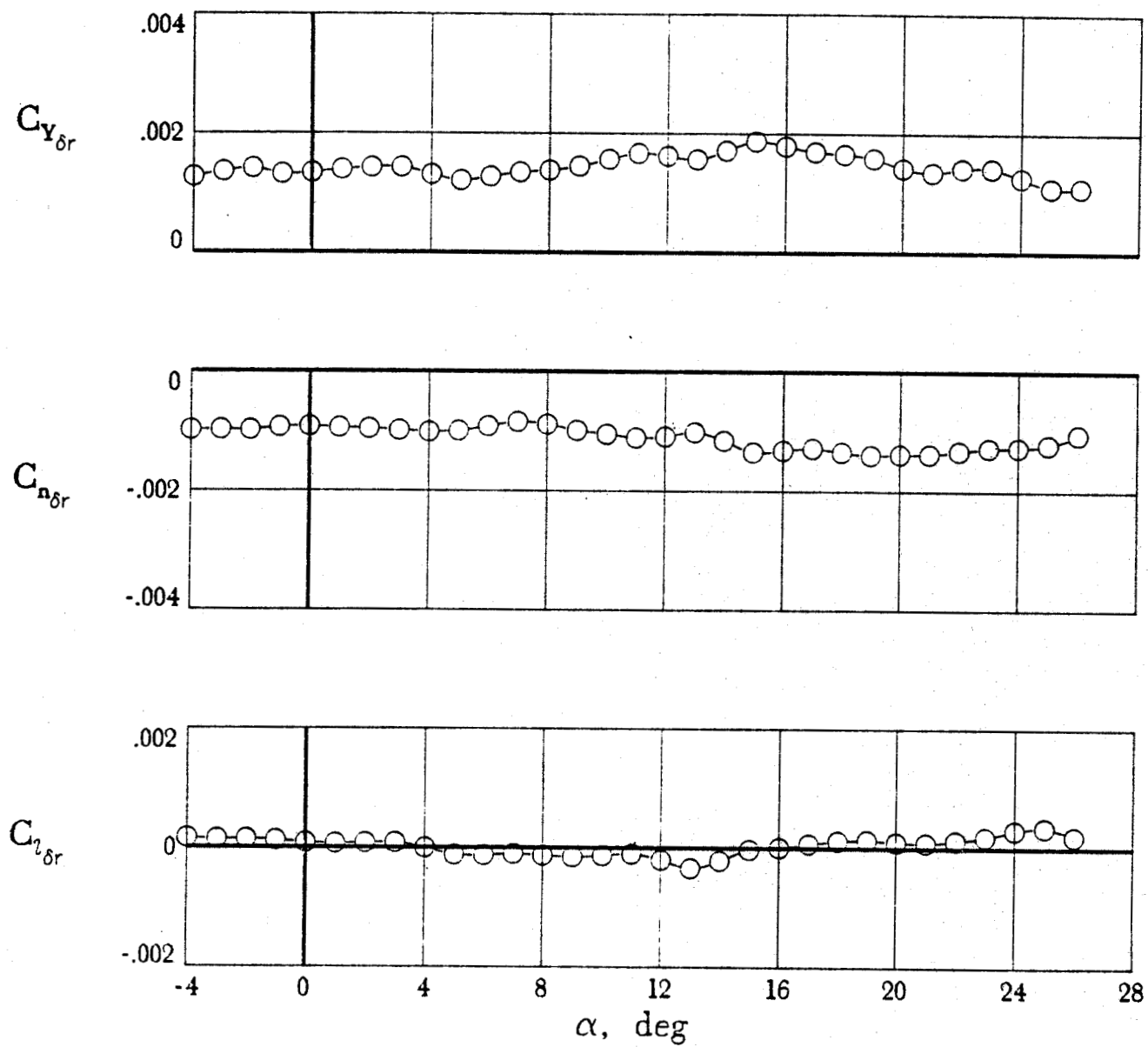
(c) $M = 0.9$.

Figure 19. Continued.



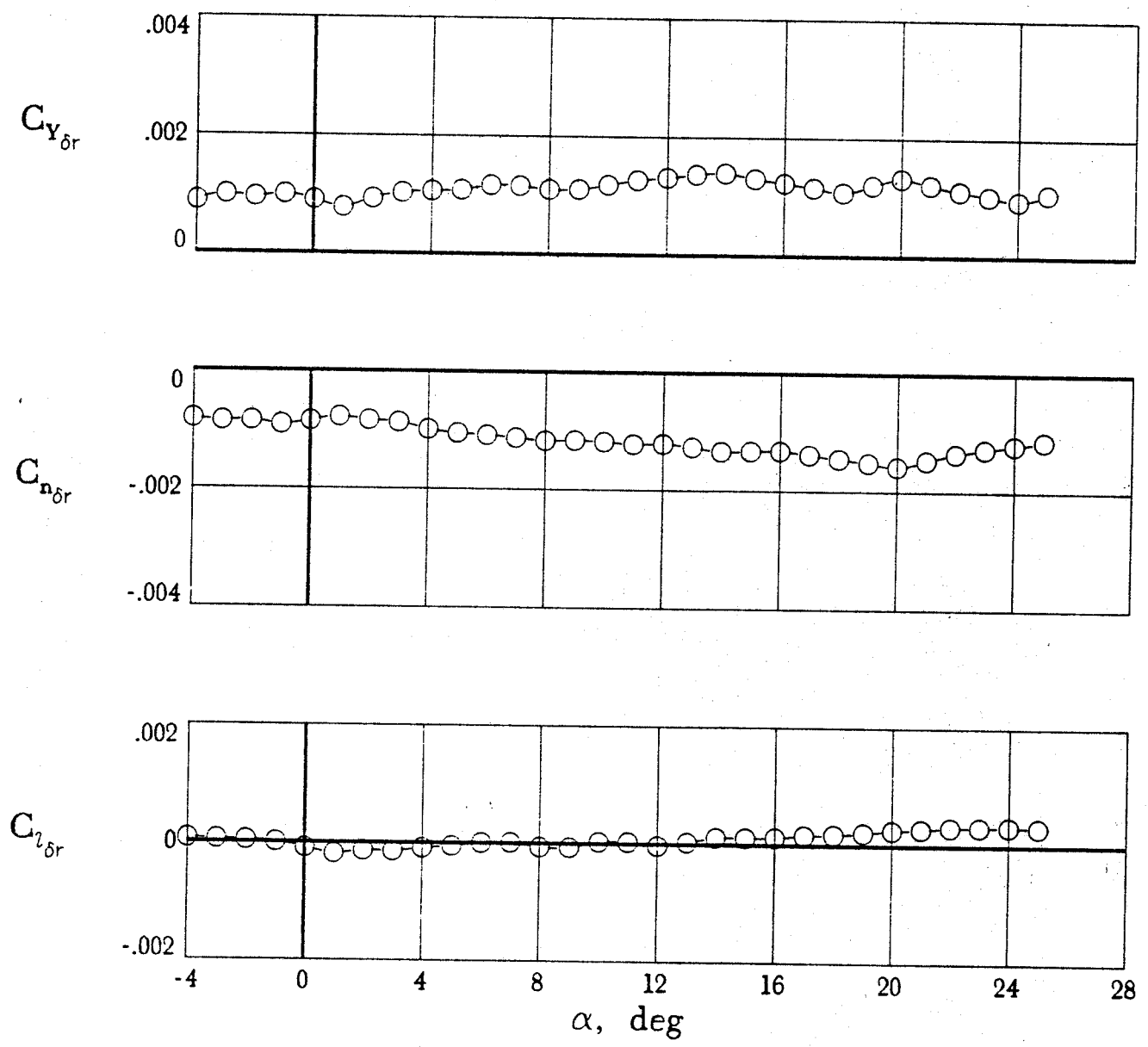
(d) $M = 0.95$.

Figure 19. Continued.



(e) $M = 1.1$.

Figure 19. Continued.



(f) $M = 1.2$.

Figure 19. Concluded.

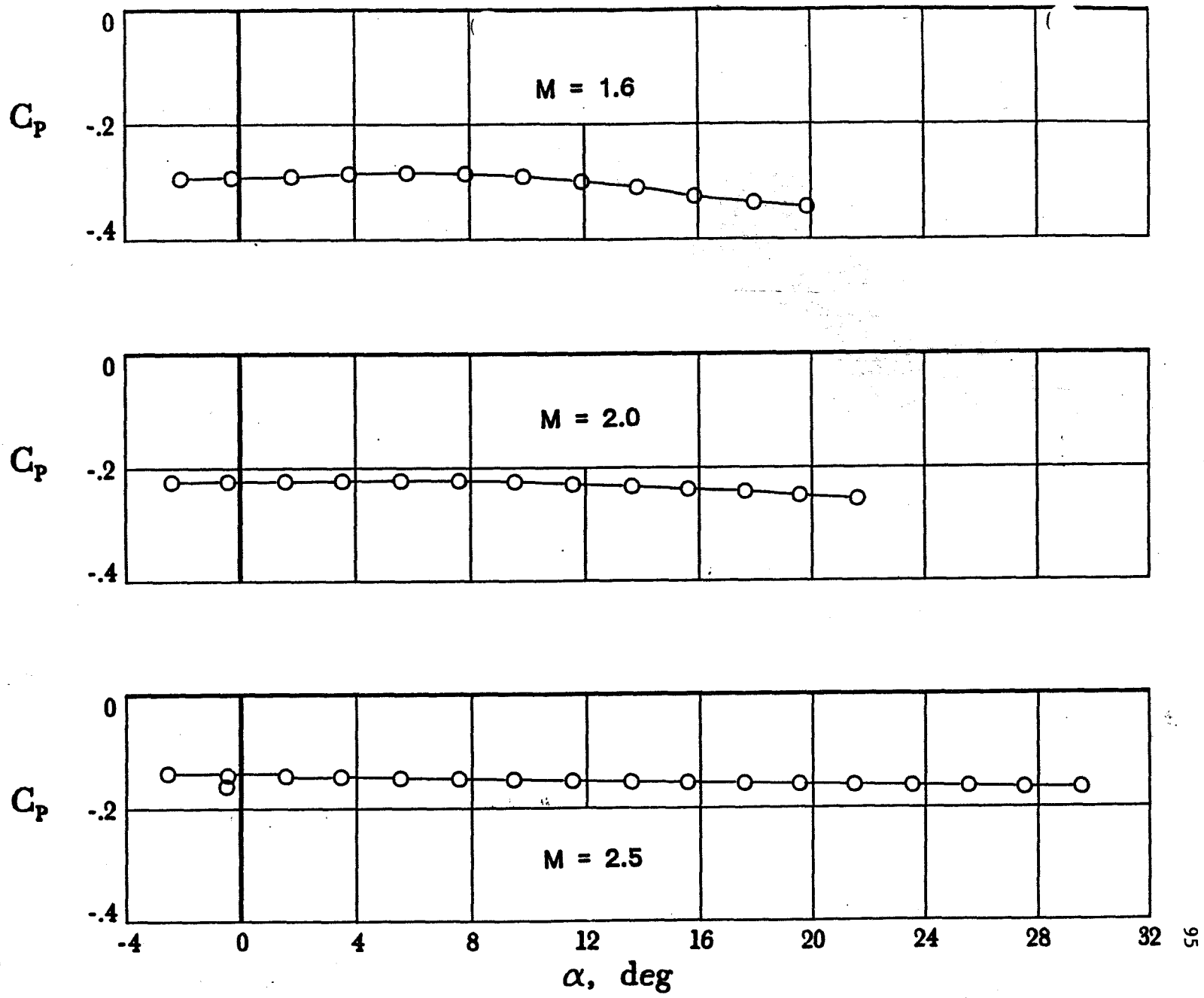


Figure 20. Model base pressures measured in supersonic investigation.

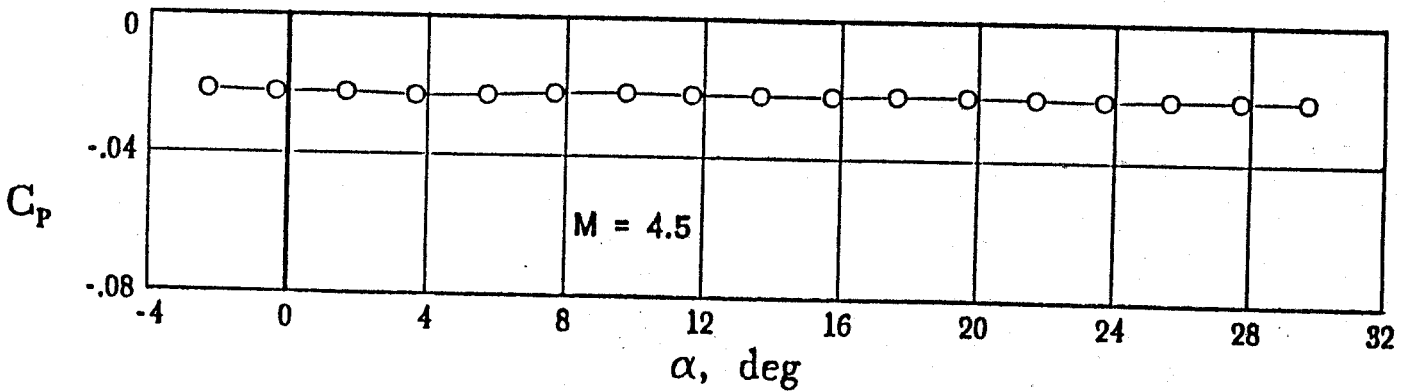
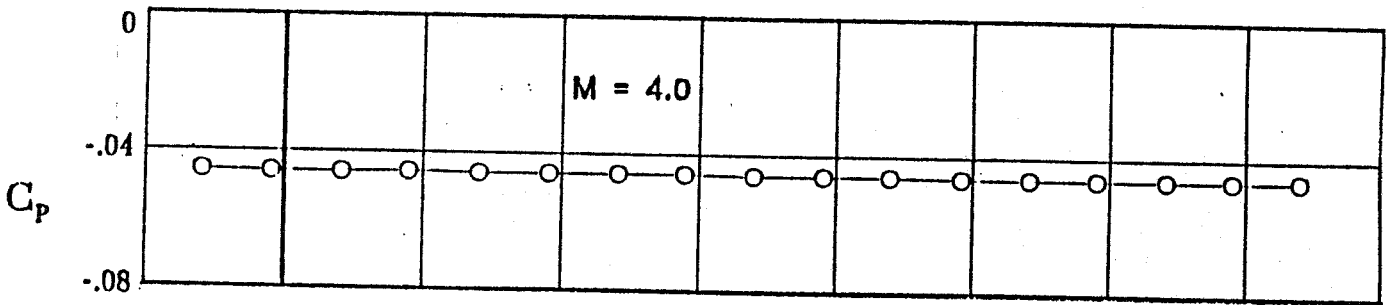
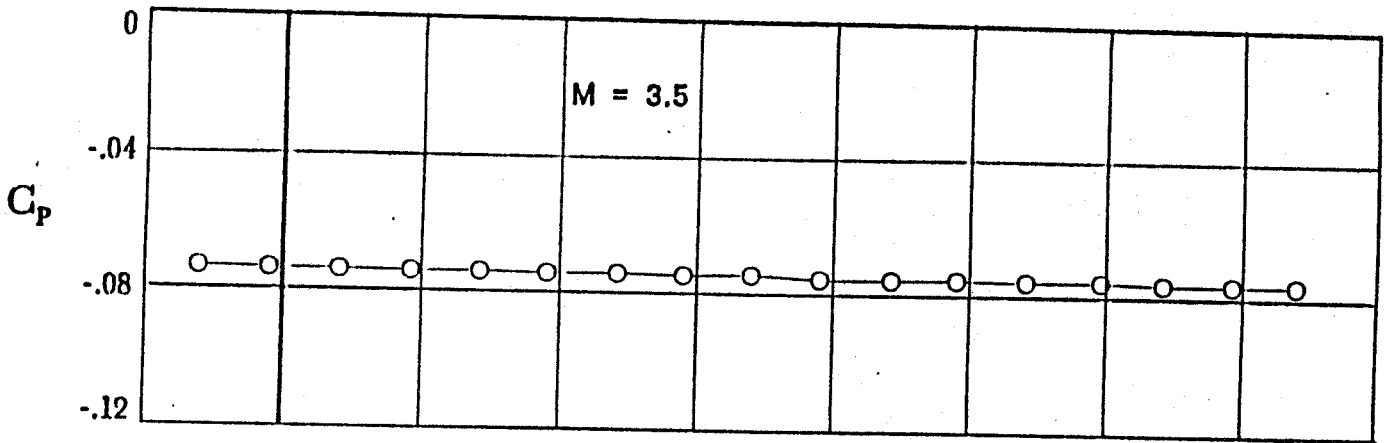
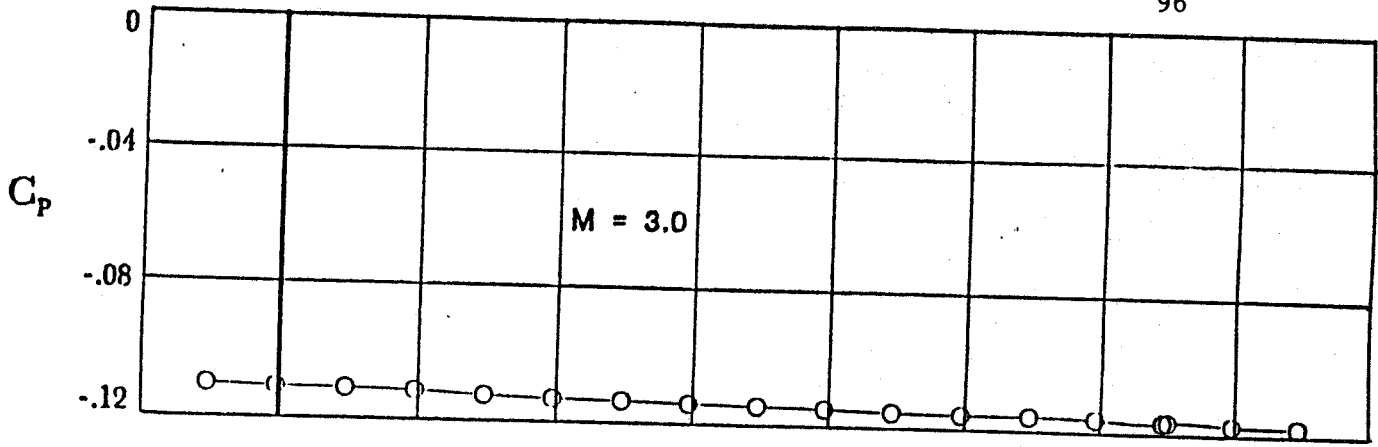
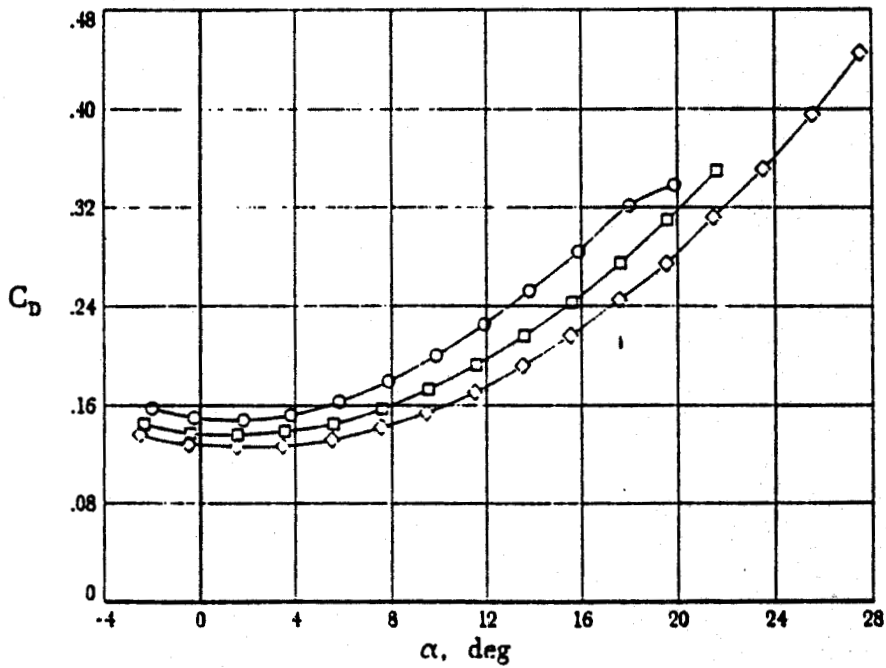
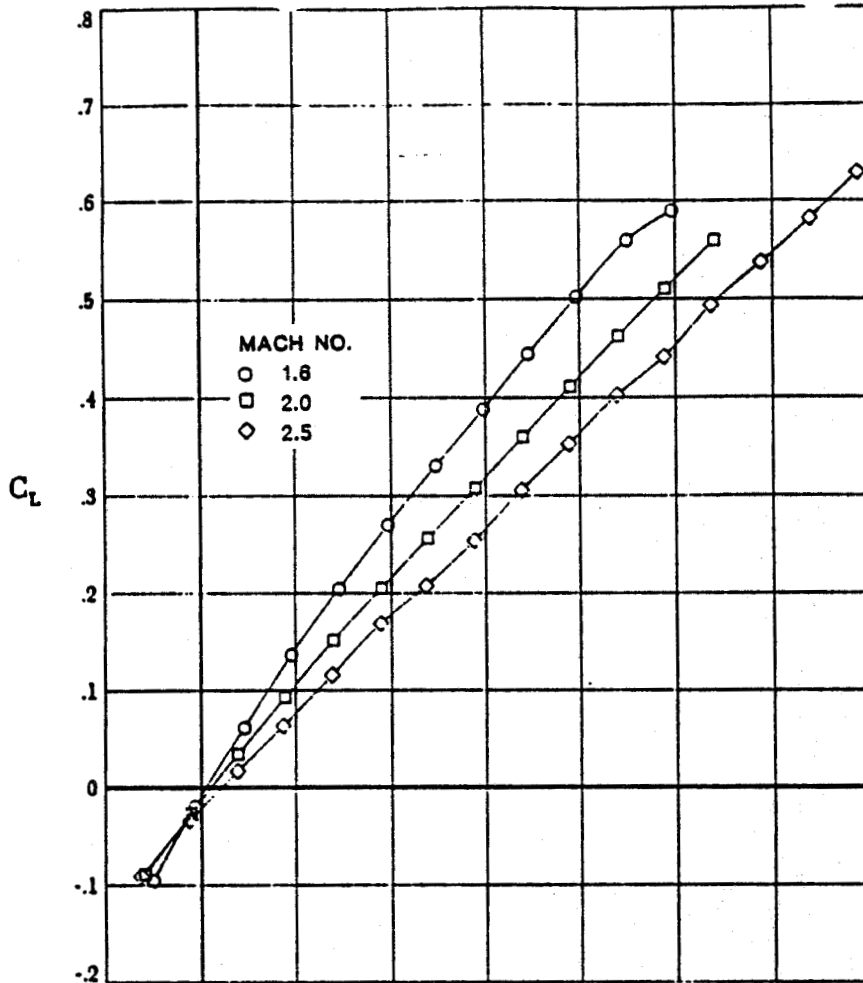


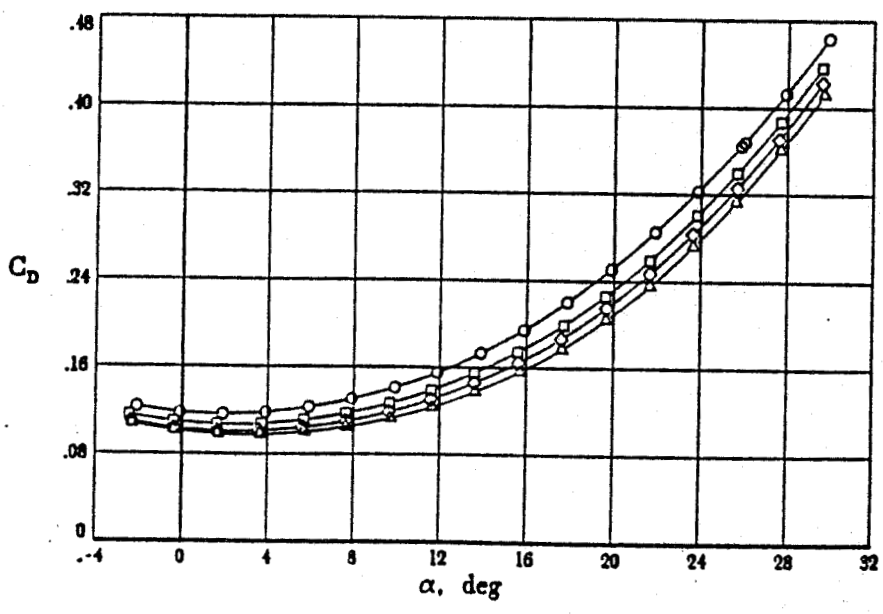
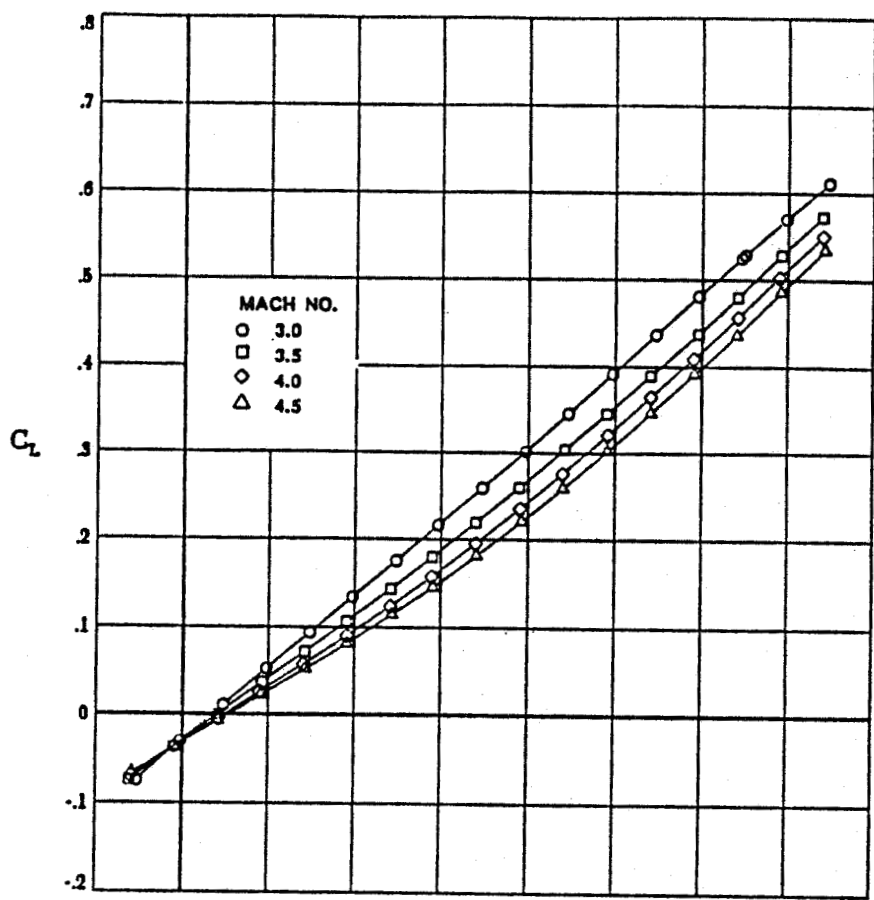
Figure 20. Concluded.

C-2



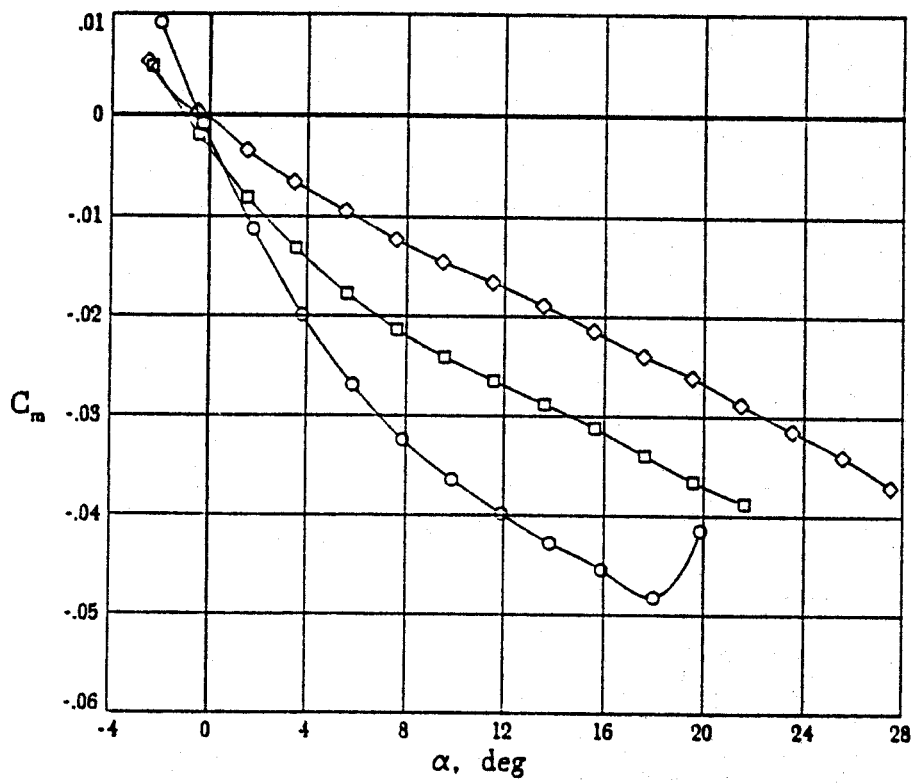
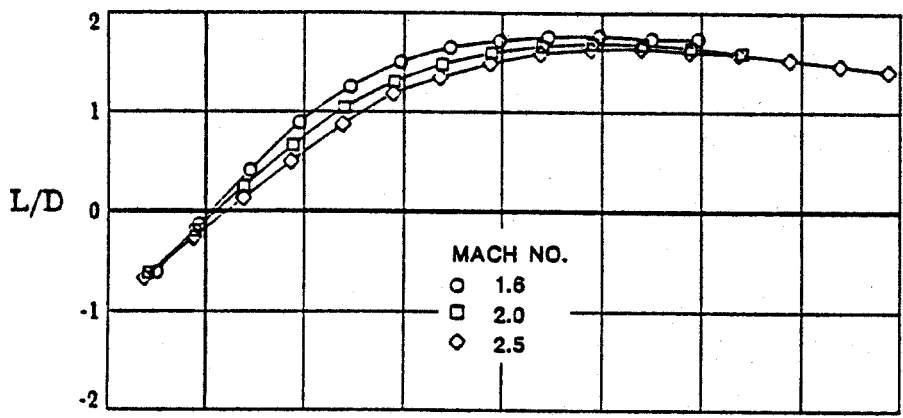
(a) C_L VS α and C_D VS α

Figure 21. Effect of Mach number variation on the supersonic longitudinal aerodynamic characteristics of the model.



(a) C_L VS α and C_D VS α

Figure 21. Continued.



(b) L/D VS α and C_m VS α

Figure 21. Continued.

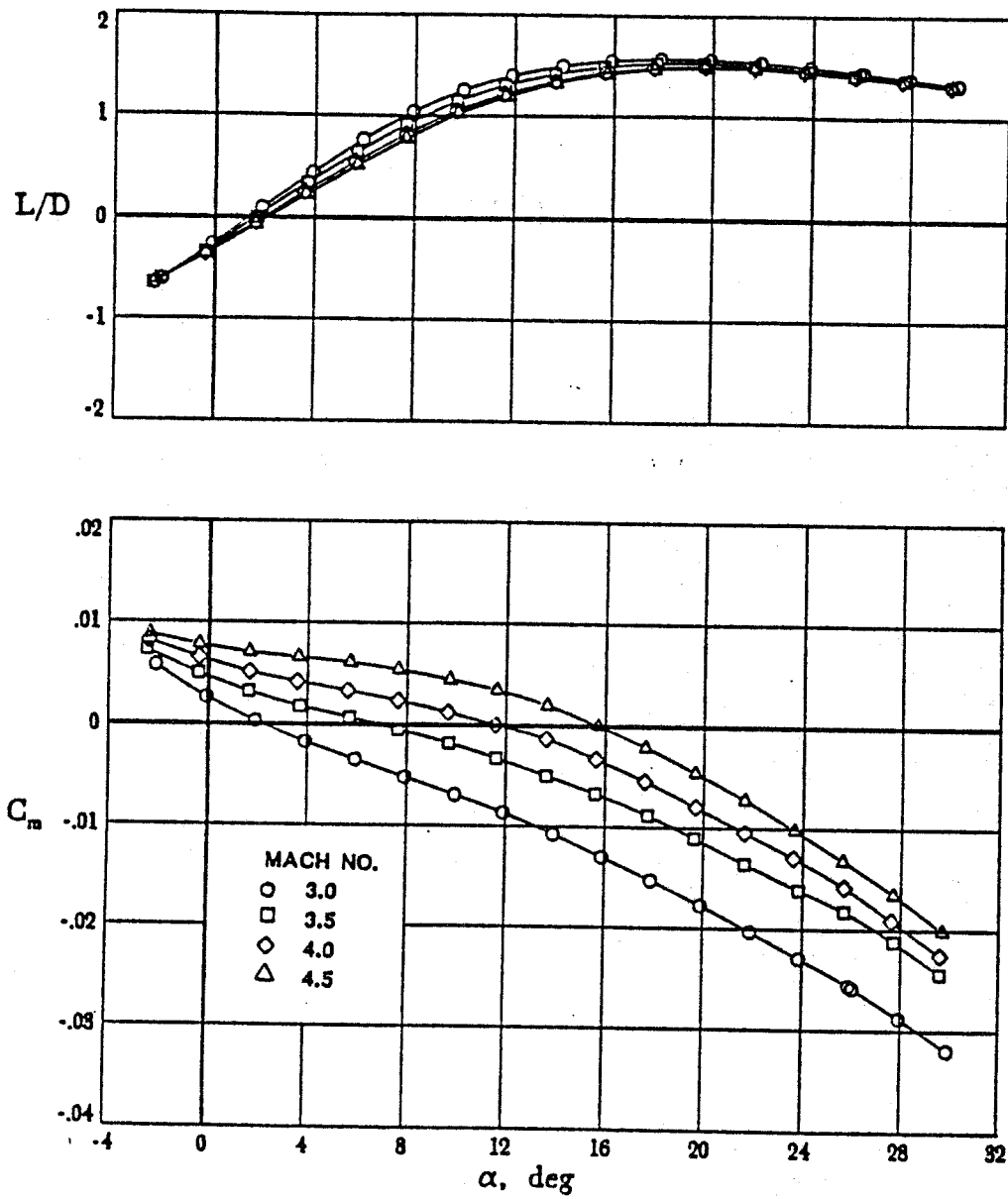
(b) L/D VS α and C_m VS α

Figure 21. Concluded.

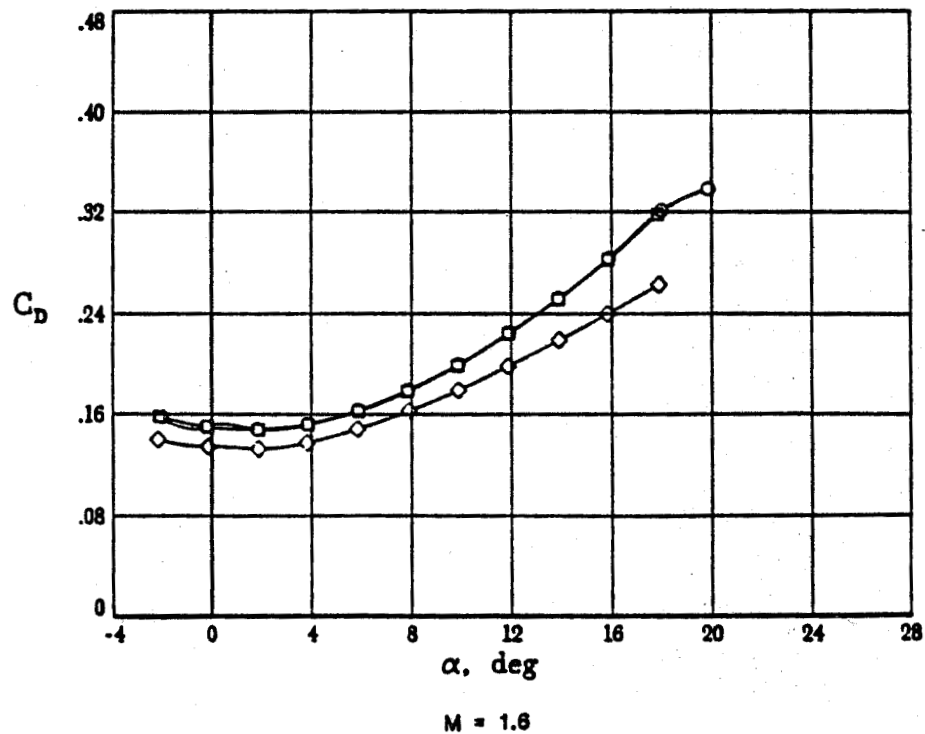
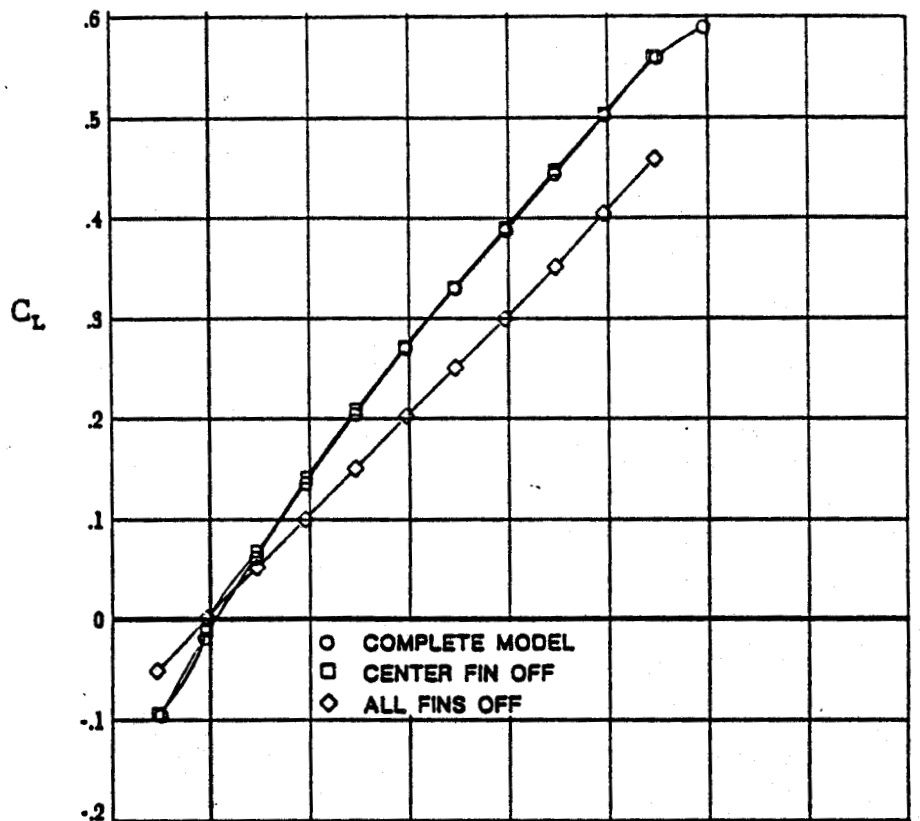
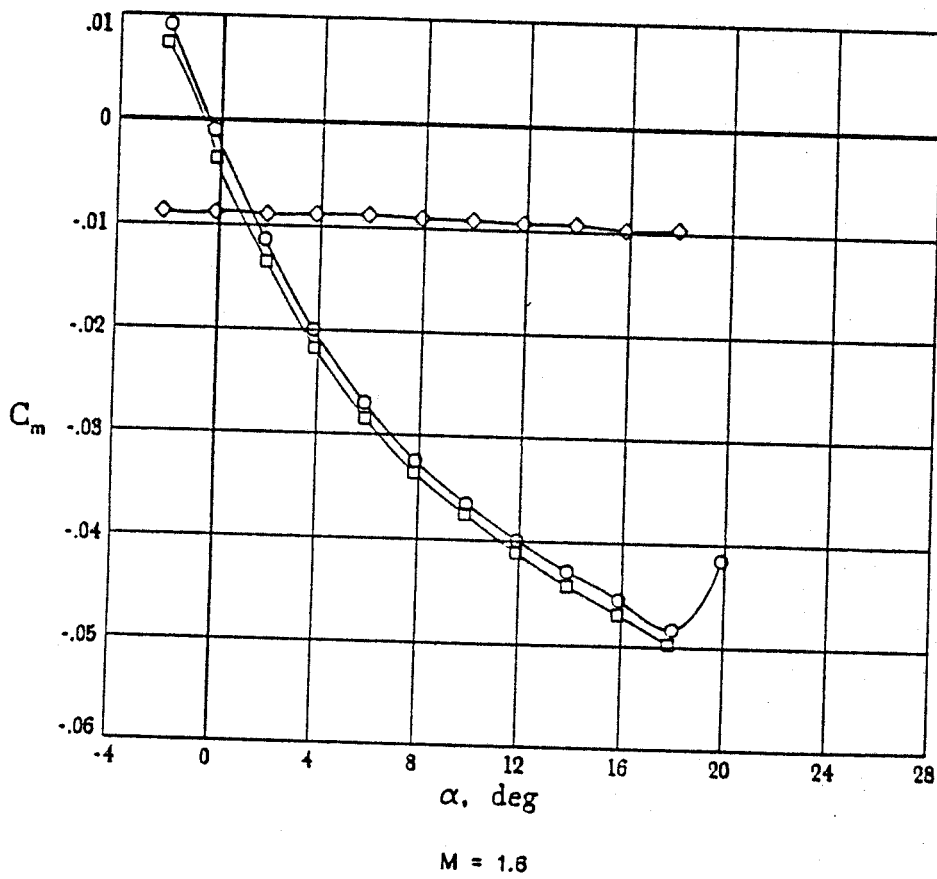
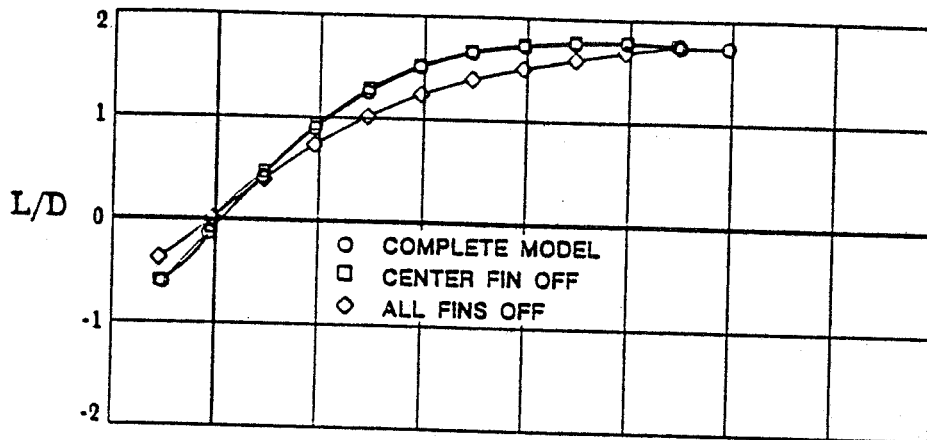
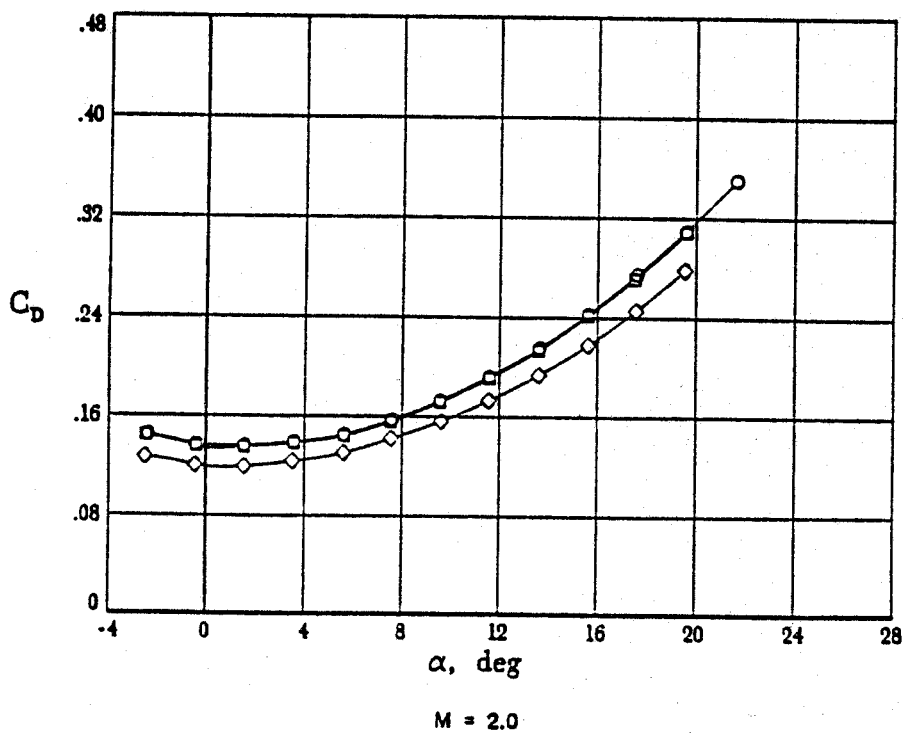
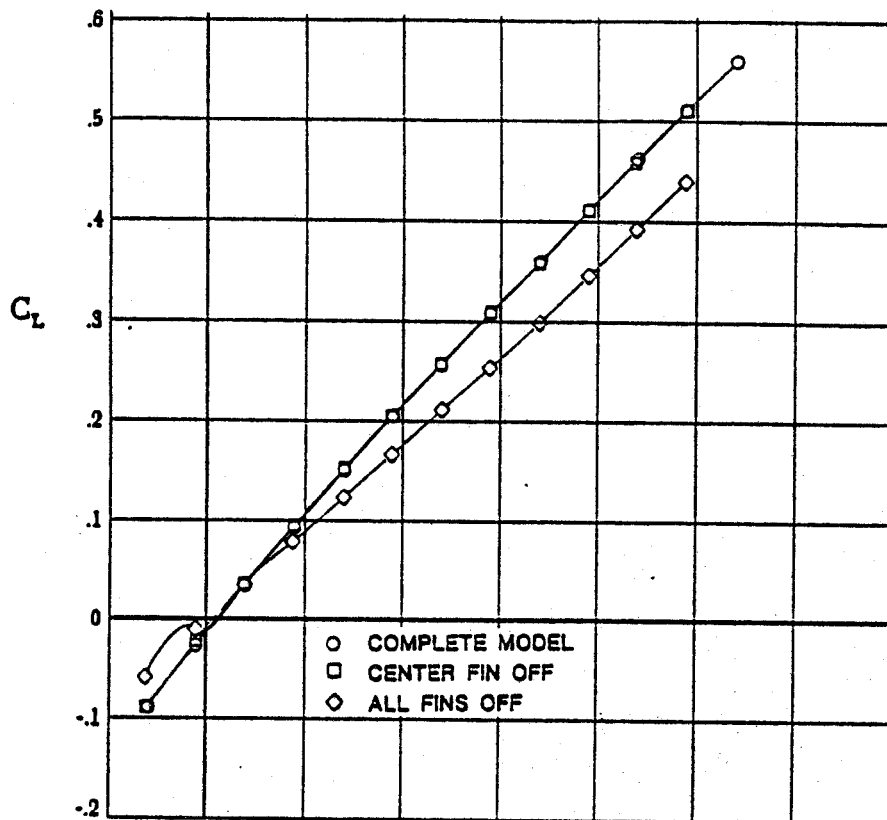
(a) C_L VS α and C_D VS α

Figure 22. Effect of fins on the supersonic longitudinal aerodynamic characteristics of the model.



(b) L/D VS α and C_m VS α

Figure 22. Continued.



(a) C_L VS α and C_D VS α
Figure 22. Continued.

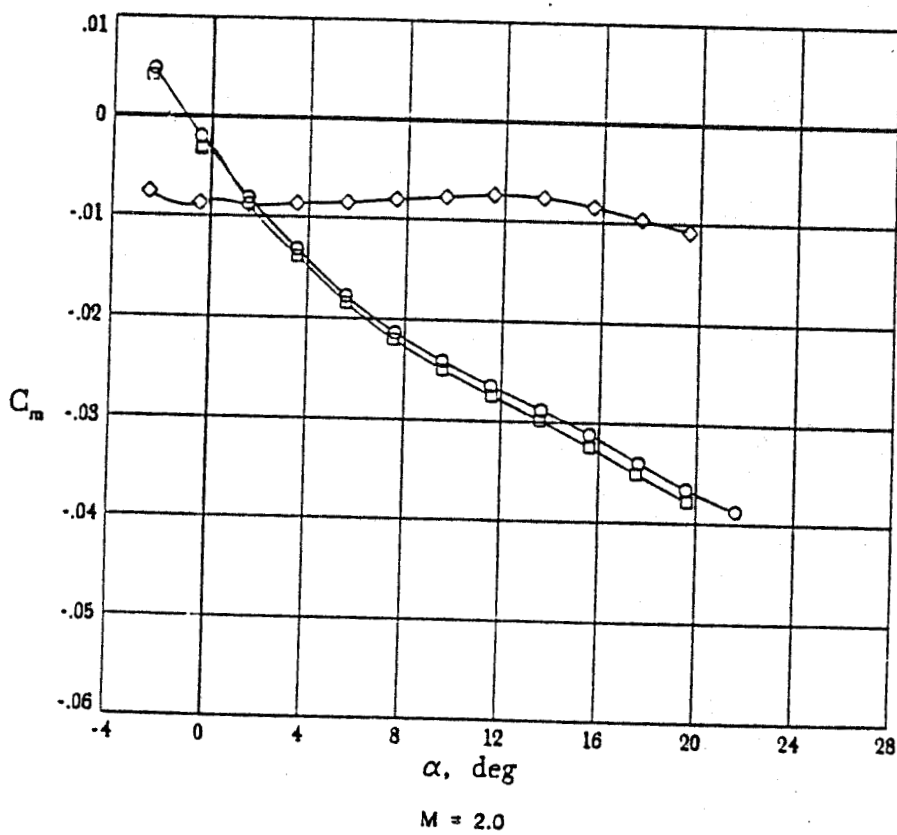
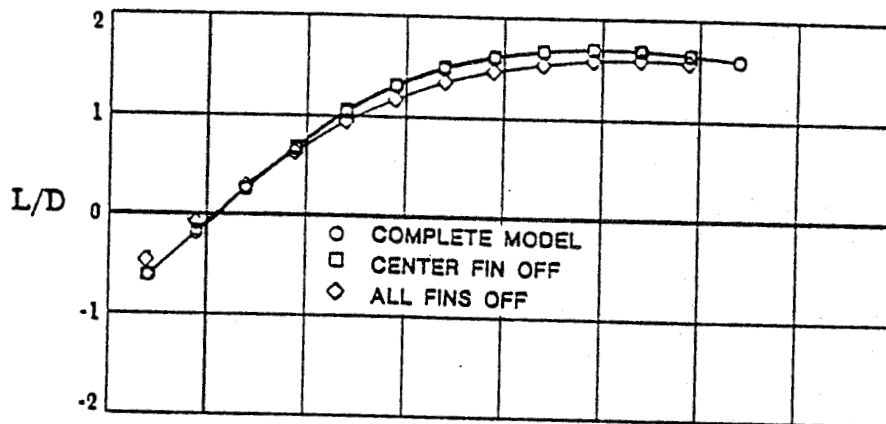
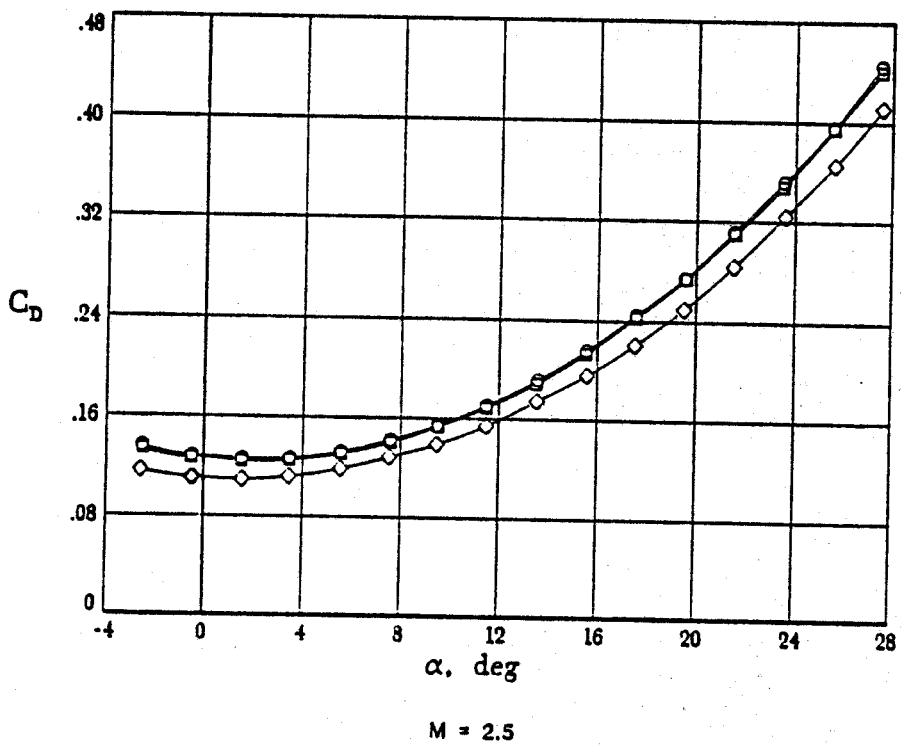
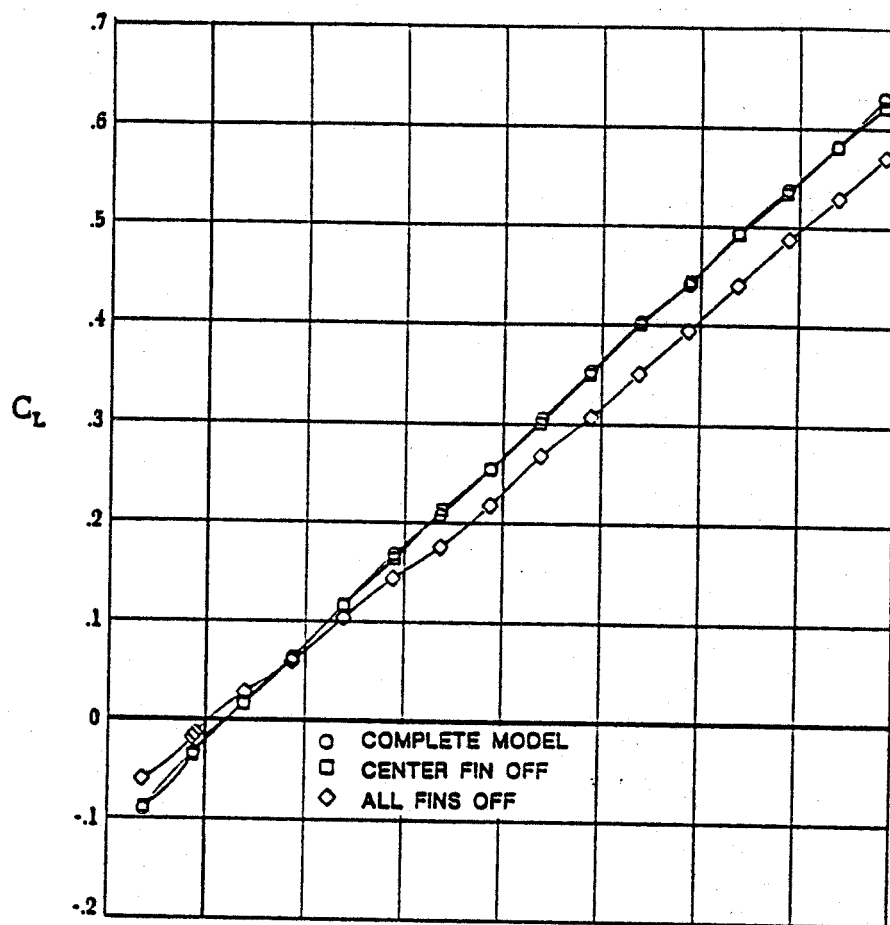
(b) L/D VS α and C_m VS α

Figure 22. Continued.



(a) C_L VS α and C_D VS α

Figure 22. Continued.

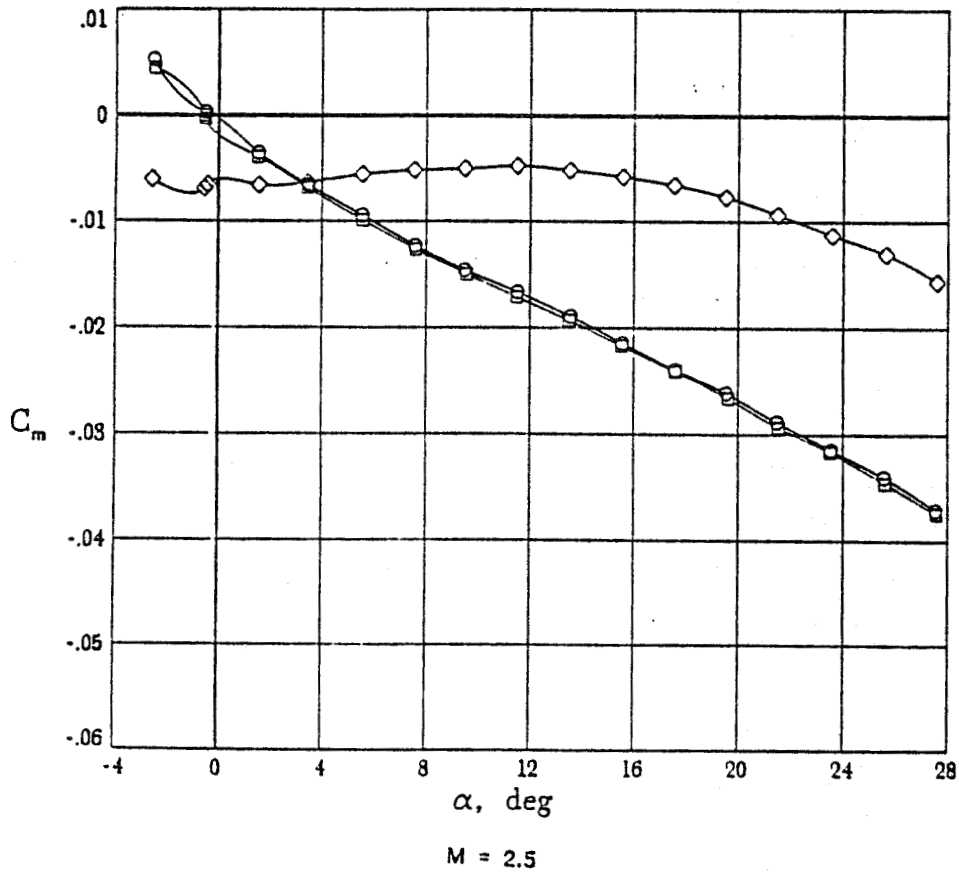
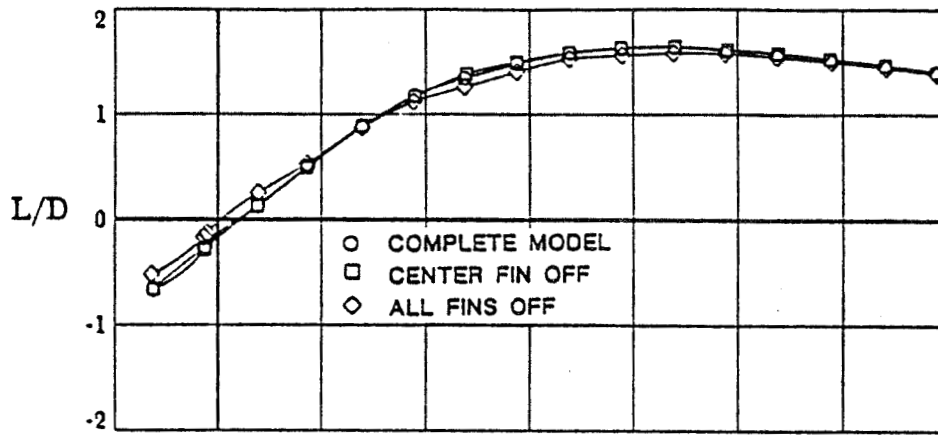
(b) L/D VS α and C_m VS α

Figure 22. Continued.

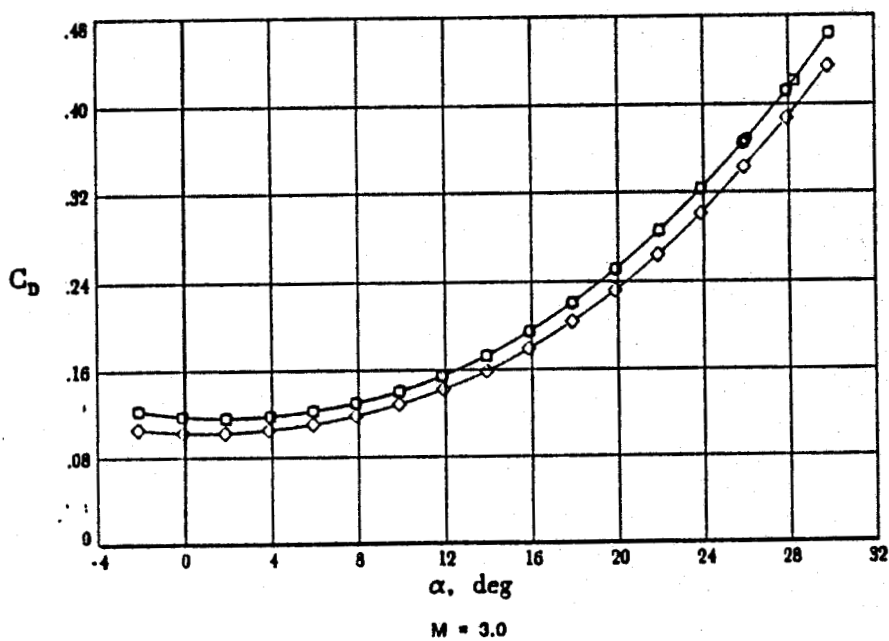
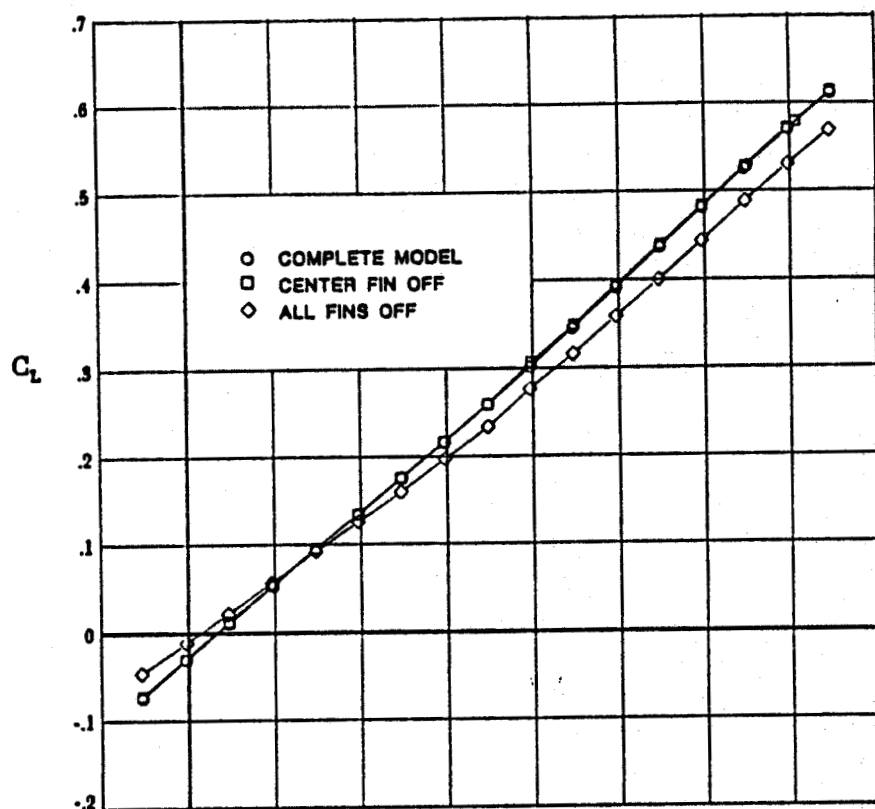
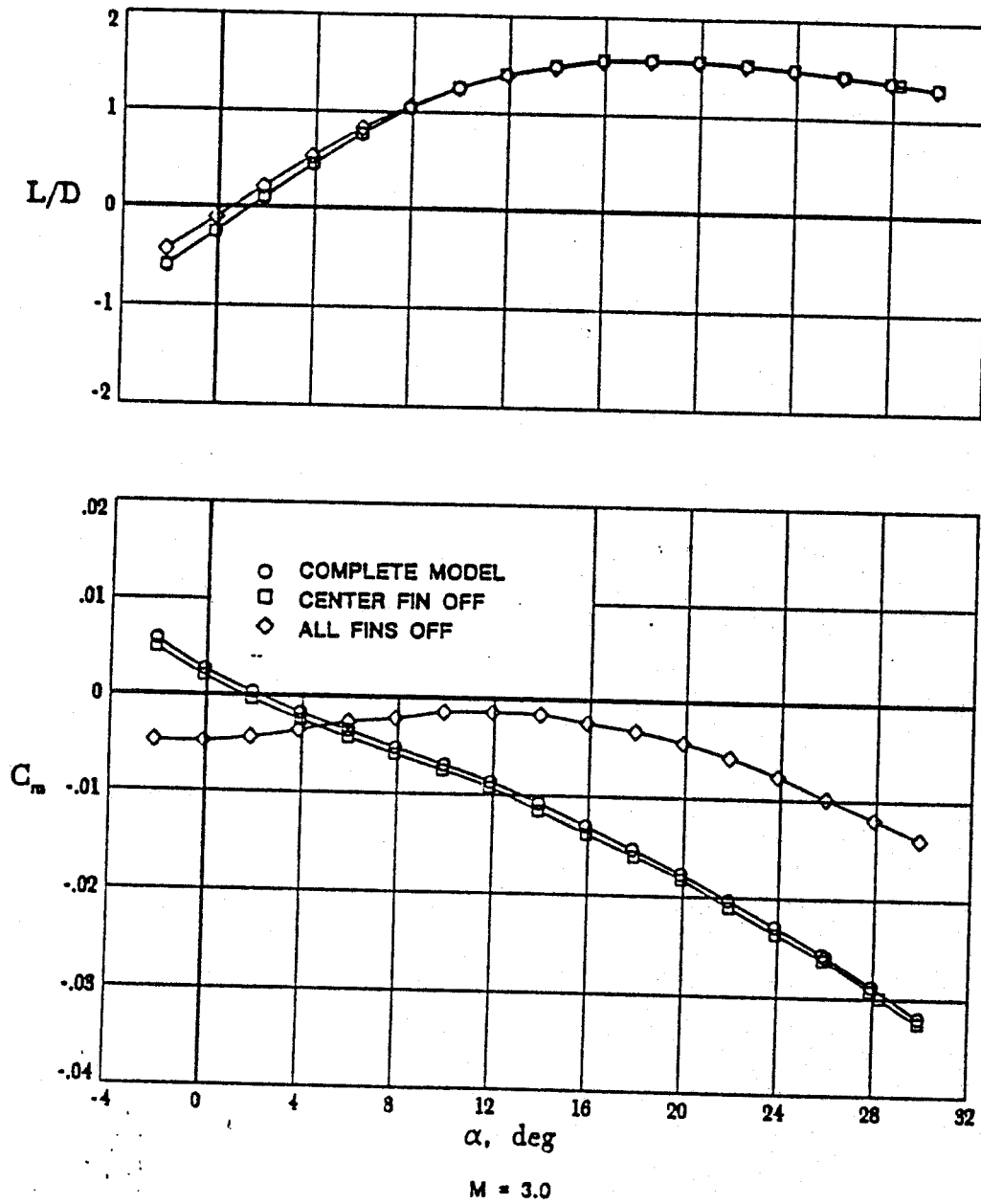
(a) C_L VS α and C_D VS α

Figure 22. Continued.



(b) L/D VS α and C_m VS α
 Figure 22. Continued.

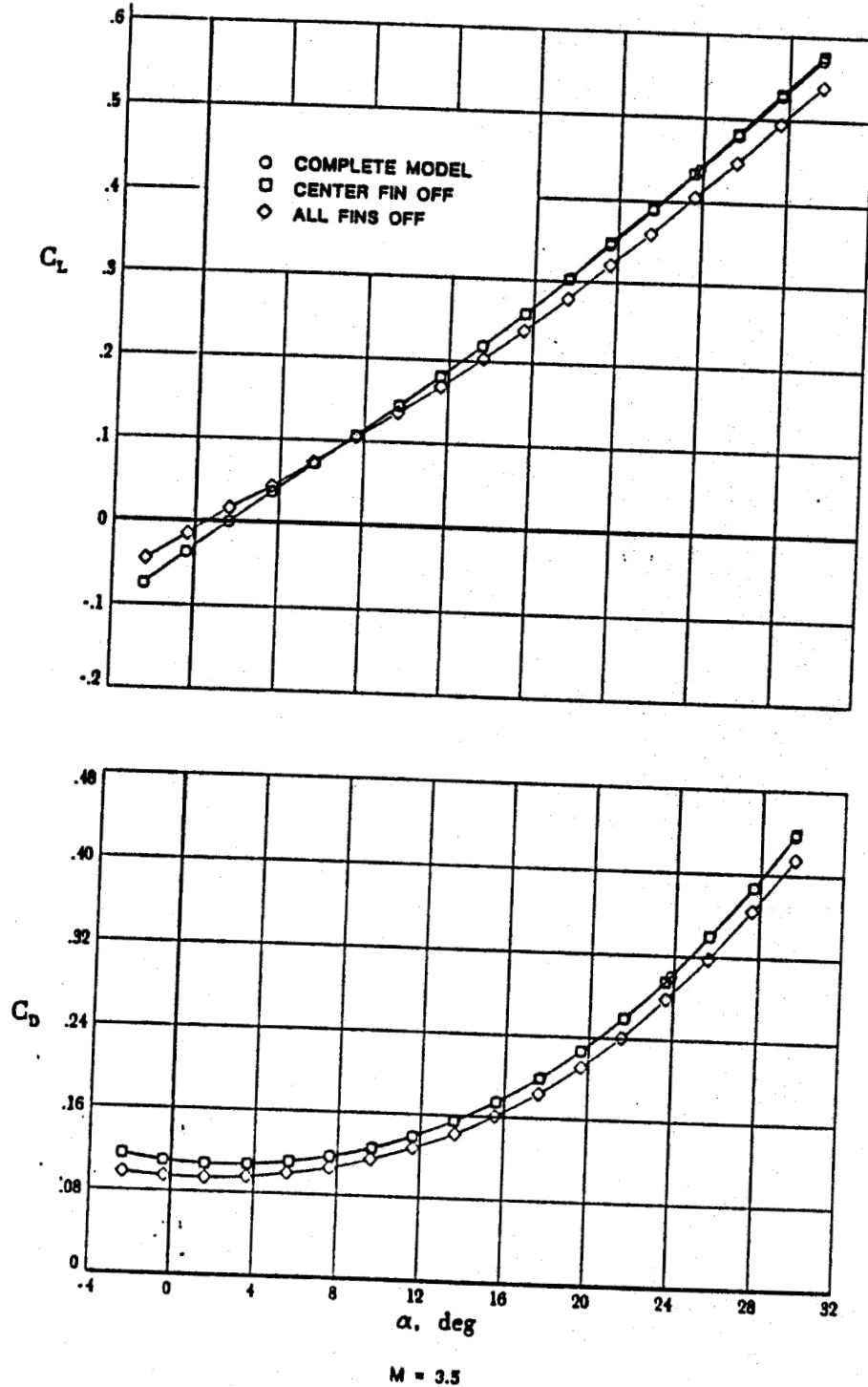
(a) C_L VS α and C_D VS α

Figure 22. Continued.

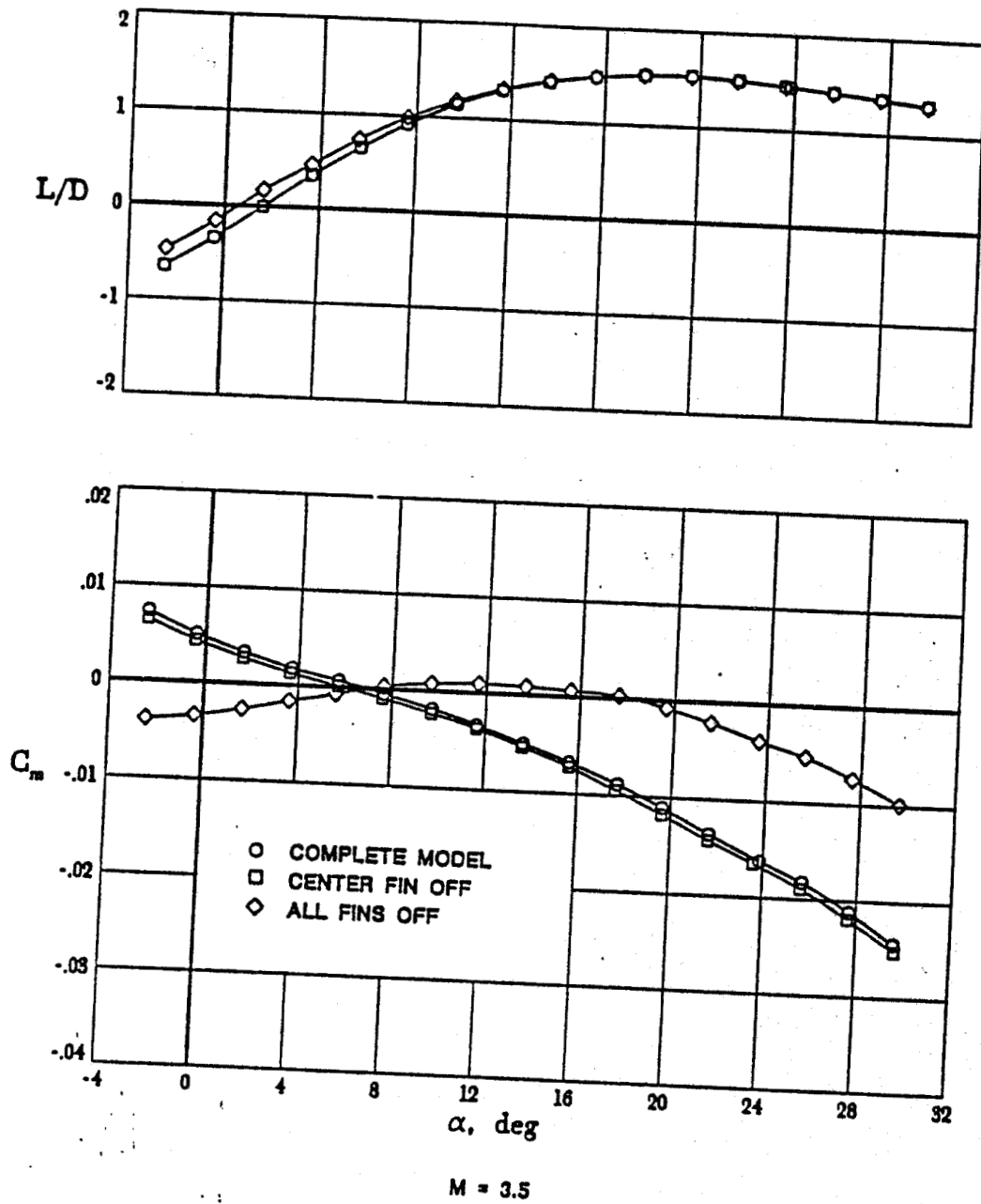
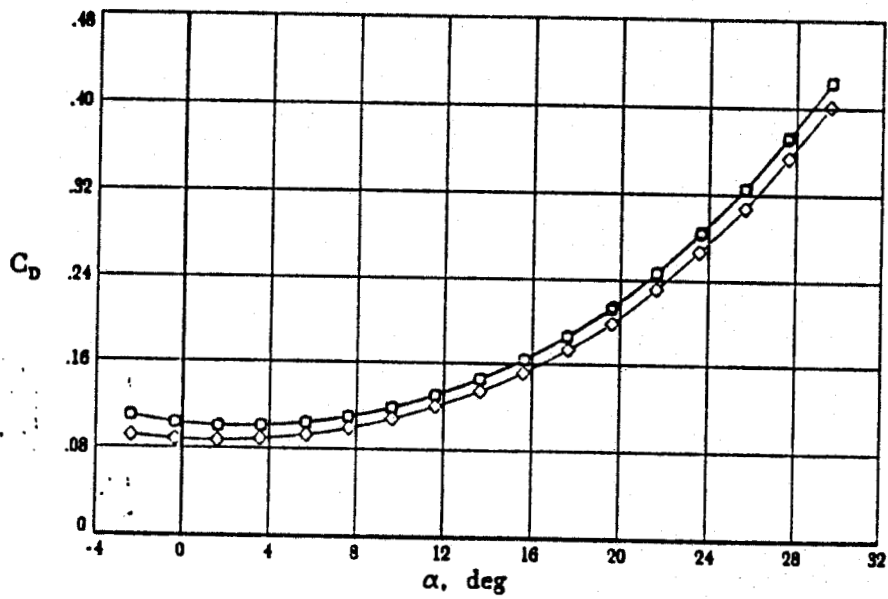
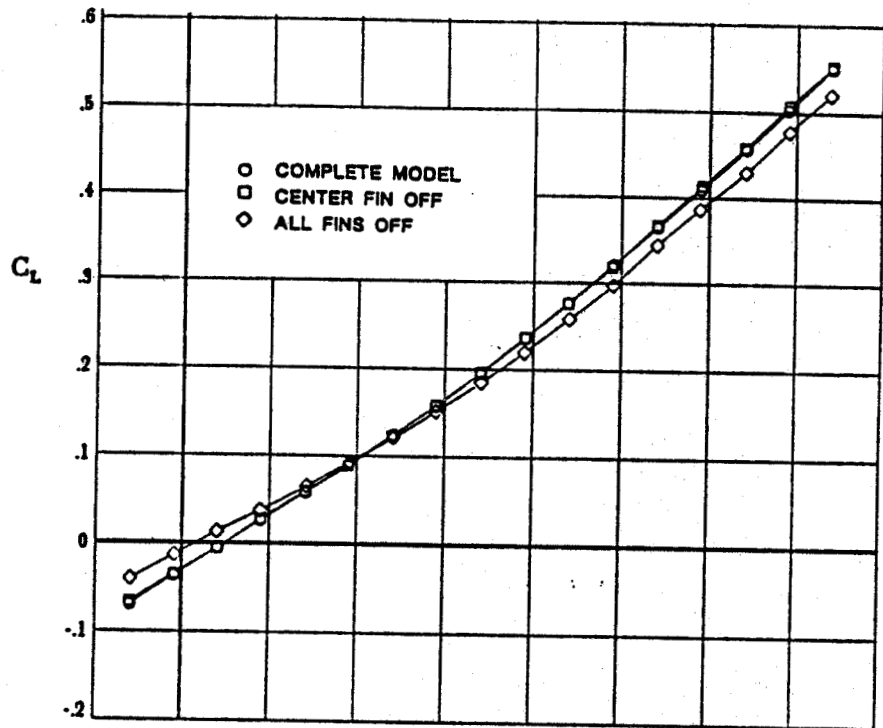
(b) L/D VS α and C_m VS α

Figure 22. Continued.



$M = 4.0$

(a) C_L VS α and C_D VS α

Figure 22. Continued.

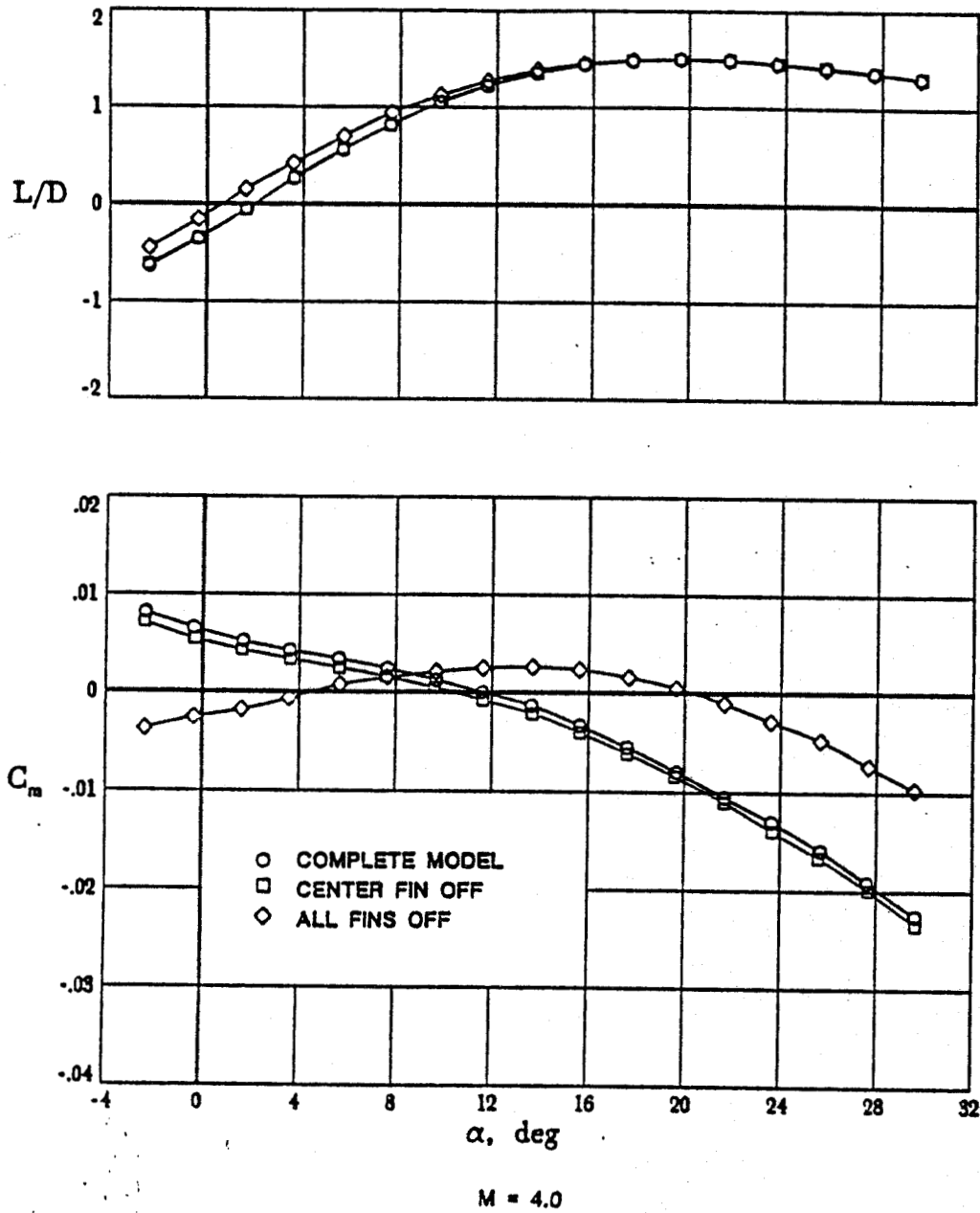
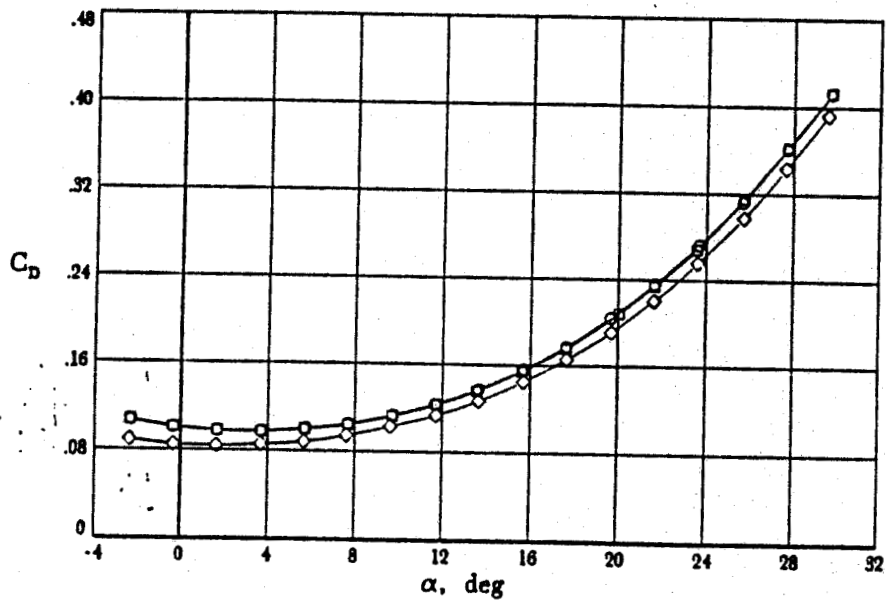
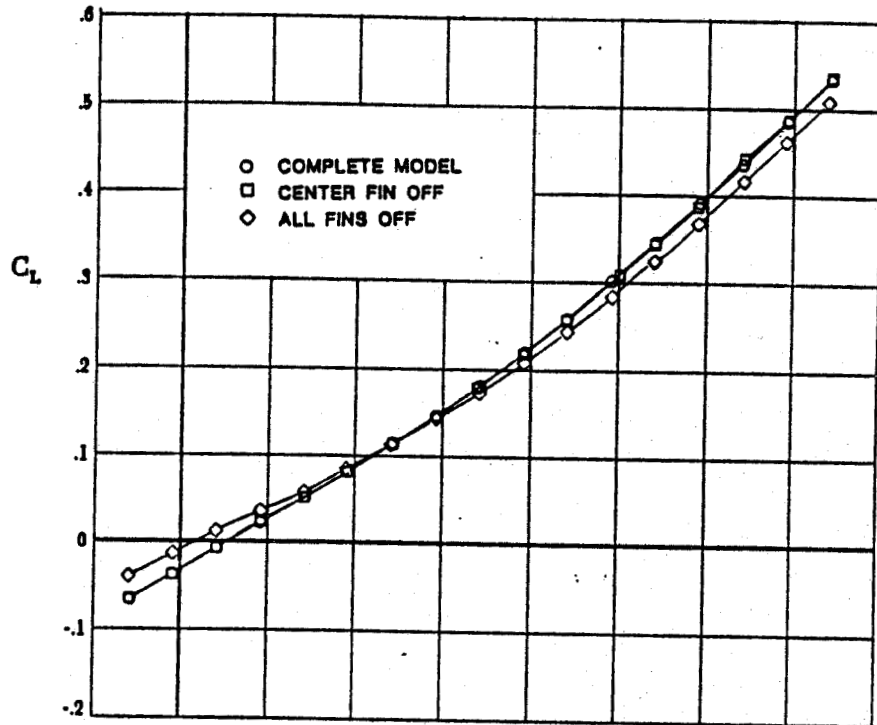
(b) L/D VS α and C_m VS α

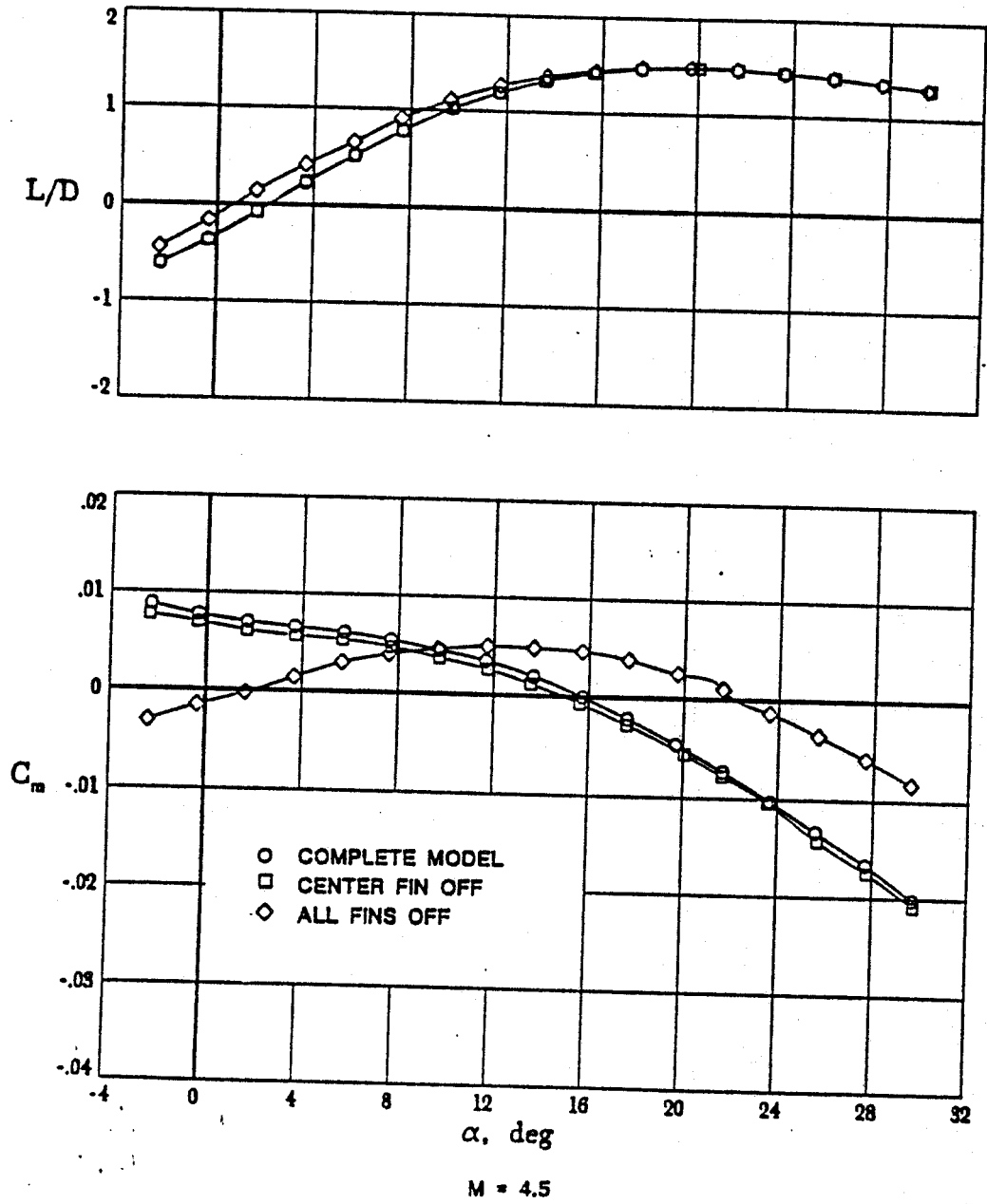
Figure 22. Continued.



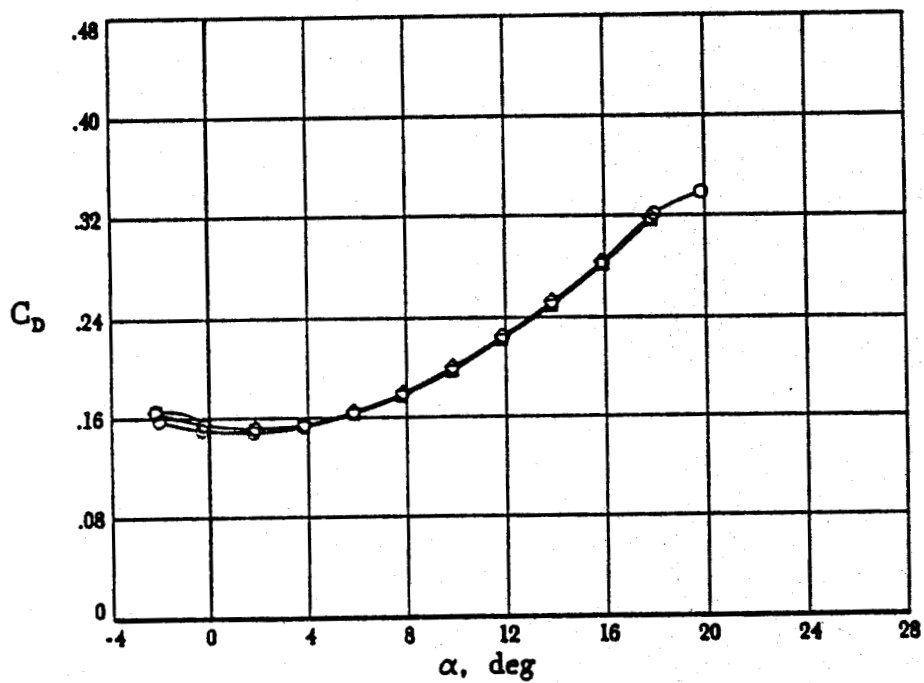
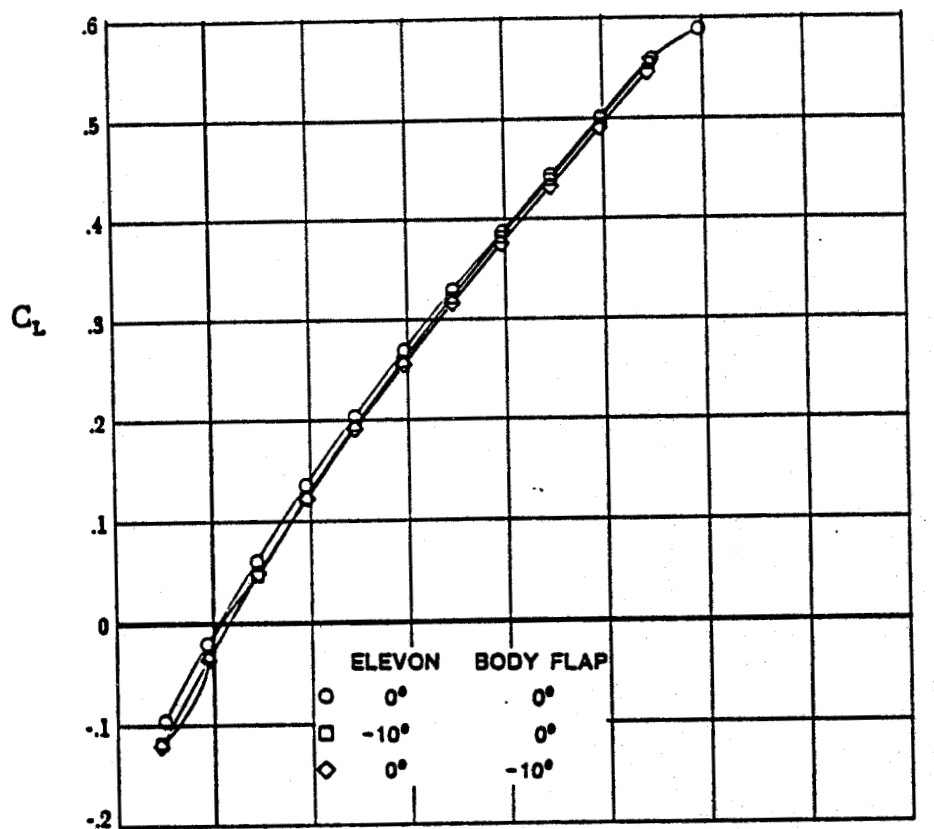
$M = 4.5$

(a) C_L VS α and C_D VS α

Figure 22. Continued.



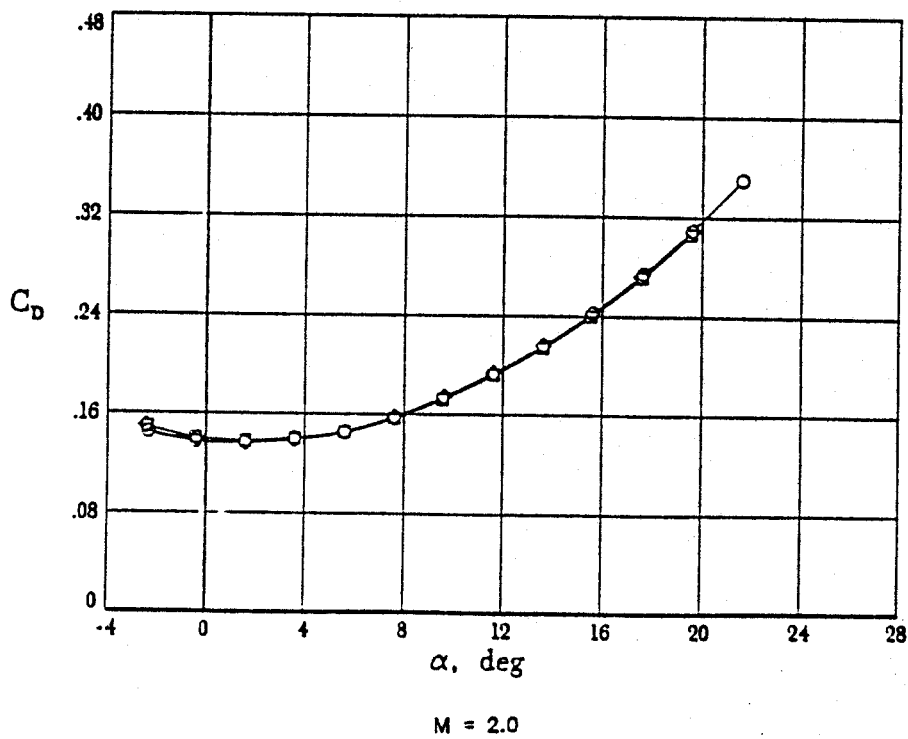
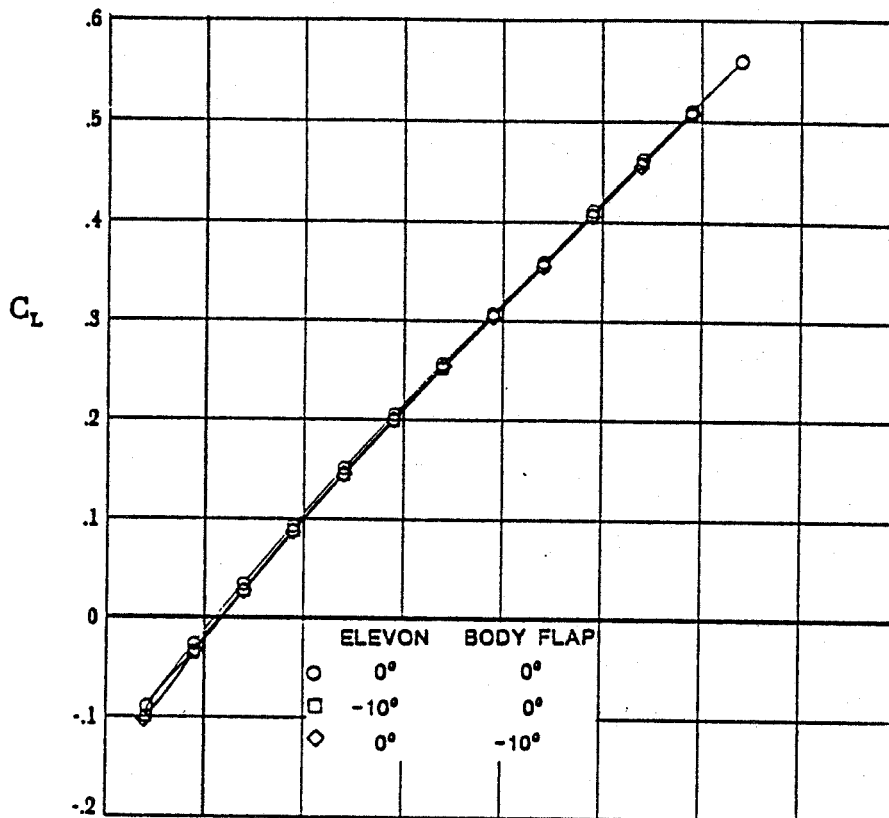
(b) L/D VS α and C_m VS α
 Figure 22. Concluded.



$M = 1.6$

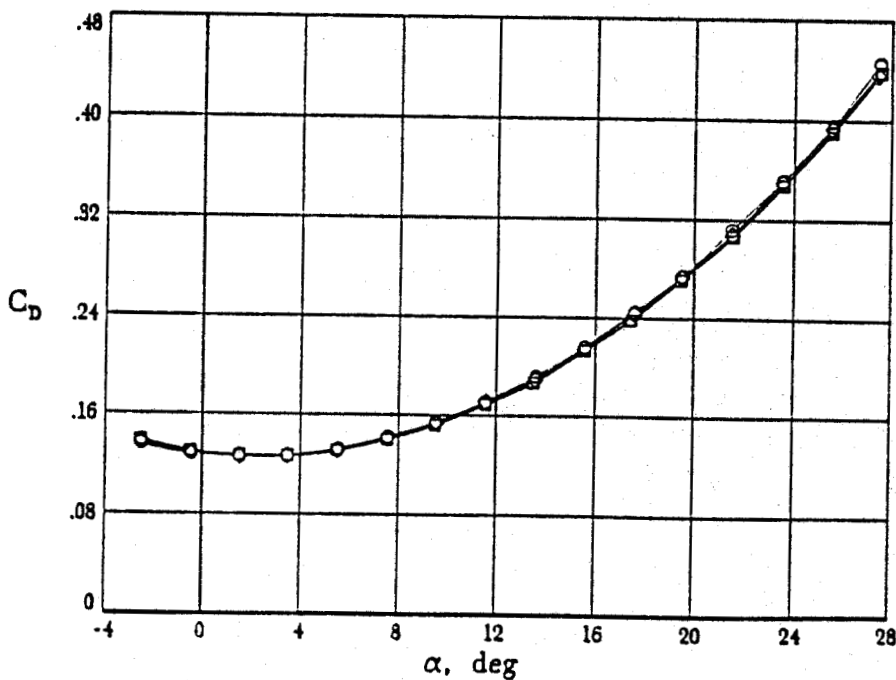
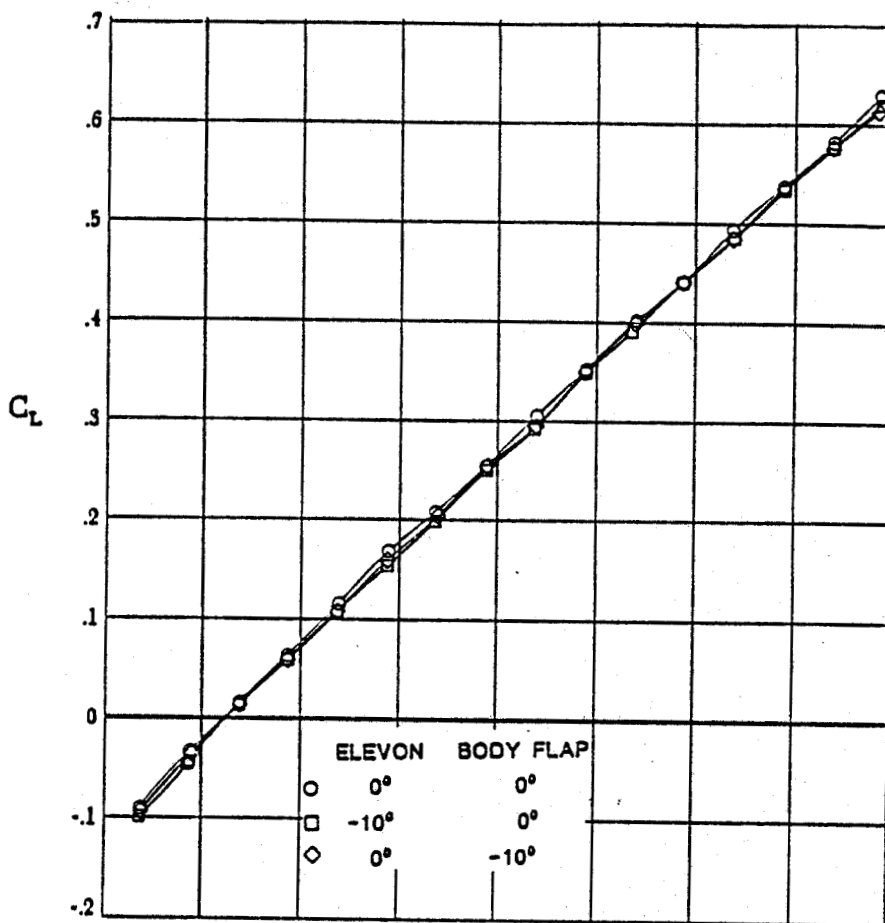
(a) C_L VS α and C_D VS α

Figure 23. Effect of elevon and body flap on the supersonic longitudinal characteristics of the model.



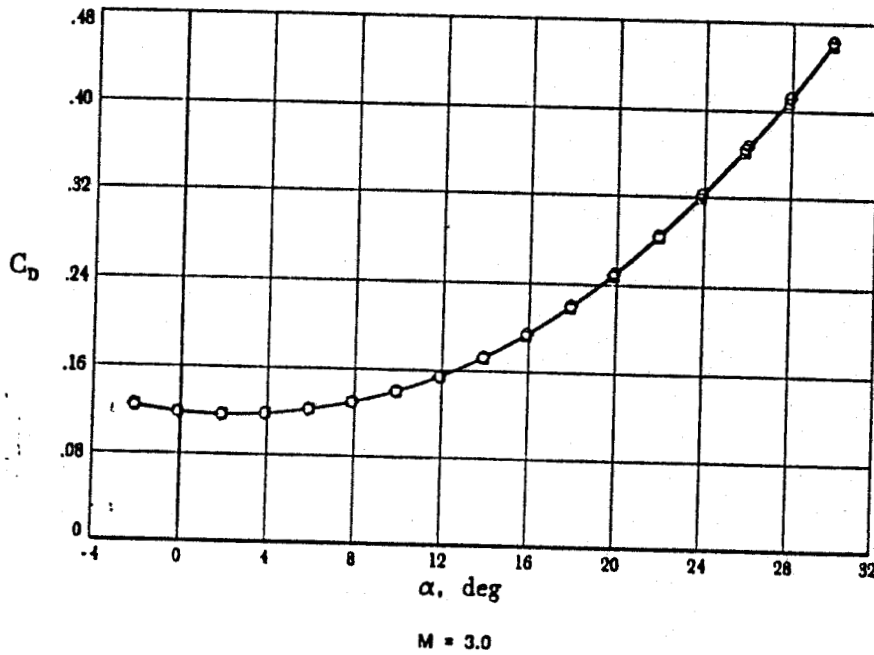
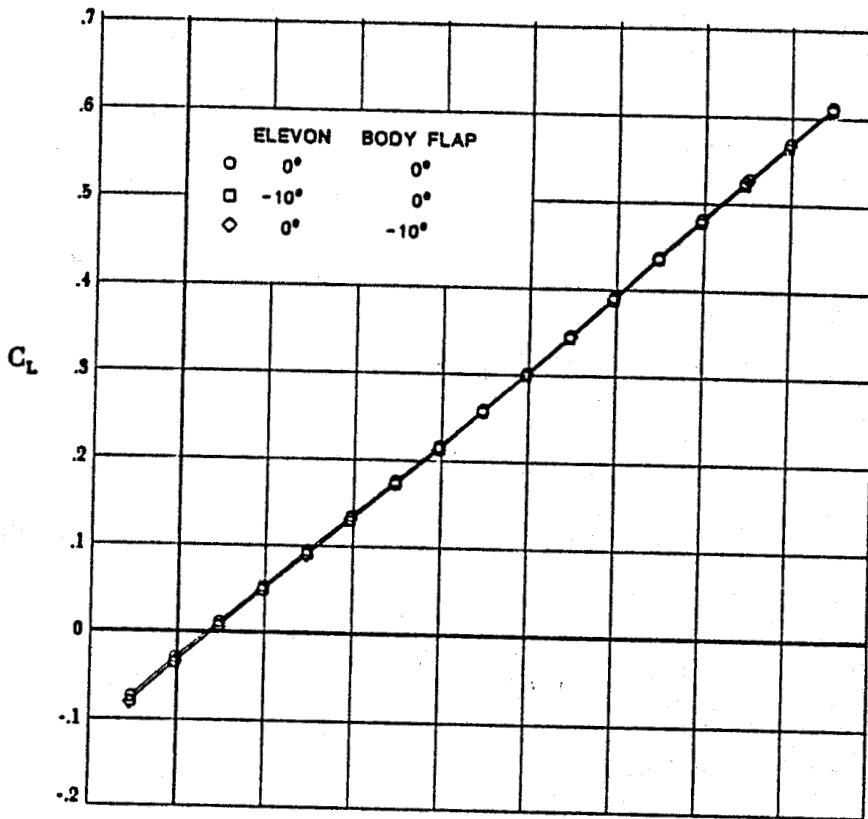
(a) C_L VS α and C_D VS α

Figure 23. Continued.

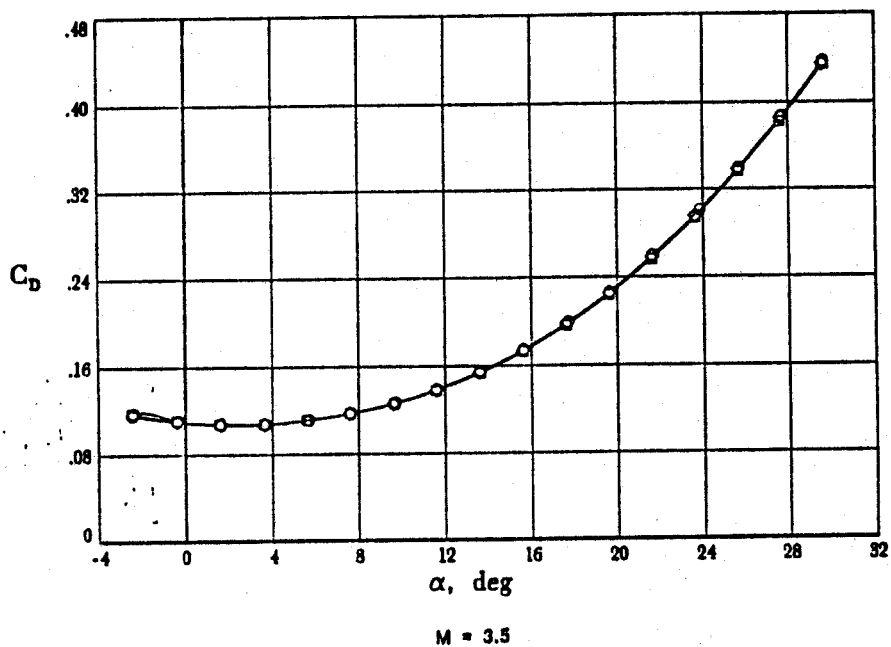
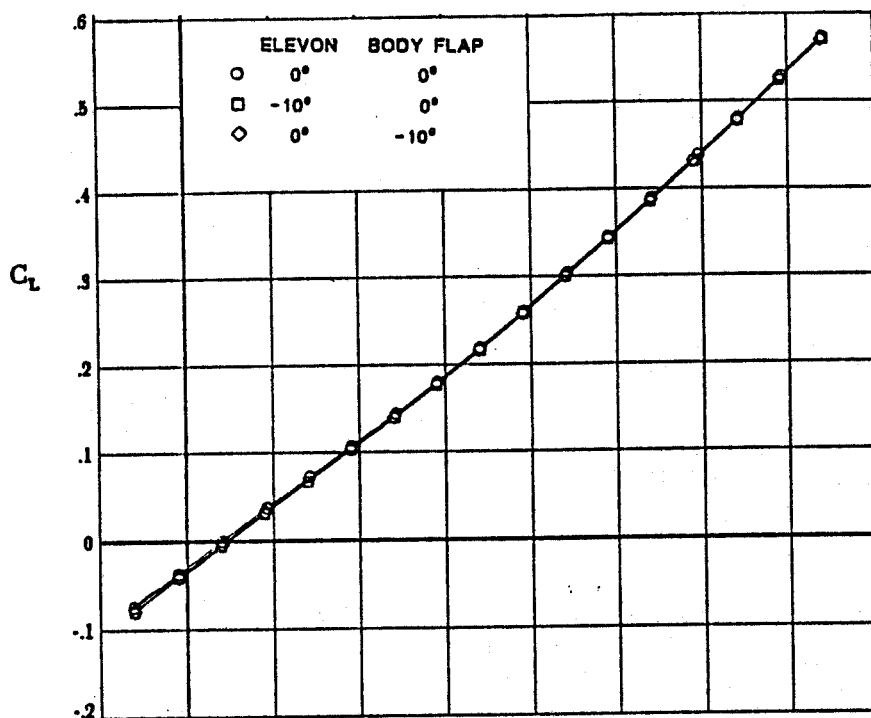


M = 2.5

(a) C_L VS α and C_D VS α
 Figure 23. Continued.

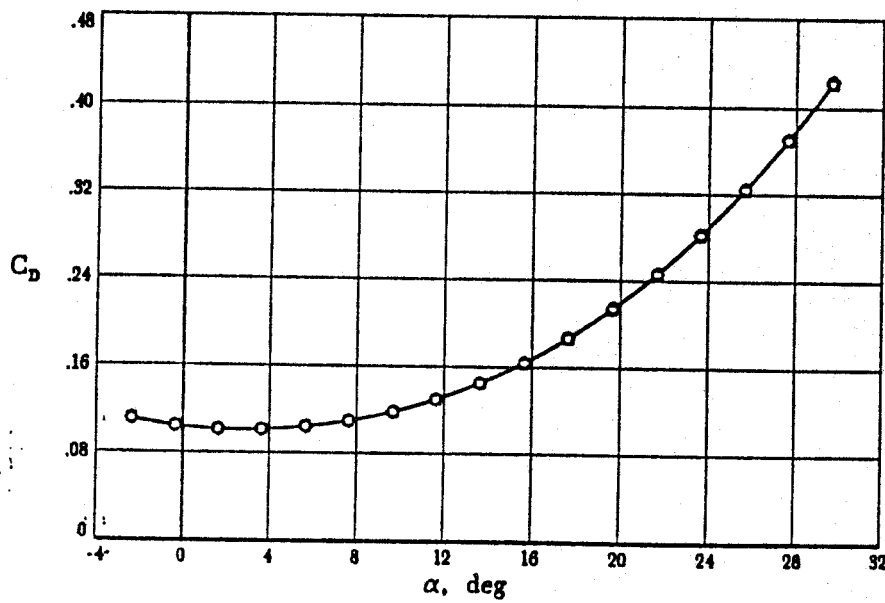
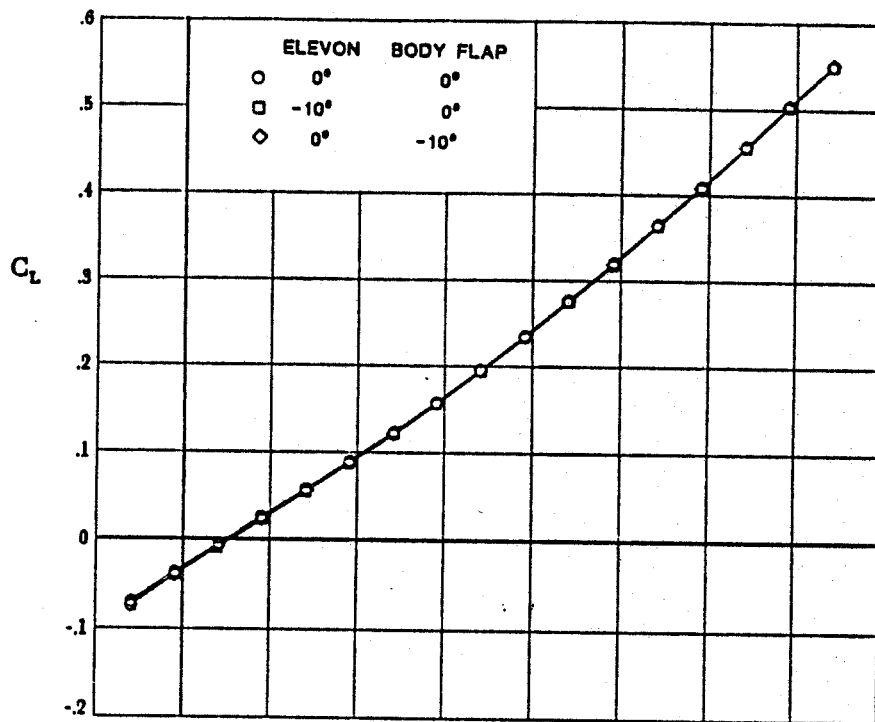


(a) C_L VS α and C_D VS α
 Figure 23. Continued.



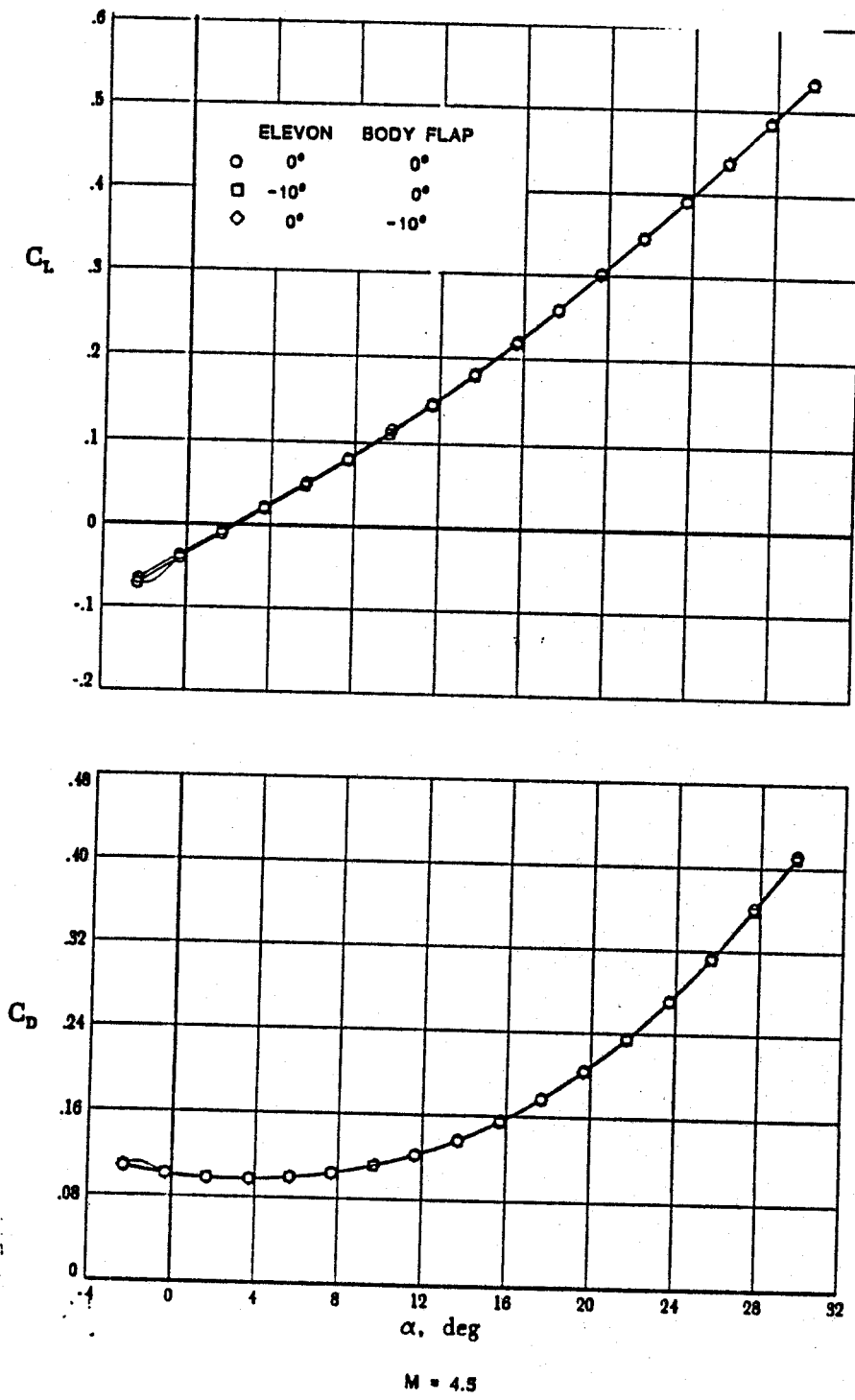
(a) C_L VS α and C_D VS α

Figure 23. Continued.



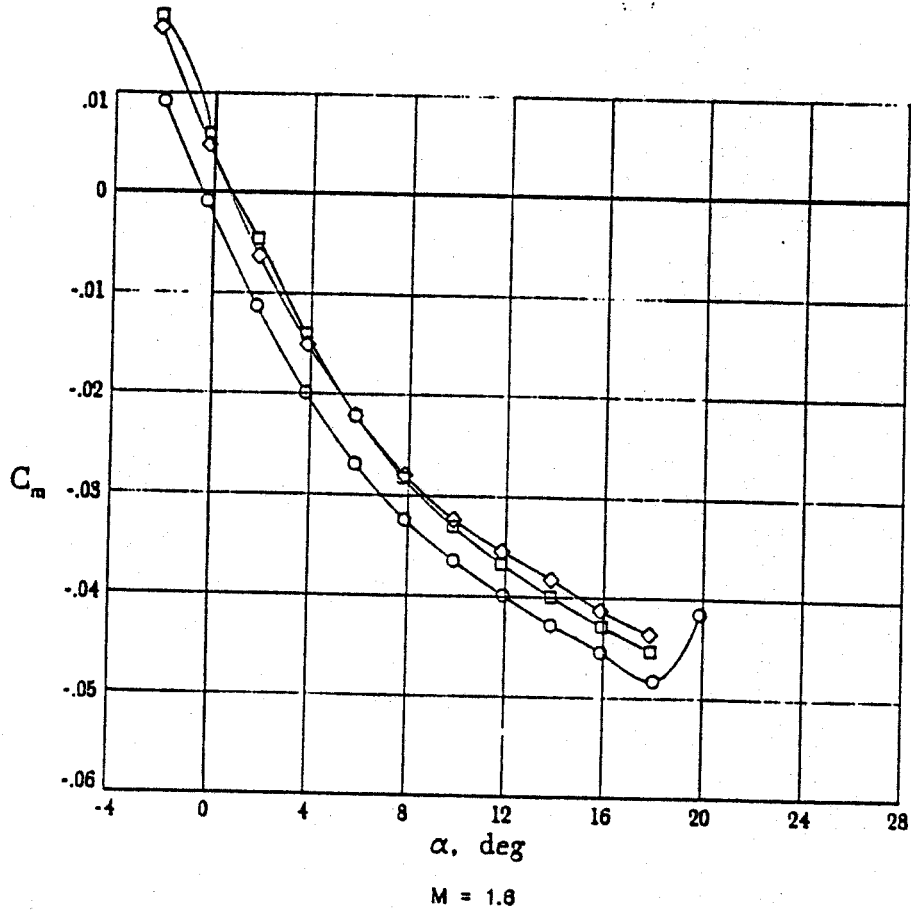
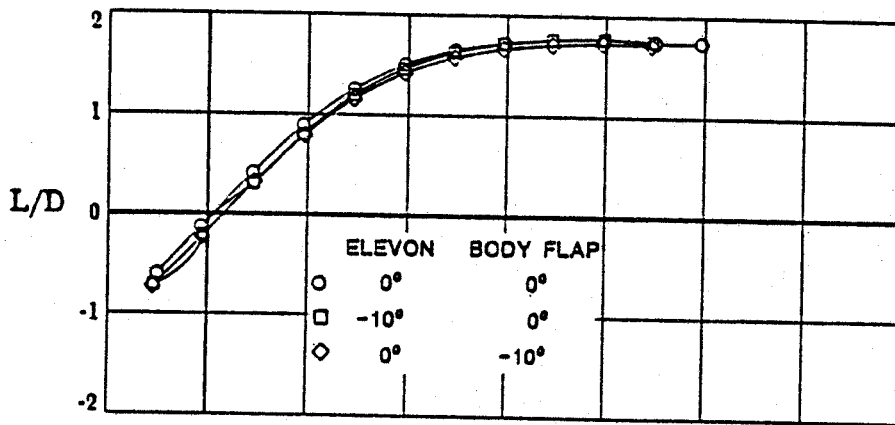
$M = 4.0$

(a) C_L VS α and C_D VS α
Figure 23. Continued.

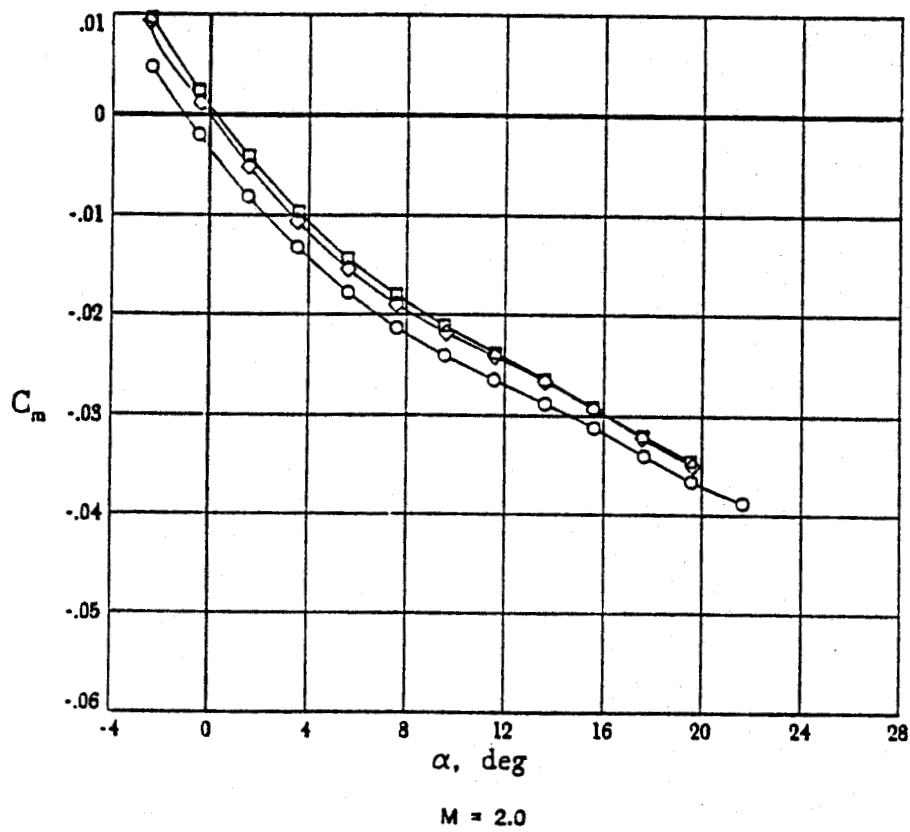
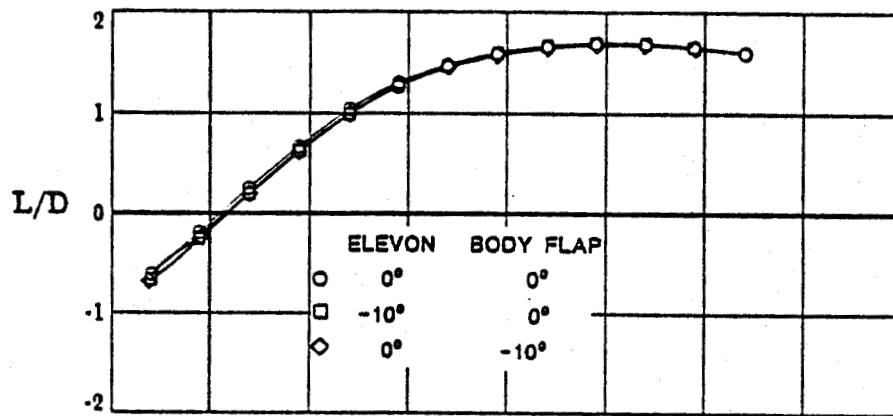


(a) C_L VS α and C_D VS α

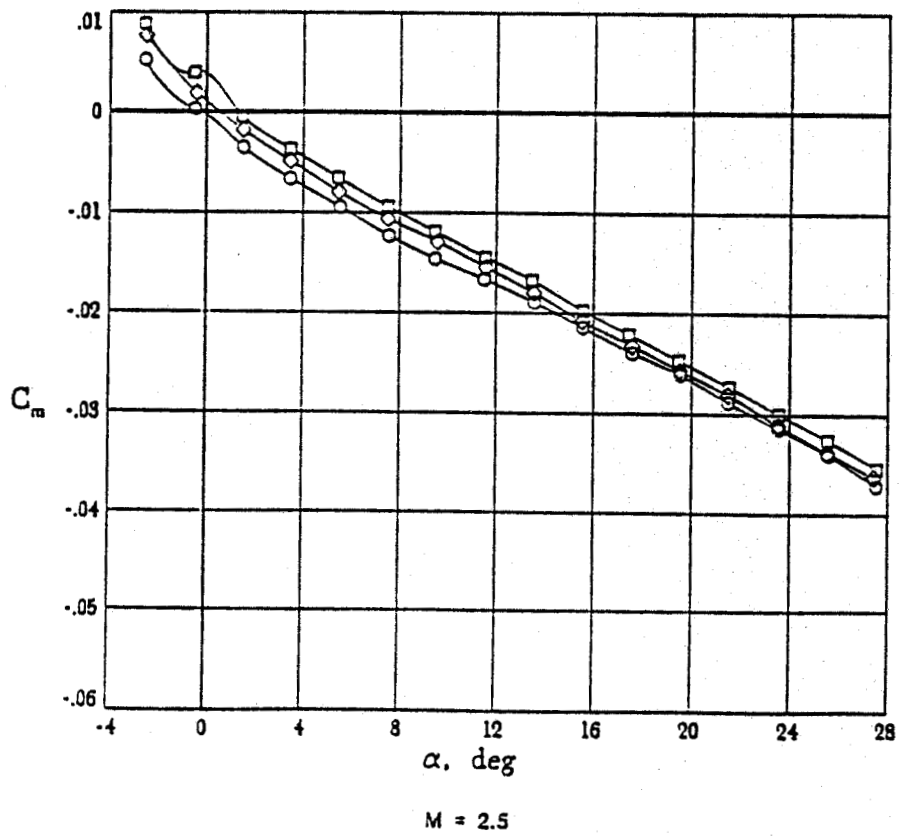
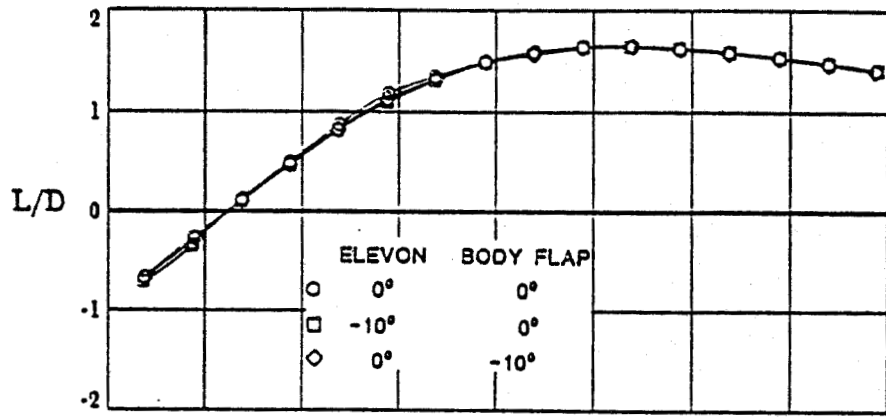
Figure 23. Continued.



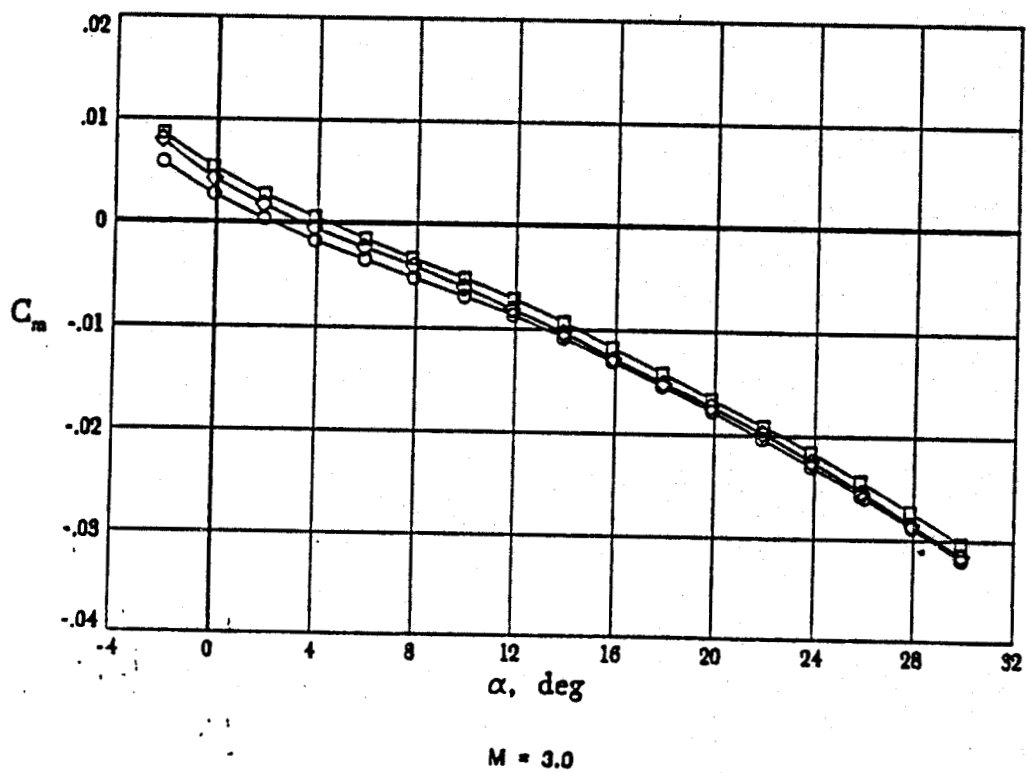
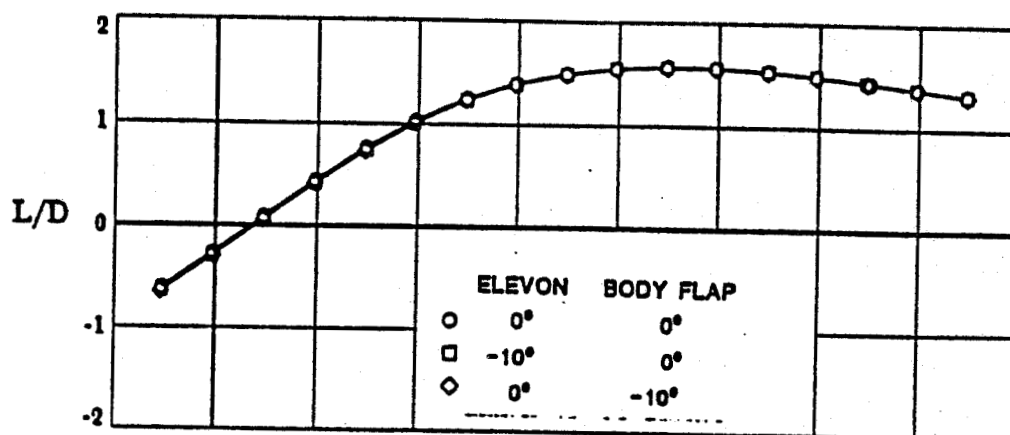
(b) L/D VS α and C_m VS α
 Figure 23. Continued.



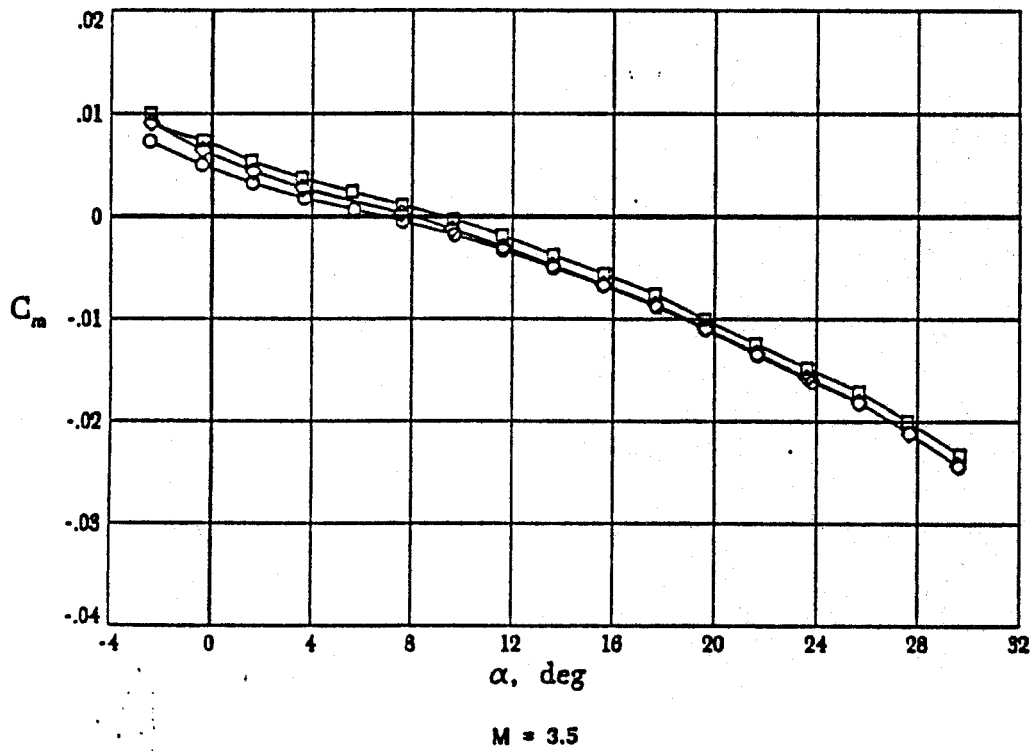
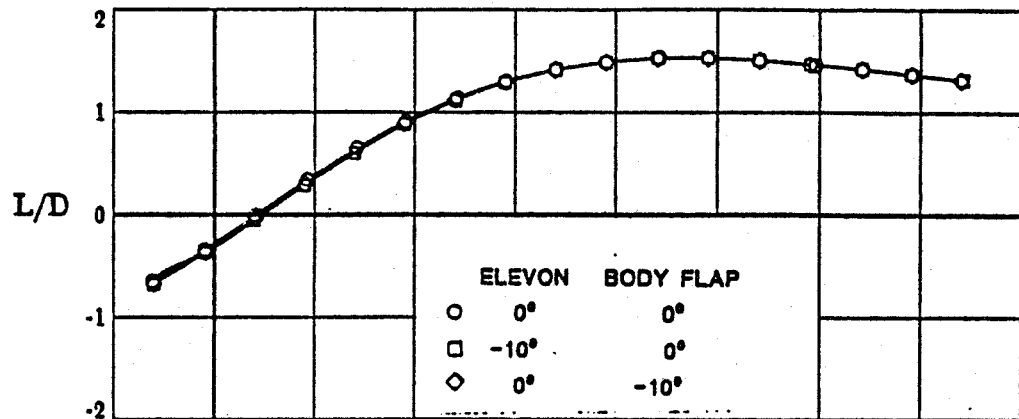
(b) L/D VS α and C_m VS α
Figure 23. Continued.



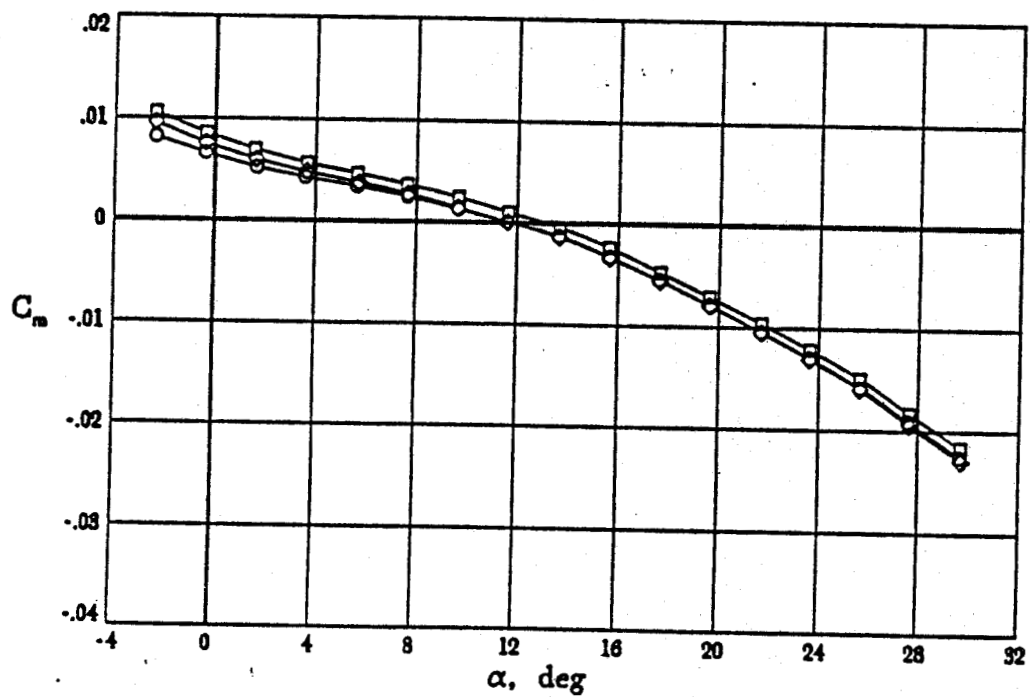
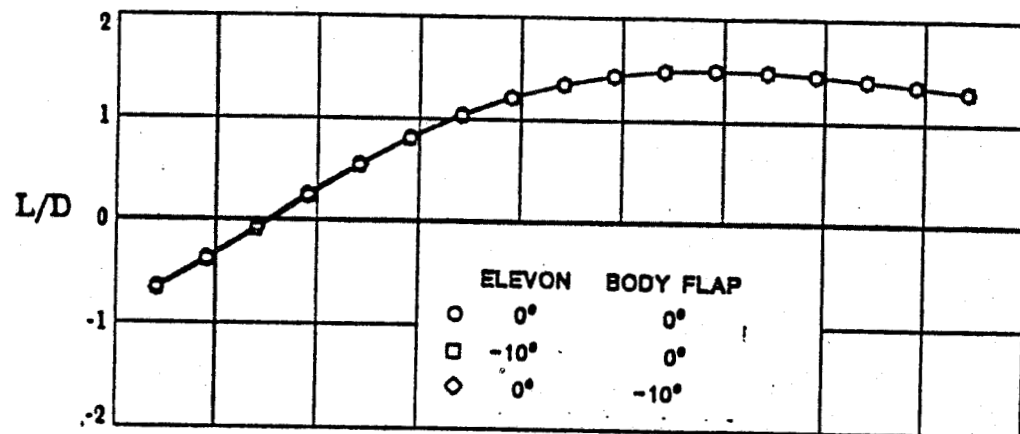
(b) L/D VS α and C_m VS α
 Figure 23. Continued.



(b) L/D VS α and C_m VS α
 Figure 23. Continued.

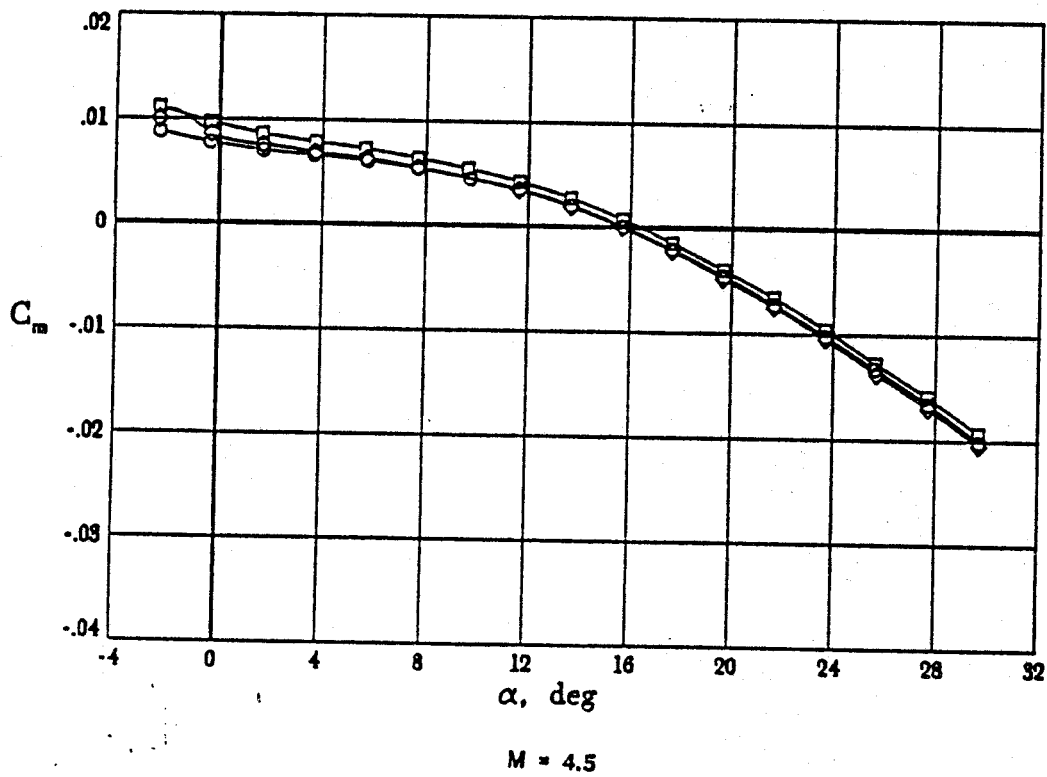
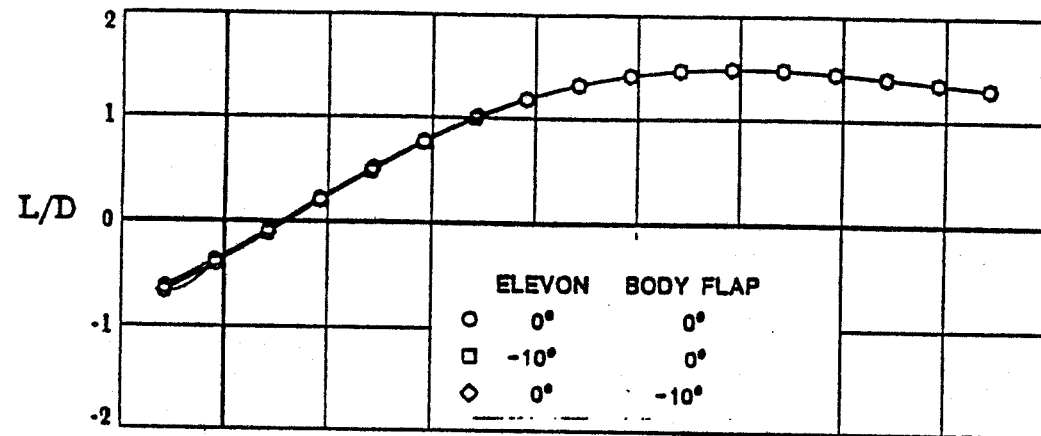


(b) L/D VS α and C_m VS α
 Figure 23. Continued.



$M = 4.0$

(b) L/D VS α and C_m VS α
Figure 23. Continued.



(b) L/D VS α and C_m VS α
 Figure 23. Concluded.

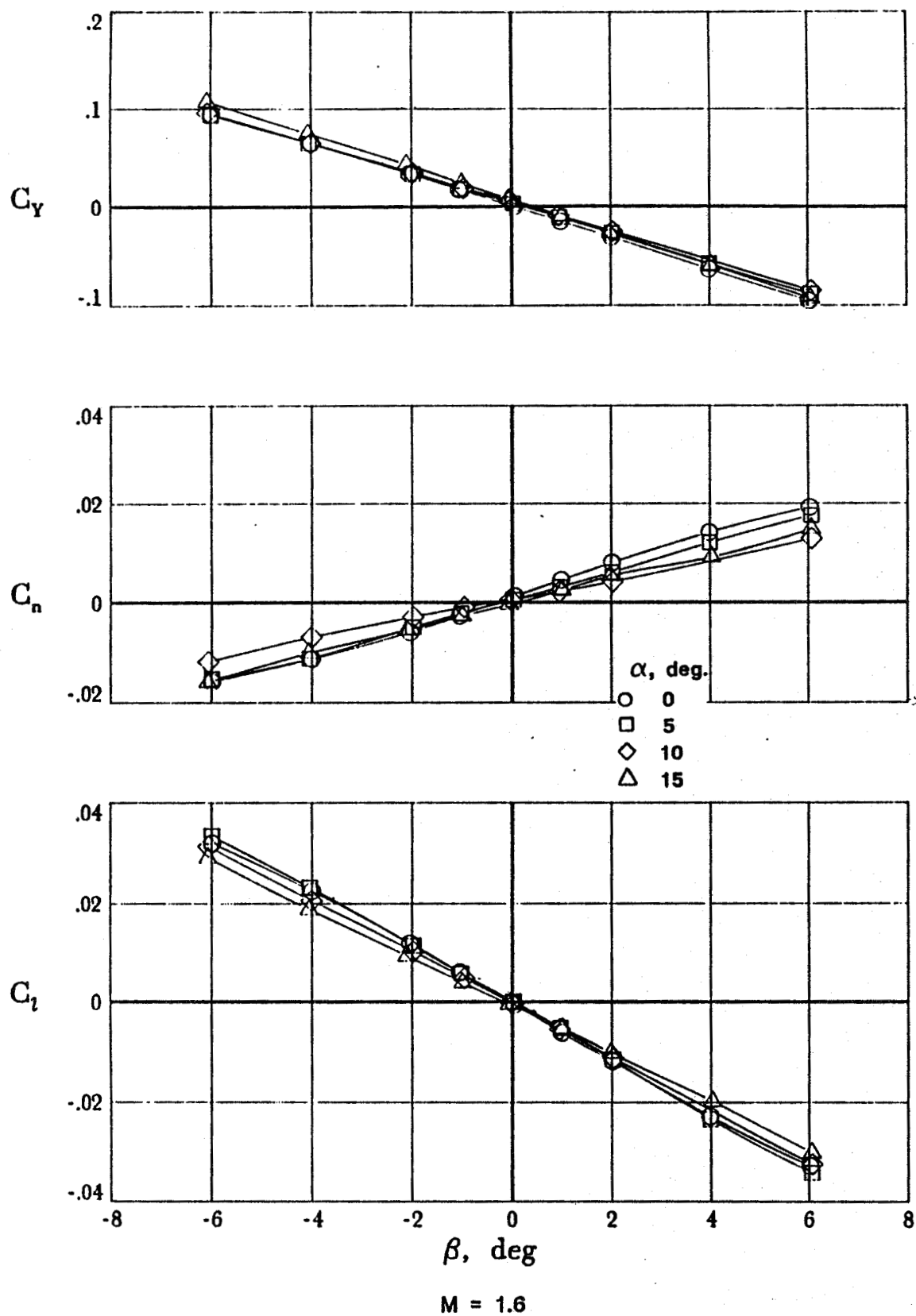


Figure 24. Variation of supersonic lateral aerodynamic characteristics with angle of sideslip.

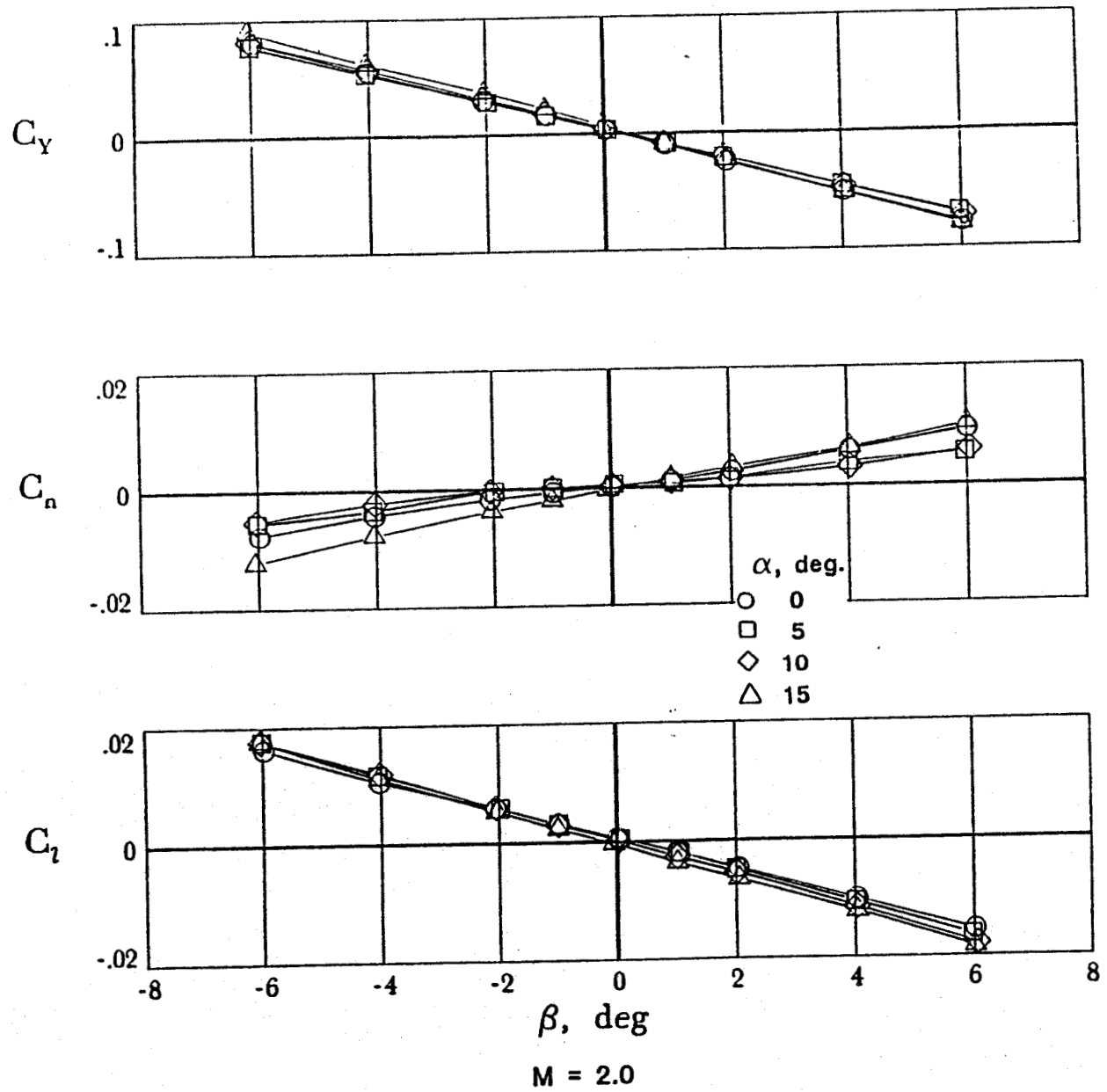


Figure 24. Continued.

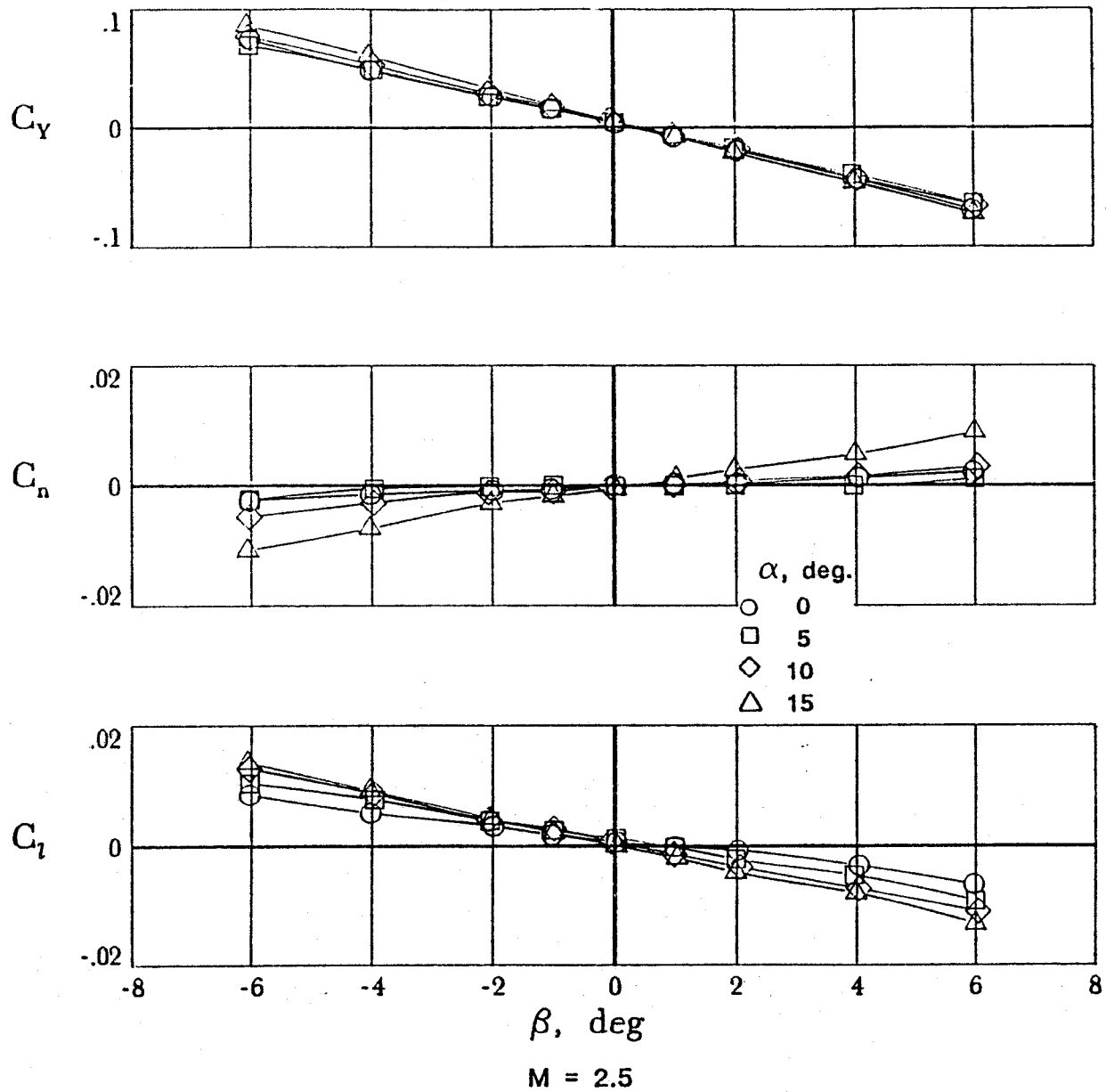


Figure 24. Continued.

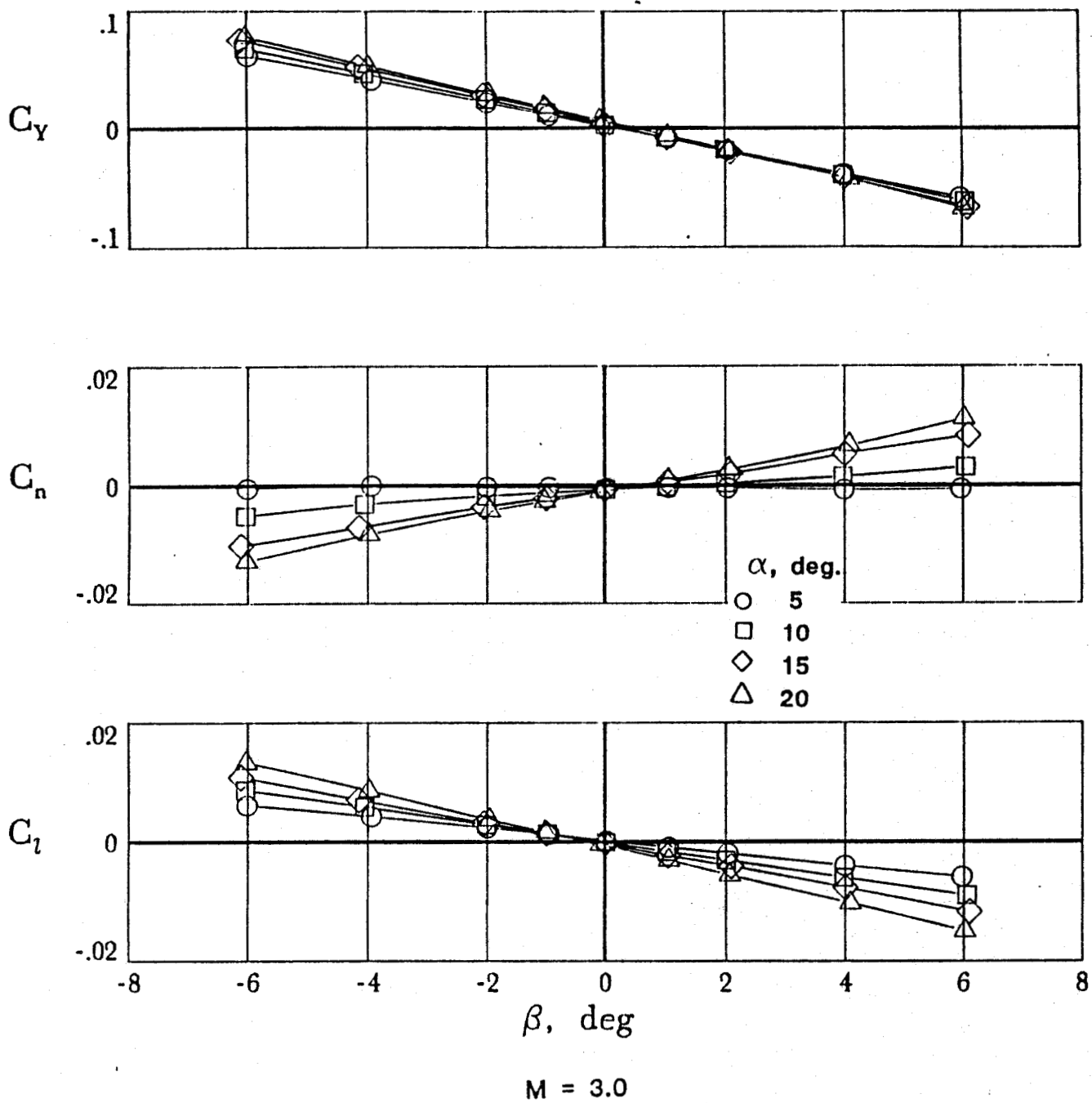


Figure 24. Continued.

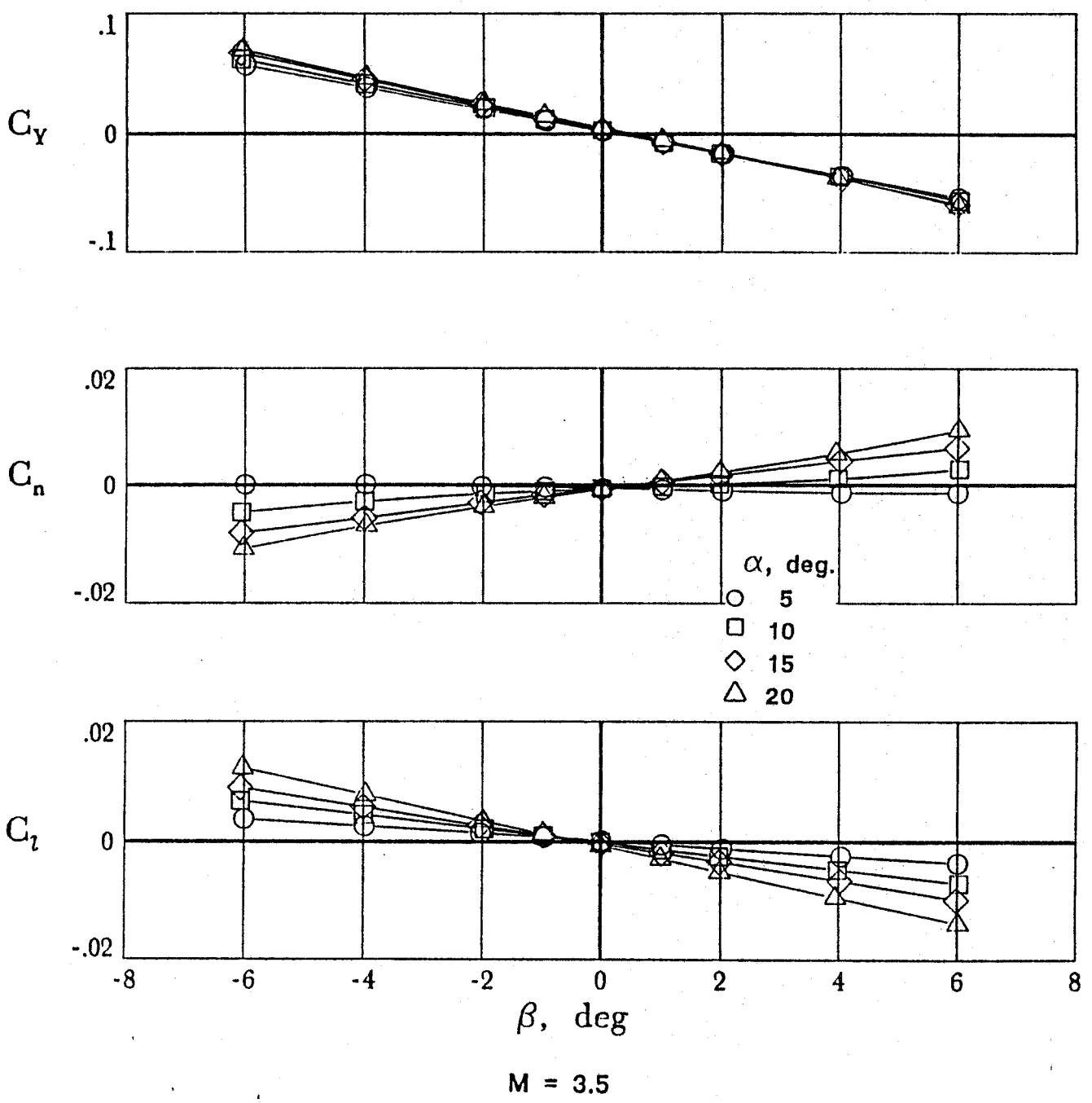


Figure 24. Continued.

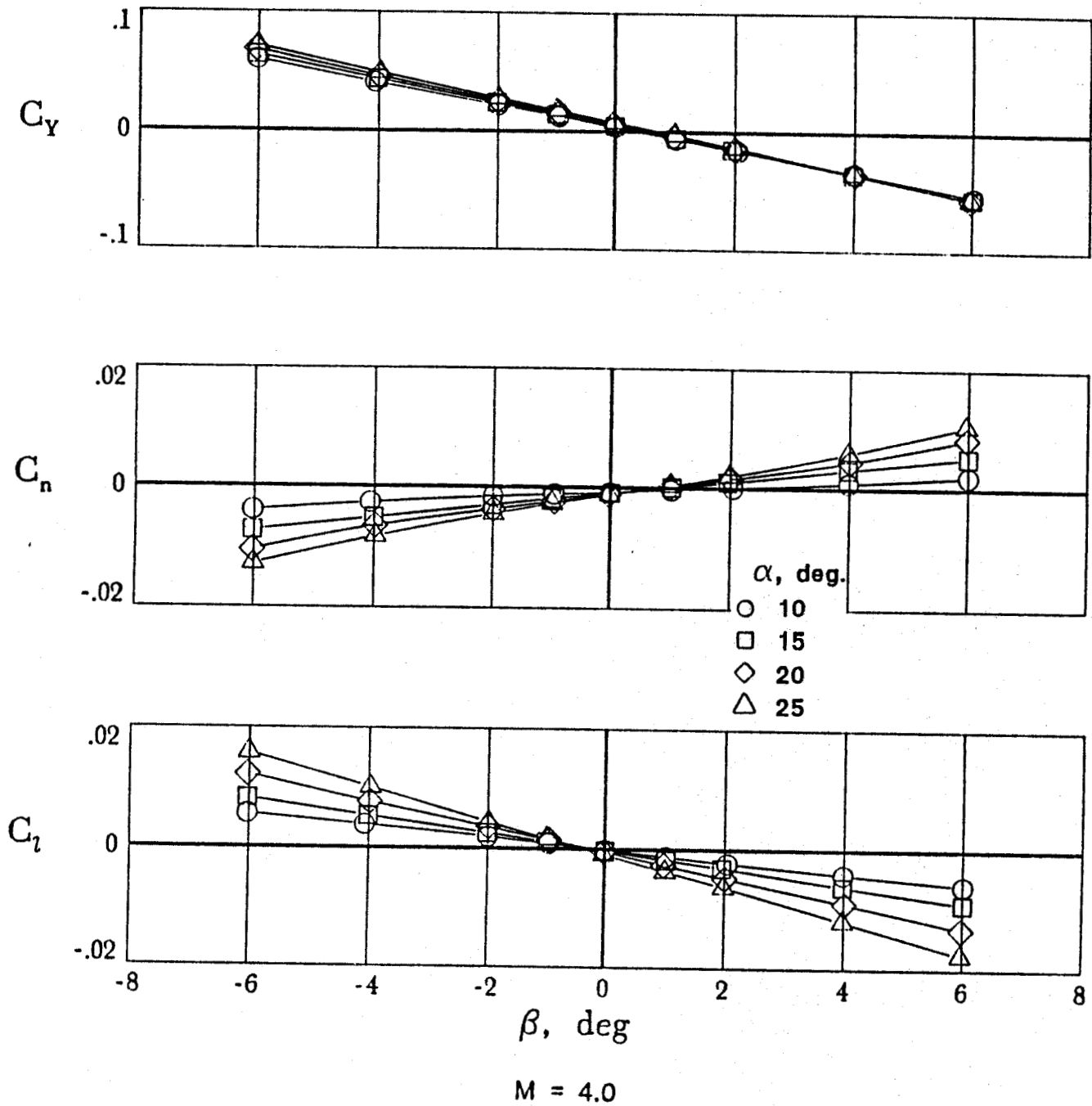


Figure 24. Continued.

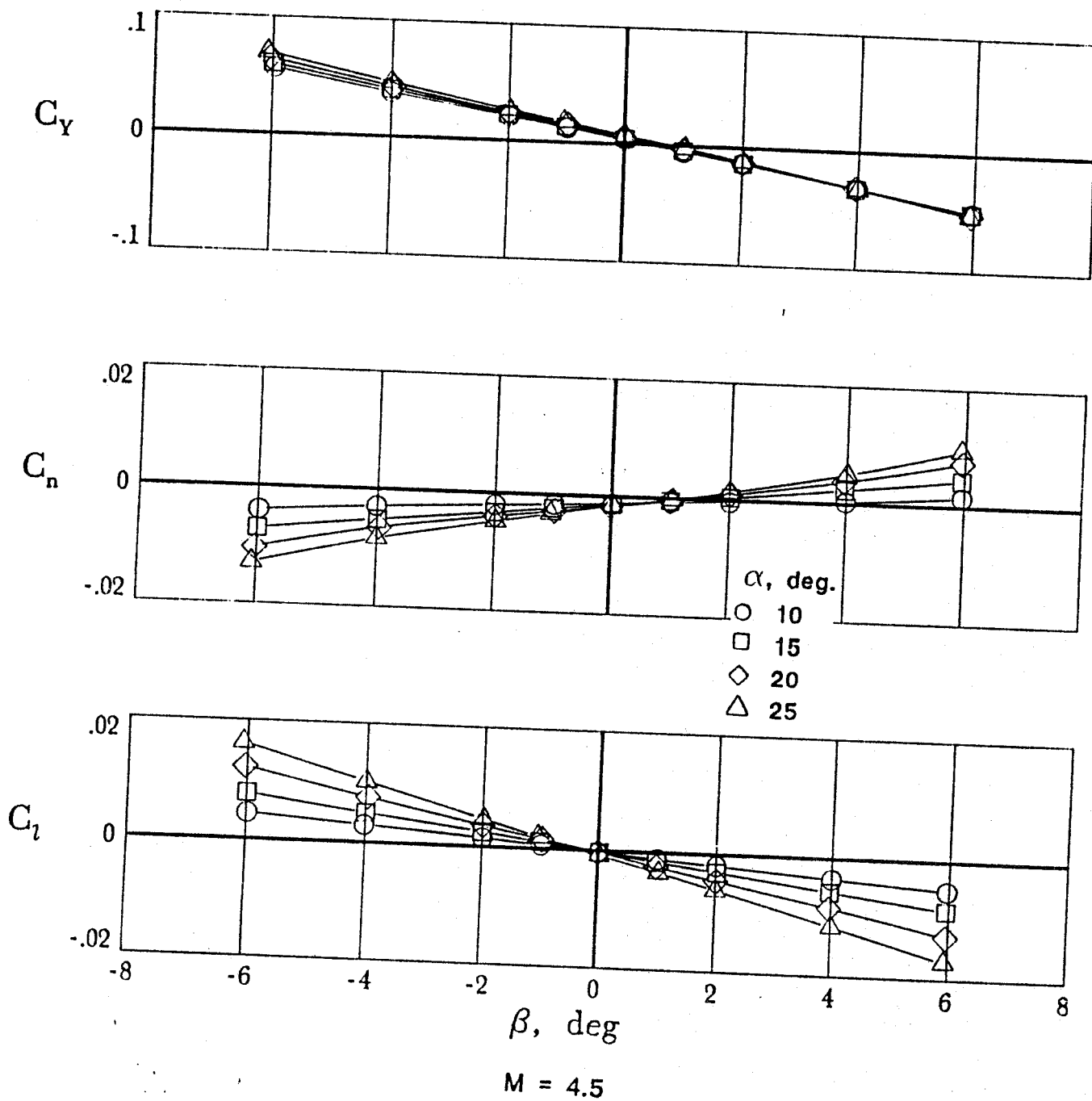


Figure 24. Concluded.

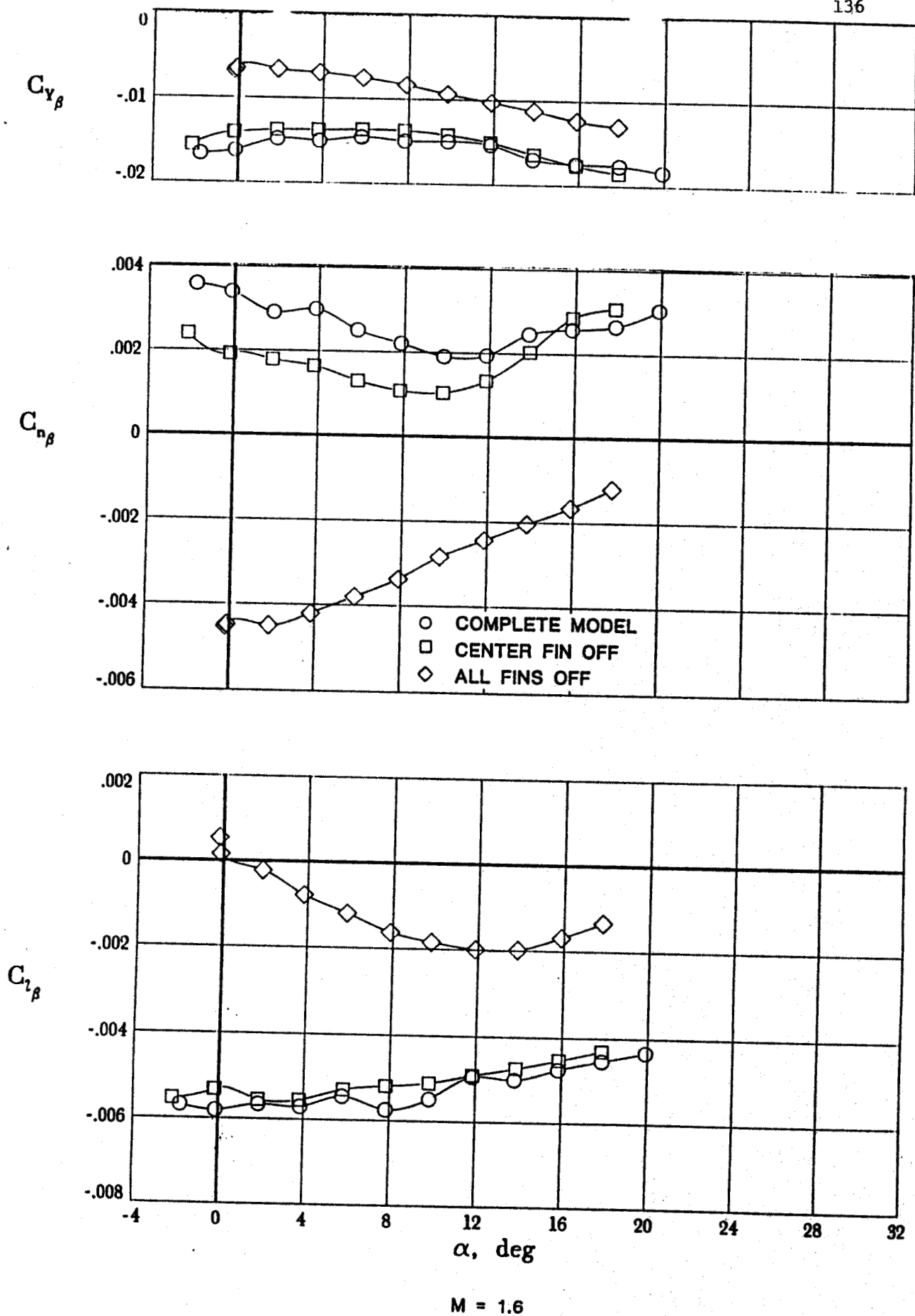
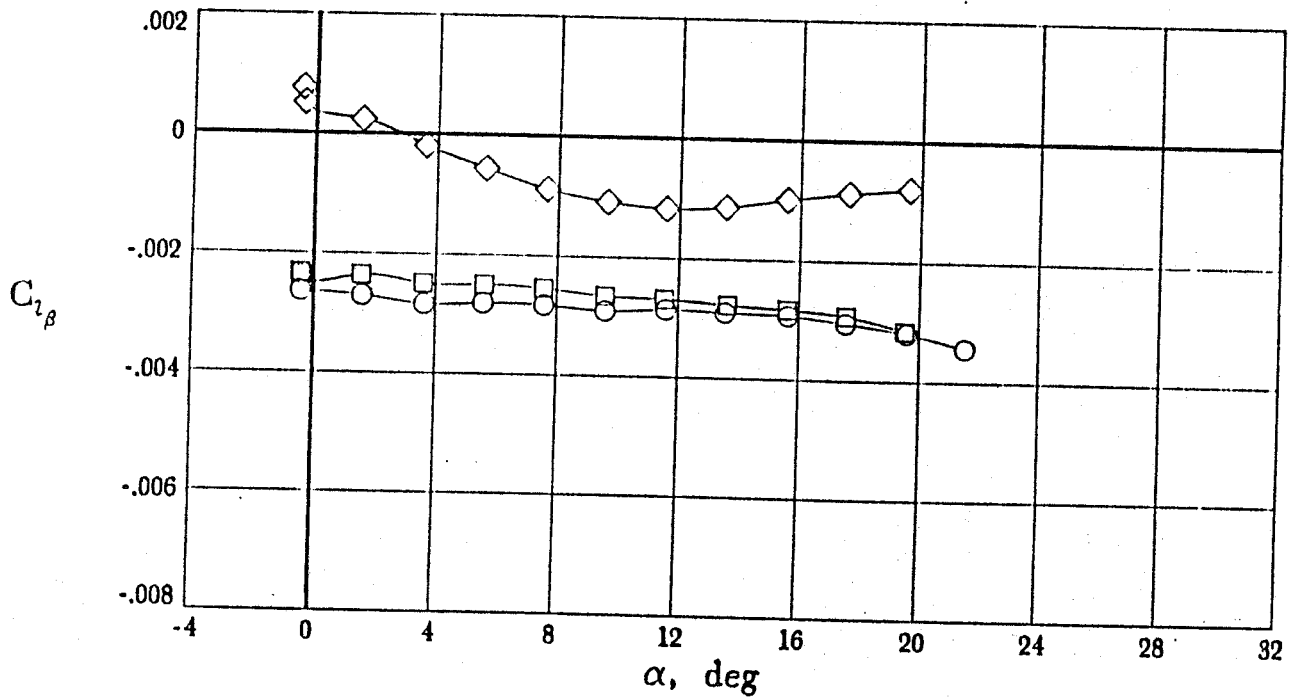
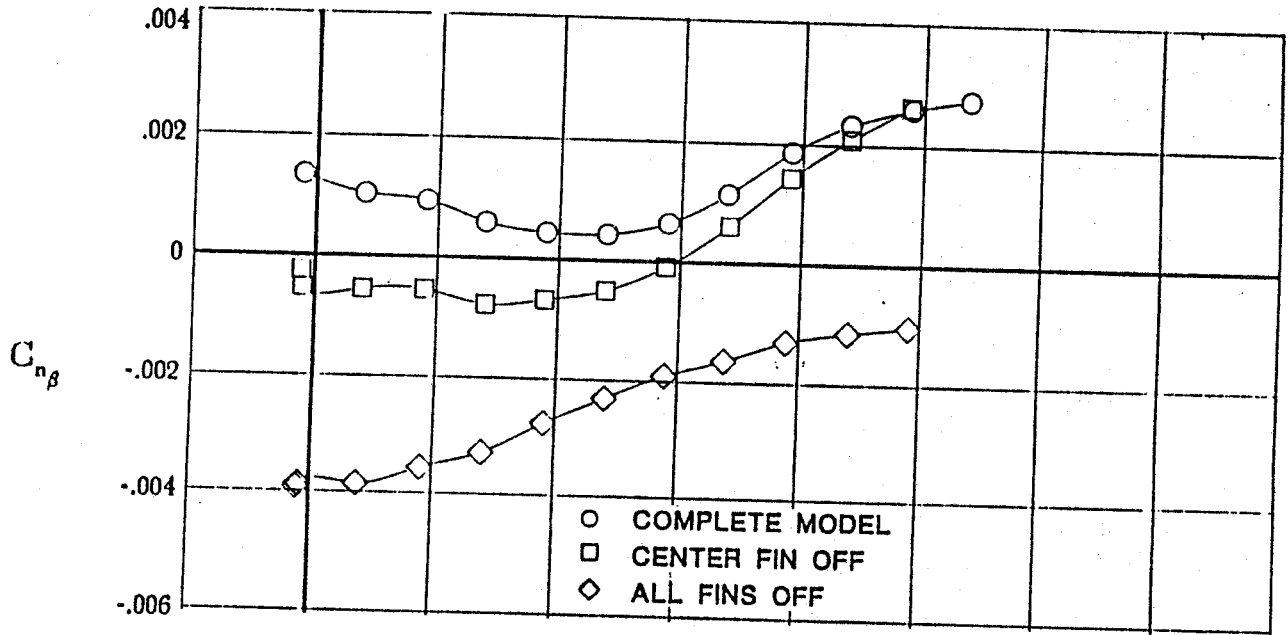
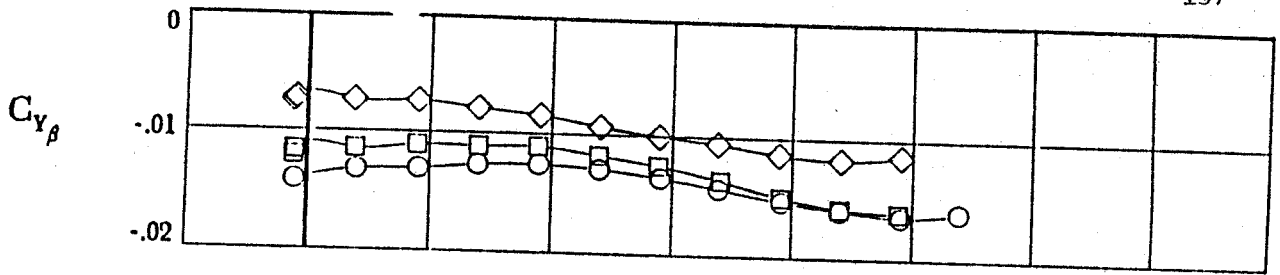


Figure 25. Effect of fins on the supersonic lateral-directional stability characteristics of the model.



M = 2.0

Figure 25. Continued.

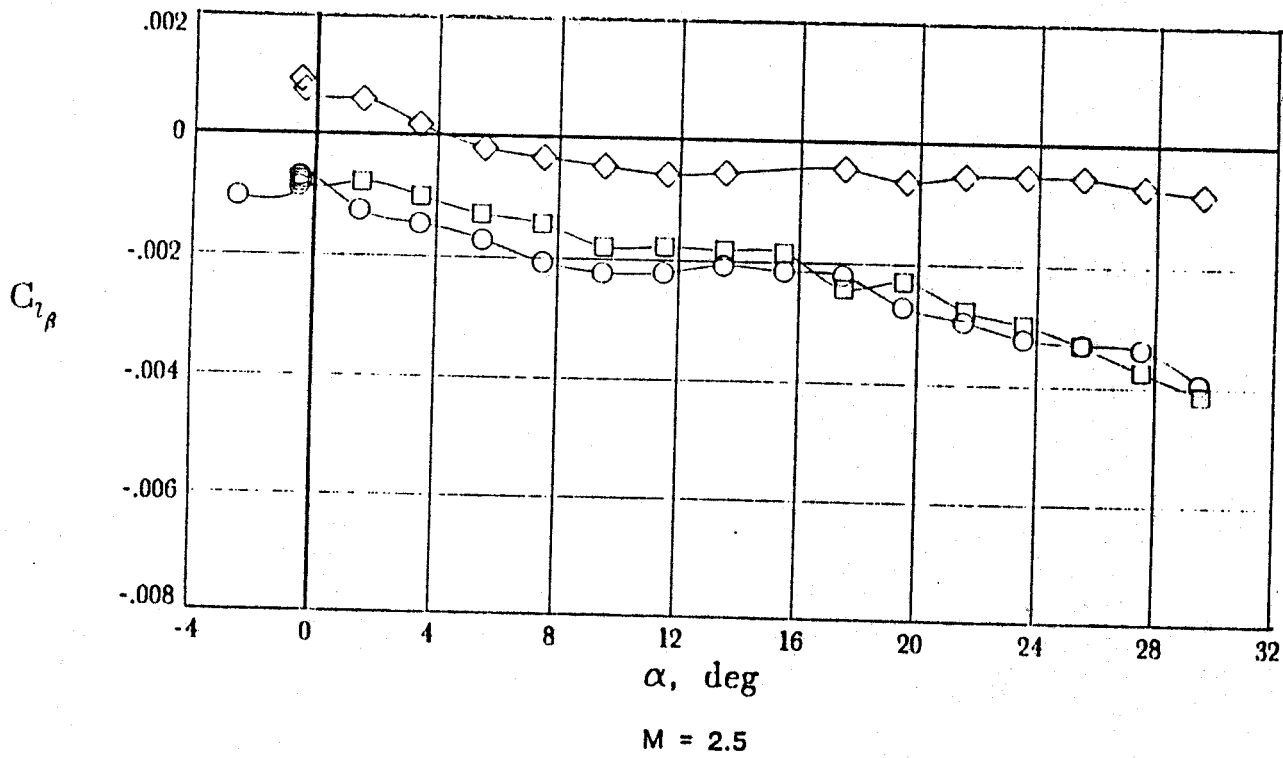
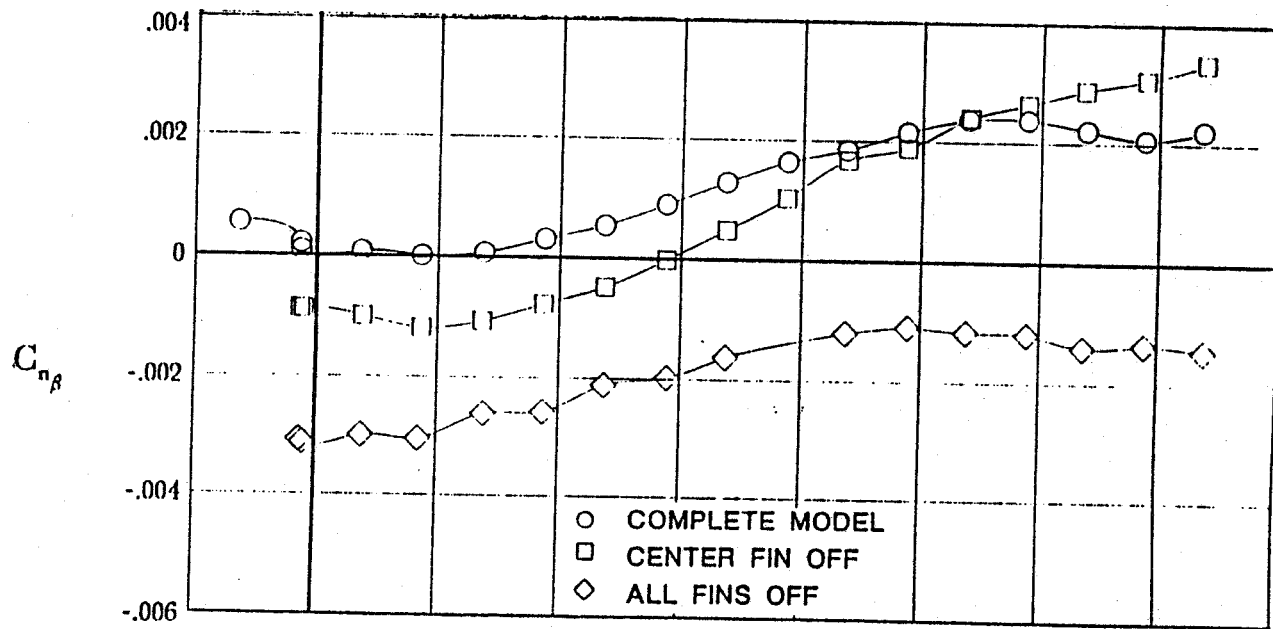
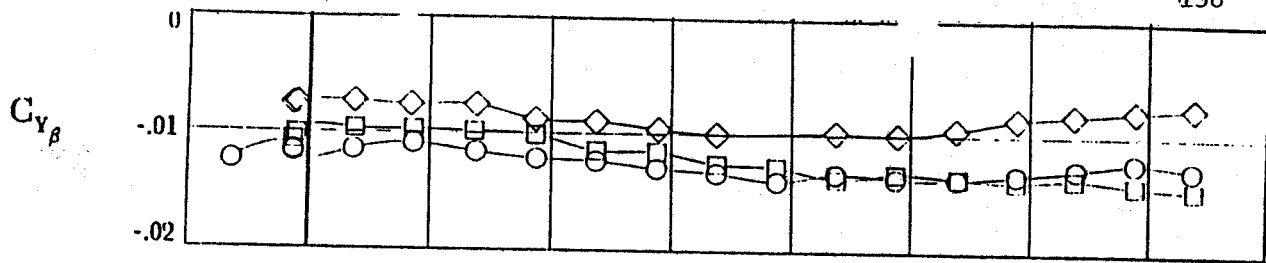


Figure 25. Continued.

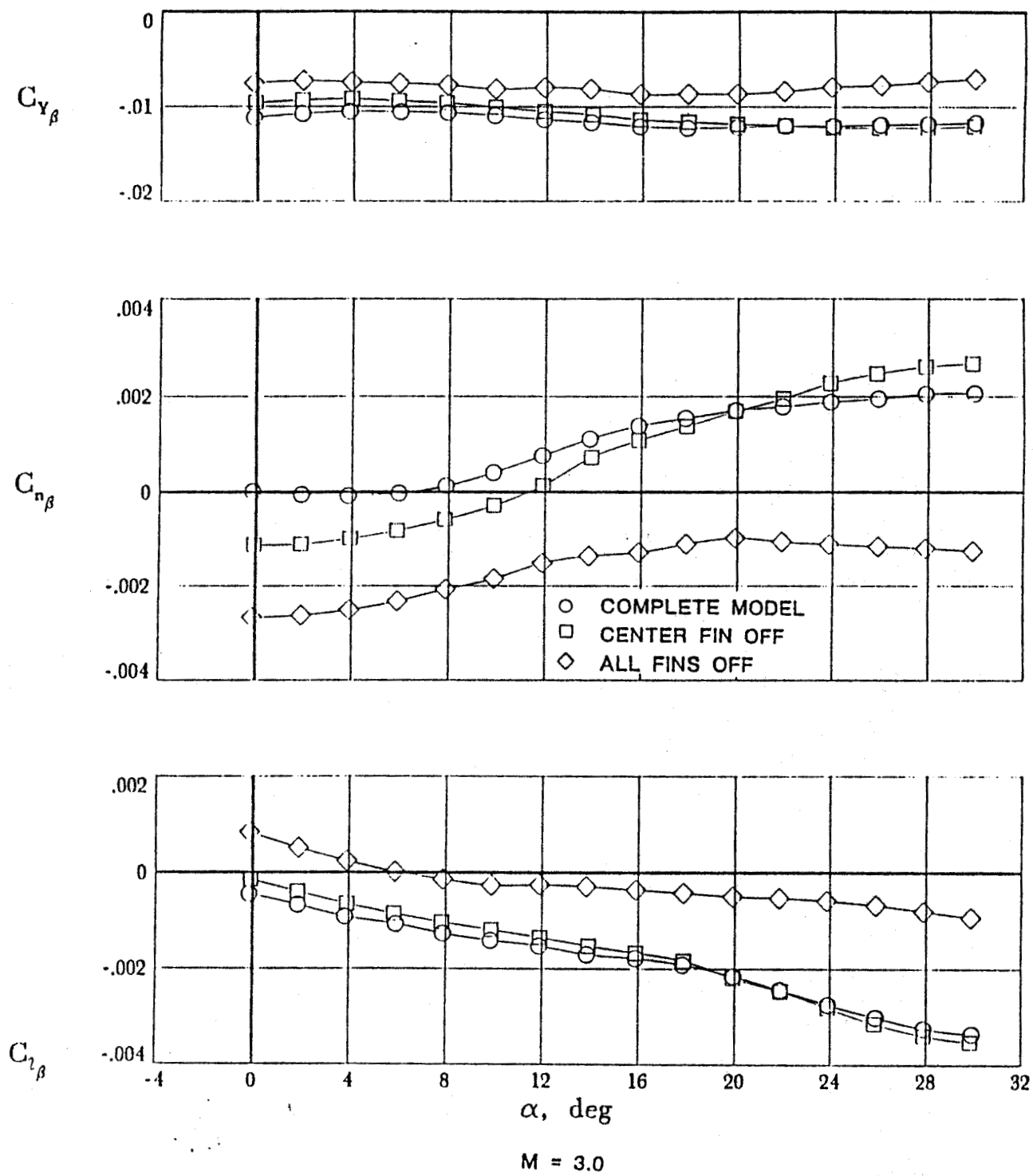


Figure 25. Continued.

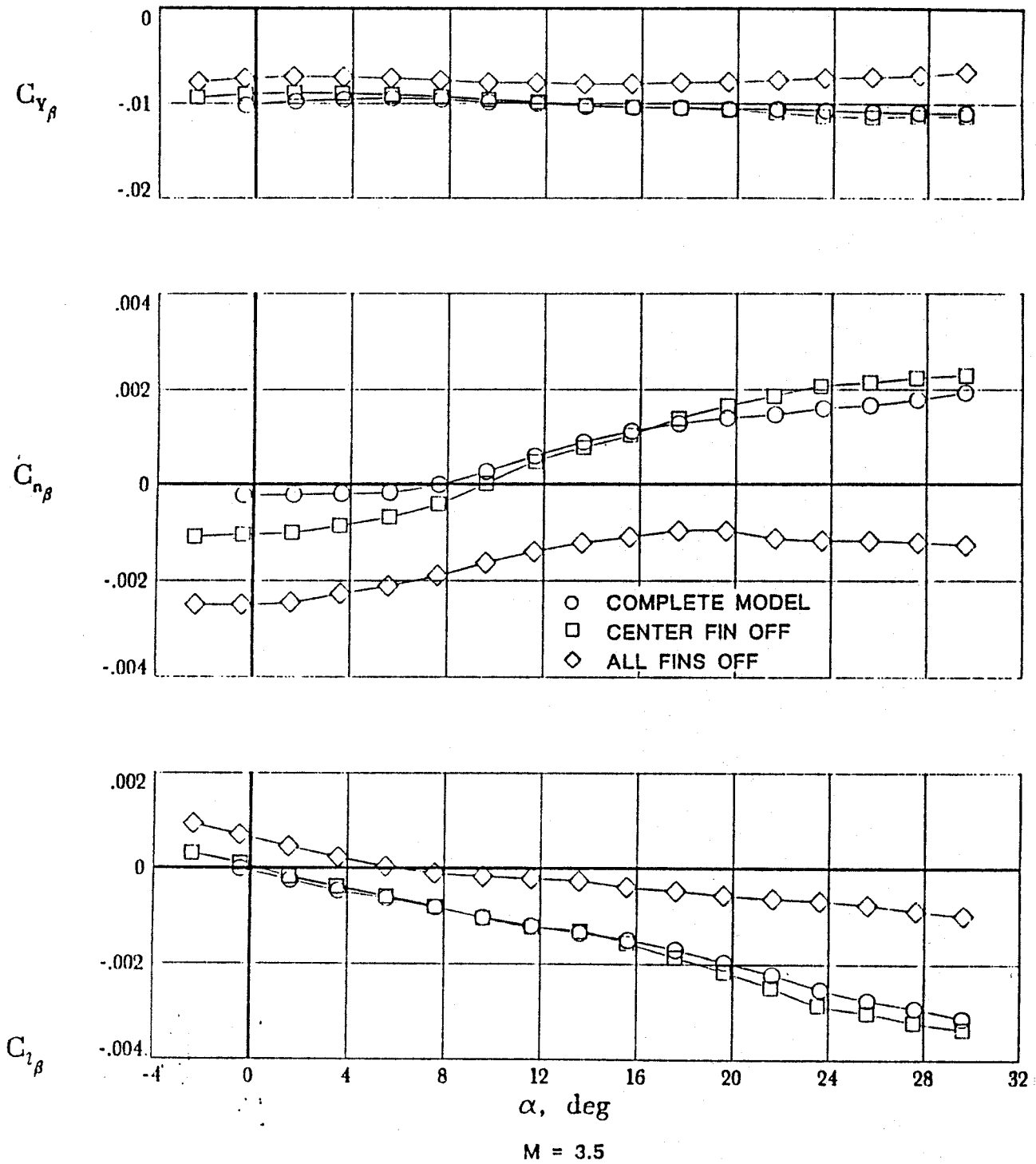


Figure 25. Continued.

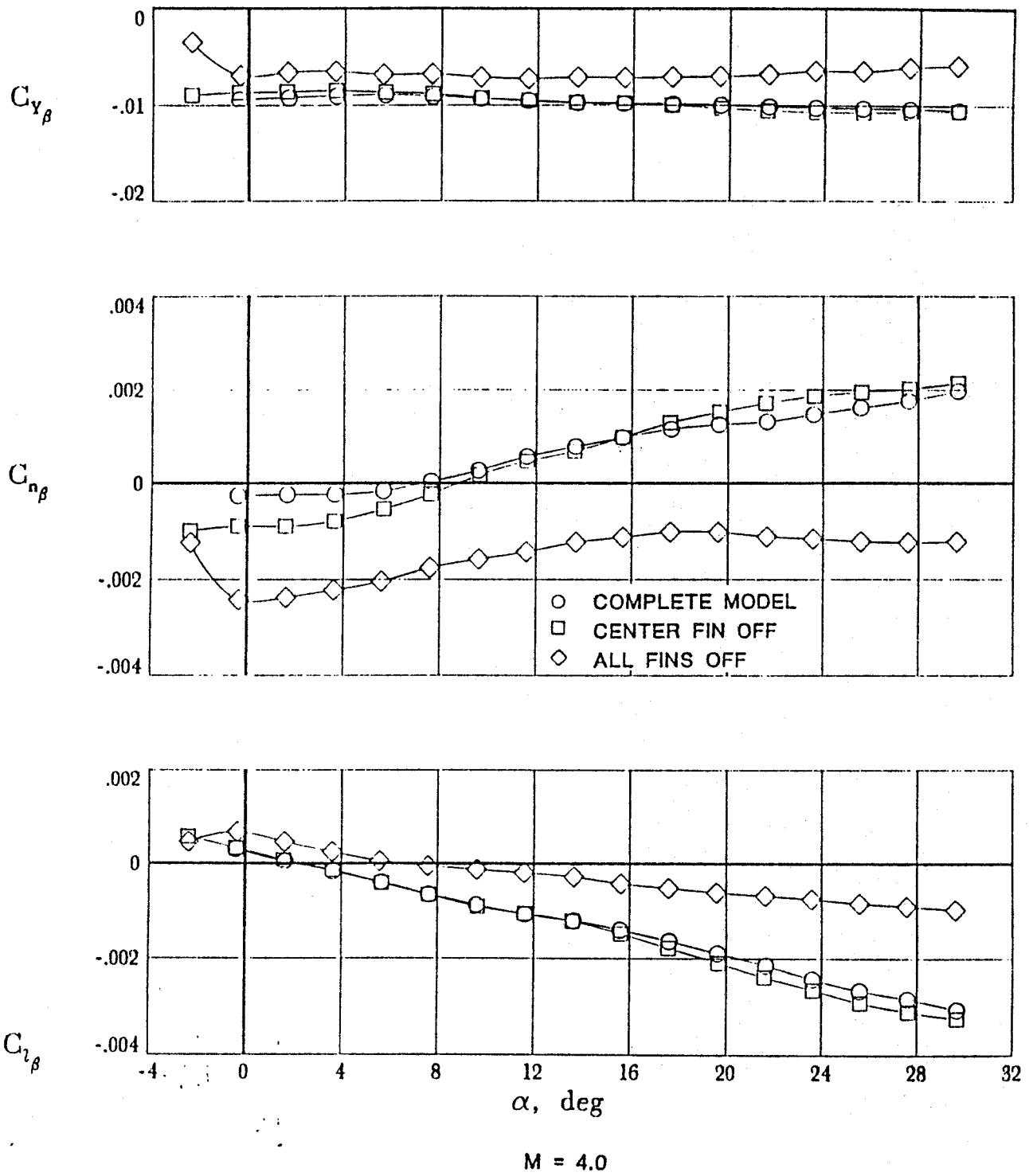


Figure 25. Continued.

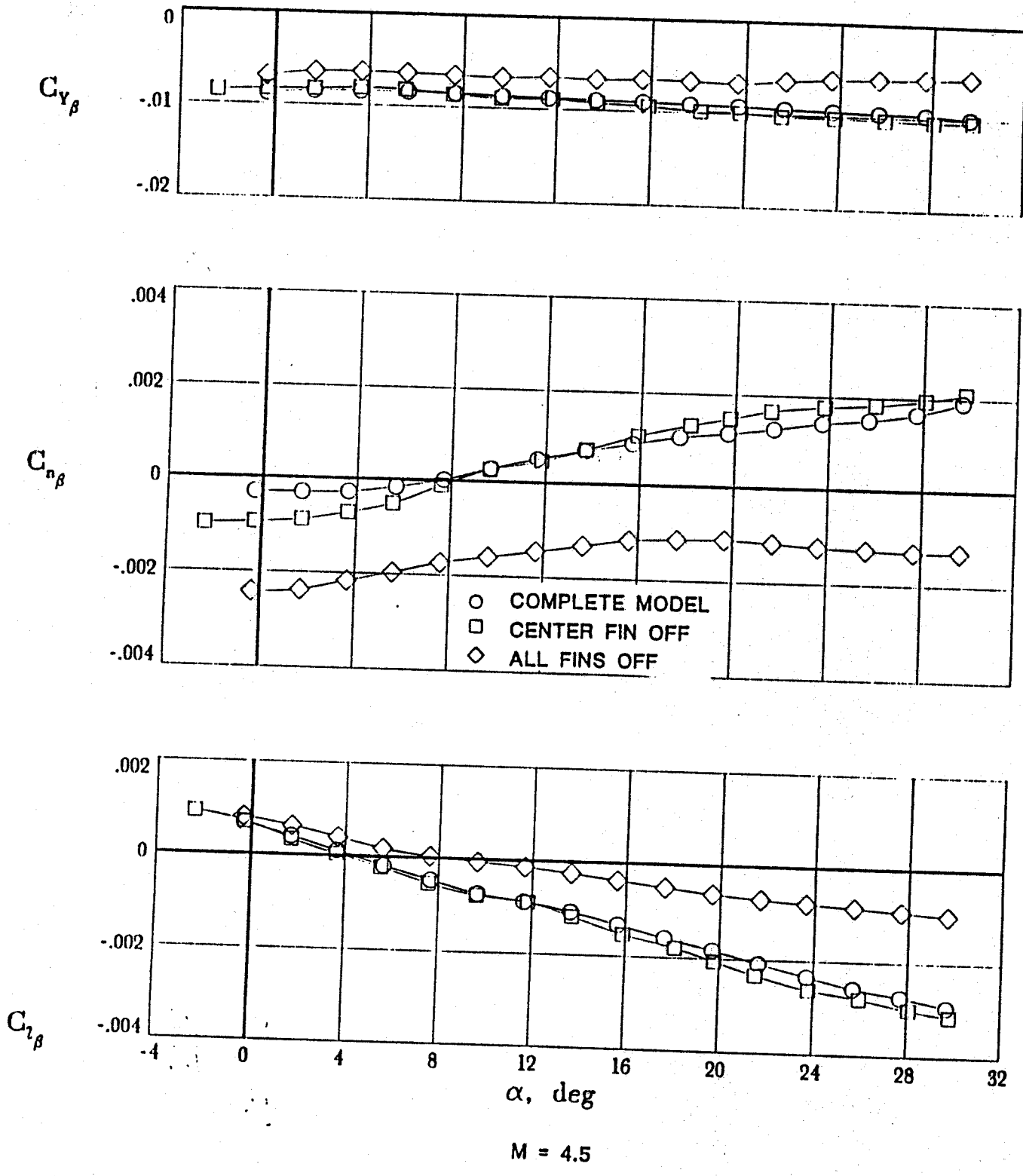


Figure 25. Concluded.

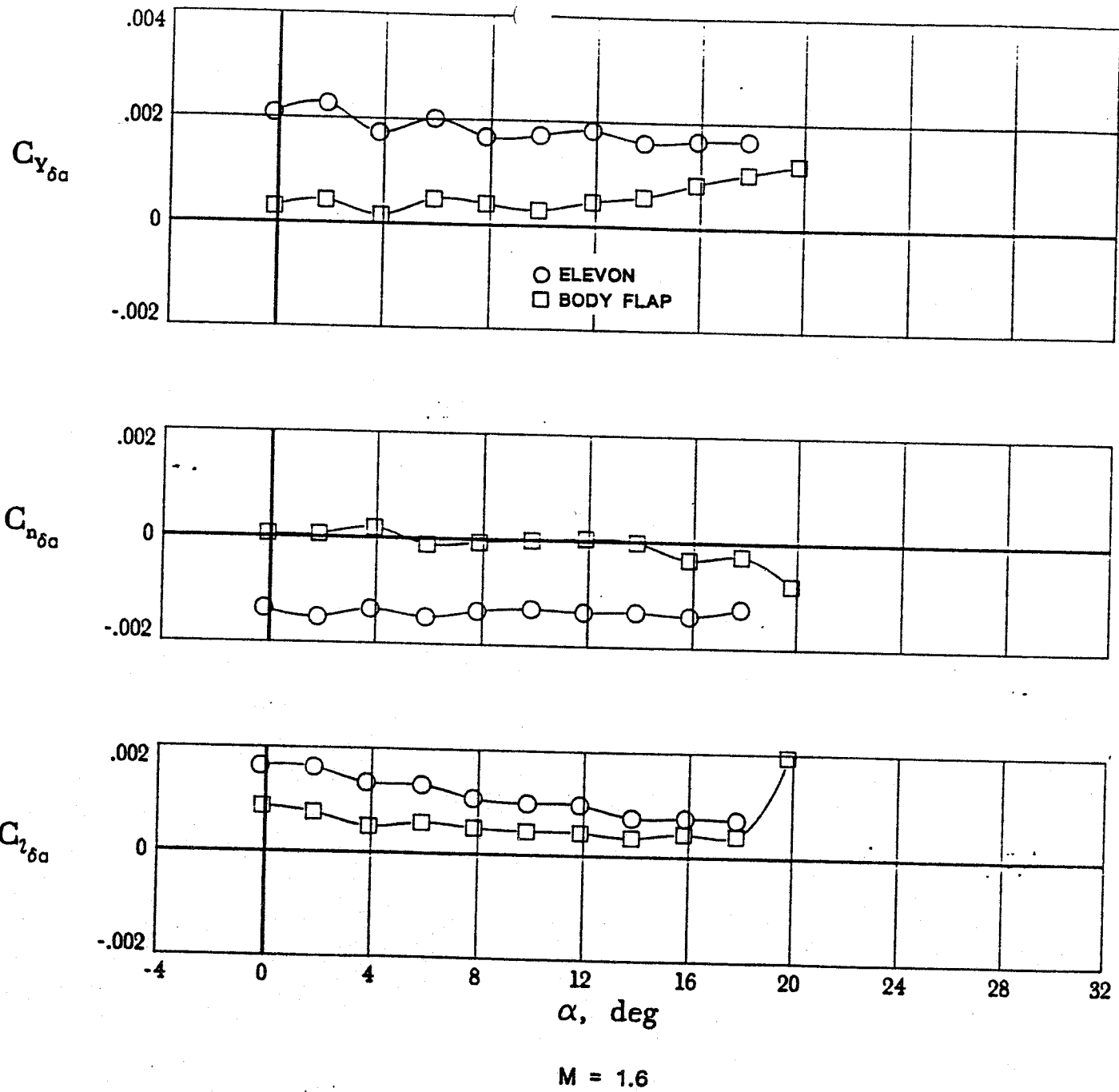
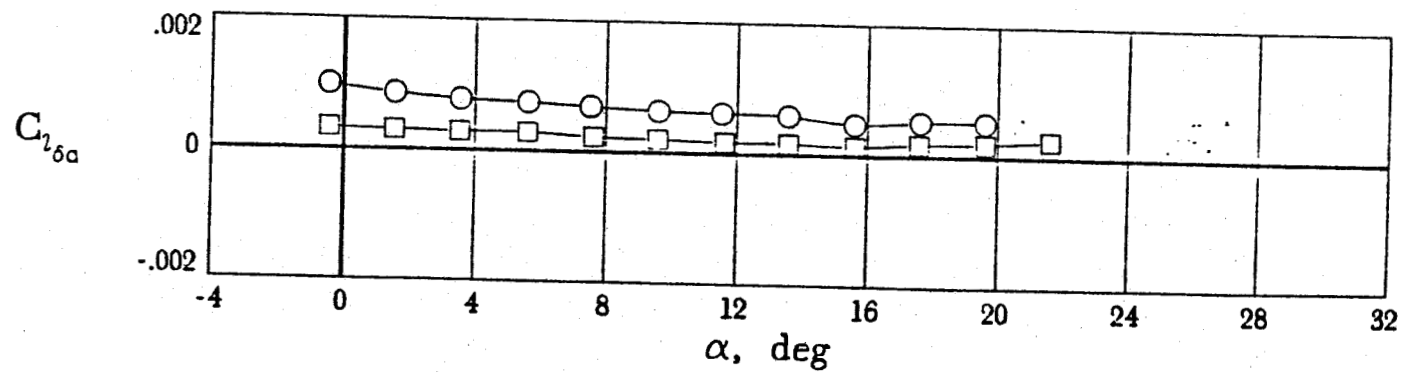
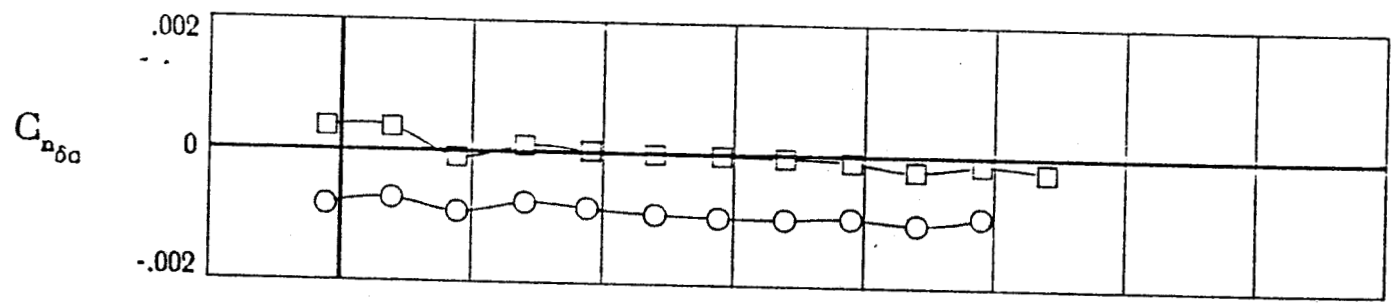
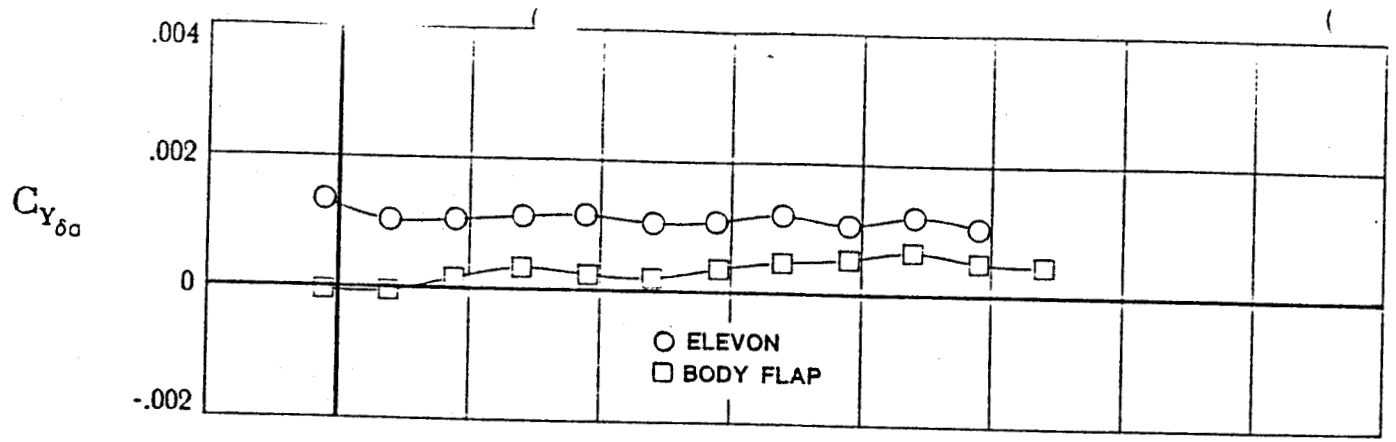
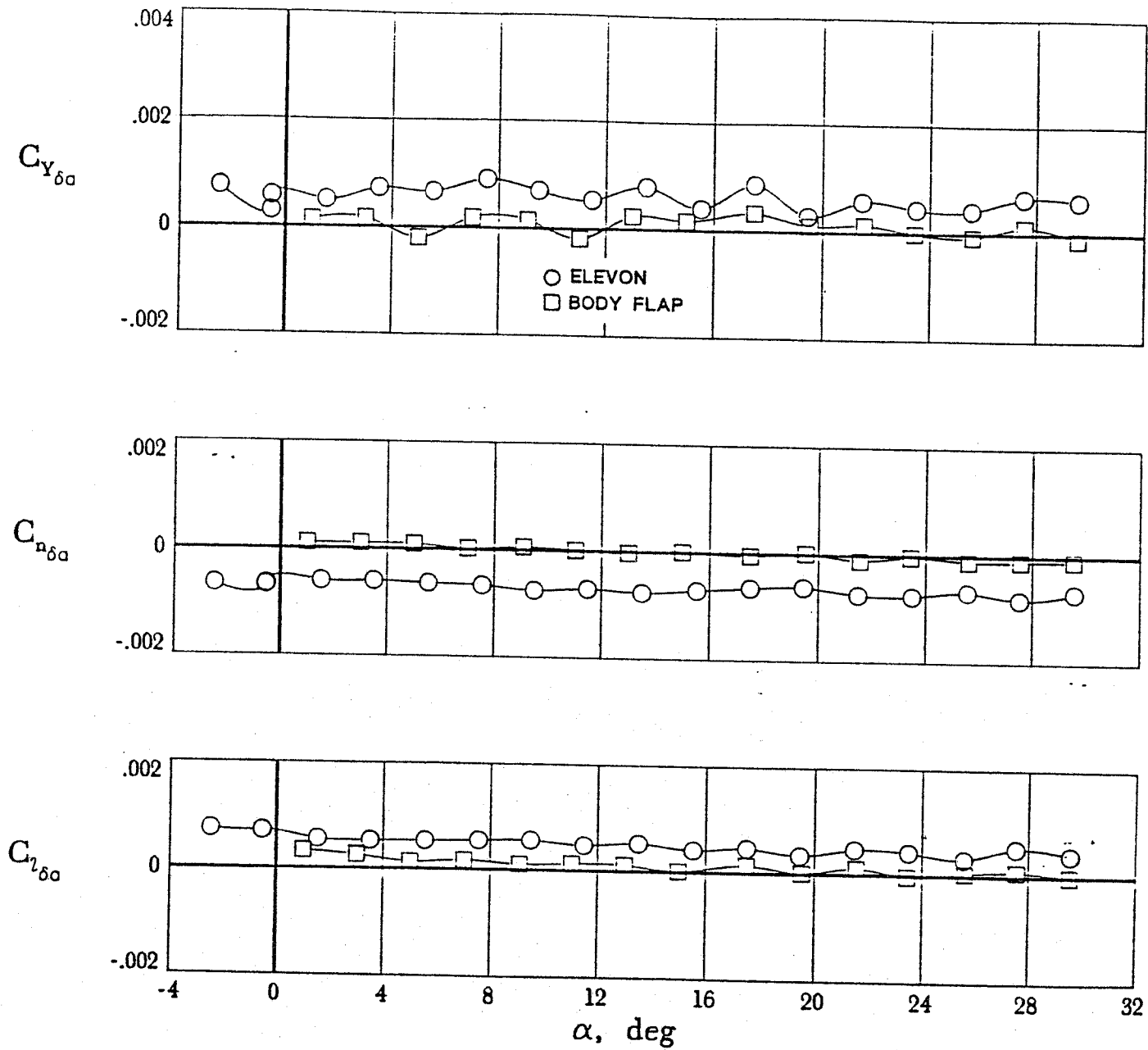


Figure 26. Supersonic roll control effectiveness.



M = 2.0

Figure 26. Continued.



$M = 2.5$

Figure 26. Continued.

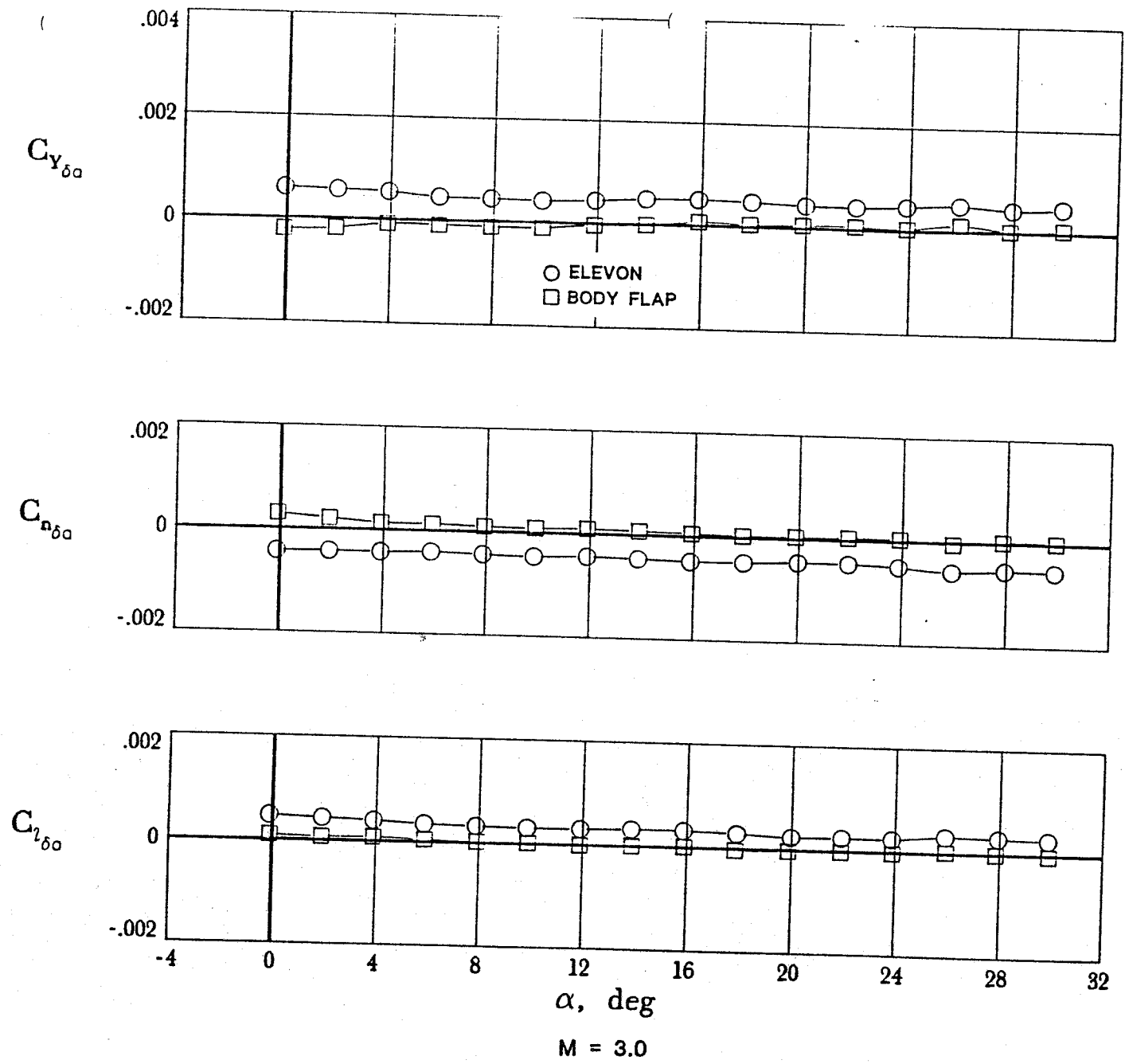


Figure 26. Continued.

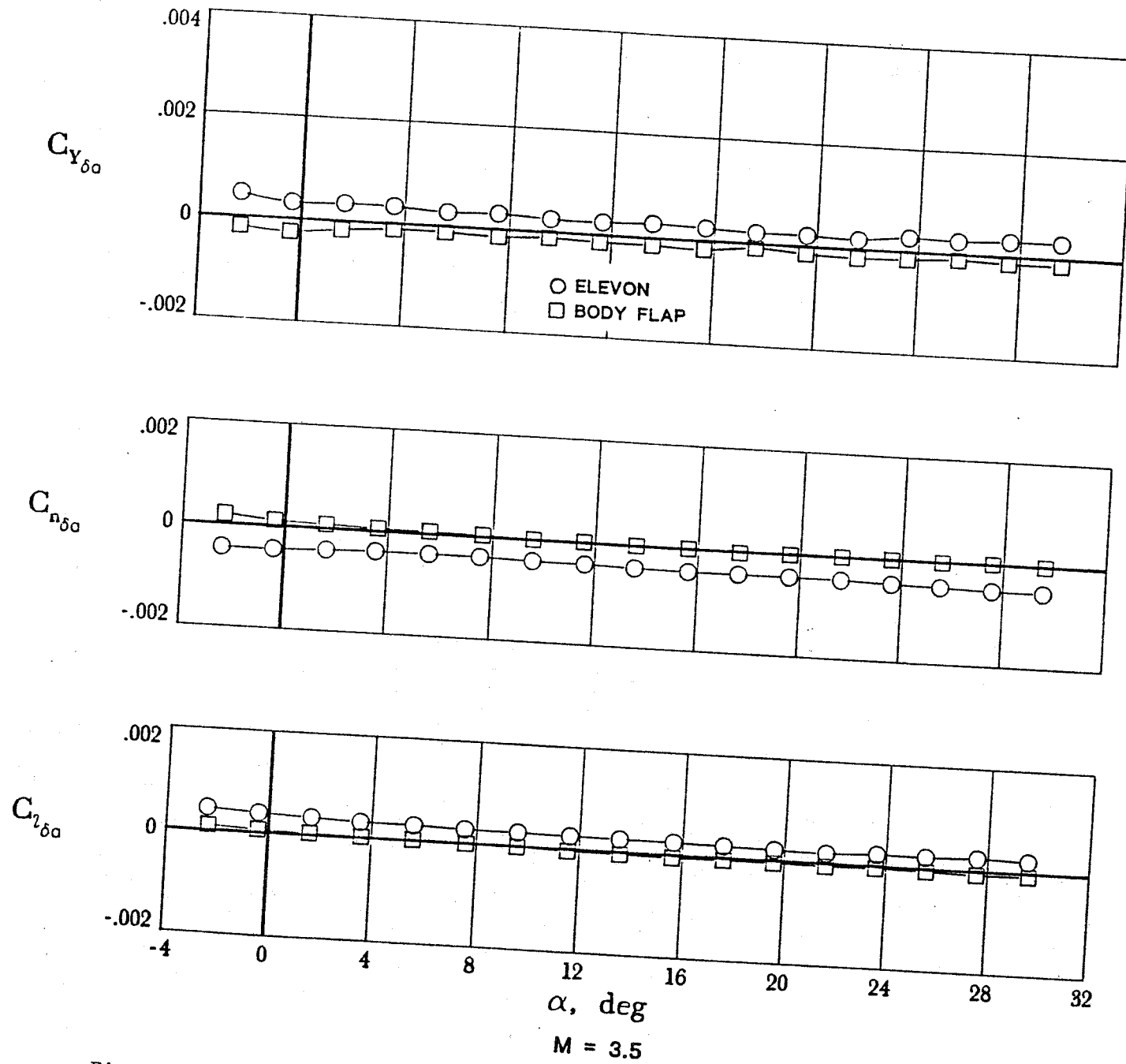


Figure 26. Continued.

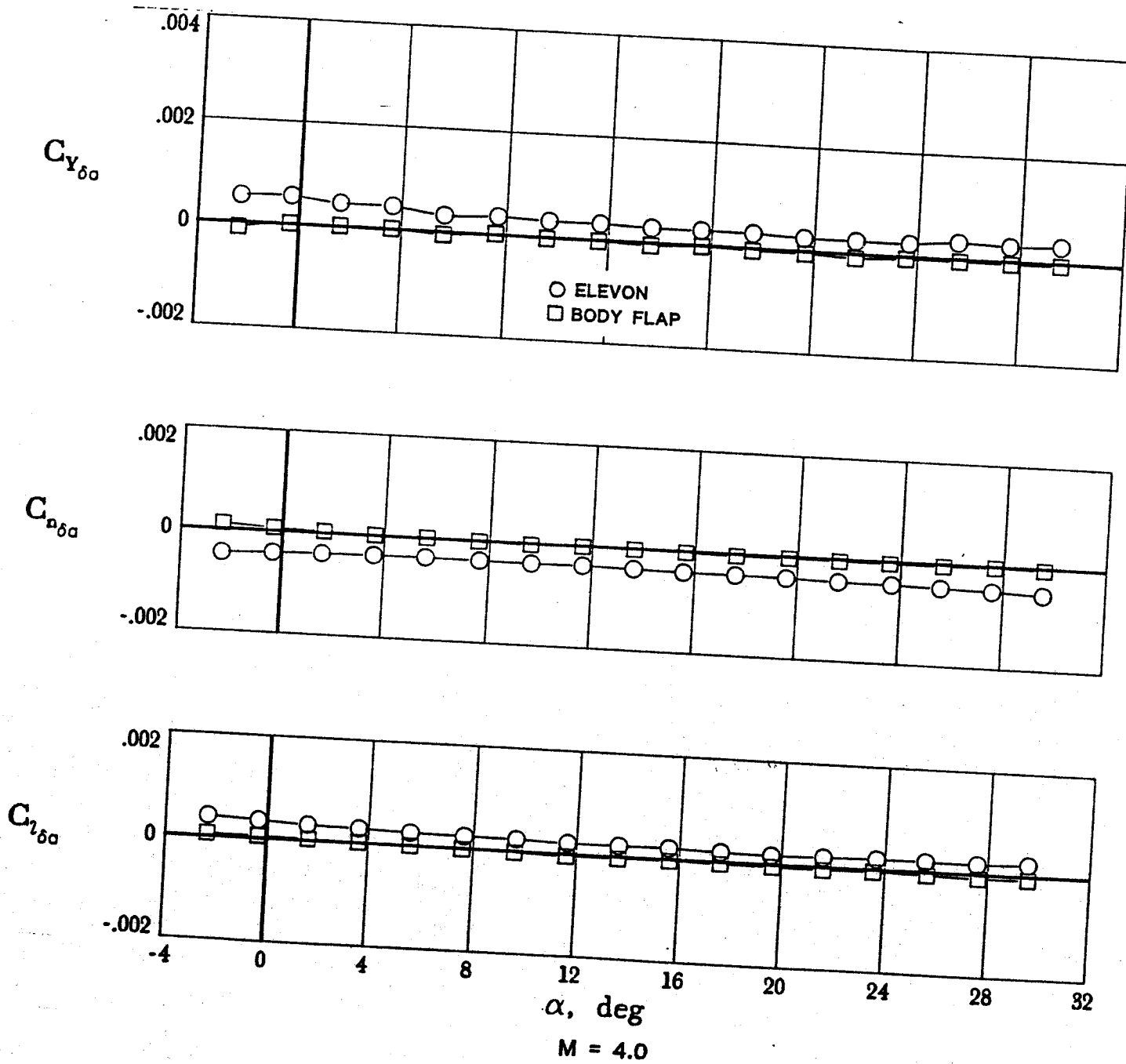


Figure 26. Continued.

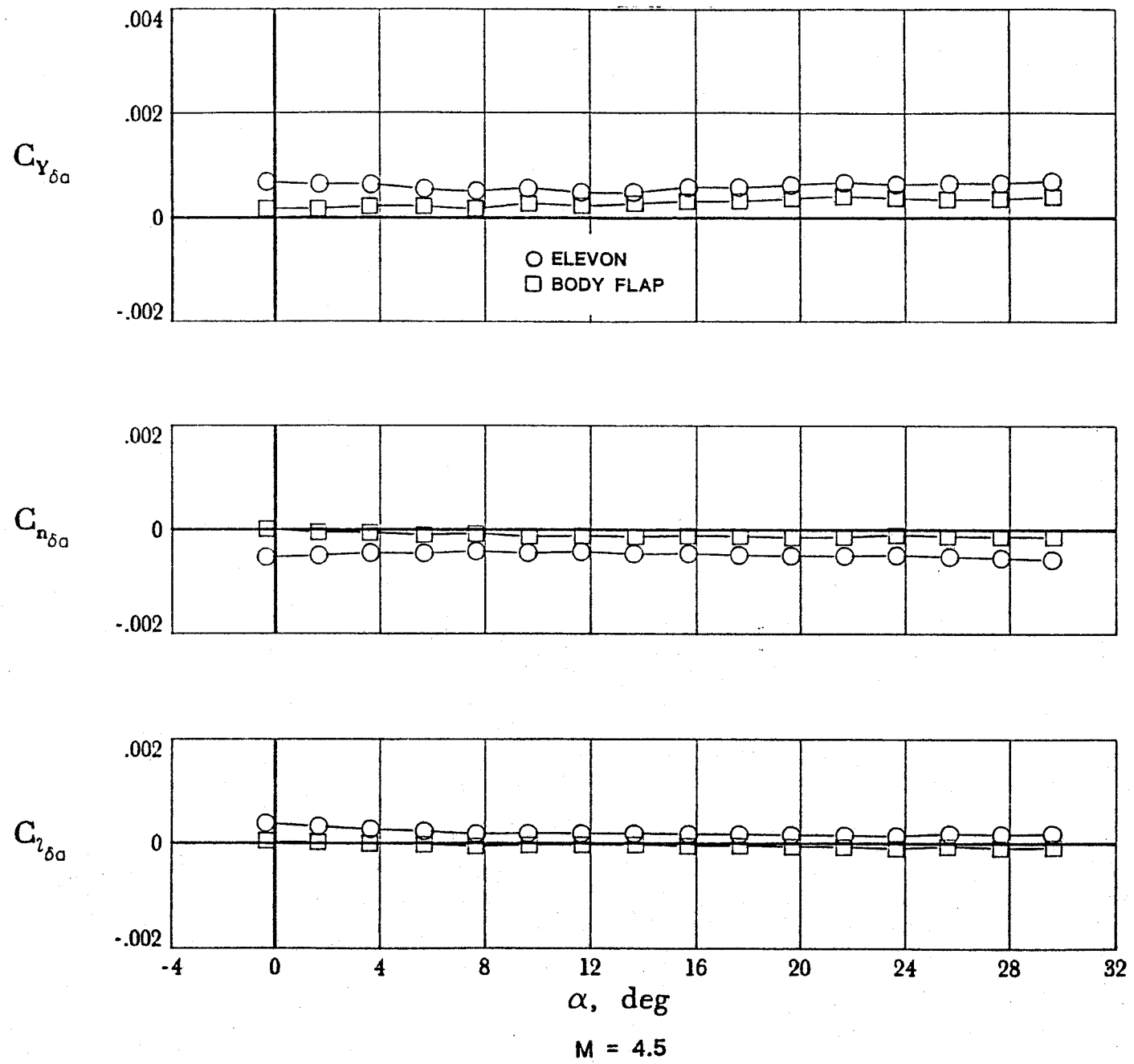


Figure 26. Concluded.

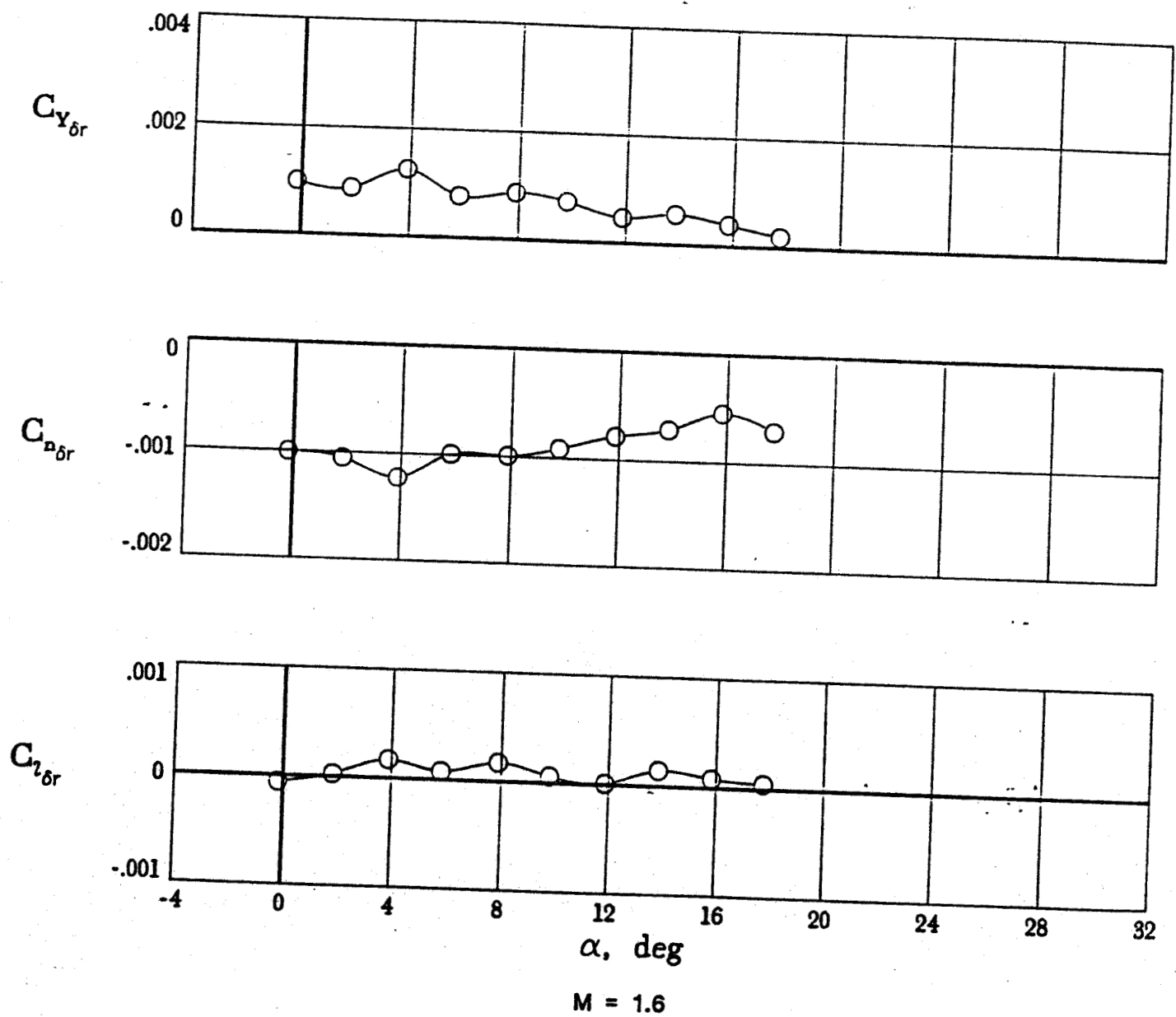


Figure 27. Supersonic yaw control effectiveness.

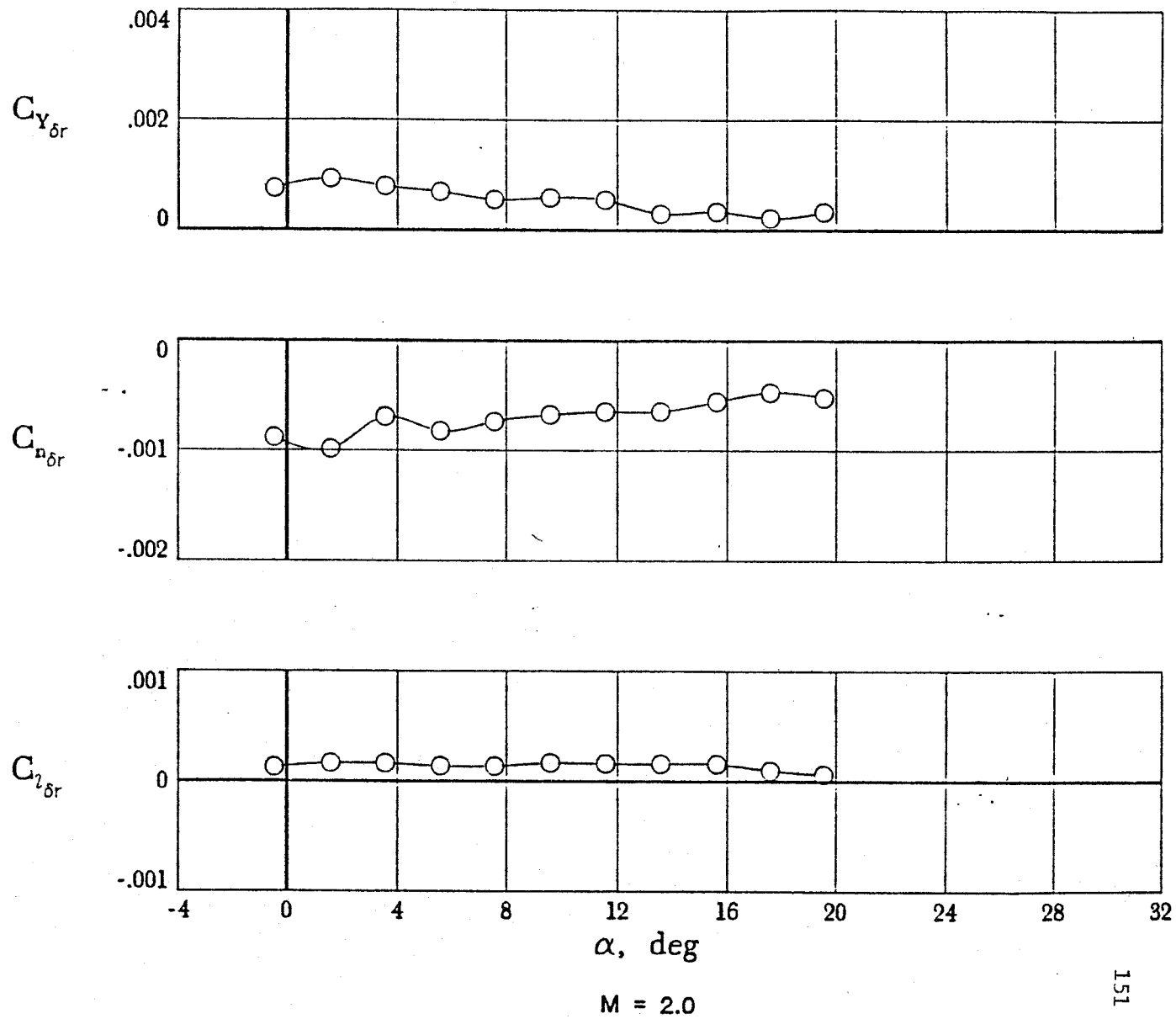


Figure 27. Continued.

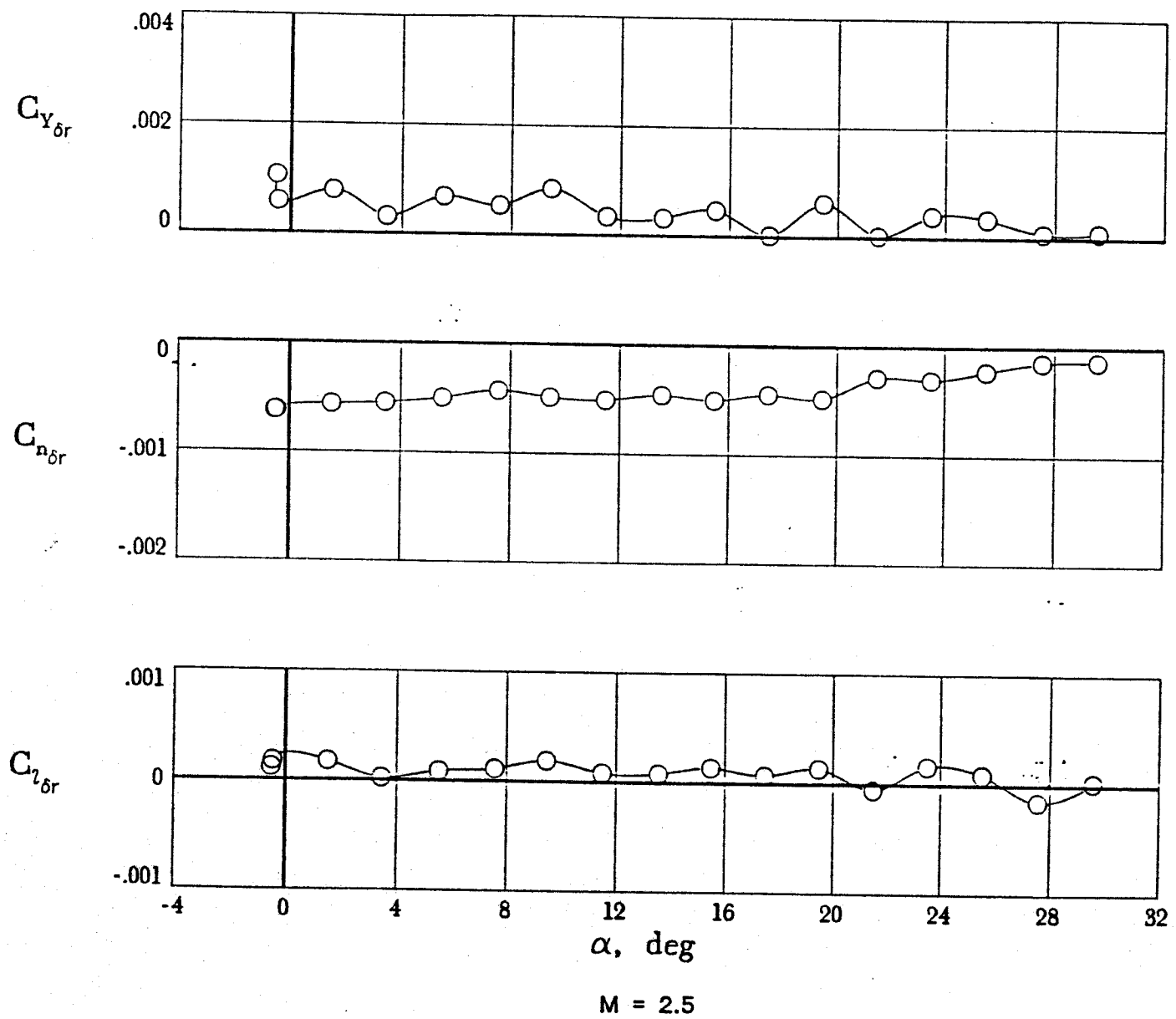


Figure 27. Continued.

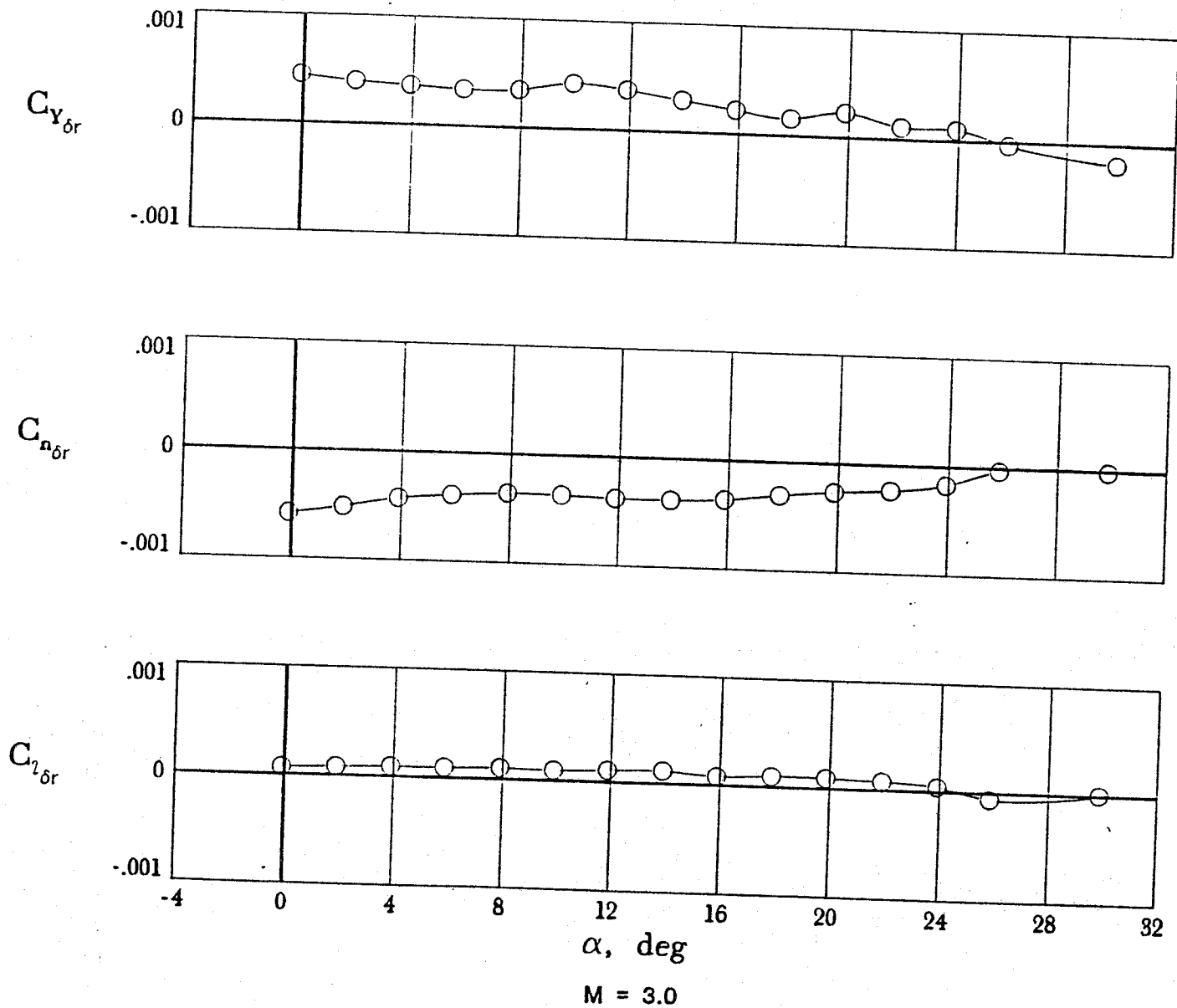


Figure 27. Continued.

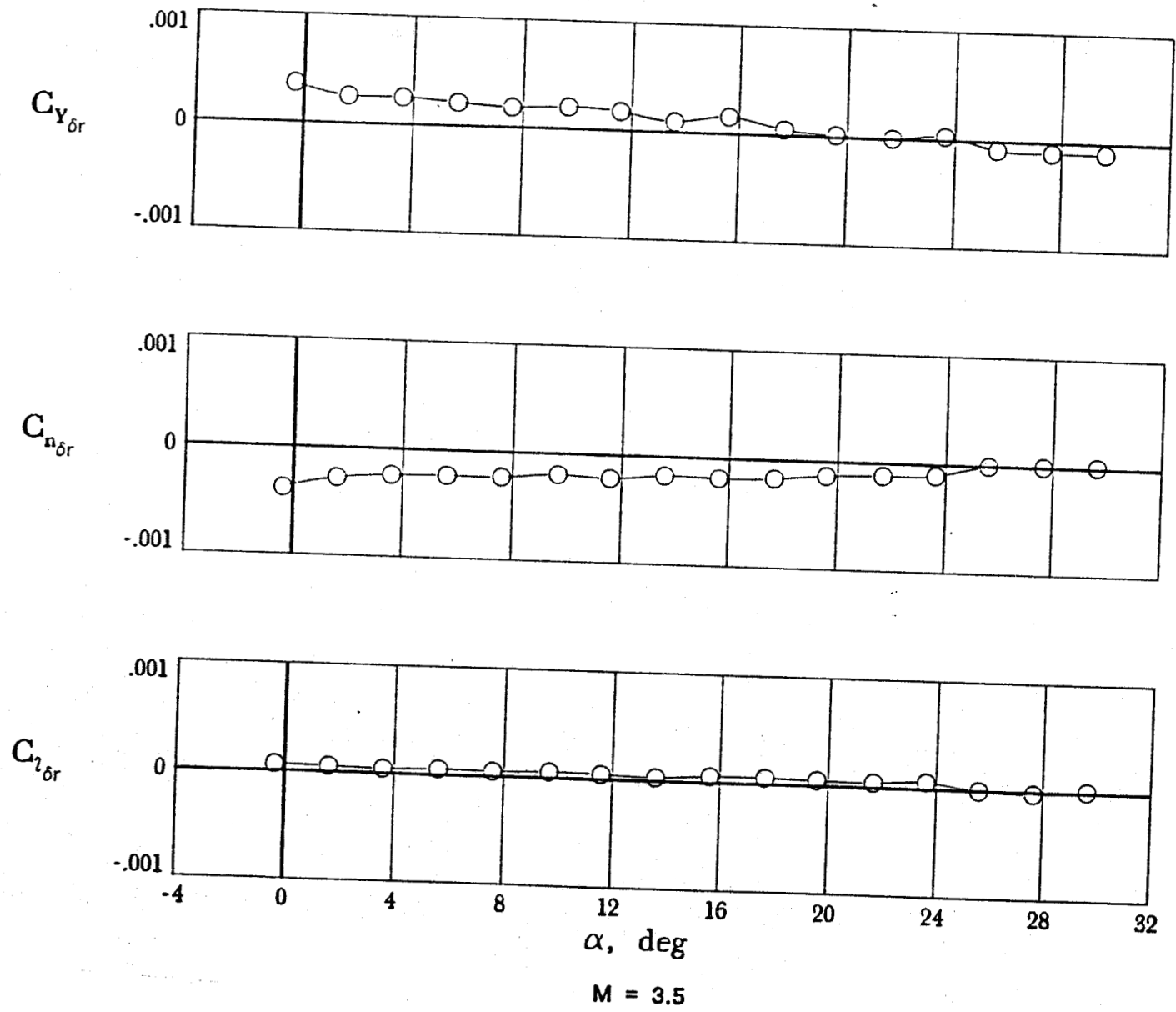


Figure 27. Continued.

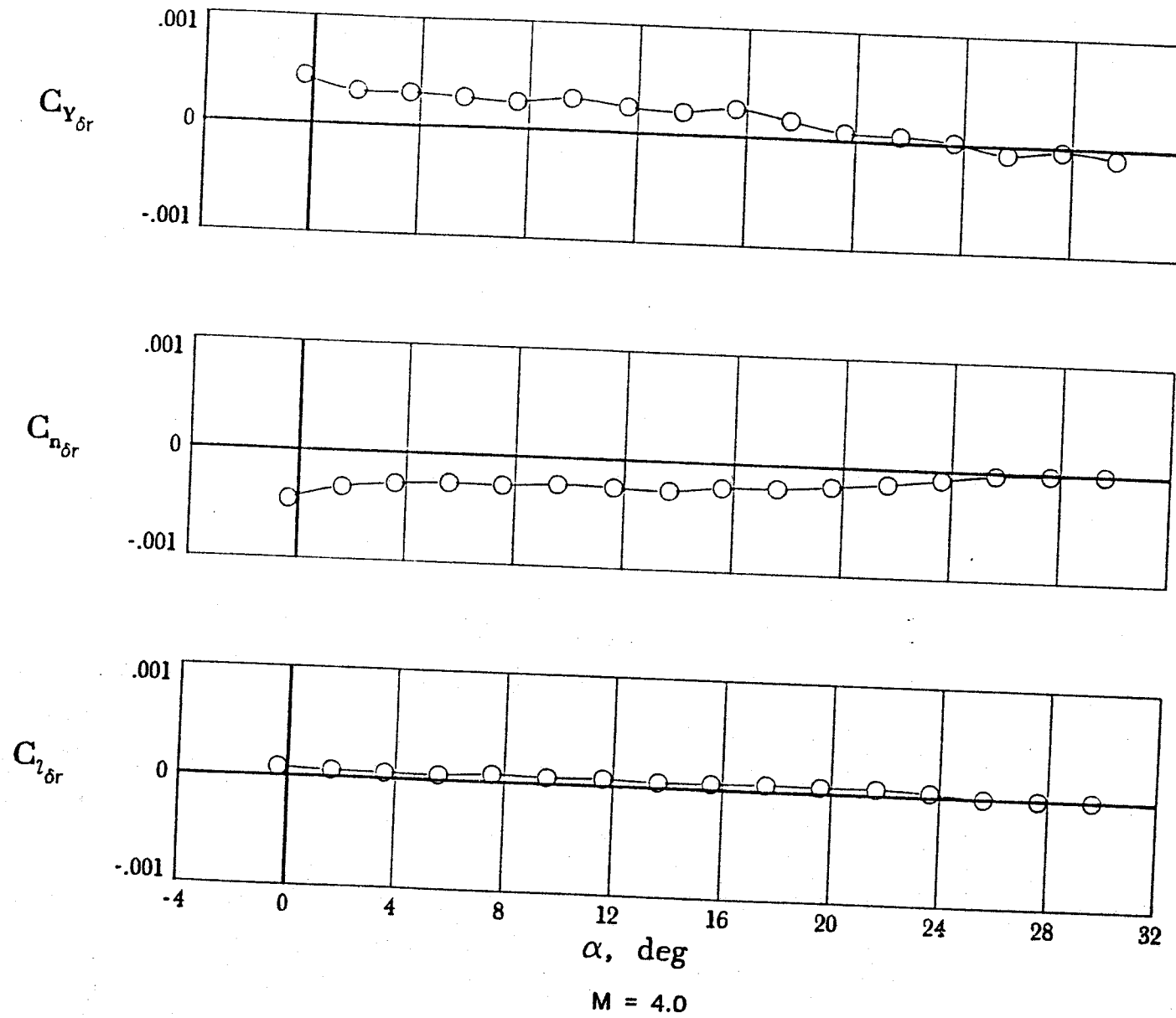
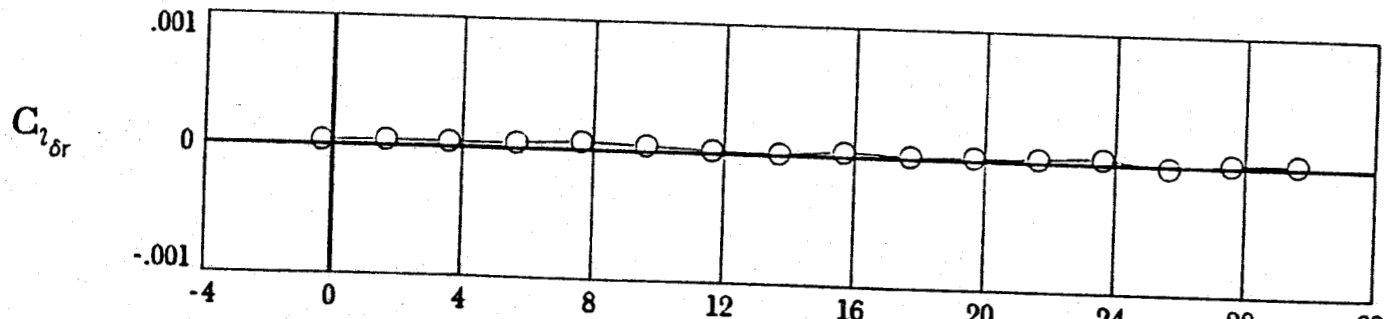
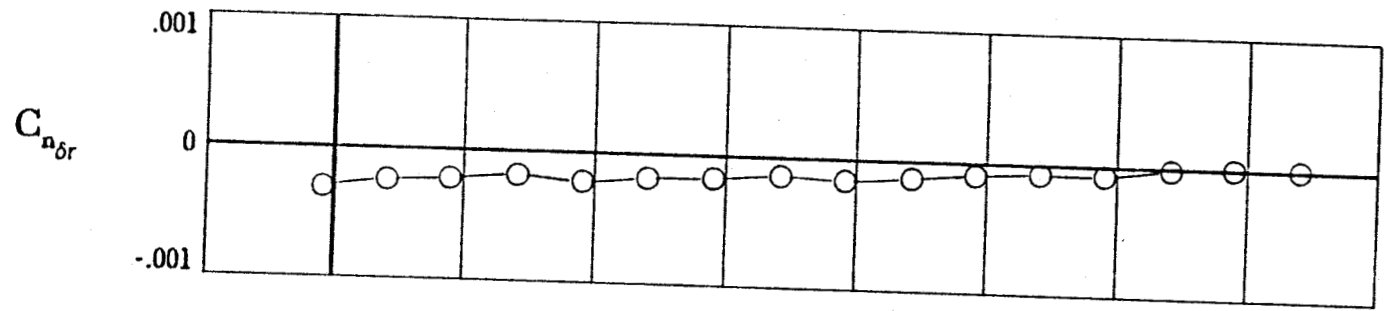
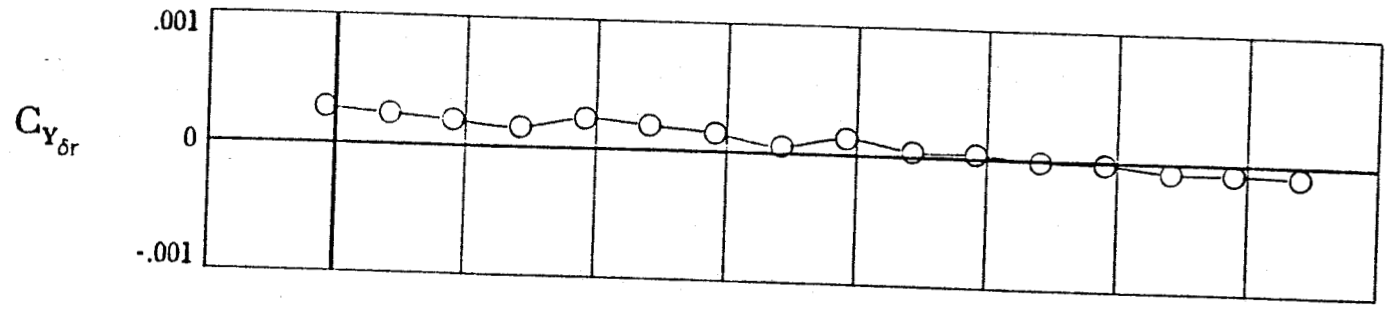


Figure 27. Continued.



α , deg

$M = 4.5$

Figure 27. Concluded.

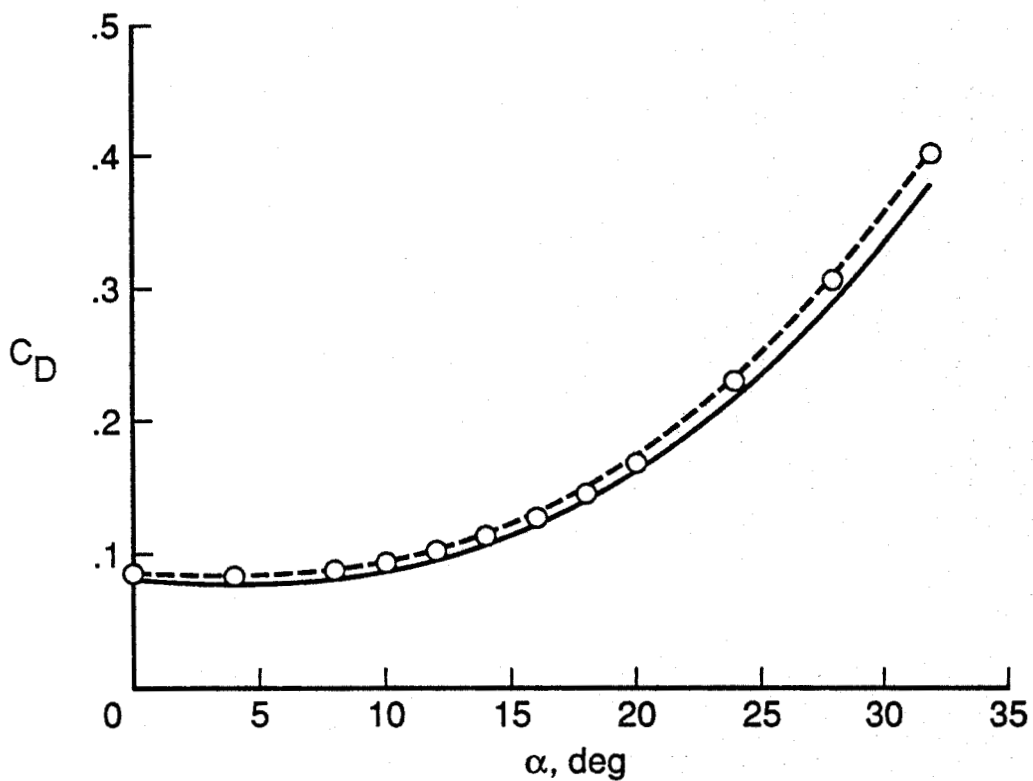
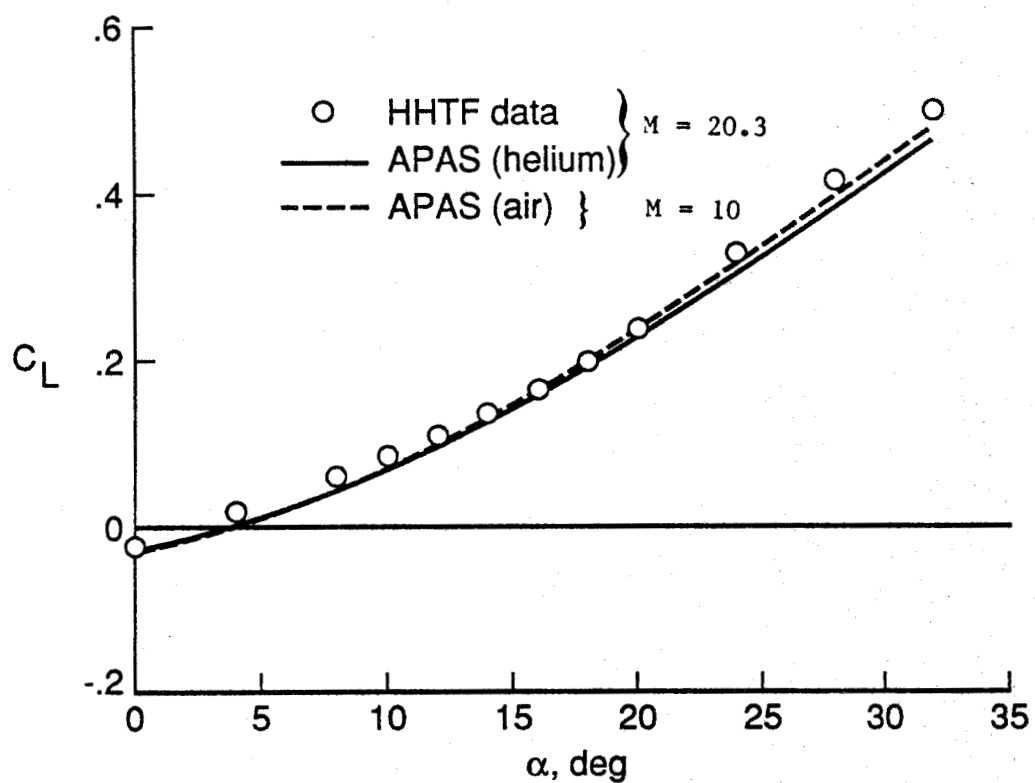
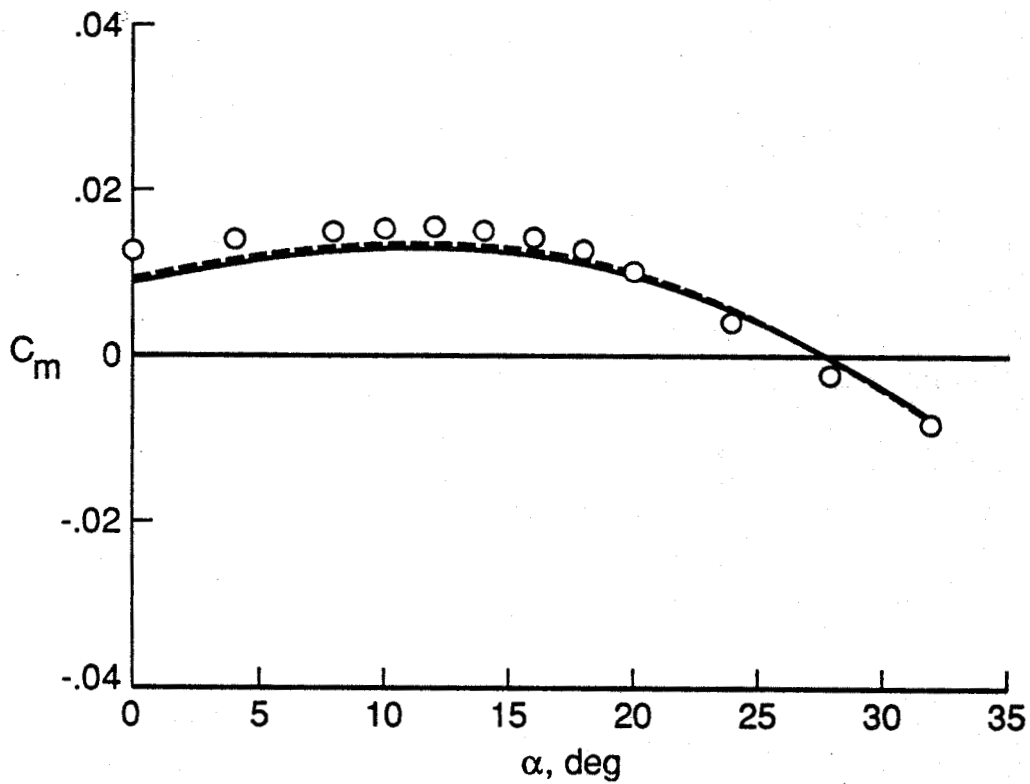
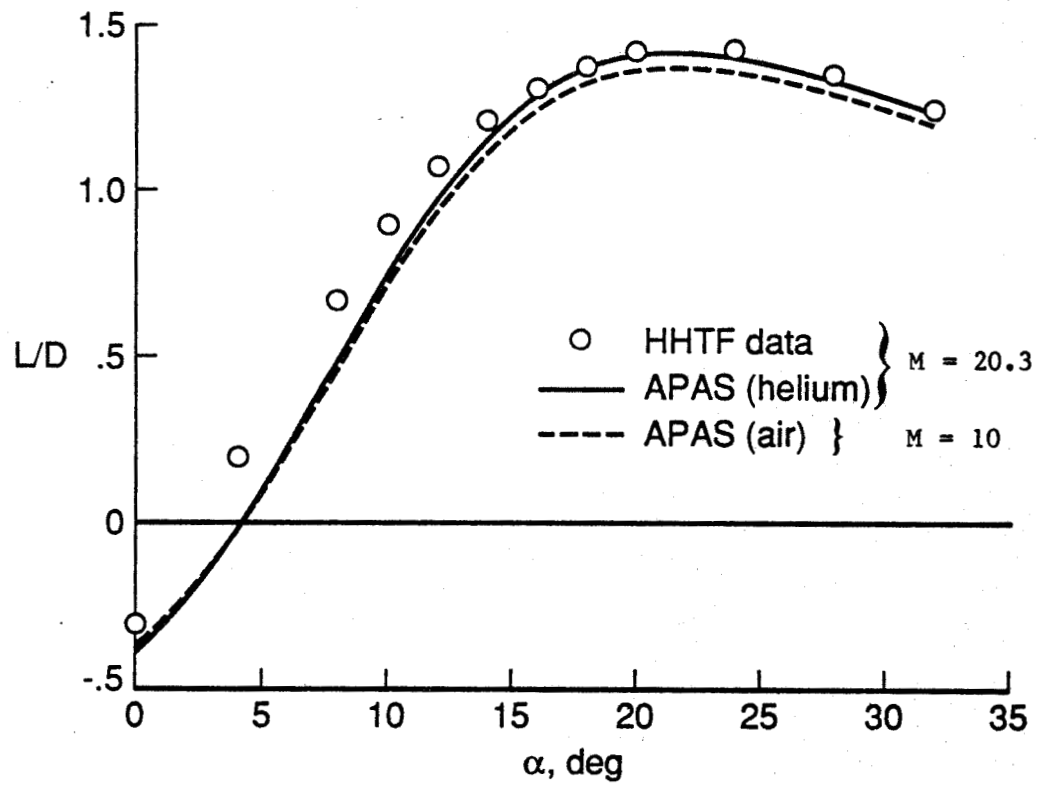
(a) C_L versus α and C_D versus α .

Figure 28. Longitudinal aerodynamics of the proposed PLS vehicle at hypersonic speeds.



(b) L/D versus α and C_m versus α .

Figure 28. Concluded.

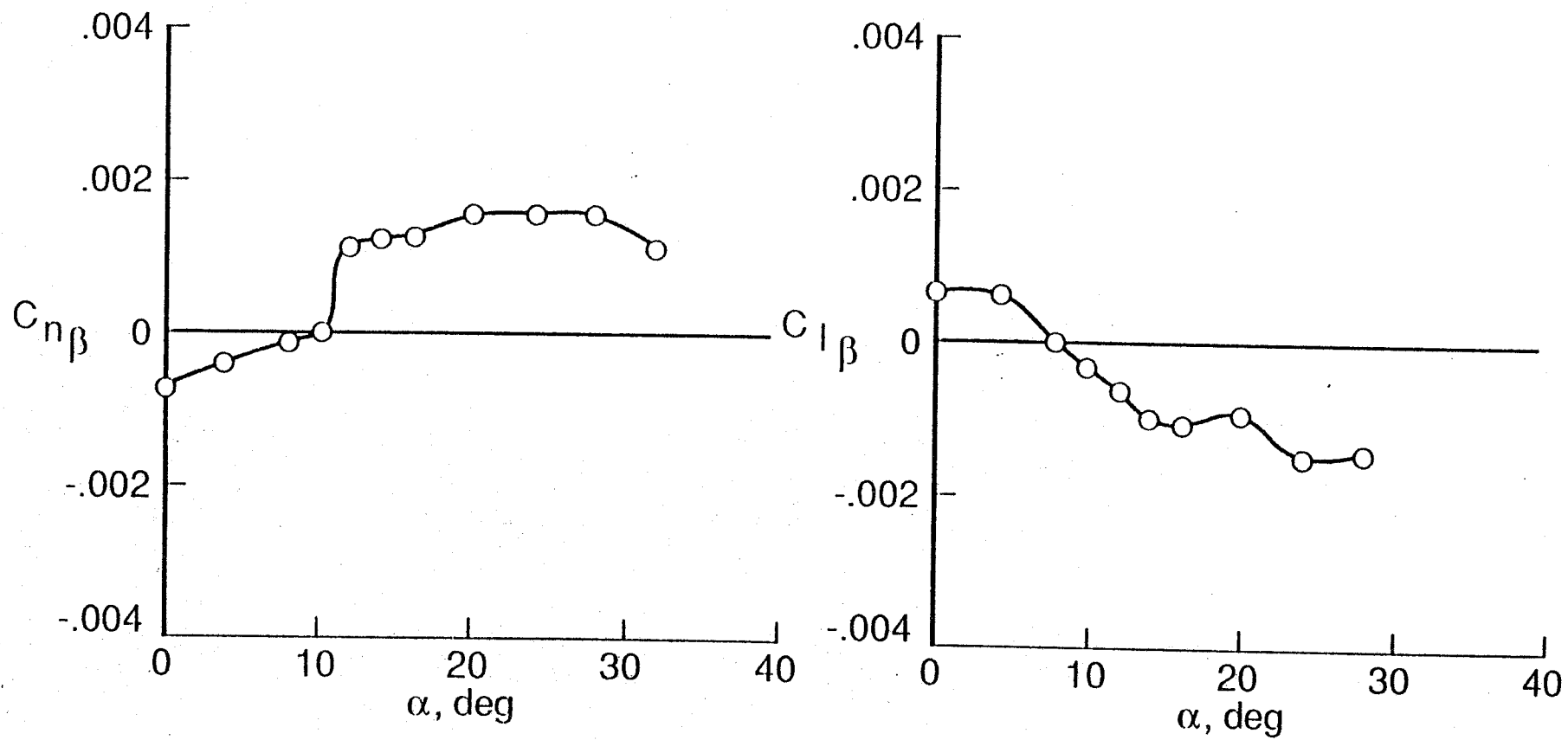


Figure 29. Lateral-directional aerodynamics of the proposed PLS vehicle at Mach 20.3 in helium.



Report Documentation Page

1. Report No. NASA TM-101641		2. Government Accession No.		3. Recipient's Catalog No.	
4. Title and Subtitle Aerodynamic Characteristics of a Proposed Personnel Launch System (PLS) Lifting-Body Configuration at Mach Numbers From 0.05 to 20.3				5. Report Date November 1989	
				6. Performing Organization Code	
7. Author(s) Christopher I. Cruz, George M. Ware, Sue B. Grafton, William C. Woods, James C. Young				8. Performing Organization Report No.	
				10. Work Unit No. 506-49-11-01	
9. Performing Organization Name and Address NASA Langley Research Center Hampton, Virginia 23665-5225				11. Contract or Grant No.	
				13. Type of Report and Period Covered Technical Memorandum	
12. Sponsoring Agency Name and Address National Aeronautics and Space Administration Washington, DC 20546-0001				14. Sponsoring Agency Code	
				15. Supplementary Notes	
16. Abstract <p>A wind-tunnel investigation has been performed to determine the aerodynamic characteristics of a proposed lifting-body personnel launch system (PLS) configuration over a Mach range of 0.05 to 20.3. The test configuration had a low-aspect-ratio body with a flat undersurface and three fins on the upper aft body. Data are presented with a minimum of analysis.</p>					
17. Key Words (Suggested by Author(s)) Aerodynamics Lifting Body Spacecraft			18. Distribution Statement Unclassified - Unlimited Subject Category 16		
19. Security Classif. (of this report) Unclassified		20. Security Classif. (of this page) Unclassified		21. No. of pages 161	22. Price A08